



UNIVERSITAT^{DE}
BARCELONA

CRISPR-Cas9 to model retinitis pigmentosa caused by mutations in splicing factors in *C. elegans*

Dmytro Kukhtar Kukhtar



Aquesta tesi doctoral està subjecta a la llicència **Reconeixement 4.0. Espanya de Creative Commons.**

Esta tesis doctoral está sujeta a la licencia **Reconocimiento 4.0. España de Creative Commons.**

This doctoral thesis is licensed under the **Creative Commons Attribution 4.0. Spain License.**



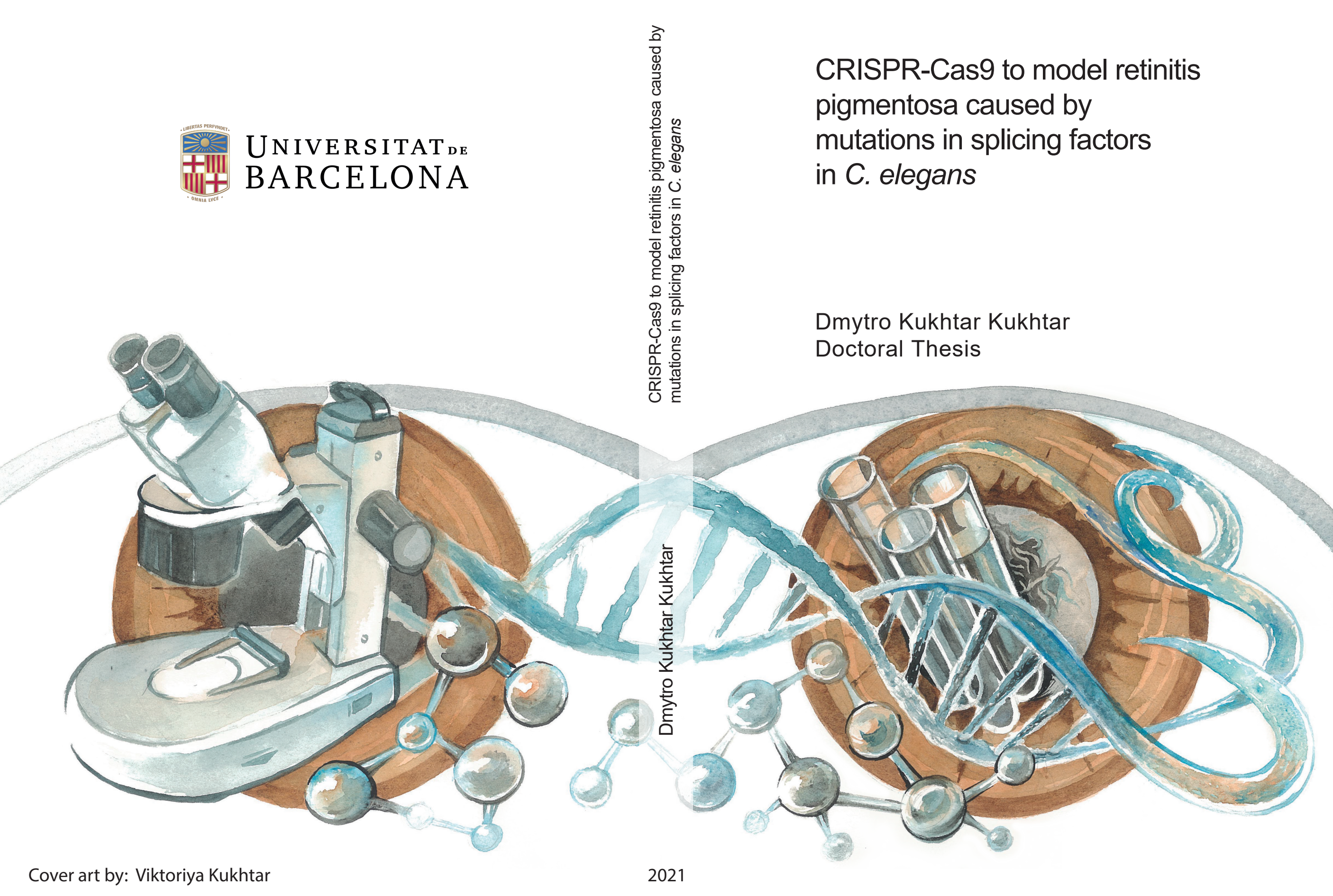
UNIVERSITAT DE
BARCELONA

CRISPR-Cas9 to model retinitis pigmentosa caused by
mutations in splicing factors in *C. elegans*

CRISPR-Cas9 to model retinitis
pigmentosa caused by
mutations in splicing factors
in *C. elegans*

Dmytro Kukhtar Kukhtar
Doctoral Thesis

Dmytro Kukhtar Kukhtar



Doctoral program in Biomedicine

**CRISPR-Cas9 to model retinitis
pigmentosa caused by mutations in
splicing factors in *C. elegans***

Thesis presented by

Dmytro Kukhtar Kukhtar

to qualify for the degree of Doctor of Philosophy in
Biomedicine by

the University of Barcelona



**UNIVERSITAT DE
BARCELONA**


Dmytro Kukhtar





This thesis has been performed in the Institute of
Biomedical Investigation of Bellvitge (IDIBELL), under
the supervision of Dr. Julián Cerón Madrigal and the
tutorship of Francesc Viñals Canal

Acknowledgments

Mirando atrás, a pesar de las dificultades y noches sin dormir, me doy cuenta de que, en realidad, no cambiaría nada. Y eso es gracias a todos los que me rodean y a quien dedico estas líneas.

Un especial agradecimiento a Julián, por tu apoyo y por ayudarme a crecer. Tu optimismo ha amenizado incluso los peores momentos. Gracias a ti no sólo he mejorado como científico, sino como persona. Por los buenos ratos y por convertir Cerón lab en una familia, más que sólo un grupo de investigación.

Un cariñoso recuerdo a quienes me han acompañado en mis primeros pasos de la vida investigadora Karinna, Lluís y Montse.

Un fuerte abrazo a la *worm family* que ha soportado mis “¿Me rascas la espalda?” y siempre han estado ahí para rascarla. Jeremy, Carmen, David y desde la distancia Xènia: ha sido un enorme placer convivir en el lab y en especial fuera de él. Necesitaría una tesis sólo para daros las gracias y voy corto de tiempo *ja, ja...* Uno de los mejores regalos que me llevo es vuestra amistad, os quiero y os tendré en el corazón siempre.

Gracias a Núria, Mariona y Miguel, aunque coincidimos poco, las risas compartidas me alegraron las últimas semanas del proyecto. En especial a mi máster favorita Núria, tus mates me han dado vida en la escritura.

Por supuesto esto no habría sido posible sin todos los que sin estar en el lab formáis parte de mi vida. Natalia i Meri m’heu ajudat sempre a veure les coses amb perspectiva i aquest treball és també gràcies a vosaltres.

Una especial dedicació a Nat, pels anys que hem compartit i que m'ha recolzat inclús en moments en que altres no ho haguessin fet.

И в завершении, я хотел бы выразить огромную благодарность своей семье. Спасибо, что всегда верили и поддерживали меня. Отдельное спасибо моей маме Виктории, которая была всегда готова помочь и чей дизайн украшает обложку этой работы. Моему папе Игорю, на которого я могу всегда положиться. Без вашей поддержки и понимания я не смог бы этого добиться. Также, я хотел бы выразить благодарность своей бабушке Елене и всем родственникам, которые сейчас находятся вдалеке.

Abstract

Retinitis pigmentosa (RP) is a rare, heterogenic, and hereditary disease that produces gradual loss of the visual field and can cause blindness. Mutations causing RP are still unknown in about 50% of the cases. By CRISPR-Cas9, we mimicked a few splicing-related RP mutations (s-adRP) in *PRPF8/prp-8* and *SRNP200/snpr-200* that were used for drug screens, identify potential disease modifiers, investigate mechanisms of the disease, and work on a system to provide functional information for gene variants.

One of the alleles generated, displaying an overt phenotype, was used in a small-scale drug screen to identify small molecules capable of alleviating the phenotype. Unexpectedly, we found an FDA-approved drug having a detrimental effect on some of the s-adRP mutant strains.

Since RP onset and progression are highly variable due to environmental or genetic modifiers, *C. elegans* could help RP prognosis by identifying such modifiers. We performed a small-scale RNAi screen on RP mutants with no overt phenotypes and found genetic interactions with other splicing-related genes: *isy-1/ISY1*, *mog-2/SNRPA1*, and *cyn-15/PPWD1*. Thus, secondary mutations in these genetic interactors could act as modifiers of the course of the disease.

The mechanism by which s-adRP mutations selectively cause retinal deterioration is unknown. We detected some hints of genome instability in s-adRP mutants, which might explain the degenerative nature of the disease.

We are taking steps towards establishing *C. elegans* as an RP diagnosis model by evaluating the functional impact of potential RP mutations, or variants of uncertain significance (VUS), in worms. For that purpose, we set a panel of features associated with s-adRP mutations, including a genetic interaction with a CRISPR-edited Slow Polymerase II mutant (*ama-1(cer135[R743H])*), mortal germline, or aberrant splicing events at specific transcripts. We partially humanized the sequence encoding the splicing factors *prp-3* in the endogenous locus to investigate if such humanization is beneficial for functional studies of VUS.

Therefore, our RP research line demonstrates the value of *C. elegans* for investigating rare diseases and for providing valuable information in search of drugs, diagnosis, and prognosis.

Table of Contents

ACKNOWLEDGMENTS	I
ABSTRACT	III
TABLE OF CONTENTS.....	V
INTRODUCTION	1
1. Splicing and disease	3
1. a. Discovery of splicing, an essential and conserved process	3
1. b. Overview of the pre-mRNA splicing mechanism	6
1. c. Splicing-transcription crosstalk: genome instability upon splicing defects	11
1. d. Pre-mRNA splicing and disease: a cause and a solution.....	14
1. e. Pre-mRNA splicing is similar between human and <i>C. elegans</i>	18
2. <i>Caenorhabditis elegans</i> is a powerful model organism	20
2. a. Basic biology and genetics of <i>C. elegans</i>	20
2. b. CRISPR-Cas9 in <i>C. elegans</i>	24
2. c. RNAi in <i>C. elegans</i>	27
2. d. Drug screens in <i>C. elegans</i>	30
3. Retinitis Pigmentosa	32
3. a. Retinal inherited disorders and retinitis pigmentosa	32
3. b. Splicing-related autosomal dominant retinitis pigmentosa (s-adRP)	35
3. c. <i>C. elegans</i> as a model to study s-adRP.....	36
AIMS	39
RESULTS.....	43
1. CRISPR-Cas9 allows mimicking of s-adRP mutations in <i>C. elegans</i>.....	45
1. a. Impact of s-adRP mutations in fertility.....	46
1. b. All s-adRP mutants cause a functional impairment.....	47

2. Prognosis: <i>weak</i> alleles permit the identification of potential disease modifiers	49
2. a. <i>Weak</i> alleles are suitable to detect genetic interactors through RNAi screens.....	50
2. b. <i>prp-8(cer22)</i> can serve as a platform for SNPs testing from genetic interactors	53
3. Therapy: A drug screen on the <i>strong</i> mutant <i>prp-8(cer14)</i> identified dequalinium as a potentially damaging molecule	58
3. a. <i>Strong</i> allele <i>prp-8(cer14)</i> is amenable for drug screens.....	59
3.b. <i>prp-8(cer14)</i> drug screen uncovers potentially damaging effects of dequalinium on <i>snrp-200</i> mutants	61
4. Mechanism – Genome instability could be present in some s-adRP mutants	63
4. a. <i>Pegl-1::gfp</i> reporter did not unveil s-adRP upregulation of <i>egl-1</i> even under hydroxyurea (HU) and UV-C induced stress	64
4. b. Single molecule Fluorescence In Situ Hybridization (smFISH) allows the detection of <i>atl-1</i> induction upon splicing defects	66
4. c. Mortal germline (Mrt) phenotype of the <i>weak</i> allele <i>prp-8(cer22)</i> points towards the presence of genome instability	70
4.d. The synthetic interaction between the <i>weak</i> allele <i>prp-8(cer22)</i> and a mutation in polymerase (Pol) II supports splicing-transcription interplay as a possible mechanism in disease	71
5. Diagnosis: <i>C. elegans</i> s-adRP models could be helpful for variants of uncertain significance (VUS) evaluation	74
5. a. <i>snrp-200(cer23)</i> <i>strong</i> allele produces specific AS events that might serve as s-adRP markers.....	75
5. b. Herboxidiene (HB) and α -amanitin treatment does not clearly magnify s-adRP alterations.....	82
5. c. Gamma radiation seems to have a stronger effect on the <i>weak</i> allele <i>snrp-200(cer24)</i>	86
5. d. Generation of a panel of features to test patient-derived VUS functional impact	88
6. Improvement of s-adRP models: <i>prp-3</i> gene tolerates partial sequence humanization.....	92
6. a. <i>prp-3</i> allows partial humanization.....	93
DISCUSSION	97

TABLE OF CONTENTS

1. CRISPR-Cas9 for the generation of s-adRP <i>C. elegans</i> models.....	99
1. a. s-adRP proteins PRPF8/PRP-8 and SNRNP200/SNRP-200	99
1. b. Functional impact of mimicked s-adRP mutations	100
2. <i>C. elegans</i> is a powerful model for the identification of genetic modifiers of s-adRP mutations.....	103
3. <i>C. elegans</i> s-adRP models as a tool for drug screens	106
4. Genome instability might be present in s-adRP mutants.....	108
5. CRISPR-Cas9 allows VUS evaluation in <i>C. elegans</i>	111
6. Humanization for s-adRP genes to improve <i>C. elegans</i> models	115
7. <i>C. elegans</i> role in personalized medicine and final remarks	117
CONCLUSIONS.....	119
MATERIALS AND METHODS	123
1. <i>C. elegans</i> maintenance and strains	125
2. Brood size, overt phenotypes, and Emb	126
3. Developmental delay assay.....	127
4. RNAi screen.....	127
6. Worm length.....	128
7. DAPI staining.....	128
8. CRISPR editing.....	129
9. Genetic crosses	133
10. Drug screen and drug treatment	134
10.a. Drug screen and validation.....	134
10. b. Herboxidiene and α -amanitin treatment	135
11. UV-C and HU treatment	135
11. a. UV-C treatment	135

11. b. HU treatment	135
12. smFISH	136
13. Mortal germline	136
14. Nanopore sequencing and semiquantitative PCR	137
14.a. RNA extraction	137
14.b. Nanopore sequencing	137
14.c. Bioinformatic pipeline	138
14.d. Semiquantitative PCR	138
15. Gamma radiation	139
16. Statistical analyses and figures.....	139
 SUPPLEMENTARY DATA.....	 141
 BIBLIOGRAPHY	 183
 LIST OF PUBLICATIONS	 209

INTRODUCTION

1. Splicing and disease

I. a. Discovery of splicing, an essential and conserved process

During the 1960s and 1970s, observations in eukaryotic cells showed that part of the nuclear RNA was exported to the cytoplasm (messenger RNA, mRNA), whereas another bigger fraction was rapidly degraded in the nucleus, named heterogeneous nuclear RNA (hnRNA) at that time. The nuclear RNA shared some characteristics with the cytoplasmic mRNA, such as 5' capping and poly-(A) tail, so some researchers hypothesized that hnRNA could be a precursor of mRNA (Berk, 2016). But the proof did not come until 1977 when hybridization of the human adenovirus 2 mRNA to viral DNA showed coupling of the mRNA to separated regions in the DNA (Chow *et al.*, 1977; Berget, Moore, & Sharp, 1977) (**Figure I. 1**). The discussion of this fundamental article stated that DNA was transcribed into a long RNA that was later processed to mRNA by joining coding regions—now known as exons— (Berget *et al.*, 1977). Later on, protection of pre-mRNA from degradation showed how pre-processed RNA was co-linear with the DNA, and it was possible to isolate partially processed intermediates with a different number of what we now call introns, supporting the previously stated theory. With the improvement of molecular techniques, such findings were extended to eukaryotic genes, demonstrating that most human genes are split into coding exons and non-coding introns (Berk, 2016).

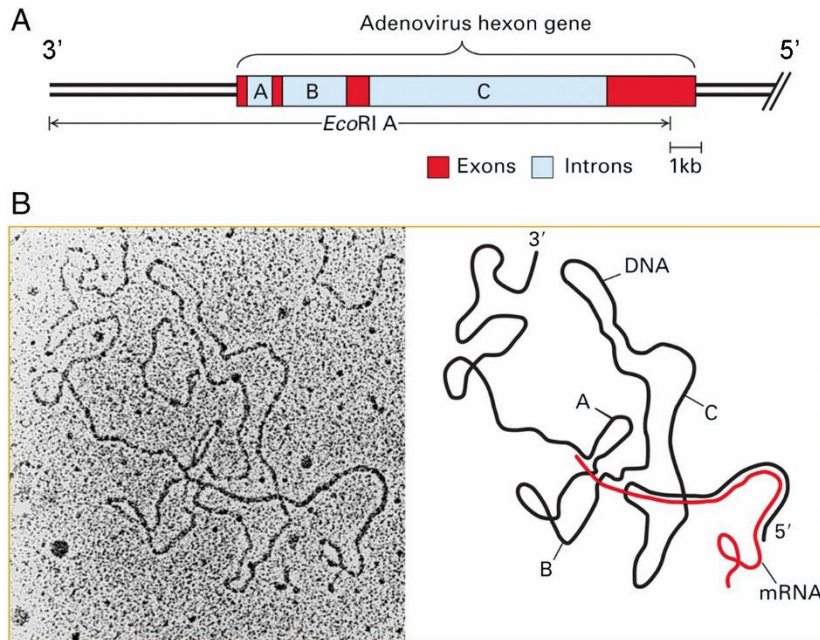


Figure I. 1: Hybrid of mRNA and the transcribed strand of its corresponding DNA fragment. A) Diagram of the exon/intron positions of adenovirus hexon gene. The site of the EcoRI A cut is indicated. B) Original electron microscopy of the mRNA/DNA hybrid (left) and the interpretation scheme (right). Reproduced from Berk 2016, the electron microscopy in panel B was retrieved from the original publication by Berget, Moore, and Sharp, in 1977.

Thus, the protein-coding sequences of genes are often intercalated by non-coding regions that must be removed. To accomplish this task, the newly transcribed pre-mRNA undergoes a process in which introns are removed and exons are joined. Such mechanism is known as splicing. Regarding the abundance of intronic regions, on average, human genes contain 21 introns and *C. elegans* genes have five (Lee & Rio, 2015).

There are four types of introns: tRNA introns, group I and group II self-splicing introns, and spliceosomal introns. The most prevalent in eukaryotes are the spliceosomal introns, which are found in all nuclear genomes and present a well-defined mechanism of splicing (Irimia & Roy, 2014). Most of the core elements needed for splicing are largely conserved

1. b. Overview of the pre-mRNA splicing mechanism

In short, splicing consists of two consecutive transesterification reactions: branching and ligation (**Figure I. 3**). A dynamic macromolecular complex called the spliceosome, formed by a set of small nuclear ribonucleoproteins (snRNP) and accessory proteins, performs splicing. To date, two different spliceosomes have been identified: a less common and absent in *Caenorhabditis elegans*, U12 snRNP-dependent spliceosome, and the most common and covered below, U2 snRNP-dependent spliceosome (Burge, Padgett, & Sharp, 1998; Wahl *et al.*, 2009; Will & Lührmann, 2011; Baralle & Baralle, 2018).

Five snRNP particles participate in U2-dependent splicing: U1, U2, U4, U5, and U6. All these snRNPs present a common set of Sm and LSm proteins and additional specific proteins in each particle. The spliceosome is not a pre-formed enzyme –it assembles *de novo* and suffers different structural rearrangements in each reaction through the activity of several proteins such as splicing factors and helicases (**Figure I. 4**). A brief description of the step-by-step process based on recent comprehensive reviews (Yan *et al.*, 2019; Kastner *et al.*, 2019; Plaschka *et al.*, 2019; Wilkinson *et al.*, 2020) is commented below:



Figure I. 3: pre-mRNA splicing occurs in two successive reactions. The first reaction, branching, consists of a nucleophilic attack of the 2'OH from the BP adenosine to the first G of the intron. In the second reaction, the 3'OH from the last nucleotide of the first exon attacks the phosphate group of the next exon resulting in exon ligation. Joined exons and a lariat intron emerge from splicing. SS: splice site, BP: branchpoint, A: branch point adenosine, p: phosphate. Adapted from Wilkinson *et al.* 2020.

There are three main pre-mRNA elements involved in the first steps of the canonical spliceosome assembly: 5' splice site (ss), branchpoint (BP), and 3'ss. There are consensus sequences that denote each of these elements (**Figure I. 5**). There is some divergence in the consensus sequences of distinct exons and introns, but the splicing efficiency is still high, indicating other regulatory elements' existence. (De Conti, Baralle, & Buratti, 2013; Baralle & Baralle, 2018; Wilkinson *et al.*, 2020).

Base-pairing of the 5' ss with the U1 snRNP leads to spliceosome assembly. In parallel, the U2AF65–U2AF35 heterodimer contacts the polypyrimidine tract and 3'ss while SF1/mBBP interacts with the BP. This conformation is known as E complex (Plaschka *et al.*, 2019; Wilkinson *et al.*, 2020). Afterward, the DEAD-box helicases PRP5 and SUB2 promote the displacement of SF1 and U2AF and recruit U2 snRNP, which interacts with U1, yielding to the formation of the A complex.

Next, the preassembled U4/U6.U5 tri-snRNP is recruited, forming the pre-B complex. The PRP8 (PRPF8 in humans) protein, implicated in retinitis pigmentosa (RP), is in the central core of U5 snRNP. The splicing factor PRP3 (PRPF3) is required for U4/U6.U5 tri-snRNP stabilization via interaction with PRP6 (PRPF6) (Liu *et al.*, 2015).

PRP28 helicase acts as an early initiator of spliceosome activation. Major rearrangements in the spliceosome lead to the disassociation of U1 from the spliceosome. In humans, the RP-related SNRNP200/BRR2 translocates and loads onto U4 snRNP, where it is ready to unfold the U4/U6 duplex, forming the B complex (Plaschka *et al.*, 2019; Wilkinson *et al.*, 2020). Once SNRNP200/BRR2 is loaded onto U4, it unwinds U4/U6 duplex leaving U6 available to pair with U2, giving rise to the B^{act} complex.

Meanwhile, at least 24 proteins, including PRP6, abandon the spliceosome and a protein shell that stabilizes the RNA catalytic core containing the PRP-19 associated nineteen complex (NTC) and PRP-19-related complex (NTR) is formed. (Wahl *et al.*, 2009; Will & Lührmann, 2011; Wilkinson *et al.*, 2020).

The promotion to B* complex, where the first transesterification reaction takes place, is stimulated by the DEAH-box ATPase PRP2. PRP2 activity leads to the destabilization of U2 protein complexes SF3a and SF3b, facilitating the displacement of U2 from the spliceosome (Plaschka *et al.*, 2019; Wilkinson *et al.*, 2020). Once the phosphate of the first G of the intron is ligated to the 2'OH of the BP (branching), the C complex is formed. PRP16 ATPase promotes the transition to the C* complex in which ligation reaction takes place, yielding to the formation of the P complex.

PRP22 ATPase catalyzes the liberation of the ligated exon leading to intronariat spliceosome (ILS). Finally, spliceosome disassembly is mediated by the PRP43 helicase resulting in individual U2, U5, and U6 snRNP particles and disaggregated NTC proteins that are ready for the subsequent reactions. (Plaschka *et al.*, 2019; Wilkinson *et al.*, 2020).

To perform its task, the spliceosome must correctly define exon-intron boundaries. As stated above, sequences around 5'ss, BP, and 3'ss are insufficient, and other regulation layers are required.

One of them is the steric hindrance. Excessively short exons are no longer included, probably due to the inability of splicing machinery to be formed. Strikingly, extremely short exons (3 to 30 nt) named microexons have been identified. To compensate the drop in splicing efficiency due to its size, they possess stronger 3'ss and 5'ss, shorter surrounding introns, and stronger regulatory elements (Li *et al.*, 2015; Ustianenko, Weyn-Vanhentenryck, & Zhang, 2017).

Conversely, a moderate extension of an exon can lead to constitutive inclusion, but excessive extension leads to exon skipping or activation of cryptic splice sites. However, there are large exons that are efficiently included if surrounded by small introns. Thus, the architecture of exons and introns seems to play an important role in delimiting these elements (De Conti *et al.*, 2013).

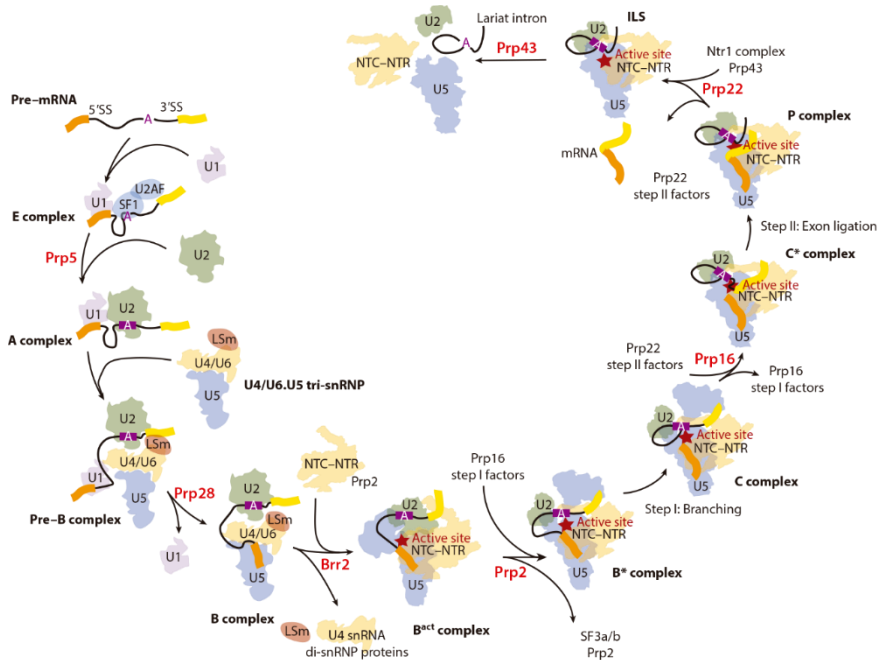


Figure I. 4: Stepwise splicing reaction. The spliceosome is assembled *de novo* in each splicing reaction, and after catalysis, all the components are released and recycled for future reactions. For this reason, splicing is often represented as a cycle. Each of the steps (from E complex to intron-lariat spliceosome (ILS)) is depicted. Helicases are represented in red. Arrows indicate the incorporation/release of components of the machinery and transitions between each step. NTC: Nineteen complex, NTR: Nineteen-related complex.

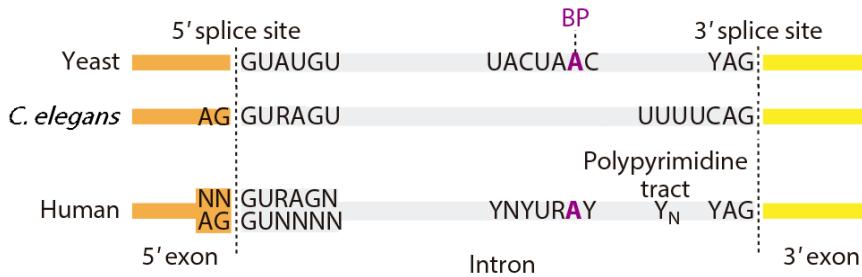


Figure I. 5: Consensus exon-intron splicing sequences. In yeast, *C. elegans*, and humans there are 5' and 3'ss consensus regions with slight dissimilarities. *C. elegans* lacks a consensus sequence in the branch point (BP) and a polypyrimidine tract but presents an extended 4U at the 3'ss. N: any nucleotide, Y: pyrimidine. Adapted from Wilkinson et al. 2020.

Another layer of regulation is the presence of intronic/exonic silencers and enhancers. Some pre-mRNAs contain regions with the ability to recruit elements in *trans* that can modulate splicing events. These *cis* sequences are named according to their position in the pre-mRNA and their role in promoting or repressing a particular splicing event as exon splicing enhancers (ESE) and exon splicing silencers (ESS), or intron splicing enhancers (ISE) and intron splicing silencers (ISS). The most studied proteins that act on such elements are serine/arginine-rich (SR) proteins and heterogeneous nuclear ribonucleoproteins (hnRNP).

Other levels of regulation such as epitranscriptomic modifications and RNA secondary structures have been described, howbeit their global effect on splicing seems to be limited (De Conti *et al.*, 2013; Shenasa & Hertel, 2019). Finally, splicing occurs co-transcriptionally, highlighting the interplay between both processes, which is discussed in the following section.

I. c. Splicing-transcription crosstalk: genome instability upon splicing defects

Approximately 80% of splicing occurs co-transcriptionally, meaning that the spliceosome catalyzes the reaction at the time that pre-mRNA is being synthesized (or DNA is being transcribed) (Girard *et al.*, 2012; De Conti *et al.*, 2013; Saldi *et al.*, 2016; Shenasa & Hertel, 2019). Thus, splicing and transcription would need to be studied as a whole.

The transcription process can regulate splicing and other pre-mRNA maturation processes such as capping and polyadenylation (Saldi *et al.*, 2016; Shenasa & Hertel, 2019). Direct recruitment of splicing factors to the Polymerase II (Pol II) via its phosphorylated C-terminal domain (CTD) is one of the mechanisms. Co-purification of the CTD with SR proteins and regulation of AS by SRp20 (also known as SFSR3) (De La Mata & Kornblihtt, 2006) as well as of RSR-2 (Fontrodona *et al.*, 2013) support this mechanism. Consistently, the inhibition of splicing affects phosphorylation of the CTD (Koga, Hayashi, & Kaida, 2015), denoting the interlink between both processes. Another interaction resides in the transcription rate. Slowing the transcription rate in yeast enhances constitutive splicing (Braberg *et al.*, 2013), and accelerating or slowing the Pol II produces alterations in AS profiles (De La Mata *et al.*, 2003; Fong *et al.*, 2014). Other indirect effects on splicing due to transcription alteration may be produced by different chromatin factors or by epigenetic marks (De Conti *et al.*, 2013; Saldi *et al.*, 2016).

One interesting observation is that impairment of splicing leads to genomic instability, and transcription seems to play a direct role in this process. During transcription, the nascent pre-mRNA can couple with DNA forming an RNA::DNA hybrid and an uncoupled DNA strand, a structure called R-loop (**Figure I. 6**) (Skourti-Stathaki & Proudfoot, 2014; Allison & Wang, 2019). Recent studies show that these structures are not mere by-products

of transcription but regulatory elements participating in diverse cellular processes such as immunoglobulin class switching recombination (Yu *et al.*, 2003), stimulation of transcription (Boque-Sastre *et al.*, 2015), and Pol II pausing downstream of the polyadenylation signal (Skourti-Stathaki & Proudfoot, 2014; Skourti-Stathaki, Kamieniarz-Gdula, & Proudfoot, 2014; Allison & Wang, 2019). Perturbation of splicing factors has been shown to increase R-loop formation and associated genome instability. Some examples are depletion of ASF/SF2 (Li & Manley, 2005), SNM1 deficiency (Jangi *et al.*, 2017), or SLU7 (Jiménez *et al.*, 2019). The up-regulation of RNaseH1, which resolves R-loops, reverses this stress (Paulsen *et al.*, 2009; Zeller *et al.*, 2016). R-loop formation was also observed after treatment with the spliceosome inhibitor Pladienolide B (Wan *et al.*, 2015). Consistently, in yeast, it was shown how intron-containing genes are less prone to accumulate R-loops, and this effect is dependent on spliceosome binding rather than splicing catalysis (Bonnet *et al.*, 2017; Tam & Stirling, 2019).

R-loops may promote genomic instability through two different mechanisms. First, R-loops promote stalling of the transcription bubble and collision with the replication fork, leading to fork collapse, double-strand DNA breaks, or incomplete replication (Tuduri *et al.*, 2009). Importantly this mechanism of stress requires dividing cells (S phase) (**Figure I. 6**). Moreover, de-regulation of R-loops can impact transcription and produce genome instability (Domínguez-Sánchez *et al.*, 2011). Another form of causing genome instability is related to the uncoupled DNA strand of the R-loop as it is a sensitive target for chemical mutagenesis or inappropriate DNA repair (Gómez-González & Aguilera, 2007; Polak & Arndt, 2008; Skourti-Stathaki & Proudfoot, 2014; Allison & Wang, 2019).

Additionally, splicing defects can cause genome instability by other mechanisms. Alterations in splicing factors may affect splicing broadly at

the genomic level or in a subset of particular genes, and these altered isoforms may lead to genome instability. This has been demonstrated for some splicing genes, including HSH155/SF3B1 and SNU114, whose alteration produces defects on α -tubulin, ultimately leading to genome instability (Tam *et al.*, 2019; Tam & Stirling, 2019). Finally, a direct link between DNA repair machinery and splicing has been observed. For example, BRCA1 interacts with splicing elements leading to up-regulation of DNA damage response genes (**Figure I. 6**) (Savage *et al.*, 2014; Tam & Stirling, 2019).

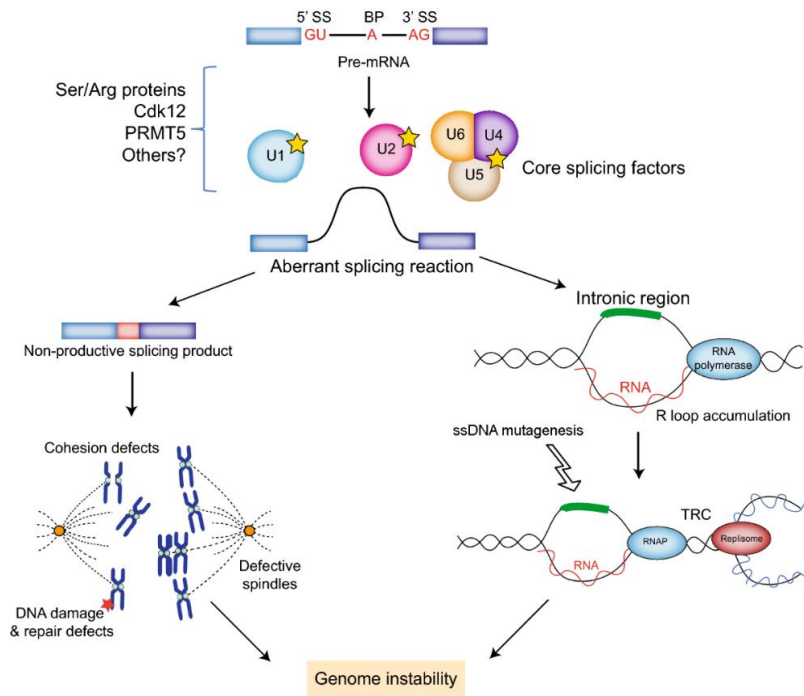


Figure I. 6: Genome instability upon splicing impairment. Affected splicing machinery leads to altered splicing products that ultimately lead to DNA damage through different mechanisms (left). Another consequence is R-loop accumulation, leading to transcription-replication conflicts (TRC) or increased mutagenesis of single-stranded DNA (ssDNA) (right). Both pathways ultimately lead to increased genome instability. Adapted from Tam & Stirling, 2019.

I. d. Pre-mRNA splicing and disease: a cause and a solution

The activity of constitutive and alternative splicing is essential for the correct production of proteins, and therefore for cellular functions. Thus, mutations leading to alterations in splicing are linked to several diseases (Sterne-Weiler & Sanford, 2014; Suñé-Pou *et al.*, 2017; Abramowicz & Gos, 2018; Montes *et al.*, 2019). As much as 22-25% of inherited diseases are likely influenced by splicing (Sterne-Weiler & Sanford, 2014), indicating that it is a common phenomenon. Such mutations can be classified into two categories: (i) *cis*, affecting signals at the pre-mRNA sequence or (ii) *trans*, affecting the proteins involved in splicing catalysis or regulation (Sterne-Weiler & Sanford, 2014; Suñé-Pou *et al.*, 2017; Abramowicz & Gos, 2018).

(i) Mutations in *cis*

This type of mutations can potentially affect different splicing key sequences of the pre-mRNA, such as the 3' ss, BP, or 5'ss as well as regulatory sequences (ISE, ISS, ESE, ESS), or create an intronic or exonic ss. The consequence of such alteration can produce exon skipping, intron retention, cryptic exon inclusion, or loss of a fragment of an exon (Sterne-Weiler & Sanford, 2014; Abramowicz & Gos, 2018). Several examples of this type of alterations have been identified and are summarized in different reviews (Sterne-Weiler & Sanford, 2014; Scotti & Swanson, 2016; Abramowicz & Gos, 2018), including the generation of an alternative 3'ss in the *HBB* gene, which ultimately produces a reduction in β -globin levels leading to β^+ -thalassemia. Other examples include cystic fibrosis, in which expansion of apolypyrimidine tract in the *CFTR* gene promotes exon nine skipping (Chu *et al.*, 1993), or congenital cataract, caused by skipping of the 3rd exon in *MIP* due to a G to A transition in a ss (Zeng *et al.*, 2013). Another interesting example is alterations in the *LMNA* gene, in which

distinct splicing mutations on the same gene produce different pathologies (Scotti & Swanson, 2016).

(ii) Mutations in *trans*

Such alterations impact the machinery that participates in the splicing reaction (Scotti & Swanson, 2016; Suñé-Pou *et al.*, 2017). A few examples of this category include:

-Amyotrophic lateral sclerosis, caused by missense mutations in *TDP-43*. TDP-43 modulates splicing in conjugation with hnRNP A1, and its pathogenic mutations produce broad effects on alternative splicing (Arnold *et al.*, 2013; Deshaies *et al.*, 2018).

-Spinal muscular atrophy, produced by homozygous deletion of *SMN1*, a gene that participates in the biogenesis of RNPs implicated in splicing and other processes. A paralog gene (*SMN2*) generates a transcript with excluded exon seven, producing a less stable protein insufficient to rescue the lack of *SMN1* completely (Li *et al.*, 2014).

-As much as 11% of inherited retinal dystrophies (IRD) are caused by mutations in splicing genes (Bacchi, Casarosa, & Denti, 2014), including *PRPF3*, *PRPF4*, *PRPF6*, *PRPF8*, *PRPF31*, *SNRNP200/BRR2* and *RP9* (Růžicková & Staněk, 2017). These genes are involved in RP, which is covered in depth in the following sections.

-AS deregulation is of great importance in different cancer types. *PRPF6* is upregulated in colorectal carcinoma, whereas heterozygous mutations or hemizygous deletions in *PRPF8* have been related to myelodysplastic syndromes (Adler *et al.*, 2014; Kurtovic-Kozaric *et al.*, 2015; Scotti & Swanson, 2016). Other recurrent mutations have been found in *SRSF2*, *U1*, *U2AF1* and *SF3B1* (Bonnal, López-Oreja, & Valcárcel, 2020). The latter has been of particular interest in our laboratory. Xenia Serrat modelled

cancer-related mutations in *sftb-1* (*C. elegans* ortholog of SF3B1) to study alternative splicing implications, identify genetic interactors with therapeutic potential, and partially humanize the gene to sensitize *C. elegans* to splicing modulators (Serrat *et al.*, 2019).

Thus, splicing alterations have shown to be the origin of different pathologies, pushing the development of therapeutic strategies to intervene on the splicing process (Suñé-Pou *et al.*, 2017; Montes *et al.*, 2019; Bonnal *et al.*, 2020). Some approved and under development strategies include the following:

(i) Antisense oligonucleotides (ASO) that bind pre-mRNA to alter the splicing of determined regions have been successfully developed to restore exon seven inclusion of *SMN2*, providing a treatment for spinal muscular atrophy (Meylemans & De Bleeker, 2019) (**Figure I. 7**). Similar approaches were developed for exon 51 skipping in the *DMD* gene to treat Duchenne muscular dystrophy (Syed, 2016). Eye-related dystrophies are also targeted with this approach (Aísa-Marín *et al.*, 2021)

(ii) Small molecules that modulate splicing have shown some efficacy in pre-clinical cancer models, and some have reached clinical trials. The most studied drugs target SF3B1, RBM39, and PRMT5 among other factors (Montes *et al.*, 2019; Bonnal *et al.*, 2020).

(iii) Spliceosomal-Mediated RNA Trans-Splicing (SMaRT) allows the substitution of a mutated fraction of the gene during pre-mRNA splicing by introducing the corrected fragment of the RNA. This approach is followed for CFTR (cystic fibrosis), Tau (FTDP-17) correction (**Figure I. 7**), as well as for RHO (RP) among others (Montes *et al.*, 2019; Aísa-Marín *et al.*, 2021).

(iv) Small interfering RNAs (siRNA) are also being developed for targeting aberrant isoforms in fibronectin gene or growth hormone deficiency (Suñé-Pou *et al.*, 2017; Montes *et al.*, 2019).

(v) Other strategies using exon-specific U1 to recognize mutated ss or genome editing by clustered regularly interspaced short palindromic repeats-Cas9 (CRISPR-Cas9) are being developed (**Figure I. 7**) (Montes *et al.*, 2019). This last strategy has enormous potential not only for splicing-related diseases but also for many other genetic pathologies.

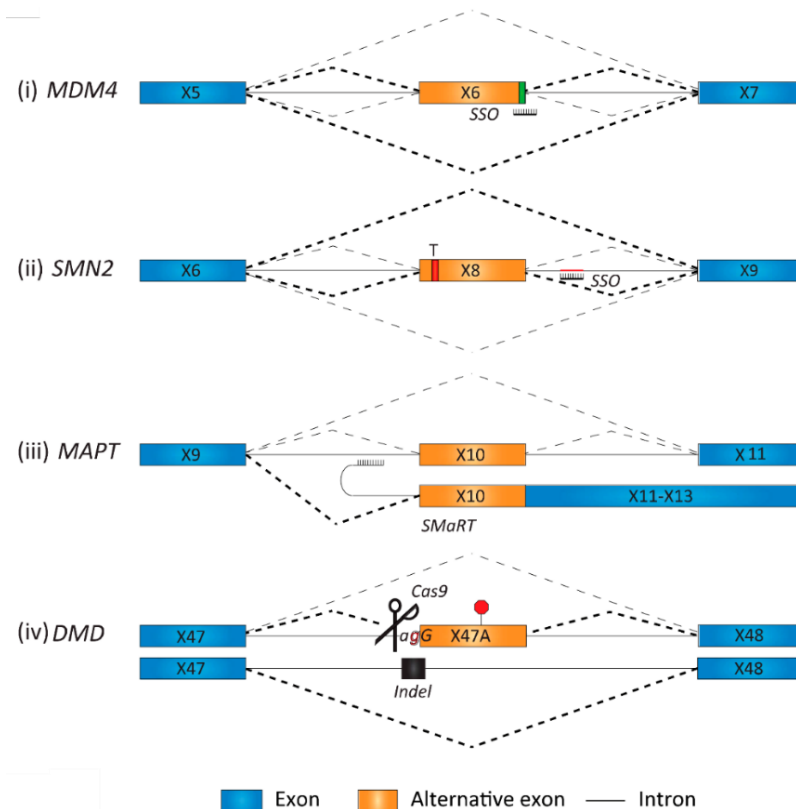


Figure I. 7: Examples of splicing specific therapeutic strategies. Splice switching oligonucleotides (SSO, also known as ASO) to promote exclusion of an exon in *MDM4* (targets tumor growth) (i) or inclusion of an exon in *SMN2* (treatment for spinal muscular atrophy) (ii). SMaRT to promote exon ten inclusion of *MAPT* (correction of Tau protein in Alzheimer disease) (iii). Use of CRISPR-Cas9 to delete a cryptic splice site in *DMD* (treatment for Duchenne muscular dystrophy) (iv). Dashed lines: spliced isoforms. Adapted from Montes *et al.* 2019.

I. e. Pre-mRNA splicing is similar between human and C. elegans

In general terms, the *C. elegans* splicing process seems similar to mammals and yeast as splicing elements are largely conserved (Wani & Kuroyanagi, 2017; Zahler, 2018). The consensus sequence of the 5' splice site is similar to human and yeast counterparts (Riddle *et al.*, 1997a), and it is degenerated in most of the exon-intron boundaries (Riddle *et al.*, 1997a; Kent & Zahler, 2000; Zahler, 2018). Worm introns contain an AG dinucleotide with a short tetra-U extension at 3' splice site (Riddle *et al.*, 1997a; Zorio & Blumenthal, 1999; Hollins *et al.*, 2005; Zahler, 2018). Moreover, there is no precise branch point consensus sequence in *C. elegans*, and little information is available about the branch point (Figure I. 3). The genome architecture differs from the human, containing shorter introns compared to exons (Zahler, 2018) (Table 1).

Table 1: Intron-exon median lengths in yeast, roundworm and human.

	<i>S.cerevisiae</i>	<i>C. elegans</i>	Human
Exon median length (bp)	233	150	133
Intron median length (bp)	148	65	1516

Adapted from (Schwartz *et al.*, 2008).

Approximately 25-35% of *C. elegans* genes undergo alternative splicing, a smaller number compared to humans (~95%), but still indicates an important role of alternative splicing in nematode biology (Ramani *et al.*, 2011; Tourasse, Millet, & Dupuy, 2017; Zahler, 2018). Notably, the different methodology used for the detection of alternative splicing between studies might impede comparison between organisms. Thus, the impact of alternative splicing in humans and *C. elegans* could be less dissimilar than initially estimated (Tourasse *et al.*, 2017).

Several examples of developmentally regulated, or sex-specific, alternative splicing events have been shown (Sibley *et al.*, 1993; Shan & Walthall, 2008; Barberan-Soler & Zahler, 2008; Zahler, 2018). The regulation of alternative splicing is directed by

cis- and *trans*-acting factors. For instance, different SR (*rsp* genes) and hnRNPs, as well as other splicing factors were identified in *C. elegans*. The mechanism of action of these elements is not uniform, and an overlap of several regulators acting on the same genes occurs (Tan & Fraser, 2017; Zahler, 2018).

Trans-splicing is a common mechanism in *C. elegans*, affecting around 84% of all genes (Tourasse *et al.*, 2017). In contrast to *cis*-splicing (intron removal), *trans*-splicing occurs between a splicing leader (SL) sequence and the 5' of the pre-mRNA exon (Allen *et al.*, 2011). This mechanism requires the same snRNP as for *cis*-splicing except for U1 (Hannon, Maroney, & Nilsen, 1991; Blumenthal, 2012). There are two distinct SL sequences: SL1 and SL2. Half of the *C. elegans* genes use SL1 for *trans*-splicing thanks to the presence of an intron-like sequence on the 5' of the first exon of the mRNA without a functional 5'ss up-stream named outtron (Conrad *et al.*, 1991; Zorio *et al.*, 1994; Allen *et al.*, 2011; Blumenthal, 2012). Around 15-17% of *C. elegans* genes are codified in operons. The SL2-guided *trans*-splicing is responsible for the split between genes in polycistronic pre-mRNAs (Spieth *et al.*, 1993; Allen *et al.*, 2011; Blumenthal, 2012). These two mechanisms are not mutually exclusive, and some pre-mRNA undergo *trans*-splicing via both SL sequences (Allen *et al.*, 2011).

2. *Caenorhabditis elegans* is a powerful model organism

2. a. Basic biology and genetics of *C. elegans*

The 1 mm long soil nematode *Caenorhabditis elegans* has become an important model organism in biosciences, with more than 1200 laboratories using it around the world (Corsi, Wightman, & Chalfie, 2015; Harris *et al.*, 2019). This extraordinary popularity has its beginnings in the 1970s, when Sydney Brenner decided to adapt this organism for laboratory means (Brenner, 1973, 1988; Riddle *et al.*, 1997b; Corsi *et al.*, 2015). Several characteristics make it an attractive platform to dissect diverse biological questions. Laboratory maintenance is easy and inexpensive on agar Petri plates due to its small size and the fact it can be fed with *Escherichia coli* bacteria. Commonly, a dissecting microscope is used to observe these roundworms on agar plates (**Figure I.7**) (Riddle *et al.*, 1997b; Corsi *et al.*, 2015). Additionally, long-term storage of *C. elegans* stocks at -80°C freezers or in liquid nitrogen tanks and subsequent recovery is possible (Sulston & Hodgkin, 1988). In brief, it possesses the manageability of a prokaryote but it is a multi-cellular eukaryotic organism with distinct tissues.

These nematodes are commonly maintained at 15°C, 20°C, or 25°C in the laboratory. Such range of temperatures is convenient to modulate temperature-sensitive phenotypes and adjust the life cycle length according to different experimental needs. A newly born worm gives rise to its progeny in only 3.5 days at 20°C (standard temperature for maintenance). This fast generation time allows fast escalating of populations.

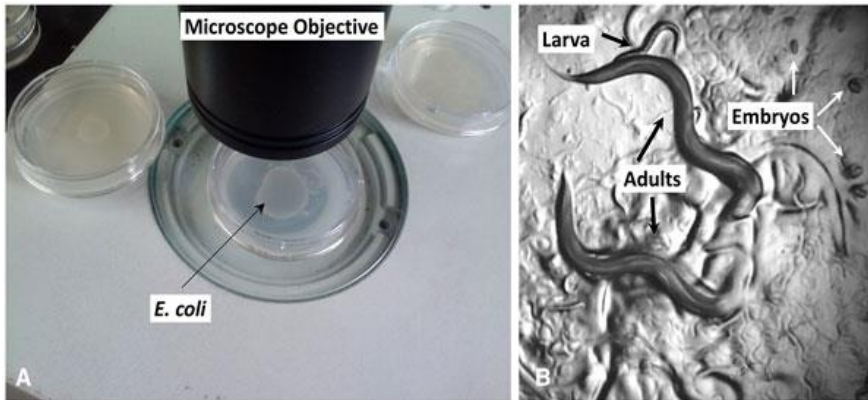


Figure I. 7: Overview of *C. elegans* maintenance and manipulation. A) Photography of a Petri agar plate with an *E. coli* lawn under a dissecting microscope. B) *C. elegans* as seen through the objective. Two adults, a larva, and a few embryos are shown on an *E. coli* lawn. Adapted from Corsi *et al.* 2015.

The embryonic development last about 16 hours. Once an embryo hatches, it becomes an L1 larva with more than half of the nuclei present in an adult worm. During postembryonic development, these L1 larvae grow in size and develop through three additional larval stages (L2, L3, and L4) to reach adulthood when they start laying eggs (**Figure I. 8**). Then, adult worms live for 10-15 additional days, which is very convenient for aging-related experiments (Corsi *et al.*, 2015; Luyten *et al.*, 2016).

When food is unavailable and larvae are crowded, *C. elegans* enters into the so-called “dauer” stage (apparent in L2). In this stage, worms are more resistant to external challenges and can survive several months (**Figure I. 8**) (Corsi *et al.*, 2015).

C. elegans can exist in two different sexual forms: hermaphrodites and males. Hermaphrodites self-fertilize, giving rise to about 300 offspring, allowing maintenance of large isogenic populations in the laboratory and being an excellent advantage for genetic studies. Males arise in extremely low proportion from a self-fertilized hermaphrodite ($\approx 0.2\%$) and are

typically used for genetic crosses with hermaphrodites to build new strains with combinations of mutations or reporters (Riddle *et al.*, 1997b; Corsi *et al.*, 2015). To our convenience, male abundance could be increased by incubating L4 hermaphrodites at high temperature (31-34°C) for a short period of time.

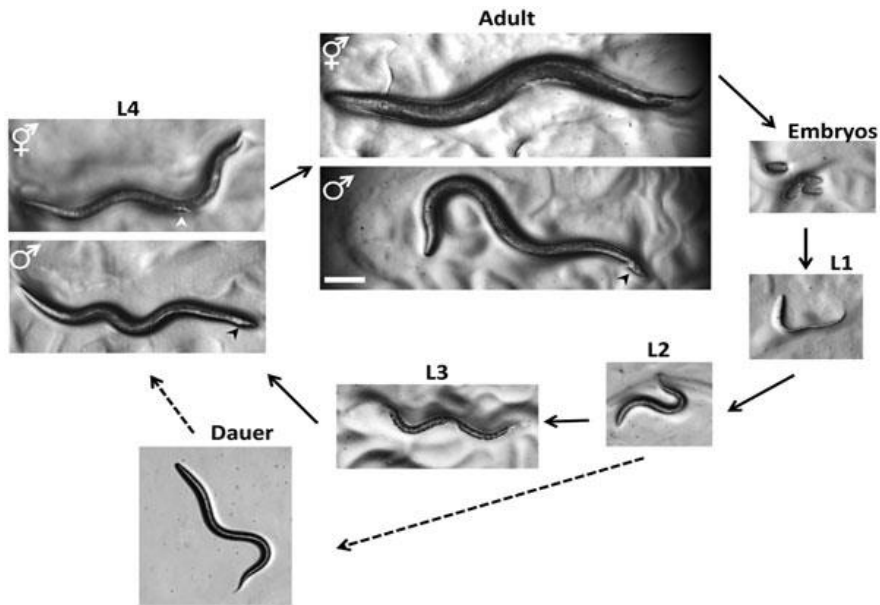


Figure I. 8: Life cycle of *C. elegans*. Images of *C. elegans* at different developmental stages as seen under a dissecting stereomicroscope. Adult males are smaller and thinner than hermaphrodites and present a fan-shaped tail (black arrow adult). Embryos give rise to L1 animals that develop through L2, L3, and L4 larval stages to reach adulthood. Worms increase in size and suffer morphological changes during development. Prior to the L4 stage, no apparent sexual distinguishable morphological features are observed. At L4, hermaphrodites present an easily discernible vulva (white arrow) and males show a little wider tail (black arrow). The alternative dauer stage is depicted. Adapted from Corsi *et al.* 2015.

The first genetic study with *C. elegans* was performed using chemical mutagenesis with ethane methyl sulfonate (EMS)s. The study's main aim was to identify affected behavior mutants; however, other phenotypes such as blistered, dumpy, roller, small, and long were found (Brenner, 1974).

C. elegans transparency and Nomarski optics (based on differential interference contrast) allow to easily observe different cell-types without the need of dissecting the animal. This feature permitted tracing the entire cell lineage of the whole organism (Sulston, Dew, & Brenner, 1975; Sulston *et al.*, 1983; Kimble & Hirsh, 1979) and describing the connectivity of all 302 neurons (Ward *et al.*, 1975; White *et al.*, 1976, 1986). Moreover, its transparency also facilitates the use of GFP and other fluorescent markers of proteins (Chalfie *et al.*, 1994). The use of GFP in worms granted a Nobel prize in Chemistry to Martin Chalfie.

The genetic pathway controlling apoptosis was another important and early finding made in *C. elegans* with significant implications in other organisms or diseases such as cancer (Ellis & Horvitz, 1986).

Two Nobel prizes in Physiology or Medicine were granted to *C. elegans* researchers. One to Sydney Brenner, John Sulston, and Robert Horvitz in Physiology or Medicine, for their initial work in *C. elegans*. The other one was awarded to Andrew Fire and Craig Mello for the discovery of RNA interference (RNAi) (Fire *et al.*, 1998). RNAi was exploited to interrogate functions of most of the *C. elegans* genes (Kamath *et al.*, 2003; Kamath & Ahringer, 2003; Rual *et al.*, 2004; Ceron *et al.*, 2007) and is being used in other organisms and developed for therapeutic means (Tiemann & Rossi, 2009).

C. elegans was the first animal to have its genome sequenced, establishing an essential milestone in genomics and relevant for studies about genome

annotation (The *C.elegans* Sequencing Consortium, 1998). Posterior unveiling of other genomes including the human (Lander *et al.*, 2001; Craig Venter *et al.*, 2001) and continuous efforts by the scientific community showed important conservation of biological pathways between species. Nearly 40% of *C. elegans* genes have predicted orthologs in humans (Shaye & Greenwald, 2011), and up to 80% of human genes have orthologs in *C. elegans* (Kaletta & Hengartner, 2006). About 40% of disease-associated genes have an ortholog in *C. elegans* (Culetto & Sattelle, 2000). Diverse cellular processes and molecular mechanisms are conserved from worms to mammals, being of particular importance for this thesis the conservation of the apoptotic pathway (Choi & Woo, 2010) and splicing (Wani & Kuroyanagi, 2017; Zahler, 2018). All the mentioned features, and the rising of CRISPR genome editing, make *C.elegans* an excellent tool to model several human diseases.

2. b. CRISPR-Cas9 in *C. elegans*

Clustered regularly interspaced short palindromic repeats-Cas (CRISPR-Cas) has emerged as a revolutionary genome-editing technique. CRISPR-Cas is a bacterial defense system against bacteriophage infection, which was first described by Prof. Francisco Mojica. This system's rationale consists of recognizing bacteriophage DNA and cleaving it selectively (Mojica *et al.*, 2005; Barrangou *et al.*, 2007). It was not long until this system was tested *in vitro* (Gasiunas *et al.*, 2012) and immediately later used to cleave specific sequences in bacteria and mammalian cells (Jinek *et al.*, 2012; Cong *et al.*, 2013; Hsu *et al.*, 2013; Lander, 2016). The vertiginous race for the optimization and adaptation of this technique led to its usage in several organisms to model genetic diseases and many other applications (Adli, 2018; Fuster-García *et al.*, 2020). Moreover, novel CRISPR systems are being identified and adapted to expand the toolbox of

not only genome editing but also CRISPR-based RNA editing tools (Matsoukas, 2018; Adli, 2018).

In brief, the most commonly used in genome editing, class 2 system relies on the Cas9 protein and a guide RNA (gRNA, generally constructed by independent transactivating RNA (tracrRNA) base-paired to CRISPR RNA (crRNA)). The cleavage is produced when the preassembled gRNA-Cas9 ribonucleoprotein encounters a 20 bp protospacer sequence complementary to the crRNA next to the protospacer-adjacent motif (PAM, for Cas9 is NGG). Then, Cas9 nuclease cut and cause a double-strand break (DSB) three nucleotides upstream of the PAM (**Figure I. 9**) (Jinek *et al.*, 2012; Dickinson & Goldstein, 2016).

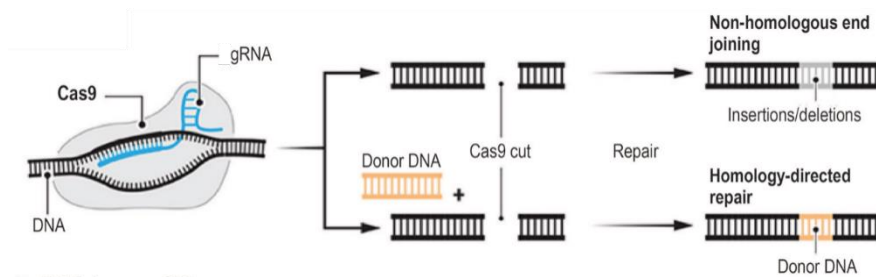


Figure I. 9: Genome editing by CRISPR-Cas9. The ribonucleoprotein complex consisting of Cas9-gRNA recognizes specific DNA regions and produces a DSB which is then repaired by NHEJ or HDR. Adapted from Matsoukas *et al.* 2018.

As a result of such cut, the eukaryotic cell activates the repair machinery to correct the damage. There are two such mechanisms: non-homologous end joining (NHEJ) and homology-directed repair (HDR). NHEJ is an error-prone repair mechanism that introduces insertions/deletions (indels) in the repair process. This mechanism might be useful to produce loss-of-function alleles, as such indels sometimes change the ORF and produce premature STOP codons. HDR is the pathway used to introduce precise modifications. It requires a repair template (ssDNA or dsDNA), with arms homologous to

the region adjacent to the DSB, to incorporate the sequence of interest into the genome (**Figure I. 9**) (Cong *et al.*, 2013; Dickinson & Goldstein, 2016).

CRISPR-Cas9 has been rapidly adopted and extensively exploited in *C. elegans* (Friedland *et al.*, 2013; Chiu *et al.*, 2013; Cho *et al.*, 2013; Kim *et al.*, 2014; Arribere *et al.*, 2014; Ward, 2015; Paix *et al.*, 2015; Dickinson & Goldstein, 2016; Dokshin *et al.*, 2018). Several characteristics make *C. elegans* an convenient organism for CRISPR-Cas editing (Vicencio & Cerón, 2021). Technically, the reagents are injected into the germ line, which is a nuclei-containing syncytium, allowing to potentially edit hundreds of individuals at the time. The short life cycle added to the hermaphroditism enables the isolation of homozygous individuals in a very short time (**Figure I. 10**). Moreover, several laboratories have elaborated optimized protocols for efficient gene editing and identification of edited lines with approaches such as co-CRISPR (Kim *et al.*, 2014; Ward, 2015; Paix *et al.*, 2015; Dickinson & Goldstein, 2016).

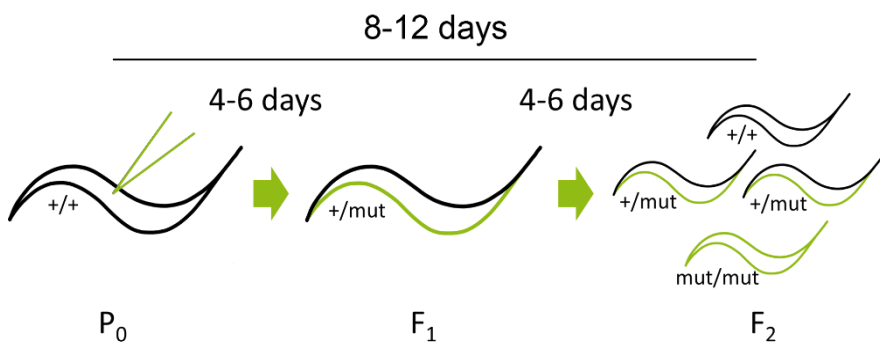


Figure I. 10: Schematic representation of the segregation of an edited hermaphrodite. After injection of P₀, heterozygous hermaphrodites are identified in F₁. By self-fertilization in the F₂, a quarter of the progeny segregates the mutation in homozygosis. The whole process can be achieved in less than a couple of weeks.

CRISPR-Cas9 permits the introduction of desired mutations and tagging genes with fluorescent reporters (FR) at the endogenous locus to study protein expression and localization *in vivo*. In our laboratory, CRISPR has been successfully used to study the role of *trxr-1* in the chemoresistance to cisplatin (García-Rodríguez *et al.*, 2018), optimize a protocol for efficient FR tagging (Vicencio *et al.*, 2019), modelling cancer mutations and sensitizing *C. elegans* to splicing inhibition by partially humanizing *sftb-1* (Serrat *et al.*, 2019), and studying NF- κ B independent functions of I κ B homologs: *nfki-1* and *ikb-1* (Brena *et al.*, 2020).

2. c. RNAi in *C. elegans*

Efficient and specific gene silencing by double-stranded RNA (dsRNA), which was firstly described in *C. elegans*, received the name of RNA interference (RNAi) (Fire *et al.*, 1998). Since its identification, the finding has been extended to different organisms and converted into a powerful reverse genetics' technique. Moreover, the description of silencing by exogenously provided dsRNA served as a starting point to decipher endogenous mechanisms of silencing by micro-RNAs, Piwi-interacting RNAs, and endogenous small-interfering RNAs (siRNA) (Grishok, 2005; Billi, Fischer, & Kim, 2014). It is worth noting that RNAi in *C. elegans* is heritable and is systemic (Kamath *et al.*, 2001; Asikainen *et al.*, 2005).

Shortly, the silencing is not directly produced by the dsRNA, which is cleaved into siRNAs by the endonuclease DICER/RDE-4 complex. The 21-25 nt long primary siRNAs, characterized by a monophosphate tag at 5', are recognized by the Argonaute RDE-1 protein, which directs the interaction with the complementary mRNA. Afterward, the RNA-dependent RNA polymerase RRF-1 is recruited to the mRNA and transcribes 22 nt long secondary siRNA, characterized by a tri-phosphate

tag. Finally, worm-specific argonautes (WAGO), directed by siRNAs, induce the cleavage of specific mRNAs. Thus, the secondary siRNAs are the main effectors of the gene silencing rather than the primary siRNAs. (Figure I. 11) Moreover, besides the classical post-transcriptional inhibition described above, a nuclear role directly controlling transcription has been described (Grishok, 2005; Min & Lee, 2007; Billi *et al.*, 2014; Gammon, 2017).

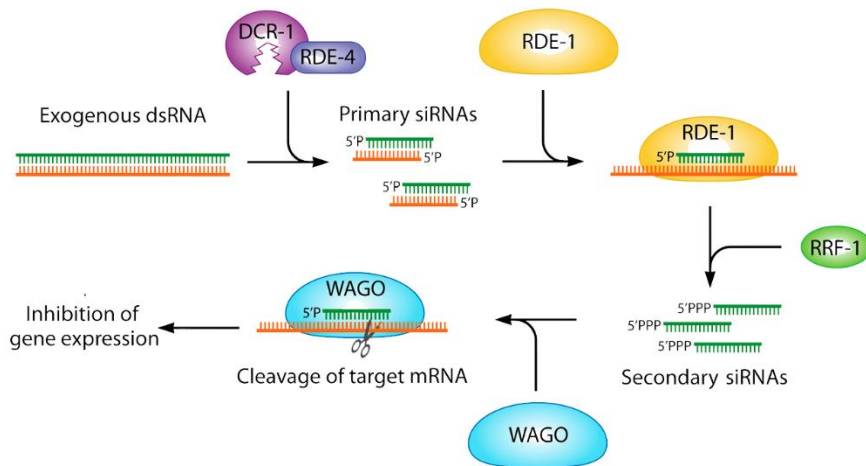


Figure I. 11: Scheme of RNAi mechanism. Exogenous dsRNA is processed into primary siRNAs which are amplified thanks to mRNA pairing by RDE-1 and RNA-dependent RNA polymerase RRF-1. Finally, WAGO directs secondary siRNAs to cleave mRNA and inhibit gene expression. Adapted from Gammon *et al.* 2017.

From a technical point of view, RNAi in *C. elegans* is easy and fast. There are three administration forms: microinjection, soaking, and feeding. dsRNA can be directly injected into the *C. elegans* gonad, and the effect is observed in the next generation. This is a reliable method from worm to worm, albeit laborious and relatively expensive (Fire *et al.*, 1998; Min & Lee, 2007). Inhibition of expression is also achieved by soaking worms into a solution with dsRNA complementary for desired gene silencing (Tabara, 1998; Min & Lee, 2007). The other alternative, and most common, is the

feeding technique, consisting of feeding *C. elegans* with bacteria expressing dsRNA. This approach is highly effective and is not dependent on expensive reagents or equipment (Timmons & Fire, 1998; Kamath *et al.*, 2001; Min & Lee, 2007; Conte *et al.*, 2015) (**Figure I. 12**).

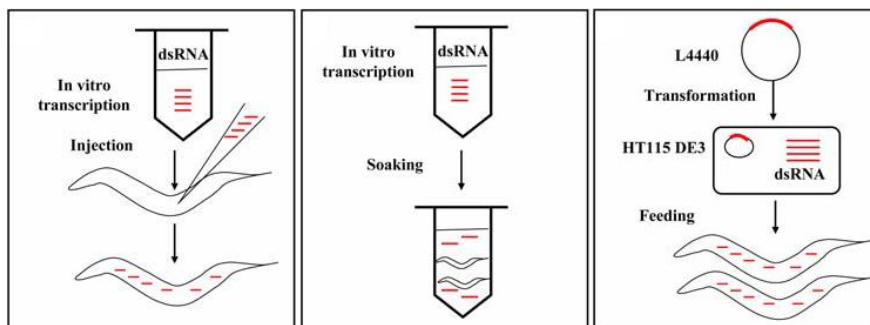


Figure I. 12: Scheme of the delivery methods of dsRNA. From left to right: injection, soaking, and feeding. dsRNA directly injected into *C. elegans*, soaking in a concentrated dsRNA solution or feeding with dsRNA expressing bacteria promote effective gene silencing.

Moreover, it allowed the construction of large libraries of bacteria expressing dsRNA targeting nearly all *C. elegans* genes. Currently, two of such libraries exist: genome-based (Arhinger's library) or open reading frame (ORF) based (ORFeome's library). In the first case, the bacterial library was constructed from genome fragments so that the resulting dsRNA contains both coding and non-coding regions (Fraser *et al.*, 2000; Kamath *et al.*, 2003). The ORFeome library only contains coding regions as it was constructed from a cDNA library, and thus it is thought to be more efficient (Rual *et al.*, 2004; Ceron *et al.*, 2007).

2. d. Drug screens in *C. elegans*

Several characteristics make *C. elegans* a potent model for drug screening to cure or alleviate diseases. First of all, the basic biological traits that placed *C. elegans* in the laboratory (small size, rapid life cycle, inexpensive maintenance, etc.) are also desirable for testing large drug libraries. Moreover, several complex diseases with different traceable and scorable phenotypes have been modelled in *C. elegans* allowing testing drugs to alleviate such alterations.

C. elegans, unlike cell cultures, present differentiated tissues and distinct cell types in the context of an organism, increasing the probability of identifying compounds more relevant for humans or other mammals. Another advantage is the possibility to test drug efficacy and initial steps of absorption, distribution, metabolism, excretion, or toxicity (ADMET) simultaneously. Finally, the availability of potent genetic tools to interrogate nearly all the genome facilitates identifying the target of a drug (Artal-Sanz, de Jong, & Tavernarakis, 2006; O'Reilly *et al.*, 2014). And now, thanks to CRISPR-Cas, if the target is not present could be placed in *C. elegans* cells through genome editing (Serrat *et al.*, 2019).

The use of *C. elegans* in high-throughput screens has been implemented relatively recently. The first reports of drug testing in roundworms date from the 1970s; however, the first screening of an extensive library was made in 2006 (Kwok *et al.*, 2006). Drug testing in agar plates implicates manual labor and larger amounts of drugs. The development of new handling liquid approaches allowed to scale up using from 24 well-plates up to 1536 well-plates. Additional advances in automatization of distribution, treatment, imaging acquisition, and analysis facilitated the implementation of high content and throughput screens (O'Reilly *et al.*, 2014). *C. elegans* has been used to identify valuable compounds for amyotrophic lateral sclerosis (Ikenaka *et al.*, 2019), antimicrobial

compounds (Moy *et al.*, 2006), anthelmintics (Partridge *et al.*, 2018), anti-aging (Matsunami, 2018), psychotic hyperphagia (Perez-Gomez *et al.*, 2018), and Alzheimer disease (Pérez-Jiménez *et al.*, 2021) among others.

Despite its many advantages, *C. elegans* still has many limitations for human disease modelling, such as the lack of certain human orthologs or reduced organ complexity (O'Reilly *et al.*, 2014). Still, settings using multicellular organisms as *C. elegans*, free of ethical-issues, allows to reduce the number of candidates to be tested in other organisms closely related to humans might be convenient (Volpatti *et al.*, 2020).

3. Retinitis Pigmentosa

3. a. Retinal inherited disorders and retinitis pigmentosa

Inherited retinal dystrophies (IRD) are a leading cause of vision loss in working-age people. Globally, IRD affect around 4.5 million worldwide, and the most prevalent of IRDs is RP (Hohman, 2017; Dockery *et al.*, 2017; Verbakel *et al.*, 2018). A study in Ireland has found more than 40% of IRDs cases accounted for RP (Dockery *et al.*, 2017), and it is estimated to affect 1.5 million people worldwide (Verbakel *et al.*, 2018). The incidence of RP is thought to be 1 per 4000 people worldwide; however, this number varies greatly in different geographic locations (Hartong, Berson, & Dryja, 2006; Parmeggiani *et al.*, 2011; Verbakel *et al.*, 2018).

Clinically, RP is manifested by initial nyctalopia (difficult vision in reduced light conditions) followed by a progressive reduction in visual acuity and field in a characteristic tunnel manner (**Figure I. 13**).

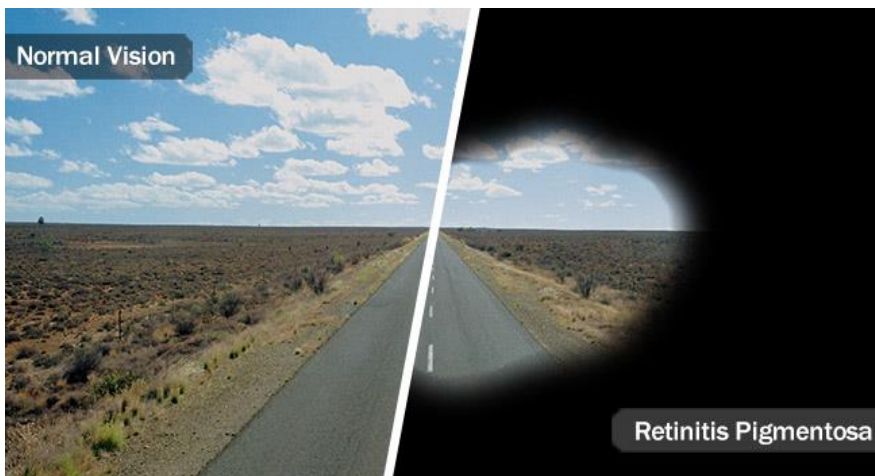


Figure I. 13: Visual field reduction in RP patients. Comparison of a scene perceived in normal conditions (left) and in patients with advanced RP (right). Retrieved from: <https://www.webmd.com/eye-health/what-is-retinitis-pigmentosa#1>.

These symptoms usually appear in adolescence, but there is considerable variability even between members of the same family (Daiger, Bowne, & Sullivan, 2007; Parmeggiani *et al.*, 2011; Verbakel *et al.*, 2018; Kiser *et al.*, 2019). The gradual loss of visual ability may ultimately lead to complete blindness. At a cellular level, these manifestations are in concordance with the initial loss of rods and posterior loss of cones and retinal pigment epithelium (RPE) observed in RP patients (Hartong *et al.*, 2006; Daiger *et al.*, 2007; Parmeggiani *et al.*, 2011; Verbakel *et al.*, 2018). Apoptosis is the mechanism by which photoreceptor loss is thought to occur, albeit the precise mechanism is still not unveiled (Wert, Lin, & Tsang, 2014; Zhang, 2016). Clinical features include fundus abnormalities such as bone-spicule deposits, attenuated retinal vessels, waxy pallor of the optic nerve, nystagmus, disease-associated refractive error, macular complications, photophobia, dyschromatopsia, or cataracts (**Figure I. 14**) (Fahim, Daiger, & Weleber, 1993; Parmeggiani *et al.*, 2011; Verbakel *et al.*, 2018). Importantly, clinical manifestations are widely varying and overlapping with other IRD. Thus, different functional and imaging techniques are used to characterize the visual function and diagnose RP differentially (Fahim *et al.*, 1993; Hartong *et al.*, 2006; Verbakel *et al.*, 2018).

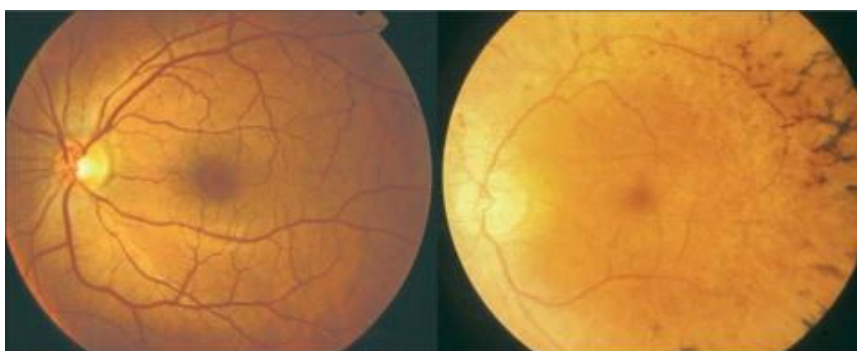


Figure I. 14: Fundi alterations in RP patients. Fundoscopy of a healthy individual (left) and an RP patient (right). Diseased eye shows attenuated vessels, optic-disc pallor, and bone-spicule deposits. Adapted from Hartong *et al.* 2006.

RP is mainly presented in a non-syndromic form (affecting only retina); however, a minor fraction of patients also present affection in other tissues in a syndromic form of the disease. Moreover, systemic affections may lead to a secondary RP as a result. The syndromic forms account for 25% of all patients being the Usher syndrome and the Bardet-Biedl syndrome the most common of this kind (Hartong *et al.*, 2006; Daiger *et al.*, 2007; Parmeggiani *et al.*, 2011; Verbakel *et al.*, 2018). Usher syndrome patients present additional neurosensory hearing loss and Bardet-Biedl patients present polydactyly, cognitive impairment, renal disease, hypogonadism or obesity. A phenocopy of RP-like symptoms may arise due to factors such as medication (e.g. Thioridazine, chlorpromazine, or quinolines) or inflammatory disease sequela among others and thus is classified as pseudo-RP. Some of these conditions are not the consequence of a genetic alteration and are amenable for treatment (Verbakel *et al.*, 2018).

Importantly, there is no cure for RP. The management is limited to the treatment of derived complications and improving the patient's functional abilities. Currently, efforts on developing strategies based on gene therapy, stem cell transplants, retinal implants, neuroprotective molecules, transcorneal electric stimulation, or optogenetics are being made (Zhang, 2016; Verbakel *et al.*, 2018).

Since the discovery of the *RHO* gene as causative of RP in 1990, more than 80 other genes have been identified (Dryja *et al.*, 1990; Daiger *et al.*, 1998; Verbakel *et al.*, 2018). It is estimated that many more genes are involved in RP since a significant number of patients still do not have a genetic diagnosis (Salmaninejad *et al.*, 2019; Perea-Romero *et al.*, 2021). As in clinical manifestations, there is an overlap of affected genes with other IRD (Verbakel *et al.*, 2018). RP genes can be classified according to their inheritance mode (Hartong *et al.*, 2006; Daiger *et al.*, 2007; Parmeggiani *et al.*, 2011; Verbakel *et al.*, 2018) (**Table 2**). However, this task has proven

difficult and inaccurate for some variants since different mutations in the same gene may be inherited in different ways provoking lack or misinterpretation of the pedigree (Daiger, Bowne, & Sullivan, 2015).

Table 2: Prevalence of RP depending on the inheritance mode.

RP inheritance mode	Aproximate percentatge of patients
Autosomal recessive RP (arRP)	50-60%
Autosomal dominant RP (adRP)	30-40%
X-linked RP	5-15%

Extracted from Verbeckel *et al.* 2018 and Hartong *et al.* 2006.

The RP genes are involved in several pathways including: phototransduction, visual cycle, ciliary structure and transport, or splicing, among others (Hartong *et al.*, 2006; Parmeggiani *et al.*, 2011; Verbakel *et al.*, 2018).

3. b. Splicing-related autosomal dominant retinitis pigmentosa (s-adRP)

RP caused by alterations in splicing factors (s-adRP) rise a still not fully unanswered question of why mutations on ubiquitously expressed and essential genes produce a tissue-specific phenotype. The degenerative nature, late and highly variable onset, and progression of the disease are also not well understood (Mordes *et al.*, 2006; Parmeggiani *et al.*, 2011; Růžičková & Staněk, 2017). Genes mutated in RP related to splicing include: *PRPF3*, *PRPF4*, *PRPF6*, *PRPF8*, *PRPF31*, *SNRNP200/Brr2*, *RP9/PAPI*, and more recently *DHX38* and *CWC27* were found (Růžičková & Staněk, 2017; Verbakel *et al.*, 2018). The s-adRP identified mutations

occur in genes that form part of U4/U6.U5 tri-snRNP components and follow an autosomal dominant mode of inheritance (**Supplementary Table I. 1**).

Different hypotheses were postulated to explain the implication of splicing alterations in RP etiology. One possible explanation might be due to higher transcriptional requirements of the retina, thus being more sensitive to alterations in splicing machinery compared to other tissues. Despite the fact that none of the s-adRP proteins participate in the splice site recognition, but in the catalysis reaction, s-adRP mutations affect AS widely and unevenly, being some transcripts more susceptible to changes. Retina-specific AS events might thus explain tissue specificity; however, there are not strong evidence yet supporting this theory. Nevertheless, comprehension of AS in the retina is essential to understand its role in pathogenesis and improve genetic diagnosis (Aísa-Marín *et al.*, 2021). Other hypotheses include pathological aggregation of mutated proteins in photoreceptors or damaged RPE cells provoking photoreceptors' cell death as secondary effect (Mordes *et al.*, 2006; Růžicková & Staněk, 2017). Although there are different hypotheses, the precise mechanism is still far from being uncovered, and different model organisms (Graziotto *et al.*, 2008; Yin *et al.*, 2011) are being used to tackle the functional impact of RP mutations .

3. c. *C. elegans* as a model to study s-adRP

RP has been modelled in several settings ranging from *in vitro* cell lines including iPSC or yeast to the generation of more complex rodent models (Towns *et al.*, 2010; Graziotto *et al.*, 2011; Brydon *et al.*, 2019). In our laboratory, *C. elegans* was used for such aim as apoptosis and splicing are highly conserved, and it is easy to manipulate while containing

differentiated tissues. Peña-Rubio *et al.* made the initial efforts to model s-adRP, taking advantage of deletion alleles of *prp-8* and *prp-31*, reporter strains, and RNAi. RNAi of splicing factors present in U4/U6.U5 tri-snRNP showed two distinct phenoclusters being U4 associated genes the ones that present milder phenotypes. Transcriptomic analyses did not show any major modifications in AS events; however, there was upregulation of the pro-apoptotic gene *egl-1* and the DNA damage sensor *atl-1*. Moreover, this upregulation was produced unevenly, being hypodermal cells the most affected tissue.

These findings set *C. elegans* as a model for s-adRP. Similar to humans, nematodes showed tissue-specific sensitivity to partial inactivation of splicing factors. Moreover, up-regulation of *atl-1* and *egl-1* led to the establishment of a working model. Based on the co-transcriptional nature of splicing, the model established altered splicing as a source of R-loop accumulation which leads to genome instability and ultimately apoptosis (Figure I. 6, 15) (Rubio-Peña *et al.*, 2015).

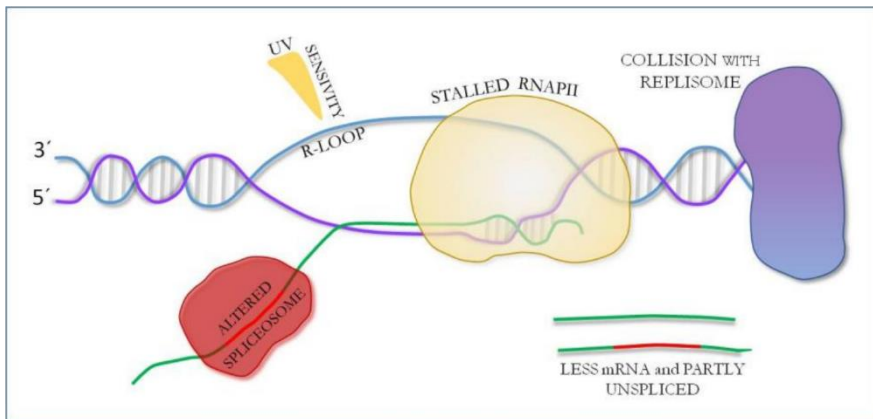


Figure I. 15: Working model based on the previous finding in *C. elegans*. Altered spliceosome induces R-loop accumulation, which leads to genomic instability through different mechanisms (sensitivity to DNA damage or replisome collision). Partially or inefficiently spliced transcripts may negatively impact retinal cells. Adapted from Karinna Rubio-Peña doctoral thesis.

The advent of CRISPR-Cas9 technology allows the construction of models to better reproduce the actual alterations of s-adRP patients. Karinna Rubio-Peña took advantage of this to model s-adRP missense mutations in *prp-8* and *snrp-200* genes. The result was four strains: two strains with strong phenotypes (*prp-8(cer14[H2302del])* and *snrp-200(cer23[V676L])*), and two strains with no overt alterations (*prp-8(cer22[R2303G])* and *snrp-200(cer24[S1080L])*) (Kukhtar *et al.*, 2020). In this thesis, I explore the utility of these strains as a pre-clinical model, and I describe potential mechanisms of the disease while expanding the toolkit of s-adRP strains.

AIMS

1. To to mimic splicing-related adRP mutations in the *C. elegans* genome using CRISPR-Cas9 and **characterize** its effects.
2. Use RNAi to identify genetic interactions with mimicked s-adRP mutations that might unveil **modifiers** of the disease.
3. To evaluate the preclinical value of *C. elegans* s-adRP mutants for **drug screens**.
4. To investigate the molecular **mechanisms** by which s-adRP splicing-related mutations cause apoptosis in specific cell types.
5. To establish the use of *C. elegans* s-adRP mutants as a diagnostic tool for **variants of uncertain significance (VUS)**.
6. To explore the limits of the splicing factor **humanization** in *C. elegans* through gene replacement of the *prp-3* gene.

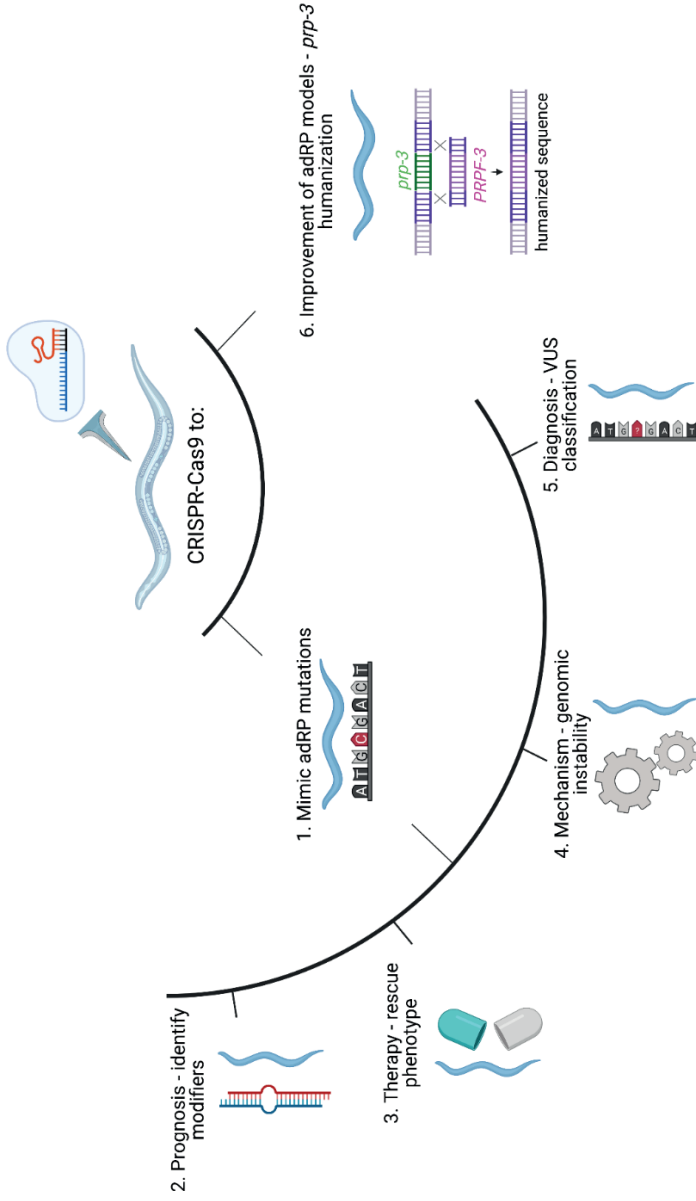
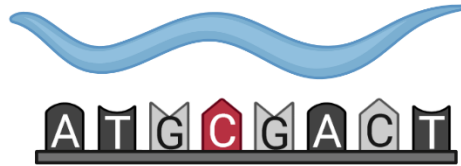


Figure A. 1: Graphical abstract of the aims pursued in this thesis project.

(1) Mimic s-adRP mutations in *C. elegans* thanks to CRISPR-Cas9 technology and use these models for (2) the identification of genetic interactors with prognostic purposes with an RNAi screen, (3) the identification of potential therapeutic agents with a drug screen, (4) the study of genomic instability as a possible trigger of the disease, and (5) development of a panel of features for variants of unknown significance (VUS) classification. Moreover, (6) to explore the limits of gene replacement at the endogenous locus to improve *C. elegans* s-adRP models.

RESULTS

1. CRISPR-Cas9 allows mimicking of s-adRP mutations in *C. elegans*



As stated in the introduction, four different strains that mimicked s-adRP mutations were generated by a former member of the laboratory (Karinna Rubio-Peña). Three strains mimic actual patients' mutations, *prp-8(cer22)*, *snrp-200(cer23)*, and *snrp-200(cer24)*, while *prp-8(cer14)* removes a residue that is affected in RP patients and was obtained unwittingly. All strains present developmental delay, and two mutants, *prp-8(cer14)* and *snrp-200(cer23)*, display overt phenotypes (Rubio-Peña, 2017; Kukhtar *et al.*, 2020). The two mutants with overt phenotypes were considered *strong* alleles, and mutants with no obvious phenotypes *weak* alleles.

I. a. Impact of s-adRP mutations in fertility

Since we observed a sterile phenotype on *prp-8(cer14)* animals, we quantified the brood size of s-adRP mutants at 25°C. *snrp-200(cer23)* worms presented a reduced brood size (about half of the progeny) (**Figure R. 1A**), and *prp-8(cer14)* animals were sterile (**Figure R. 1B**). Thus, the characterization of the brood size confirms the two *strong* alleles have an important impact on fertility, while *weak* alleles do not show this effect. The temperature-sensitive sterility of *prp-8(cer14)* allows its maintenances at 15°C, thus facilitating the development of the project with all four strains (**Figure R. 1B**).

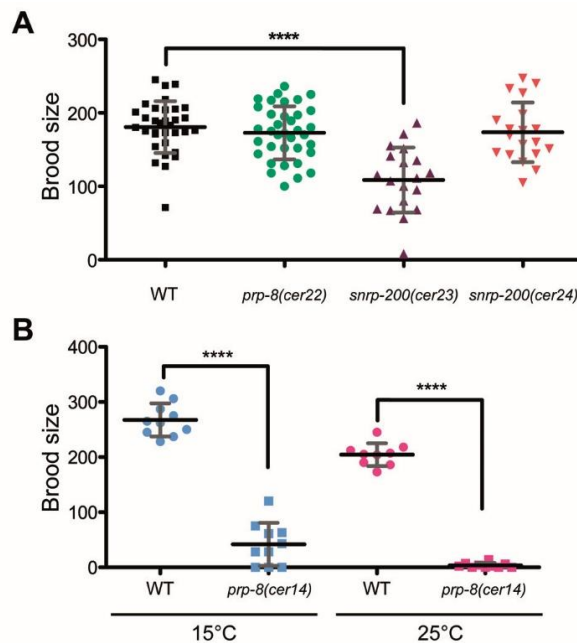


Figure R. 1: s-adRP mutants *prp-8(cer22)* and *snrp-200(cer23)* present altered fertility. Brood size of s-adRP mutants at 25°C (A) and of the *prp-8(cer14)* at permissive (15°C) and restrictive (25°C) temperature (B). (A) The brood size of *snrp-200(cer23)* animals is significantly reduced compared to wildtype (N=2; n≥20). (B) The brood size of *prp-8(cer14)* at permissive temperature is reduced and complete sterility emerges at restrictive temperature (N=1; n≥10). (A) Kruskal-Wallis with Dunn's post-hoc was applied. *ns* indicates not significant and **** $p < 0.0001$. (B) Mann-Whitney test was applied to compare mutant to WT at each temperature. **** $p < 0.0001$. Collaborative results between Karinna Rubio-Peña and Dmytro Kukhtar.

1. b. All s-adRP mutants cause a functional impairment

Karina Rubio-Peña observed diverse overt alterations in the *strong* alleles. (Rubio-Peña, 2017; Kukhtar *et al.*, 2020). Formal quantification at 25°C confirmed *snrp-200(cer23)* displays a variety of postembryonic phenotypes at low penetrance and embryonic lethality (Emb) (**Figure R. 2**).

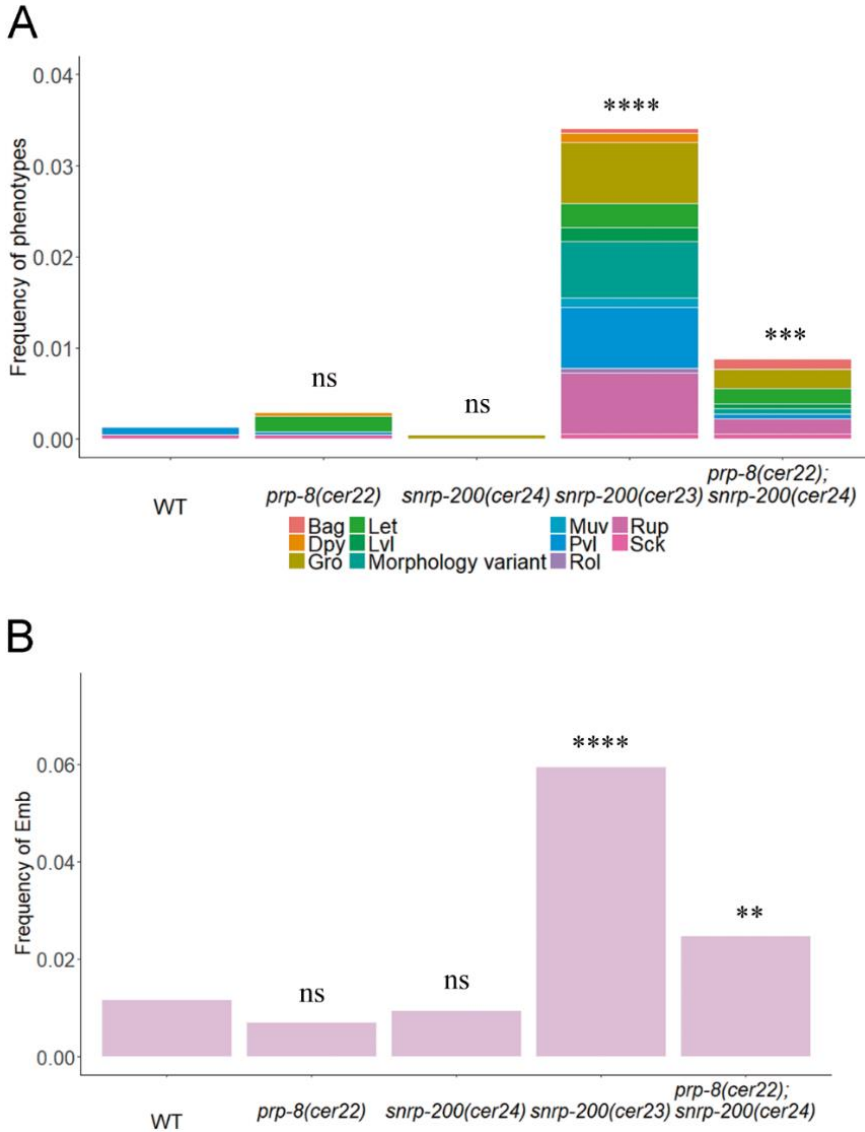


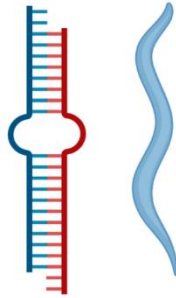
Figure R. 2: *snrp-200(cer23)* along with the double mutant *prp-8(cer22); snrp-200(cer24)* presents higher frequency of embryonic lethality and pleiotropic phenotypes.

(A) Cumulative frequencies of overt phenotypes under the stereomicroscope and (B) frequency of dead embryos laid (N=1, n \geq 1753). *prp-8(cer14)* is not included as it is sterile at 25°C. χ^2 comparing each of the mutant strains to the wildtype (WT) was applied. *ns* indicates not significant, **p<0.01, *** p<0.001 and **** p<0.0001.

Abbreviations: Bag: bag of worms, Dpy: dumpy, Gro: slow growth, Let: lethality, Lvl: larval lethality, Muv: multivulva, Pvl: protruding vulva, Rol: roller, Rup: ruptured, Sck: sick.

These alterations were not observed on *weak* alleles. To uncover the functional impact of *weak* alleles, a double mutant of *prp-8(cer22)* and *snrp-200(cer24)* was generated. This strain presents increased pleiotropic phenotypes in a synergistic manner and additive Emb percentage. This data shows that although *weak* alleles do not show overt phenotypes, there is a functional impact caused by these mutations (**Figure R. 2**).

2. Prognosis: *weak* alleles permit the identification of potential disease modifiers



As mentioned in the introduction, a considerable variation in onset and progression of RP exists, often in members of the same family carrying the same mutation (Kiser *et al.*, 2019). This variability probably arises due to environmental and genetic factors. Identifying elements that could predict how the disease will evolve is not only of interest for patients, but it can also point towards novel therapeutic strategies.

C. elegans' powerful genetics can help in identifying other genetic alterations that modify the effect of s-adRP mutations. For that means, I performed an RNAi screen on the *weak* alleles *prp-8(cer22)* and *snrp-200(cer24)* to identify potential genetic modifiers of the disease.

2. a. Weak alleles are suitable to detect genetic interactors through RNAi screens

Weak alleles without apparent functional alterations are suitable for screens in search of genetic interactors that worsen their impact, thus pointing to genes that might guide patient prognosis.

I gathered a library of 98 validated bacterial clones expressing dsRNA targeting genes related to the splicing process (**Supplementary table R. 1**). Splicing-related genes were selected as they would have more chances to functionally interact with s-adRP mutants; however, any group of genes is amenable for such screens.

I performed the RNAi screen in 24-well plates, testing RNAi clones in duplicates in wildtype (WT) and the mutant background (**Figure R. 3 A**). As a result, three enhancers of *prp-8(cer22)* were identified: *isy-1*, *cyn-15*, and *mog-2*.

isy-1(RNAi) produces stronger larval arrest (Lva) in mutants (**Figure R. 3 B and D**), while *cyn-15(RNAi)* and *mog-2(RNAi)* induce nearly 100% sterility only in mutants, but not in the WT (**Figure R. 3 C and D**).

A careful look into the germline of the RNAi treated worms confirmed *isy-1(RNAi)* produces animals with undeveloped germlines while *cyn-15(RNAi)* and *mog-2(RNAi)* produce masculinization of germline (Mog) phenotype (**Figure R. 4 and R. 5**).

We show how s-adRP *weak* alleles can be used for RNAi screens that might be escalated in size. The identification of three *prp-8(cer22)* modifiers supports our strategy for the identification of other genes involved in disease development and validates the use of *weak* alleles for this aim.

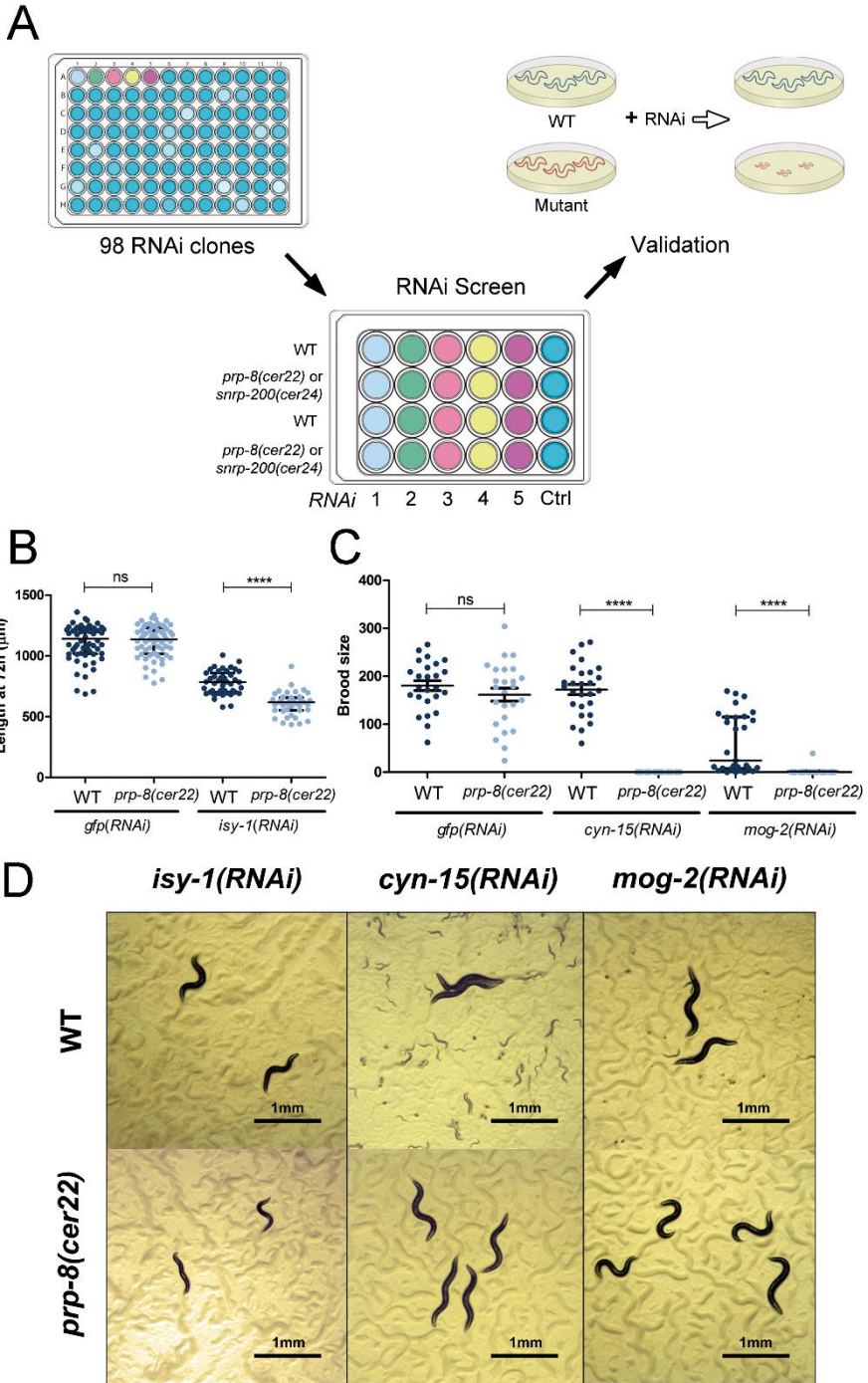


Figure R. 3: General procedure of the RNAi screen (A) and characterization of the identified genetic modifiers of *prp-8(cer22)*.

(A) Schematic of the RNAi screen procedure. 98 splicing-related genes were assayed on WT, *prp-8(cer22)*, and *snrp-200(cer24)* mutants in a 24-well plate format. Hits were validated on individual agar plates. (B) Body length of WT and *prp-8(cer22)* animals at 72 h post L1, grown at 25°C (N=3; n≥61). Each dot represents the body length of a single worm, and bars represent the median with interquartile range (IQR). (C) Progeny of WT and *prp-8(cer22)* mutants (N=2; n≥25). Each dot represents the offspring of a single worm, and bars represent the median with IQR. (D) Representative images of WT and *prp-8(cer22)* animals fed with RNAi clones targeting *isy-1*, *cyn-15* and *mog-2*. Kruskal-Wallis with Dunn's post-hoc analysis: *ns* indicates not significant and **** $p < 0.0001$.

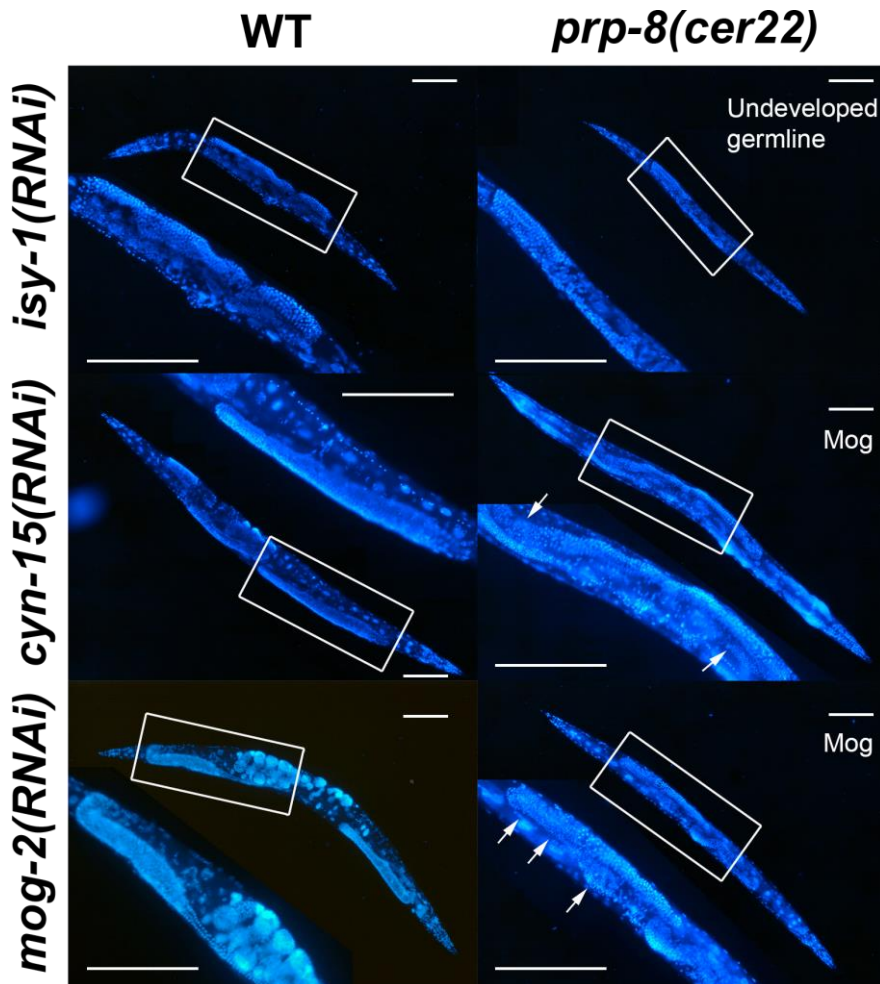


Figure R. 4: DAPI staining of *prp-8(cer22)* worms shows undeveloped germlines upon *isy-1(RNAi)* and Mog phenotype in *cyn-15(RNAi)* and *mog-2(RNAi)*.

isy-1(RNAi) induces undeveloped germlines in both WT and *prp-8(cer22)*, more prominent in mutants with smaller size and abnormal morphology. In *cyn-15(RNAi)* and *mog-2(RNAi)*, WT worms present normal morphology, while mutants show an abnormal accumulation of sperm (arrows) known as Mog phenotype. Scale bars 100 μ m.

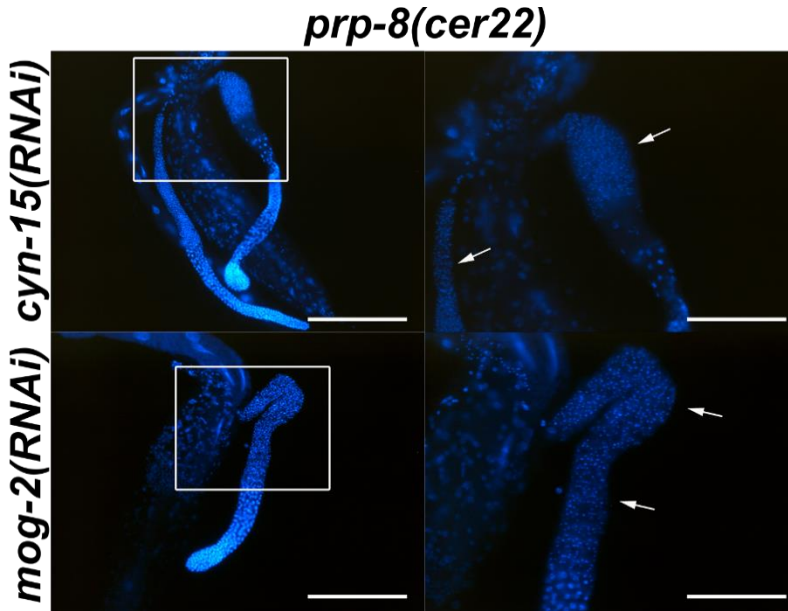


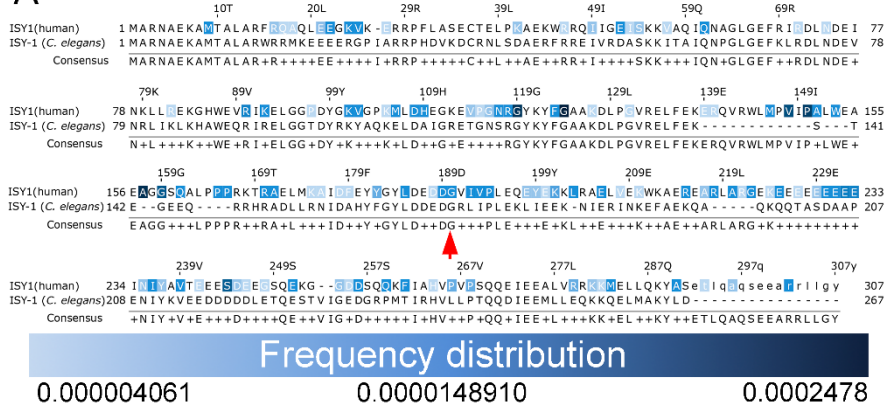
Figure R. 5: DAPI staining of the gonads of *cyn-15(RNAi)* and *mog-2(RNAi)* confirms Mog phenotype. Scale bars 100 μ m.

2. b. *prp-8(cer22)* can serve as a platform for SNPs testing from genetic interactors

Once we identified genes that interact with the *weak* mutant *prp-8(cer22)*, we wondered whether single nucleotide polymorphisms (SNPs) that cause missense mutations in human orthologs of *isy-1* (*ISY1*) and *cyn-15* (*PPWD1*) could genetically interact with *prp-8(cer22)* allele as well, explaining the patients' variability in disease progression. For this purpose, from the 20 most prevalent SNPs from healthy individuals retrieved from gnomAD (Karczewski *et al.*, 2020), I selected one residue for each gene that may have an impact on the protein when mutated based on *in silico* predictors from Ensembl (Hunt *et al.*, 2018; Zerbino *et al.*, 2018) and are

conserved in *C. elegans*. In parallel, I also produced a small deletion allele of *cyn-15* covering nine residues from the first WD40 repeat, presumably an essential domain for the protein function (Jain & Pandey, 2018) (**Figure R.6**).

A



B

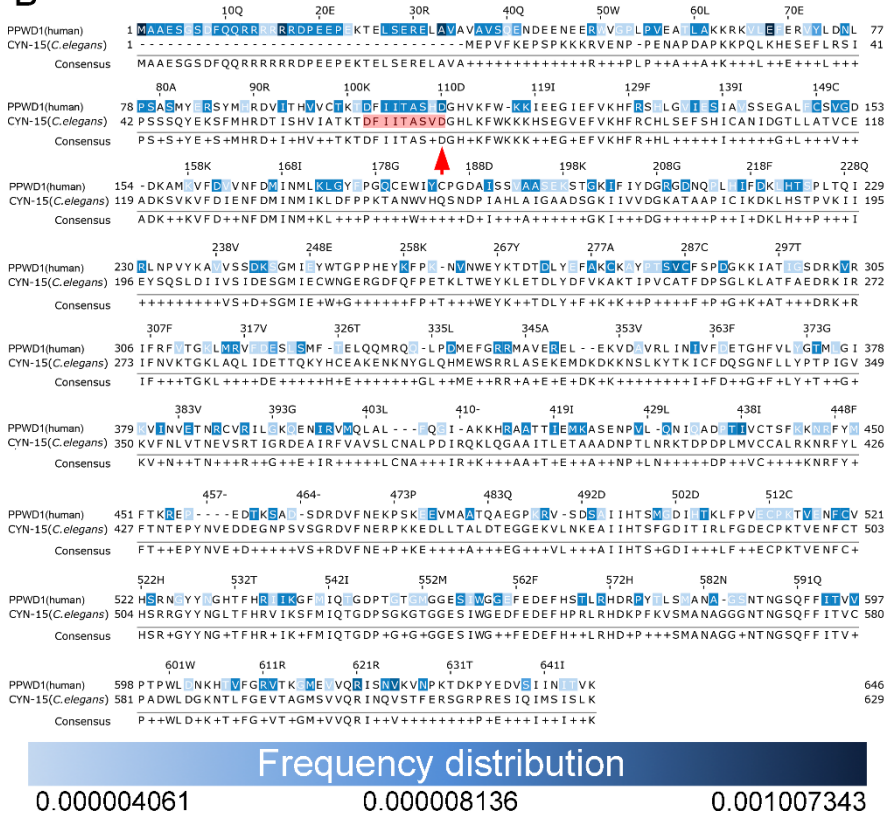


Figure R. 6: Alignment of ISY-1 (A) and CYN-15 (B) with their human counterparts ISY1 and PPWD1. Blue shade indicates residues affected by missense mutations in healthy individuals. The intensity of shades corresponds to the frequency of each mutation with the maximum, median, and minimum indicated. Arrows point to the residues for which mutations were generated, and the shaded red area denotes the deletion allele of *cyn-15*.

Thus, we generated three mutant strains by CRISPR-Cas9: *isy-1(cer115[G170S])*, *cyn-15(cer119[D74Q])* and *cyn-15(cer173[D66_D74del])*. None of the three strains had any overt phenotype. A more careful characterization showed that the two missense mutations did not present developmental delay nor alterations in fertility and did not interact with *prp-8(cer22)* (**Figure R. 7**).

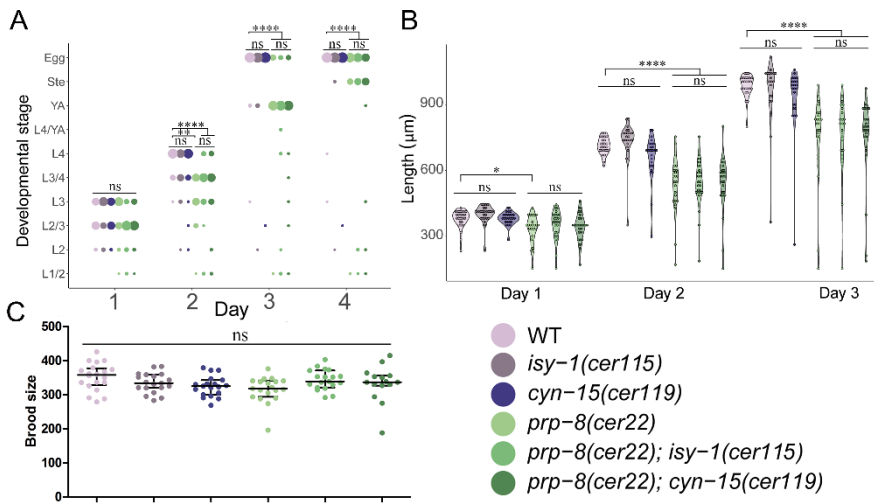


Figure R. 7: *isy-1(cer115[G170S])* and *cyn-15(cer119[D74Q])* do not present developmental delay (A and B), nor fertility alterations (C) alone or in combination with *prp-8(cer22)*. (A) Developmental timing. The size of each dot is proportional to the percentage of the population at a given developmental stage, starting with a synchronized population and grown at 20°C (N=2, n \geq 81). χ^2 comparing each of the mutant strains to the WT was applied. *ns* indicates not significant, ** p<0.01, and **** p<0.0001. (B) Violin plot of the length distribution of a synchronized population across time at 20°C, each dot represents the length of an individual worm (N=1, n \geq 22). (C) Brood size. Each dot represents the brood of an individual worm (N=1, n \geq 15). (C, D) Kruskal-Wallis with Dunn's post-hoc analysis was used. *ns* indicates not significant, * p<0.05, and **** p<0.0001.

Isolation of the double mutant of *cyn-15(cer173)* deletion allele with the *prp-8(cer22)* resulted impossible at any temperature as such worms are sterile, suggesting a synthetic interaction. A deeper look into the progeny of *prp-8(cer22); cyn-15(cer173[D66_D74del])/+* showed no effect of *cer173[D66_D74del]* allele alone, nor in heterozygosis; however, double mutants were sterile (**Figure R. 8**). Hence, I confirmed the interaction identified in the RNAi screen with a genetic mutant of *cyn-15*.

Although I did not identify any interaction between SNPs mimicked from humans and the *prp-8(cer22)* mutant, presented findings demonstrate how CRISPR-Cas9 in *C. elegans* can be easily implemented to test genetic interactions in a mutant background.

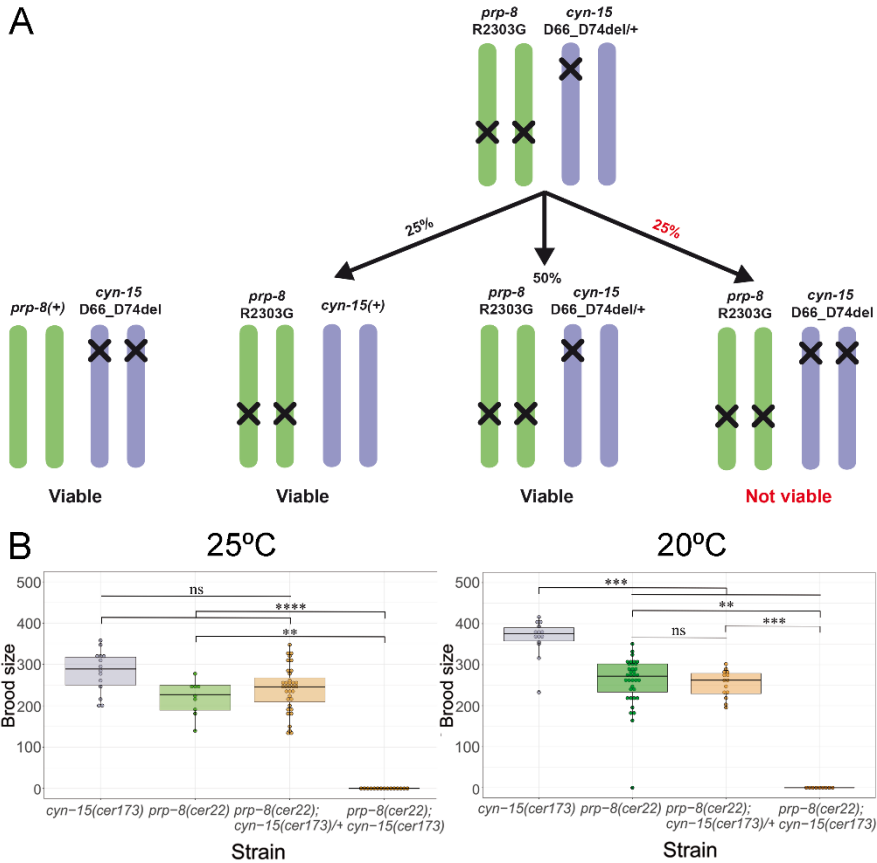
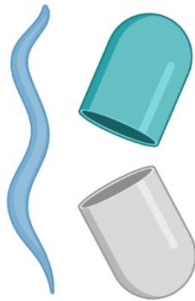


Figure R. 8: *cyn-15(cer173[D66_D74del])* interacts genetically with *prp-8(cer22)*.

(A) Schematic representation of the segregation pattern. Mutations are represented as cross marks in chromosomes (bars), and percentages indicate the expected segregation rates. I was able to maintain *cyn-15(cer173[D66_D74del])* as homozygotes. Around 25% of singled worms from *cyn-15[D66_D74del]/+* heterozygotes on *prp-8(cer22)* background were sterile. Genotyping by PCR showed that all sterile worms were homozygotes for the *cyn-15[D66_D74del]*. (B) Progeny of the *cyn-15(cer173[D66_D74del])* and of the singled-out worms from *prp-8(cer22); cyn-15(cer173[D66_D74del])/+* at 25°C (left) and 20°C (right) (N=1; n>9). Each dot represents the offspring of a single worm, bars represent the median with the IQR, and whiskers the ± 1.5 product of IQR. Kruskal-Wallis with Dunn's post-hoc analysis: ns indicates not significant, ** p<0.01, *** p<0.001, and **** p<0.0001.

3. Therapy: A drug screen on the *strong* mutant *prp-8(cer14)* identified dequalinium as a potentially damaging molecule



The lack of effective treatments for RP encourages the search for personalized therapies. Genome editing and stem cell therapy are promising horizons; however, their application in clinics for RP is still distant. Thus, the implementation of other approaches that could alleviate the progression of the disease is of significant interest. One strategy to identify novel drugs is through a screen of a library of compounds. Typically, a hit from such a screen would take years until it arrives to the clinics; however, if the identified molecule has already been approved for its use in humans, this period would be drastically shortened. With this in mind, I proceeded to screen a library of primarily FDA-approved small molecules in the *prp-8(cer14) strong* allele to identify potential treatments.

3. a. *Strong allele prp-8(cer14) is amenable for drug screens*

The temperature-sensitive *prp-8(cer14)* is an ideal strain for drug screens as the rescued sterility would be easily detected. Using a library of 929 drugs, mostly FDA-approved (**Supplementary Table R. 2**), I screened for any compound capable of rescuing *prp-8(cer14)* sterility. *C. elegans* is particularly convenient for such experiments as it can be grown in liquid medium in 96 well-plates, allowing thus the scaling of the drug screen.

The effect of drugs in animals was studied using a movement tracker device WMicrotracker (PhylumTech & InVivo Biosystems) (*i*), and by visual scoring (*ii*) (**Figure R. 9**).

(*i*) Since *prp-8(cer14)* worms are sterile at 25°C, motility at *prp-8(cer14)* wells will be lower than WT at day four when F1 larvae appear. (**Figure R. 10**).

(*ii*) Visual scoring showed obvious phenotypes in about 16% of tested drugs, validating our library. Even though we did not observe any rescue, we observed a correlation of visually observable phenotypes and reduction in motility, indicating that motility may be used as an indicator of toxicity (**Figure R. 10**).

In summary, we demonstrate how the *strong* allele *prp-8(cer14)* is amenable for small molecule screens. I validated the efficacy of our drug library and observed a correlation between motility recordings and animal fitness. Unfortunately, I did not identify any drug that rescues *prp-8(cer14)* sterility.

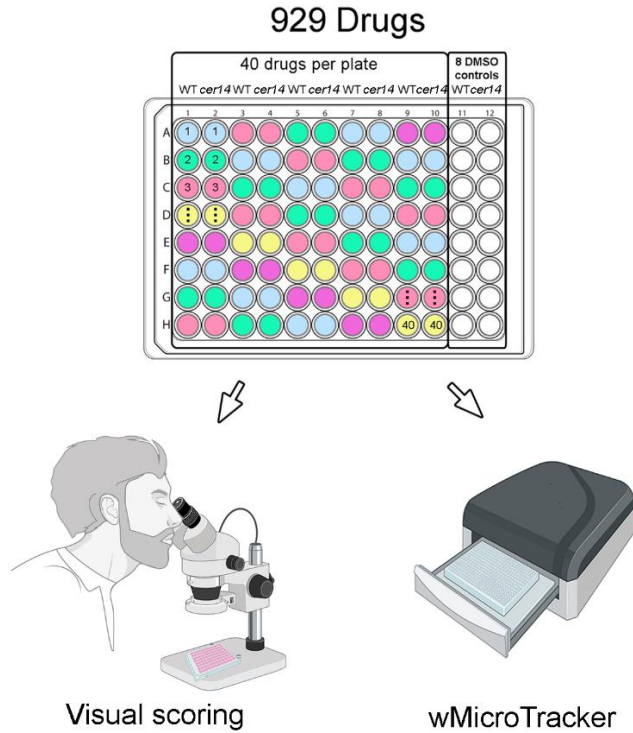


Figure R. 9: Drug screen scheme.

Representation of the drug screen procedure. Drugs were tested in liquid medium at a final concentration of 50 μM and 0.5% DMSO, being 40 drugs tested per each 96-well plate. Plates were scored visually in search of a differential response between *prp-8(cer14)* and WT, and motility was recorded with the WMicrotracker device.

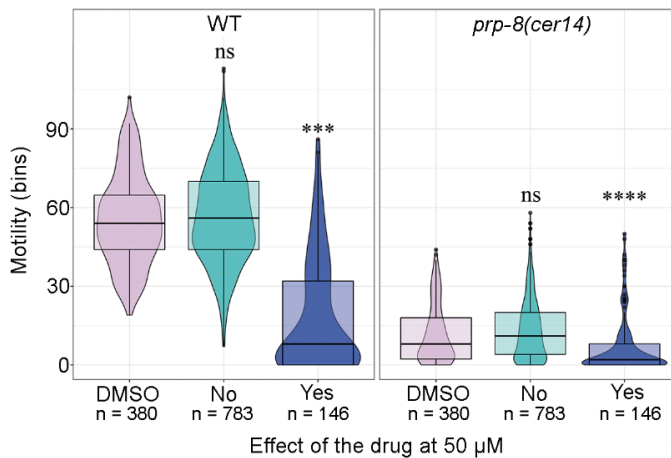


Figure R. 10: Motility results of WT and *prp-8(cer14)* classified by the presence (Yes) or absence (No) of visually observable drug effect.

Violin plot and boxplot of the motility of WT and *prp-8(cer14)* worms. *prp-8(cer14)* animals present reduced motility even at control conditions. In both WT and *prp-8(cer14)*, the motility is drastically reduced in the case of drugs causing a phenotype. Box plots indicate the median with the IQR and whiskers the ± 1.5 product of IQR. Kruskal-Wallis with Dunn's post-hoc analysis comparing the motility of the drugs that did have (Yes) or not (No) visible effects on worms to control DMSO condition was applied. *ns* indicates not significant, *** $p < 0.001$, and **** $p < 0.0001$.

3.b. *prp-8(cer14)* drug screen uncovers potentially damaging effects of dequalinium on *snrp-200* mutants

To our surprise, I found drugs that produce a stronger phenotype in mutants compared to WT, indicating a toxic synergy between s-adRP mutations and the compound. All four candidates are FDA-approved drugs and could be prescribed to RP patients. These molecules are potentially harmful by inducing more substantial side effects or even worsening RP progression.

I proceeded with the validation of four identified compounds on agar plates: dequalinium chloride, flutamide, doxycycline hyclate, and dronedarone (**Figure R. 11** and **Supplementary Figure R. 1**). The *strong* alleles *prp-8(cer14)* and *snrp-200(cer23)* show artefactual resistance to the drugs, probably due to their reduced body size. Similarly, inexplicable resistance in *prp-8(cer22)* worms treated with doxycycline is seen (**Supplementary Figure R. 1**). Only dequalinium chloride consistently affected more severely *snrp-200* mutants at precise concentrations (**Figure R. 11**).

Our findings demonstrate that *C. elegans* can not only be valuable for molecule screens with therapeutic means but also as a tool to identify potentially toxic interactions between drugs and particular genotypes.

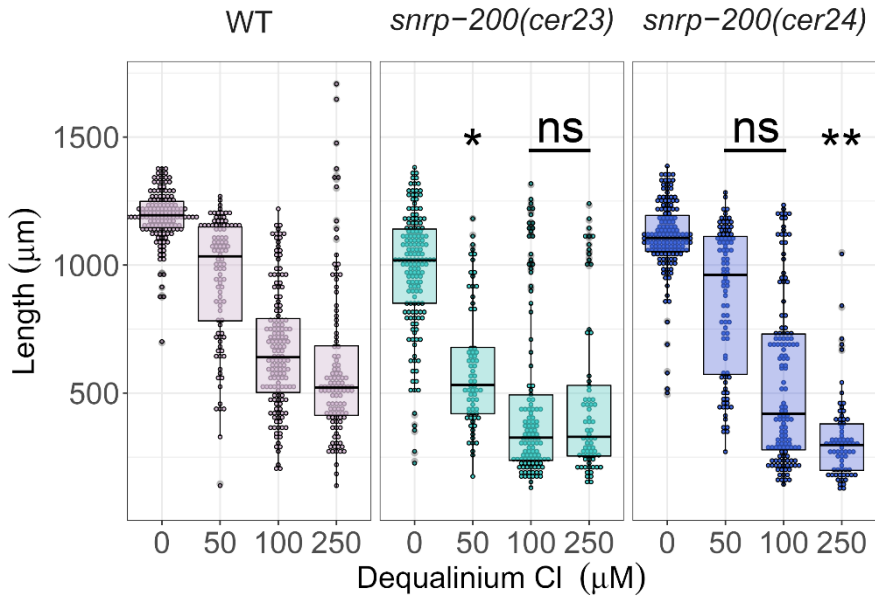
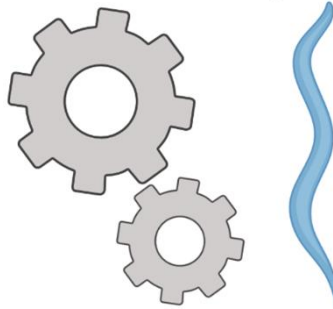


Figure R. 11: Dequalinium chloride produces sensitivity in *snrp-200* mutants.

Worm length of WT and s-adRP strains upon treatment with dequalinium chloride (N=3, except N=2 at 50 µM; n≥69). Each dot represents the length of an individual worm, box plot indicates the median with the IQR, and whiskers the ± 1.5 product of IQR. The difference between control concentration 0 and the tested drug concentrations in WT worms was compared to the difference in the mutants. Aligned rank transformation followed by two-way ANOVA and F test to test interaction was applied. *ns* indicates not significant, * $p < 0.05$ and ** $p < 0.01$. The *snrp-200(cer23)* mutant shows sensitivity at 50 µM concentration of dequalinium Cl and the *snrp-200(cer24)* at 250 µM.

4. Mechanism – Genome instability could be present in some s-adRP mutants



Rubio-Peña *et al.* (2015), based on RNAi experiments, proposed genome instability might lead to apoptosis as a potential mechanism involved in disease etiology. The interplay between splicing and transcription might provide a rationale for DNA damage accumulation due to splicing defects and explain the degenerative nature of the disease. This hypothesis is supported by the fact that knockdown of *s-adRP* genes produces upregulation of the genome instability marker *atl-1* (*ATR* in humans) and the pro-apoptotic gene *egl-1*. Moreover, the upregulation of *egl-1* was primarily seen in somatic seam cells (Rubio-Peña *et al.*, 2015). Thus, we were interested in studying if the same molecular alterations occur in our *s-adRP* mutants supporting this hypothesis.

4. a. *Pegl-1::gfp* reporter did not unveil s-adRP upregulation of *egl-1* even under hydroxyurea (HU) and UV-C induced stress

To further explore if s-adRP mutants also present increased expression of *egl-1*, I crossed them with a reporter strain carrying 3 kb of the upstream region of *egl-1* fused to 2xNLS and GFP (*Pegl-1::gfp*). However, none of the s-adRP mutant backgrounds seemed to induce ectopic GFP expression at standard growing conditions.

We hypothesized exposure to DNA damaging elements such as hydroxyurea (HU) and UV light could uncover the sensitivity of s-adRP mutants, as these treatments induce upregulation of both *egl-1* and *atl-1* (Rubio-Peña *et al.*, 2015). The *strong* allele *snrp-200(cer23)* was initially chosen to assess if *Pegl-1::gfp* was induced as a result of HU and UV exposure.

A HU dose-dependent increase in *Pegl-1::gfp* signal was observed in WT and *snrp-200(cer23)* with no apparent sensitivity of the mutant (**Figure R. 12 A and B**). Surprisingly, when other s-adRP strains were treated with 10 mM HU for 48h, both *prp-8* mutants showed fewer cells expressing GFP than the control (**Figure R. 12 D**). Premature cell death might explain this finding in such strains, resulting in less GFP-expressing nuclei.

Similarly, up-regulation of *Pegl-1::gfp* but not sensitivity is observed upon UV light treatment of the *strong* allele *snrp-200(cer23)* (**Figure R. 12 C**). The *strong* allele *prp-8(cer14)* was the only mutant that might have sensitivity to this agent (**Figure R. 12 E**). A deeper look into the data showed high inter-experimental variability, which indicates low reliability of the *Pegl-1::gfp* signal (**Supplementary Figure R. 2**). Thus, *Pegl-1::gfp* reporter strain seems not to be an adequate tool to answer our question, probably due to the lack of other *cis*- and *trans*-regulatory regions controlling GFP expression.

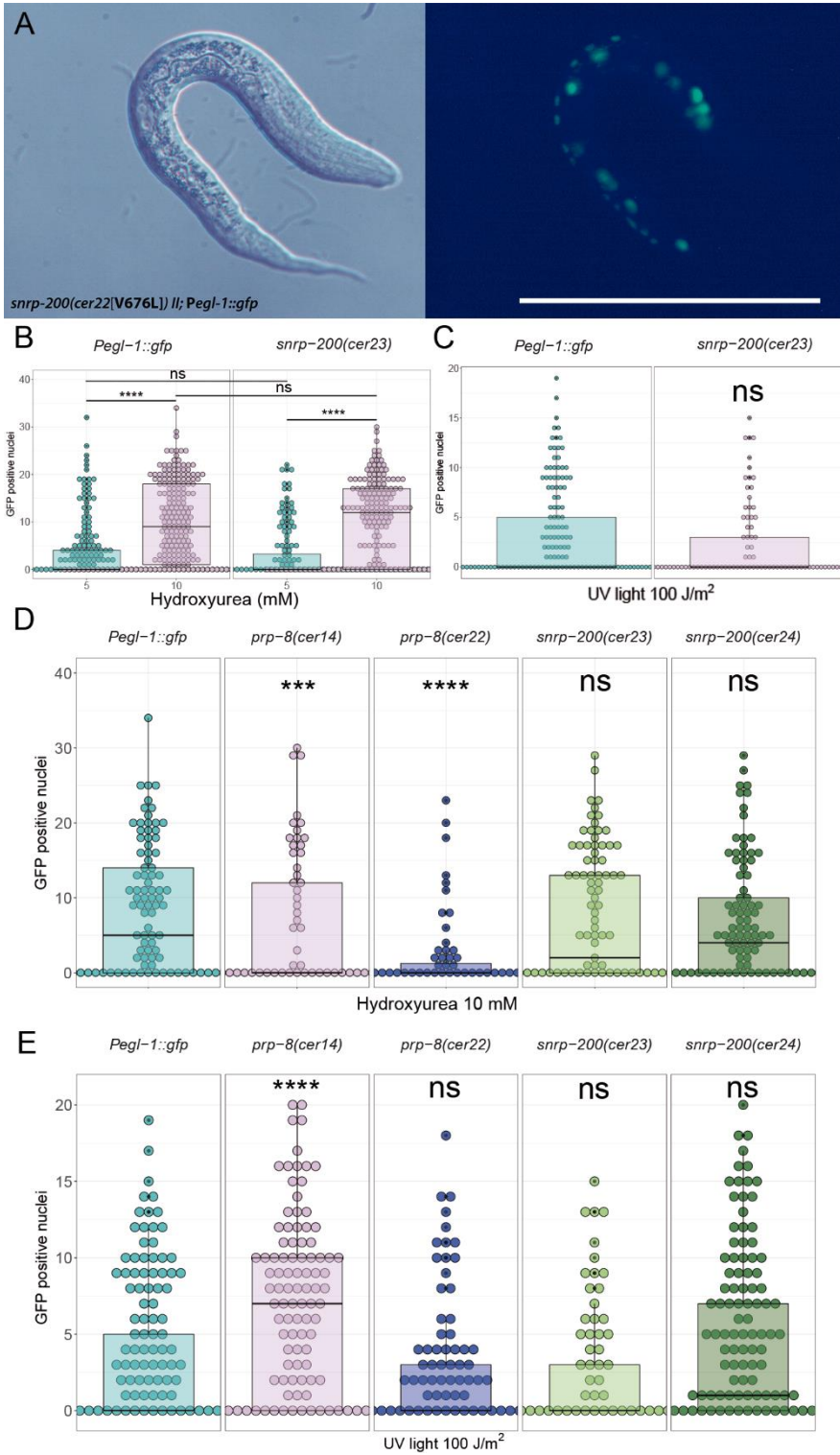


Figure R.12. HU and UV light induce up-regulation of an *egl-1* reporter with no clear sensitivity in s-adRP mutants.

(A) *snrp-200(cer22)* worms expressing the *Pegl-1::gfp* construct and treated with HU show ectopic GFP expression. Scale bar 100 μ m. (B-E) Green fluorescence quantification in s-adRP strains crossed with *Pegl-1::gfp* (simplified with the name of s-adRP strain) upon exposure to HU (B and D) and UV light (C and E). Both treatments induce GFP expression in the *strong* allele *snrp-200(cer23)*; however, no sensitivity is observed (B, N=4, n \geq 156 and C, N=3, n \geq 89). *prp-8* mutants show a reduction in the number of GFP expressing cells upon HU treatment compared to WT (D, N=2, n \geq 65), and *prp-8(cer14)* might be sensitive to UV (E, N=3, n \geq 89). Each dot represents the number of GFP expressing cells, bars represent the median with the IQR and whiskers \pm 1.5 product of IQR. Kruskal-Wallis with Dunn's post-hoc analysis between concentrations (B) and to WT conditions (B-E): *ns* indicates not significant, *** p<0.01 and **** p<0.0001.

4. b. Single molecule Fluorescence In Situ Hybridization (smFISH) allows the detection of *atl-1* induction upon splicing defects

Along with *egl-1*, the DNA damage marker *atl-1* was also upregulated upon RNAi of s-adRP genes (Rubio-Peña *et al.*, 2015). We were interested to see if our s-adRP mutants induced such upregulation and if this occurred in somatic tissues. Instead of using a reporter strain, I took advantage of smFISH, a technique that allows detection of individual transcripts, thus providing quantitative information about gene expression along with its localization. smFISH is based on the hybridization of fluorescently tagged oligonucleotides along an mRNA of interest, enriching the signal in the transcript locus resulting in discrete fluorescent foci (**Figure R. 13**). This approach not only allows the detection of specific gene expression but poly (T) tagged probes show the overall distribution of transcripts (**Supplementary Figure R. 3**).

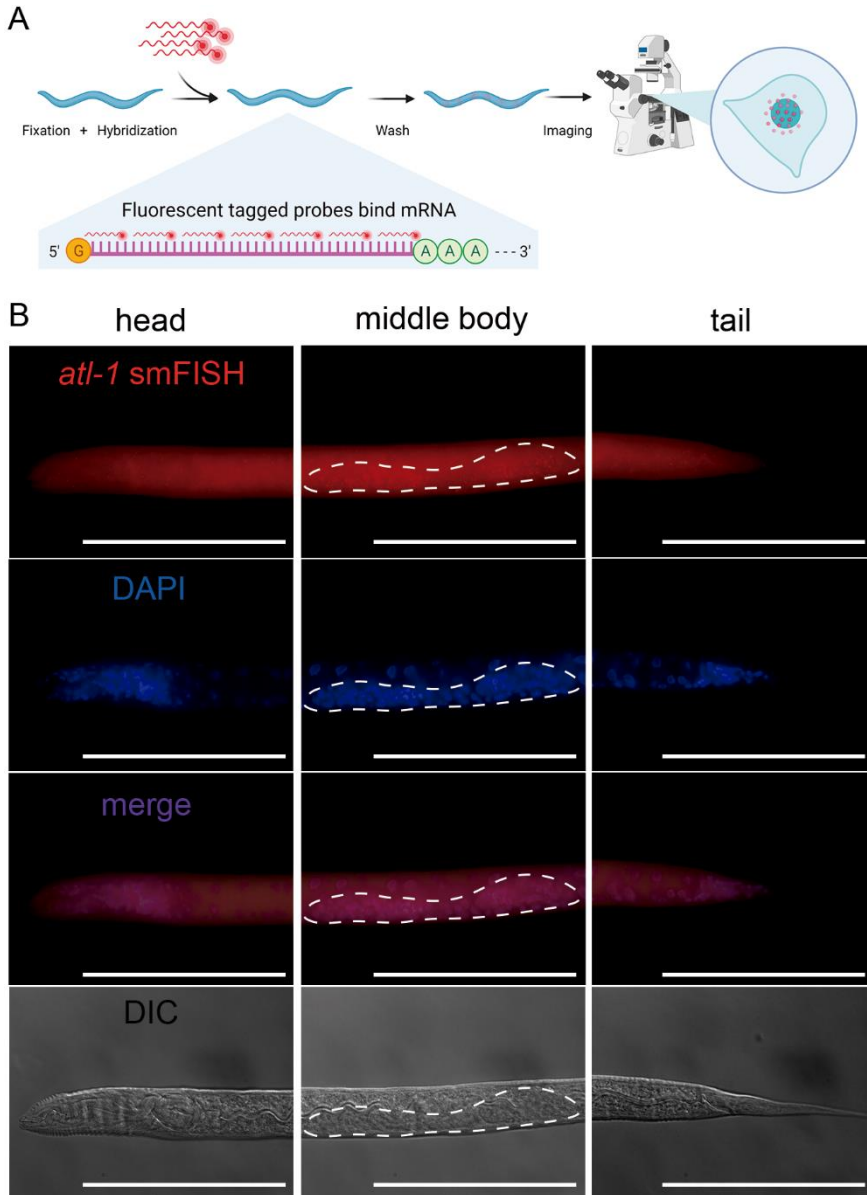


Figure R. 13: Schematic of smFISH procedure (A) and *atl-1* smFISH results in the whole animal (B). (A) In fixed animals, fluorescently tagged probes complementary to the desired transcript are incubated to allow its hybridization. After washing, the sample is visualized in an inverted fluorescent microscope. Each detected spot corresponds to a single transcript locus. (B) Images of smFISH using an *atl-1* probe with DAPI counterstaining in wildtype L3 larvae. Accumulation of foci indicates an increased expression in the germline (dashed lines), and some transcripts are also present in somatic nuclei. Scale bar 100 μ M.

atl-1 smFISH showed high expression of the gene in the germline. Unexpectedly, *atl-1* transcripts were detected in somatic cells across the whole body (**Figure R. 13 B**). We selected the *strong* allele *snrp-200(cer23)* for subsequent testing for *atl-1* upregulation in the soma. I used *prp-8(RNAi)* as a positive control as it was previously shown to strongly induce *atl-1* expression (Rubio-Peña *et al.*, 2015). As expected, *prp-8(RNAi)* caused an immense increase in *atl-1* transcription in somatic cells across the whole body (**Figure R. 14**). Neurons did not show this induction, probably due to their resistance to exogenously induced RNAi (data not shown). Such an evident increase in *atl-1* mRNA expression was not clearly seen in *snrp-200(cer23)* worms (**Figure R. 14**).

In summary, I successfully achieved detection of *atl-1* transcript through smFISH. *atl-1* expression was mainly located in germ cells; however, some signal was seen in the soma. Thus, a mild *atl-1* induction by s-adRP mutations might be camouflaged by basal signal and not clearly detected. However, the strong splicing defect induced by *prp-8(RNAi)* has clearly shown *atl-1* induction in the soma, indicating splicing defects activate DNA damage response.

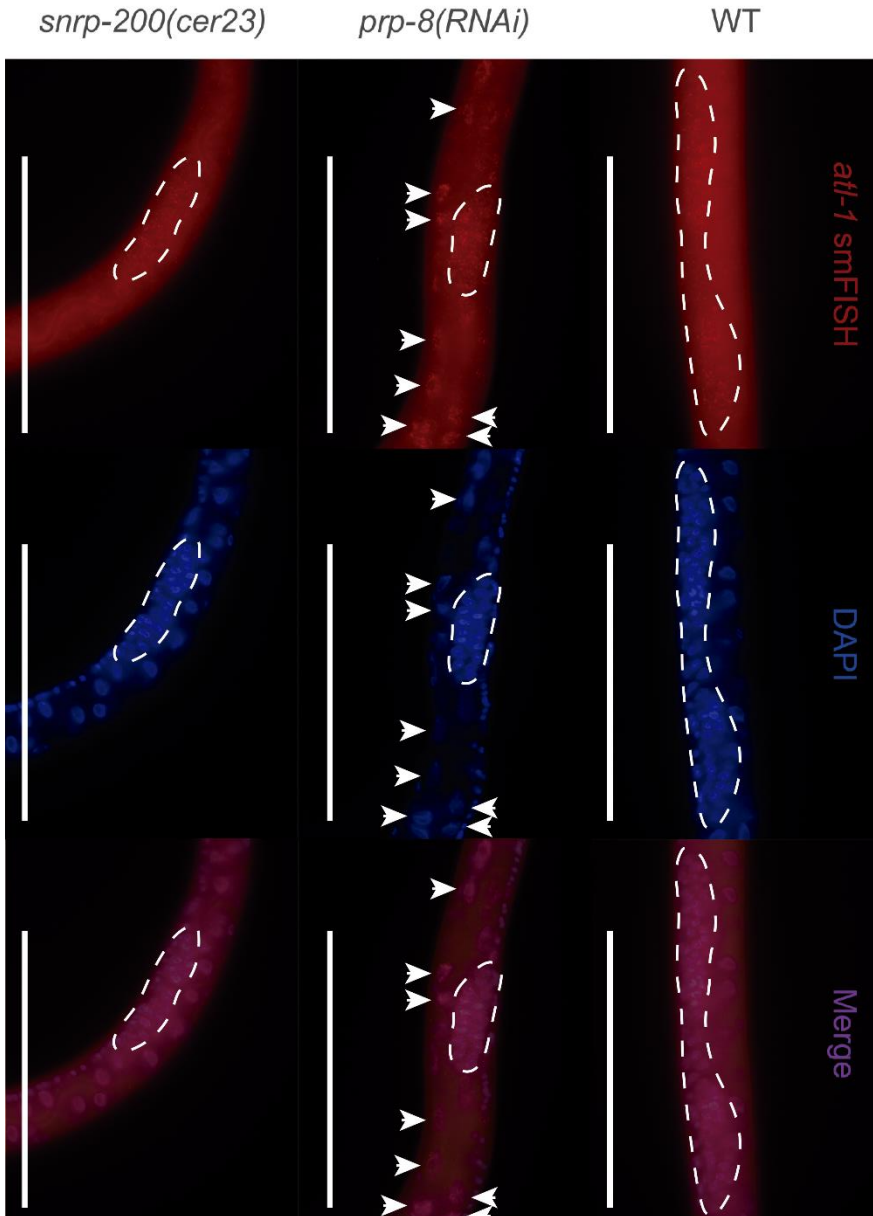


Figure R. 14: *prp-8(RNAi)* induces *atl-1* overexpression in somatic cells as revealed by smFISH. *atl-1* transcripts appear in the nuclei of somatic cells (arrows) when *prp-8* is downregulated. *snrp-200(cer23)* has no evident upregulation in somatic cells compared to WT. Scale bar 100 μ m.

4. c. Mortal germline (Mrt) phenotype of the *weak* allele *prp-8(cer22)* points towards the presence of genome instability

As *egl-1* and *atl-1* expression did not clearly show s-adRP mutations were causing apoptosis or DNA damage, we moved to a different strategy. We wondered if our s-adRP strains present mortal germline (Mrt), a phenotype observed in *C. elegans* mutants affected in telomerase activity and DNA damage checkpoints among others (Ahmed & Hodgkin, 2000; Gartner, Boag, & Blackwell, 2008; Yanowitz, 2008).

Mrt consists in a gradual reduction in brood size until complete sterility of strains maintained over generations. To test this hypothesis, at 25°C six L₁ larvae were transferred to a fresh plate every two generations, and the brood size was scored at different generations during the experiment. All alleles present a reduction in the brood size over generations, being the *strong* allele *snrp-200(cer23)* and the *weak* allele *snrp-200(cer22)* particularly affected, with the latter achieving complete sterility (**Table R. 1 and Figure R. 15**).

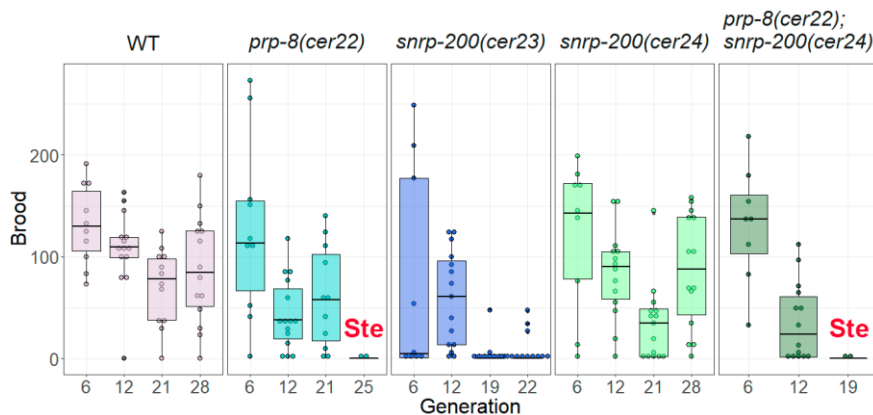


Figure R. 15: All strains present different degrees of fertility reduction at 25°C after several generations, with *prp-8(cer22)* having the most substantial effect that results in complete sterility.

Each dot represents the brood size of a single worm, and bars represent the median with the IQR and whiskers ± 1.5 product of IQR ($N=1, n \geq 8$). *prp-8(cer14)* is not included as it presents temperature-sensitive sterility at 25°C.

Table R. 1: Mrt of *prp-8(cer22)* and *prp-8(cer22); snrp-200(cer24)*.

Strain	Generation at which sterile (replicate 1/ replicate 2)
<i>prp-8(cer22)</i>	25/22
<i>prp-8(cer22); snrp-200(cer24)</i>	19/23

This experiment shows how splicing alterations derived from mimicking s-adRP mutations cause a mortal germline phenotype, which is characteristic of mutants responsible for DNA integrity, pointing thus towards the presence of DNA damage.

4.d. The synthetic interaction between the *weak* allele *prp-8(cer22)* and a mutation in polymerase (Pol) II supports splicing-transcription interplay as a possible mechanism in disease

In previous results, we detected evidence that alteration of splicing either by RNAi or s-adRP mutations induces genome instability. To investigate if the interplay between splicing and transcription plays a role in this effect, I mimicked in *C. elegans* a missense mutation of Pol II that affects its transcriptional rate (Chen *et al.*, 1996) (**Figure R. 16**). This mutation was initially identified in *Drosophila melanogaster* (Chen *et al.*, 1993), and studies in human cell lines confirmed its functional impact in splicing (Fong *et al.*, 2014).

ama-1(cer135[R743H]) has overt phenotypes and developmental delay *per se*, suggesting a functional impact on *C. elegans* transcription. I crossed the *ama-1(cer135)* with the s-adRP mutations in search of synthetic interactions. I did not observe any synergistic effect in terms of

developmental delay, embryonic lethality (Emb), or obvious phenotypes (**Supplementary Figure R. 4**).

On the contrary, brood size quantification unveiled a synthetic interaction between *ama-1(cer135)* and the *weak* allele *prp-8(cer22)* as the drop in progeny size of double mutants is not explained by the additional effect of each mutation alone (**Figure R. 17 A**).

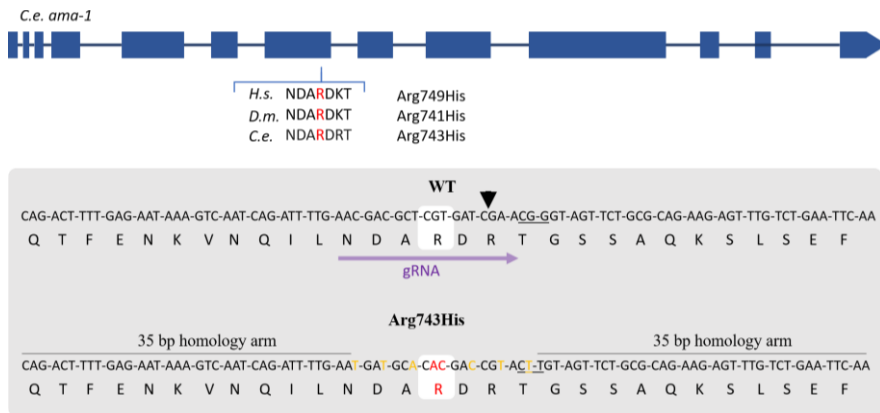


Figure R. 16: Exon-intron representation of the *ama-1* gene with the location of R743H mutation and the CRISPR-Cas9 design to model it. The R743 residue is codified in exon 7 of the gene. Local alignment between human (*H.s.*), *D. melanogaster* (*D.m.*), and *C. elegans* (*C.e.*) shows the residue of interest is conserved. The top row of the shadowed grey area pictures the edited region with the codon of interest (white shadow). The PAM sequence is underlined with the cut site indicated by an arrow. The gRNA direction is depicted. The bottom row shows the repair template provided with 35-bp homology arms, the missense mutation of interest (red), and silent mutations (orange) introduced to avoid re-cutting by Cas9 and to facilitate genotyping by PCR.

In summary, s-adRP mutations could produce genome instability as suggested by the Mrt phenotype. Moreover, the interaction of the *weak* allele of *prp-8(cer22)* with the *ama-1(cer135)* missense mutation indicates splicing defects have an impact on transcription, suggesting a plausible mechanism for genome instability.

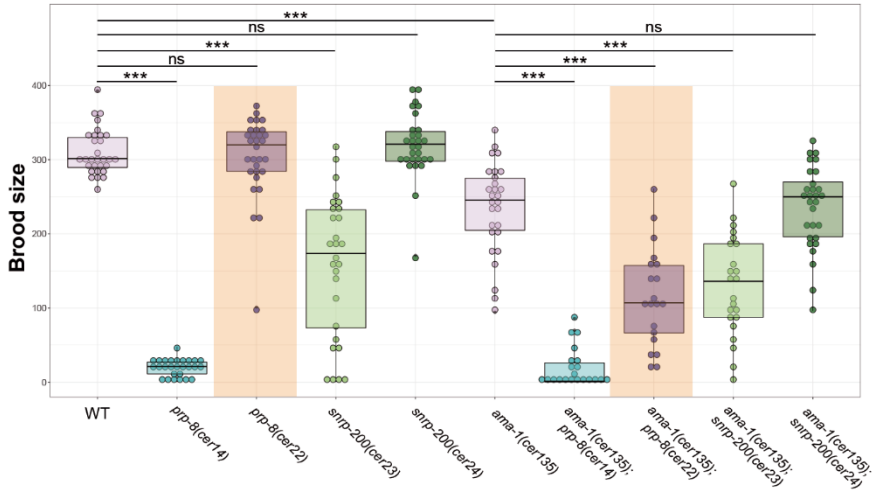
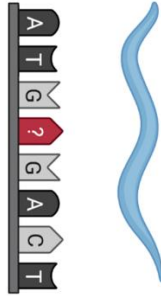


Figure R. 17: Brood size characterization revealed a synthetic interaction between *ama-1(cer135)* and the weak allele *prp-8(cer22)*. Brood size of s-adRP mutants alone and on the *ama-1(cer135)* background grown at 20°C. Shaded areas denote *prp-8(cer22)* alone and crossed with *ama-1(cer135)* mutant. Each dot represents the brood size of a single worm, and bars represent the median with the IQR and whiskers ± 1.5 product of IQR (N=2, $n \geq 21$). Kruskal-Wallis with Dunn's post-hoc analysis: ns indicates not significant and *** $p < 0.001$.

5. Diagnosis: *C. elegans* s-adRP models could be helpful for variants of uncertain significance (VUS) evaluation



Many RP patients still do not have a genetic diagnosis justifying the need for detection of novel genes and mutations involved (Zhang, 2016; Verbakel *et al.*, 2018; Birtel *et al.*, 2019). Genome and exome sequencing are being actively implemented into clinics for this task. By sequencing, lots of mutations and variants have been identified; however, it is not always easy to establish if such genetic modifications are causing disease, especially in the case of novel mutations (missense or isolated cases). We propose using *C. elegans* to model newly identified variants and VUS to assess its potential implication in RP through functional assays or association with biomarkers.

Our results demonstrate how some phenotypic features might be used as indicators of altered function in s-adRP mutants, such as the presence of postembryonic or germline phenotypes and interaction with *cyn-15(cer173)* or *ama-1(cer135)* mutants. In this section, we expand the panel of parameters that can be used for VUS study. As proof of principle, we examined a VUS identified by our collaborator Dr. Miguel Carballo.

5. a. *snrp-200(cer23)* strong allele produces specific AS events that might serve as s-adRP markers

The advent of third generation sequencing techniques allows sequencing of whole transcripts facilitating the identification of AS events that might be missed with the assembly of short-read sequencing. PacBio and Oxford Nanopore Technologies (ONT) are the leading companies in those technologies. Conveniently, ONT offers the affordable, portable device MinION with a protocol that enriches the sample for full transcripts. Moreover, nanopore sequencing is not only suitable for DNA, but it can directly sequence RNA molecules, avoiding bias induced by enzymatic retro-transcription or PCR amplification and providing information about RNA modifications.

We decided to take advantage of nanopore-based technology for the identification of AS events specific to s-adRP mutations. I proceeded with the RNA sequencing from mixed populations of WT and *snrp-200(cer23)*, as this is a *strong* allele and would presumably present more alterations. Two approaches were followed: cDNA-PCR and direct-RNA-based sequencing. The former relies on reverse transcription and PCR amplification of transcripts with primers that would enrich the sample for full transcripts. In contrast, the latter allows direct sequencing of RNA molecules avoiding enzyme-induced bias (**Figure R. 18**). Since we were interested in qualitative changes rather than quantitative, we sequenced each sample once.

For both direct RNA and cDNA-PCR approaches, WT samples led to smaller yields than those of the mutant as WT samples were the first to be sequenced and were thus subjected to protocol optimization. Direct RNA sequencing produced fewer reads than the cDNA-PCR approach; however, the quality filtering, which indicates the reliability of the signal for base calling, showed slightly better results for direct RNA. However, the cDNA-

PCR absolute number of profitable reads is higher due to better performance in the total sequenced transcripts (**Table R. 2**). In both cases, reads that are filtered out correspond to smaller lengths (**Figure R. 19**). Curiously, the mean and median read lengths, as well as the longest read sequenced, are longer without amplification compared to PCR amplified samples. A closer look at the read length distribution shows over-representation of fragments around 1000 bp in cDNA-PCR compared to direct RNA, thus explaining the shift of the read length parameters and indicating PCR bias towards these lengths (**Table R. 2; Figure R. 20**).

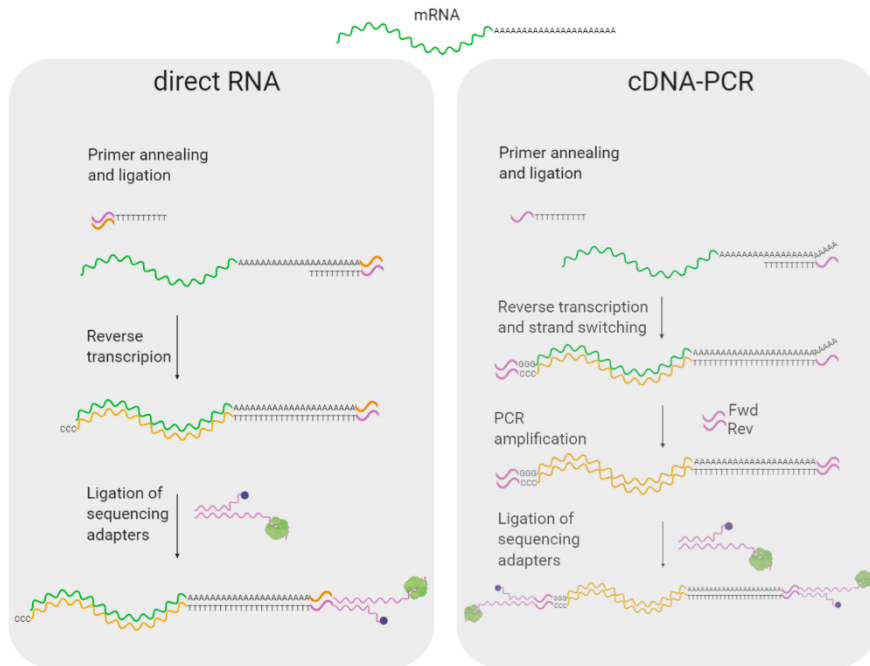


Figure R. 18: Comparison of sample preparation in direct RNA sequencing and cDNA-PCR approach. In direct RNA method, an optional reverse transcription step is followed by adapters ligation needed for sequencing. Although a retro-transcription is performed to enhance sequencing, mRNA remains as the sequenced molecule. In cDNA-PCR method, PCR amplification is performed before adapter ligation, and cDNA is the molecule being sequenced

Table R. 2: Sequencing results characteristics.

Kit Sample	direct RNA		cDNA-PCR	
	WT	<i>snrp-200</i> (<i>cer23</i>)	WT	<i>snrp-200</i> (<i>cer23</i>)
total reads	812.926	2.262.147	4.246.298	8.556.627
%QC filter passed	93,9%	96,5%	81,8%	81,4%
Mean read length	1.048 bp	1.079 bp	972 bp	858 bp
Median read length	1.322 bp	1.357 bp	1.157 bp	1.044bp
Longest read	16.541bp	22.116 bp	9.486 bp	9.181 bp

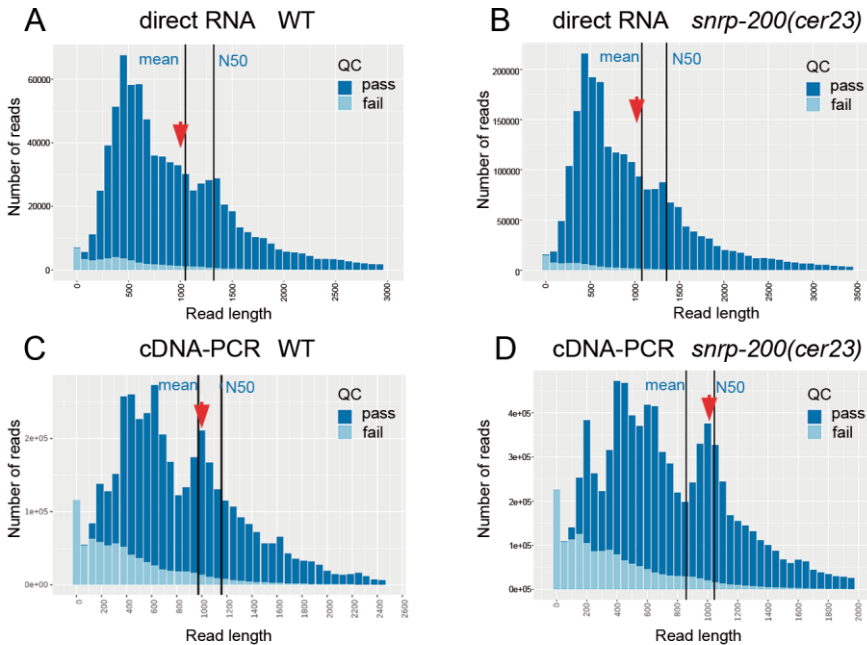


Figure R. 19: Histograms of the distribution of reads by length. Distribution of quality-control (QC) passed and failed reads of direct RNA (A and B), and cDNA-PCR (C and D) approaches. Mean read length and median (N50) are depicted. Overall, a preference towards smaller reads during sequencing is observed. In all cases, reads that fail to pass QC are primarily encountered in the lower range of lengths. The red arrow points to the enrichment of reads seen in cDNA-PCR compared to the absence in direct RNA approach around 1000 bp, indicating a possible PCR bias.

Nanopore sequencing is a relatively new technique, so there is not much user-friendly software for data analysis available. cDNA-PCR data were subjected to the analysis due to higher amounts of total reads sequenced. I applied a pipeline developed and released by the Nanopore community to identify novel isoforms by comparing the transcripts from our dataset to an annotated reference transcriptome (**Figure R. 20**).

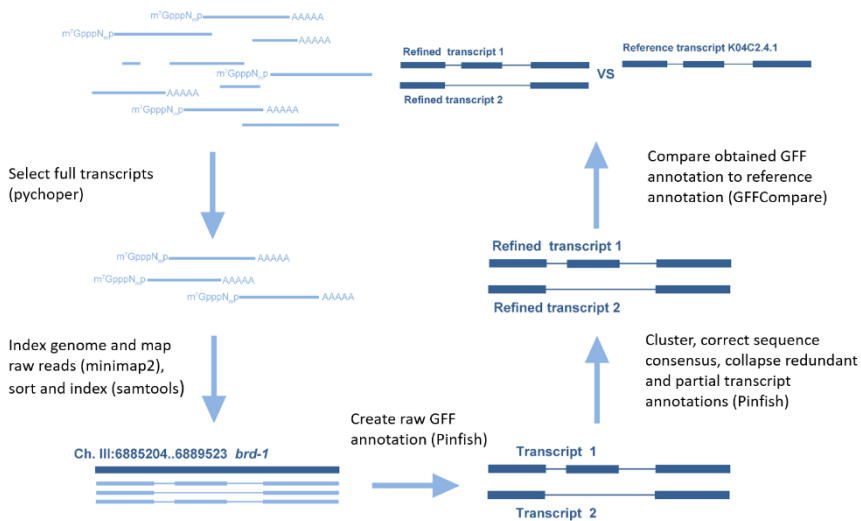


Figure R. 20: Simplified schematic of the analysis pipeline applied. Steps are indicated with the bioinformatic tools in parentheses. After selection for complete transcripts and alignment, an annotation GFF file is generated. After several phases of refinement, the generated annotation from sequencing is compared to the reference, and alternative intron-exon boundaries are identified.

Afterward, manual curation of the candidates was performed, and only high confidence hits were subjected to the posterior validation, and double checked with the direct RNA sequenced samples (**Figure R. 21**).

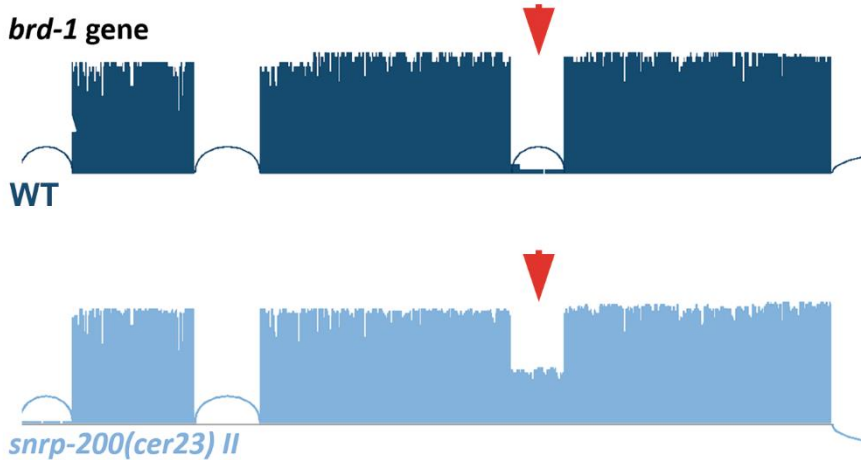


Figure R. 21: Example of coverage histograms showing an intron retention event in the *brd-1* gene. Reads that cover the whole transcript are enriched with the bioinformatic pipeline, providing coverage histograms that nicely reproduce exon (bars) and intron (bridges) boundaries. The red arrow points to the intron between exons 8 and 9 where no mapped reads are observed in the wildtype; however, around half of the reads map to this location in the *snrp-200(cer23)* mutant.

Curiously, even the WT sample led to the identification of several novel exon-intron boundaries compared to the annotated transcriptomic data. I only considered events observed in the *snrp-200(cer23)* dataset and not in the WT. This approach led to the identification of AS events present in *snrp-200(cer23)* and completely or nearly completely absent in the WT. Six of such events were selected for further validation: *brd-1*, *rnf-1*, *pcm-1*, C05C10.7, F11A10.6, and *ugt-50*. (Table R. 3).

Table R. 3: Summary of the hits' numbers from the bioinformatic pipeline and manual curation.

Sample	Hits from pipeline (n° transcripts/ n° genes)	Manual revision (n° total/ n° to validate)
WT	352 / 322	10 / 6 to validate
<i>snrp-200(cer23)</i>	530 / 479	

I performed a semiquantitative RT-PCR on the RNA extracted from mixed populations to validate AS events with primers specifically designed to distinguish different isoforms. *brd-1* and C05C10.7 present intron retention events while *rmf-1* and F11A10.6 present exon skipping.(**Figure R. 22**).

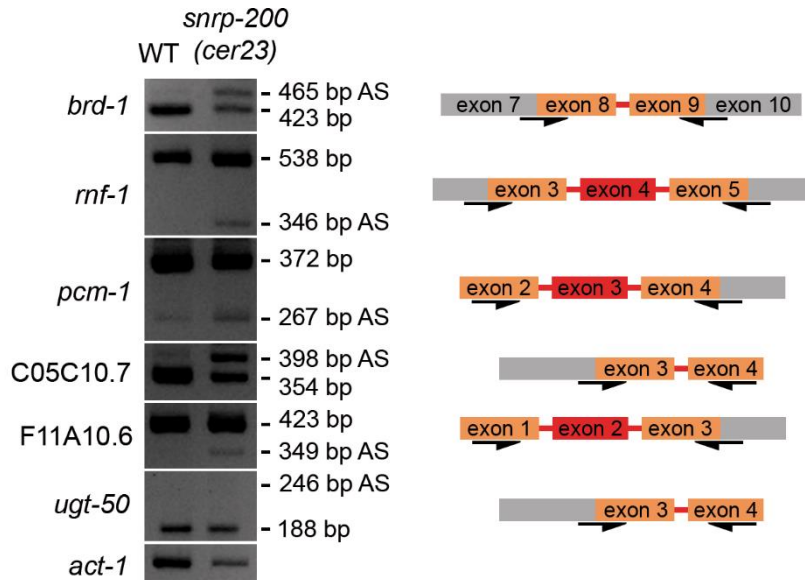


Figure R. 22: Four out of six candidates were successfully validated by semiquantitative RT-PCR. On the left, gels showing electrophoresis results with the alternatively spliced (AS) and canonically spliced transcript sizes depicted. On the right, a schematic of the design of primers (arrows) for the semiquantitative RT-PCR and affected introns and exons (red) are shown. Only *brd-1*, *rmf-1*, C05C10.7, and F11A10.6 clearly show alternative splicing events. Intron retention is observed in *brd-1* and C05C10.7, while *rmf-1* and F11A10.6 show exon skipping. Actin (*act-1*) was used as an endogenous control.

To see if such events occur in other s-adRP mutants, I performed a semiquantitative-PCR from RNA extracted from other strains. I firstly used synchronized populations grown at 25°C at 27 h (L3/L4 stage), 40 h (Young adults with no embryos inside), and 50 h (Egg-laying adults) post L1. The strong allele *prp-8(cer14)* was the only allele with visible defects on *brd-1*, *rmf-1*, and C05C10.7 at 50 h (**Supplementary Figure R. 5**). A re-extraction of RNA of mixed populations and of embryos purified with hypochlorite

treatment showed that *snrp-200(cer23)* reproducibly presents AS events on *brd-1*, *rnf-1*, and C05C10.7 during embryonic development. However, the low AS signal cannot fully explain the differences observed in the mixed populations, suggesting other stages might be affected. (**Figure R. 23**).

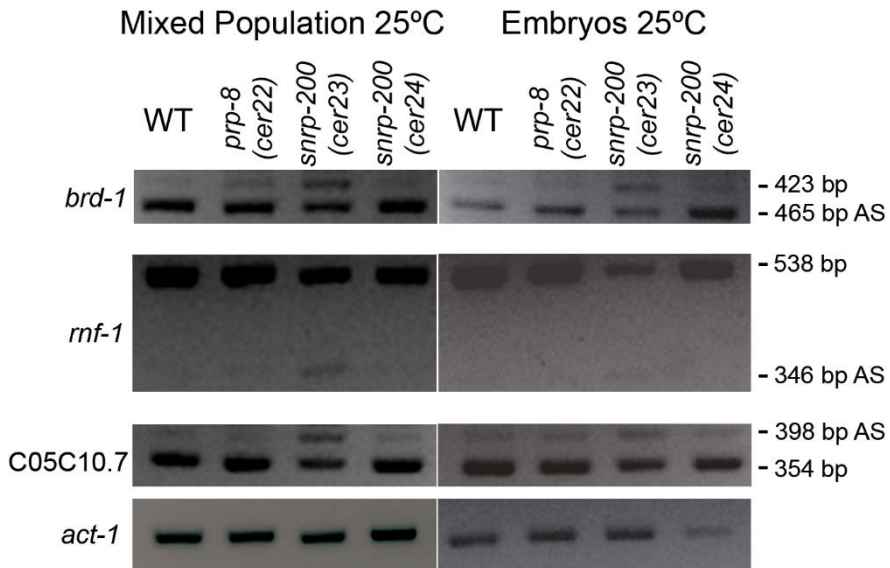


Figure R. 23: Semiquantitative RT-PCRs of mixed population (left) and embryos (right) show AS events in *brd-1*, *rnf-1*, and C05C10.7. Gels showing electrophoresis results with the alternatively spliced (AS) and canonically spliced transcript sizes depicted. AS in three of the validated genes are enriched only in *snrp-200(cer23)* mutant after RNA extraction. Actin (*act-1*) was used as an endogenous control.

Summing up, I demonstrate how nanopore-based technology can be used to identify AS events specific to some s-adRP mutants. These events are amenable to be used as molecular markers to evaluate newly identified mutations and VUS related to s-adRP, helping thus in the evaluation of pathogenicity.

5. b. Herboxidiene (HB) and α -amanitin treatment does not clearly magnify s-adRP alterations

The genetic interactions between the deletion allele of *cyn-15(cer173)* or *ama-1(cer135)* and the *weak* allele *prp-8(cer22)* are indicative of how splicing or transcriptional defects could magnify functional alterations produced by a splicing-related mutation without overt phenotypes. This points to a strategy to identify functional alterations produced by VUS in splicing-related genes.

While *C. elegans* has a short life cycle, a genetic cross is needed to assess such interaction between VUS and genetically altered splicing or transcription, slowing the evaluation process. To overcome this hindrance, we explored the use of two small molecules: herboxidiene (splicing modulator) (Hasegawa *et al.*, 2011) and α -amanitin (affects transcription) (Montanaro, Novello, & Stirpe, 1971) to induce splicing and transcriptional defects.

HB targets SF3B1, a splicing factor recurrently mutated in myelodysplastic syndrome and other tumors (Bonnal, López-Oreja, and Valcárcel 2020). A former member of the lab (Xènia Serrat) tested HB on *C. elegans* and did not observe any response due to slight differences in the drug binding pocket of SFTB-1 (worm homolog of SF3B1). She introduced small modifications by CRISPR-Cas9 to resemble the human structure of the protein in the drug binding site (*sftb-1(cer144)*), thus sensitizing *C. elegans* to HB (Serrat *et al.*, 2019). I crossed *snrp-200* s-adRP mutants and the slow Pol II *ama-1(cer135)* with *sftb-1(cer144)* while the double mutant *prp-8(cer22); sftb-1(cer144)* was CRISPR-Cas9 engineered by X. Serrat as both genes are located in the same chromosome. HB treatment on the humanized background was successful, but hypersensitivity in s-adRP mutants was not observed. In the *strong* allele *snrp-200(cer23)* and the slow Pol II allele *ama-1(cer135)*, resistance is seen by a mechanism that we still

do not understand. In any case, differences between the WT and s-adRP mutants were not as overt as we would like to implement HB to identify the functional impact of VUS (**Figure R. 24**).

To test whether pharmacological alteration of transcription enhances s-adRP functional impact, we used α -amanitin, a drug that targets Pol II affecting its transcriptional rate. As in the case of HB, this drug causes larval arrest of the worms. Curiously, a previous screen for α -amanitin resistant mutants in *C. elegans* discovered *ama-1(m322)* mutation (Rogalski, Bullerjahn, & Riddle, 1988), which was later identified as equivalent to the slow Pol II *D. melanogaster* R741H (Bowman, Riddle, & Kelly, 2011). We tested α -amanitin on the *ama-1(cer135)* allele, which presented resistance to the drug as expected (**Figure R. 25**). However, I did not detect α -amanitin sensitivity in s-adRP mutants in different drug concentrations. Thus, we discarded the use of α -amanitin as a rapid test for uncovering the functional impact produced by s-adRP mutations (**Figure R. 25**).

In summary, pharmacological impairment of splicing with HB and transcription with α -amanitin failed as rapid tests to detect the functional impact of s-adRP mutations.

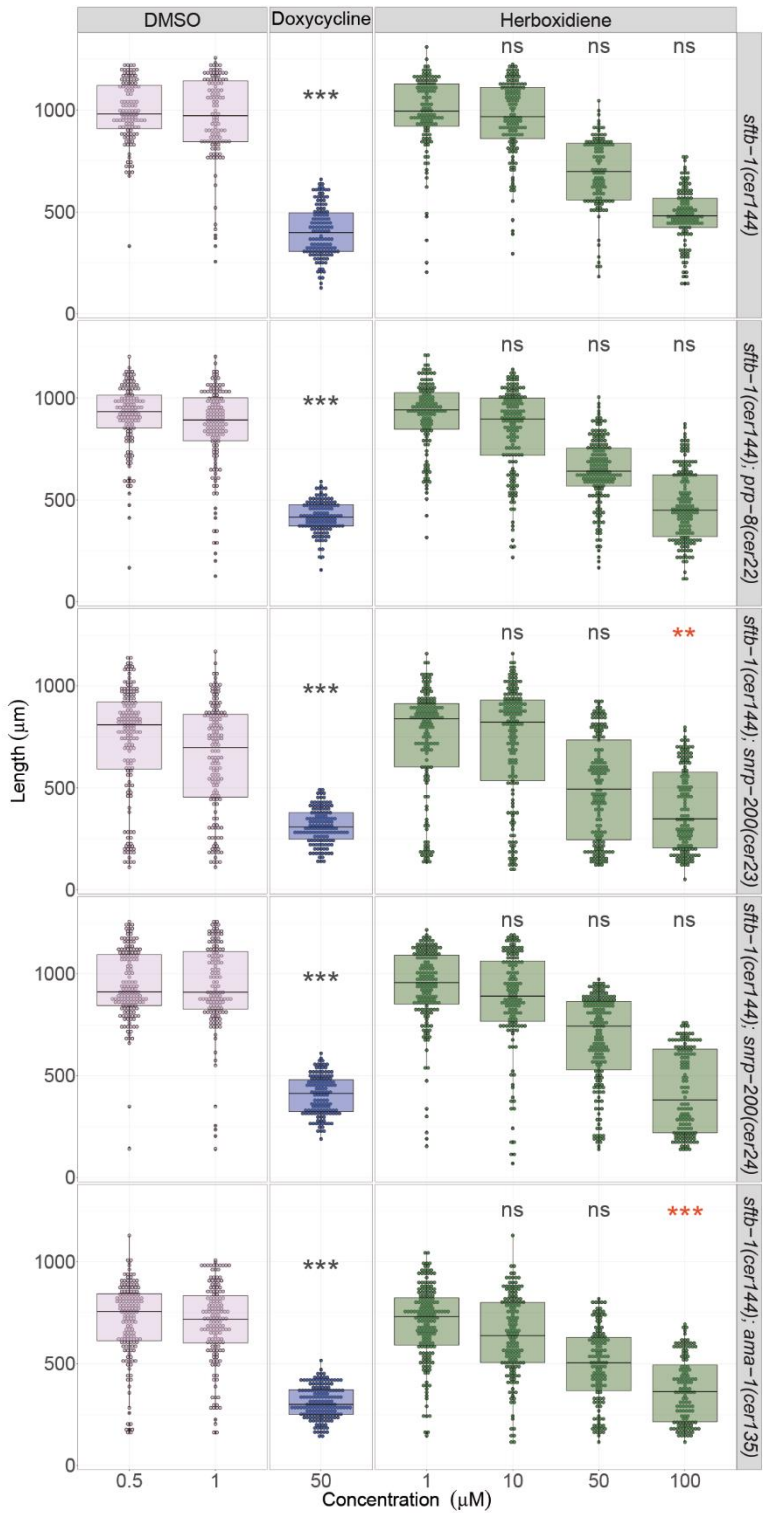


Figure R. 24: Herboxidiene induces sensitivity of the *strong* allele *snrp-200(cer23)* and the slow Pol II mutant *ama-1(cer135)*.

Worm length of WT and s-adRP strains upon treatment with herboxidiene and doxycycline as a positive control (N=3, n \geq 123). Each dot represents the length of an individual worm, box plot indicates the median with the IQR, and whiskers the ± 1.5 product of IQR. The difference between control concentration 0 and the tested drug concentrations of the WT was compared to the difference of the mutants. Aligned rank transformation followed by two-way ANOVA and F test to test interaction was applied. *ns* indicates not significant, ** p<0.01 and *** p<0.001. The positive and negative control conditions were compared by a Mann-Whitney test. The red color of the asterisks indicates that the observed differences stand against our initial hypothesis of sensitivity.

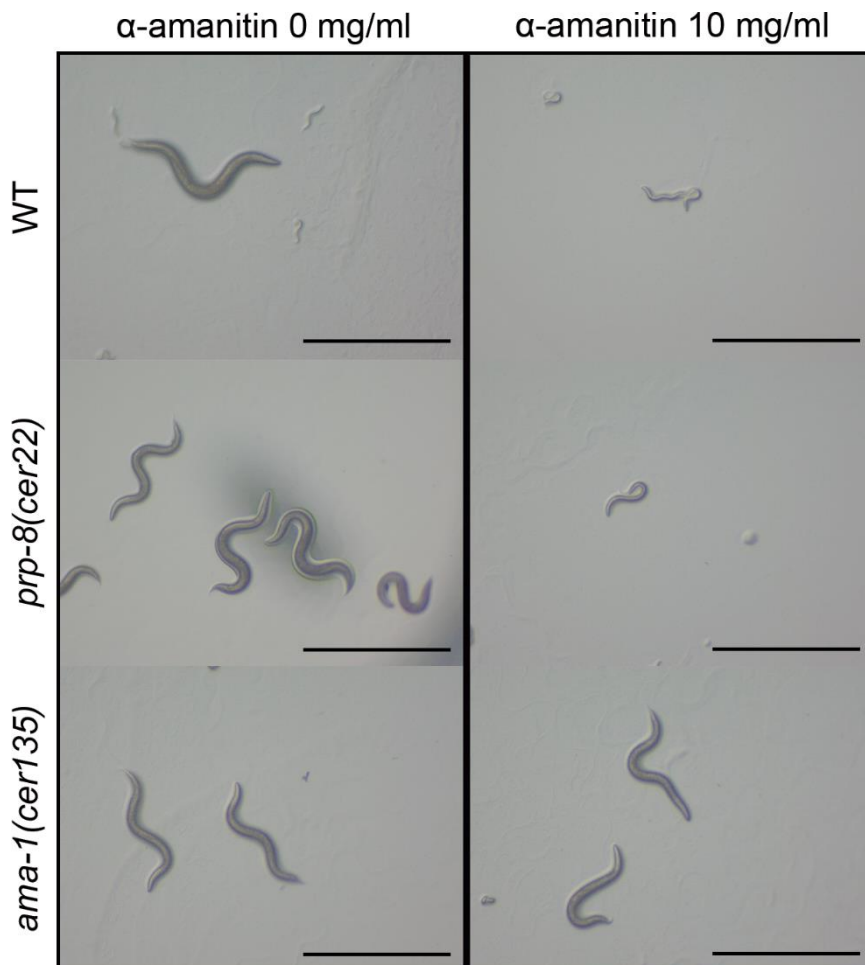


Figure R. 25: Representative picture of α -amanitin-treated *weak* allele *prp-8(cer22)* and the slow Pol II *ama-1(cer135)*. α -amanitin induces larval arrest in the WT and the s-adRP mutant but not in the *ama-1(cer135)* mutant. Scale bar 1 mm.

5. c. Gamma radiation seems to have a stronger effect on the weak allele *snrp-200(cer24)*

A pharmacological approach to enhance the functional consequence of s-adRP mutations did not give the expected result. Thus, we induced DNA damage with gamma radiation as an additional agent that may uncover the sensitivity of these mutants to DNA damage. A synchronized population of L1 worms was irradiated with different doses of gamma radiation, and the size of survivors was measured at 72 h. As a positive control, a strain from the *C. elegans* knockout consortium with mutations in *met-2* and *set-25* was used, as it was previously reported to present genome instability (Zeller *et al.*, 2016). *met-2(n4256); set-25(n5021)* animals show sensitivity to gamma radiation as expected, and the weak allele *snrp-200(cer24)* was also sensitive (**Figure R. 26**).

This preliminary data suggests gamma radiation could be used for VUS testing, and it encourages a more profound study of this effect.

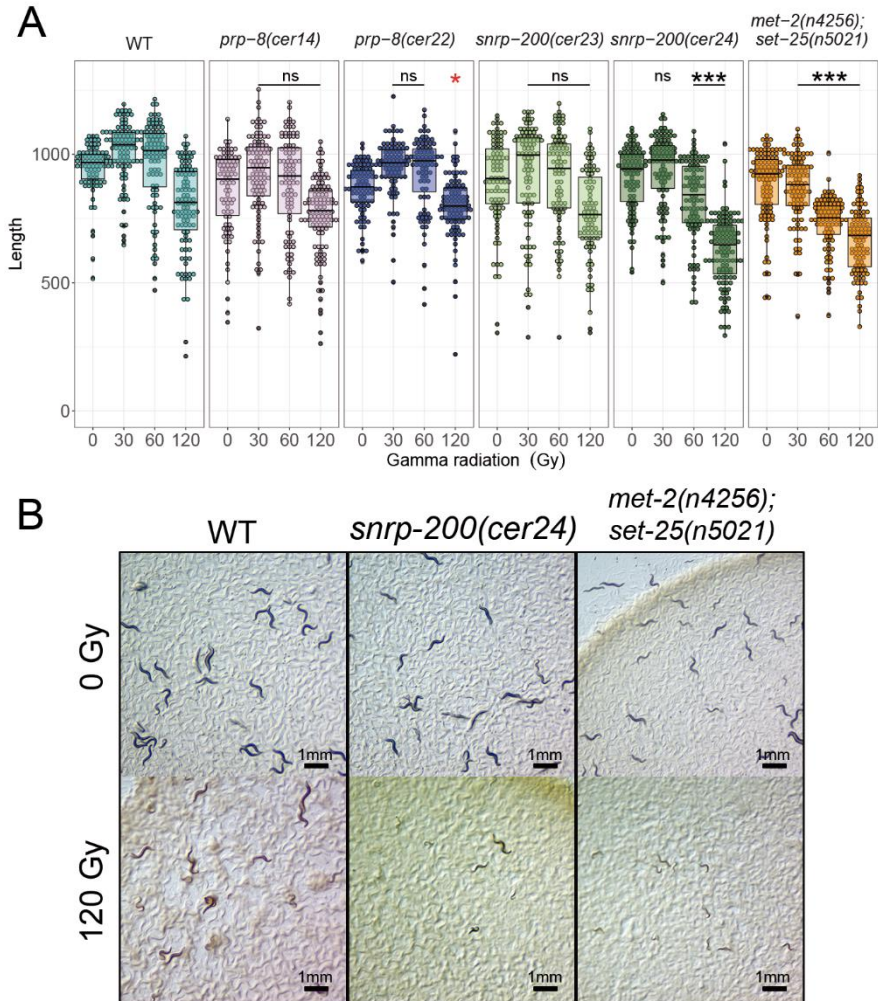


Figure R. 26: Weak s-adRP *snrp-200(cer24)* mutant is sensitive to gamma radiation.

(A) Worm length upon irradiation with different doses of gamma radiation ($N=1$, $n \geq 81$). Each dot represents the length of an individual worm, box plots indicate the median with the IQR, and whiskers the ± 1.5 product of IQR. The difference between dose 0 and each of the tested doses of the WT was compared to the difference of the mutants. Aligned rank transformation followed by two-way ANOVA and F test to test interaction was applied. *ns* indicates not significant, * $p < 0.05$ and *** $p < 0.001$. The red asterisk indicates apparent resistance of the strain. (B) Representative images of WT and sensitive strains. The sensitivity is detectable even without quantification.

5. d. Generation of a panel of features to test patient-derived VUS functional impact

With the previously obtained results, we gathered a panel of features derived from our s-adRP mutants that can indicate if a given mutation has a functional impact. These features might be helpful to provide functional data about VUS and therefore help in the assessment of their pathogenicity (Table R. 4).

Table R. 4: Panel of features identified in s-adRP mutants

	<i>prp-8(cer14)</i>	<i>prp-8(cer22)</i>	<i>snrp-200(cer23)</i>	<i>snrp-200(cer24)</i>
1 Overt phenotypes	+	-	+	-
2 Veiled phenotypes (Gro, Rbs, Mrt...)	+	+	+	+
3 <i>cyn-15(cer173)</i> interaction	-	+	-	-
4 <i>ama-1(cer135)</i> interaction	-	+	-	-
5 Detected AS events	+	-	+	-
6 Sensitivity to gamma radiation	-	-	-	+

Gro: Growing defects; Rbs: Reduced brood size; Mrt: Mortal germline.

To determine whether this panel can be used for VUS characterization, I mimicked the *PRPF8* Ala2125Thr variant (*prp-8(cer210[A2118T])* in *C. elegans*), a VUS that was identified by the team of our collaborator Dr. Miguel Carballo at Terrassa hospital. There is not enough information to classify it as a pathogenic or benign variant, remaining thus as a VUS. Along with this mutation, the in frame pathogenic Val2325_Glu2330 deletion of *PRPF8* (*prp-8(cer209T2319_E2325del)*) in *C. elegans* was mimicked (Martínez-Gimeno *et al.*, 2003) (Figure R. 27).

Notably, the generation of the VUS variant was achieved by a modified version of the Cas9 enzyme named SpG Cas9 (Walton *et al.*, 2020), which presents missense mutations that permit edition in NGN PAM sequences

instead of the conventional NGG. Thus, we provide data on *in vivo* use of SpG Cas9, which expands the spectrum of potentially editable genome regions (**Figure R. 27**).

I began with the characterization of the growing delay (Gro) phenotype and the identification of AS defects in both mutants. None of the mutants seems to present developmental delay or AS defects described above (**Figure R. 28**). Other features described in the panel still have to be further assayed.

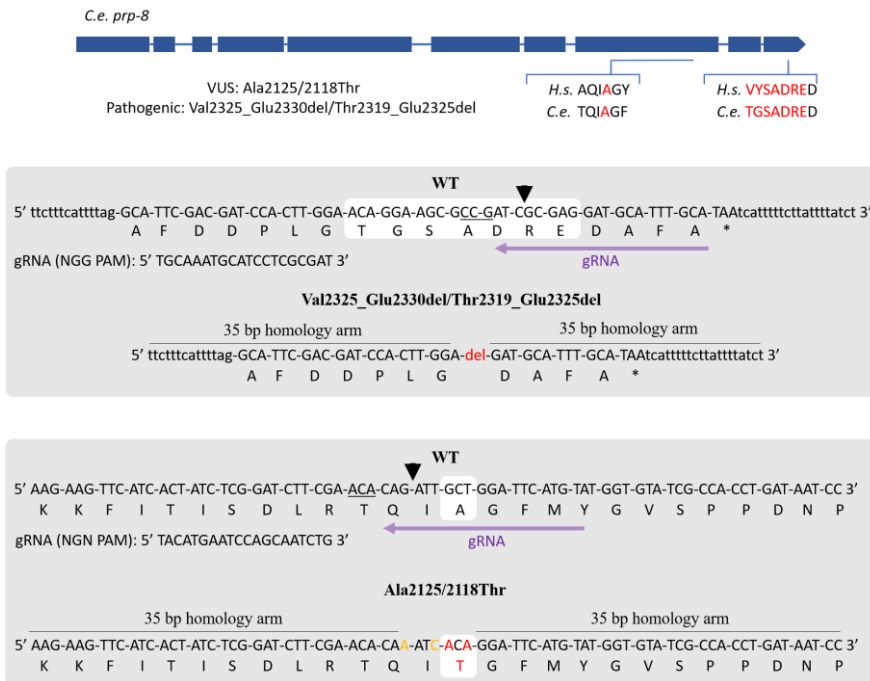


Figure R. 27: Exon-intron representation of *prp-8* gene with the location of A2118T and T2319_E2325del mutations and the CRISPR-Cas9 designs.

A2118 residue is located in exon 8, alignment between human (*H.s.*) and *C. elegans* (*C.e.*) shows the residue of interest is conserved. T2319_E2325del locates at the last exon, and five of seven affected residues are conserved. The top of the shadowed grey area pictures the edited region with the codon of interest (white shadow). PAM is underlined with the cut site indicated by an arrow. The gRNA direction and sequences are depicted. On the bottom, the repair template provided with 35 bp homology arms, mutations of interest (red), and silent mutations (orange) to avoid re-cutting by Cas9 and facilitate genotyping by PCR are shown. Capital letters denote exon sequences and lowercase introns.

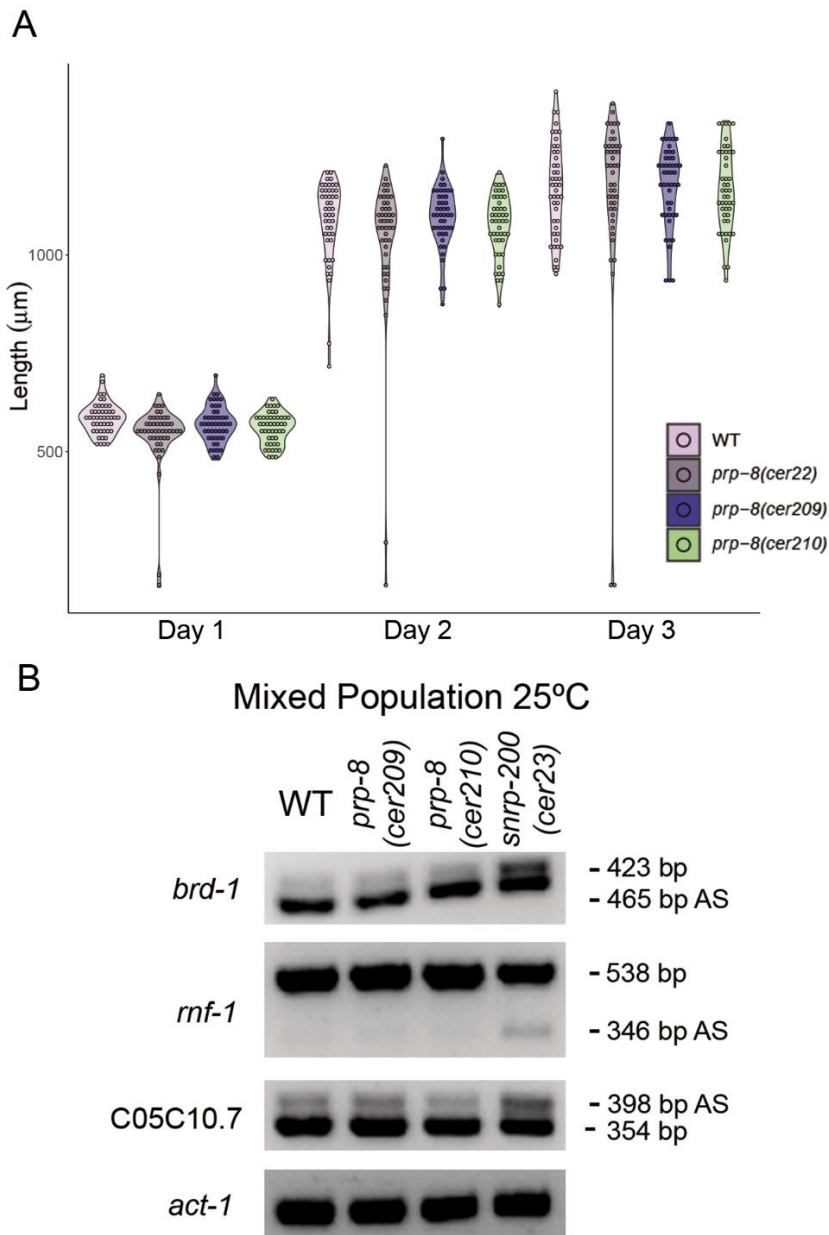


Figure R. 28: Developmental delay or AS are not present in the VUS $prp-8(cer210[A2118T])$ or the pathogenic variant $prp-8(cer209T2319_E2325del)$.

(A) Violin plot of the length distribution of a synchronized population across time at 20°C, each dot represents the length of an individual worm (N=1, n \geq 45). (B) Gels showing electrophoresis results with the alternatively spliced (AS) and canonically spliced transcript sizes depicted. $snrp-200(cer23)$ is used as a positive control. Actin (*act-1*) is used as an endogenous control.

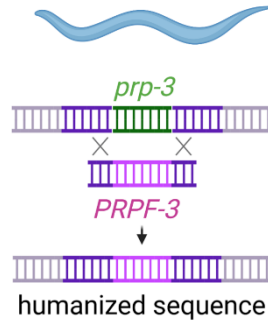
RESULTS

The current data does not support the presence of a functional impact by the newly engineered VUS and the pathogenic deletion; however, further validation is needed. Nevertheless, we show the ease of CRISPR-Cas9 to model novel mutations in *C. elegans*. The usage of SpG Cas9 *in vivo* demonstrates the ability of a more flexible Cas9 use on NGN PAM, expanding the editable genome. And finally, we propose a panel of features to evaluate the functional impact of VUS, which might have a clinical impact.

6. Improvement of s-adRP models: *prp-3*

gene tolerates partial sequence

humanization



Splicing genes are highly conserved across evolution from yeast to humans. *C. elegans* is not an exception. Most of the s-adRP missense pathogenic variants are amenable to be modelled by CRISPR-Cas9 (**Supplementary Table I. 1**). However, subtle differences in protein sequences can have a substantial impact on the function. One example is the humanized *sftb-1* in which only five residue changes are sufficient to provide sensitivity to HB (Serrat *et al.*, 2019). Thus, functional alterations provoked by s-adRP mutations in human proteins might be missed when modelled in other organisms. To overcome this obstacle, we decided to explore the humanization of the *prp-3* gene by substituting the coding sequence for the human *PRPF3* in the endogenous locus.

6. a. *prp-3* allows partial humanization

Previous efforts of functional replacement in *C. elegans* have been focused on non-essential genes and did not conserve all endogenous regulatory regions (McDiarmid *et al.*, 2018; Zhu *et al.*, 2020). To begin with the functional replacement of s-adRP genes, we chose PRP-3 due to its relatively small size and number of exons, and the fact that s-adRP mutations are clustered in a short region. PRP-3 presents an additional challenge to achieving a functional replacement as it is a core splicing factor and it is thus essential for worm viability. Human PRPF3 is slightly larger in length compared to PRP-3 and has an additional domain in the C-terminus. Still, the PRP3 and DUF1115 domains are conserved, suggesting the human protein might be functional in *C. elegans* (**Figure R. 29**).

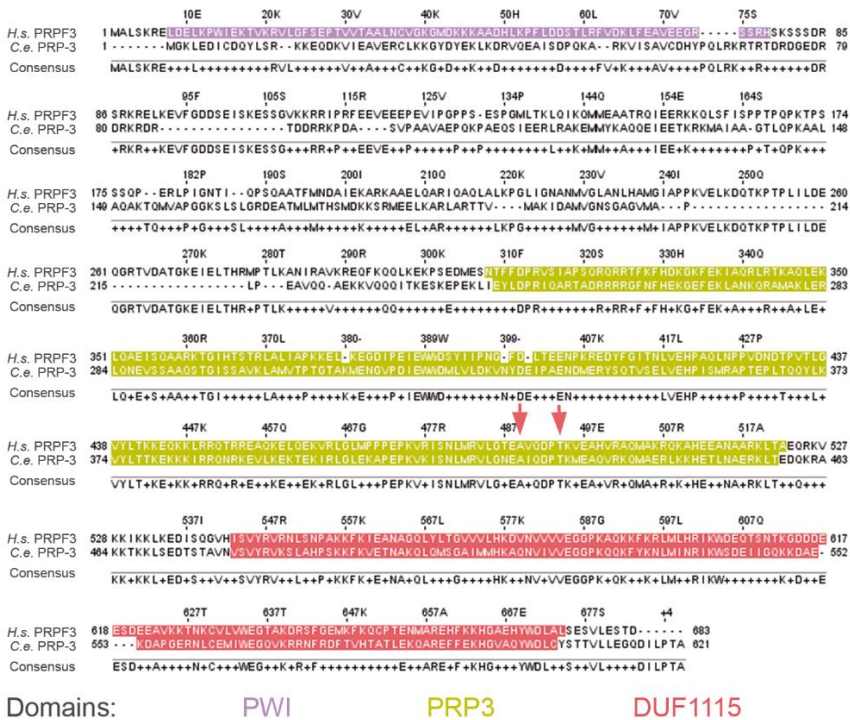


Figure R. 29: Alignment of human PRPF3 and *C. elegans* PRP-3 shows PRP3 and DUF1115 domains are conserved.

Colour shades denote identified domains in each of the proteins. Red arrows mark s-adRP mutations selected for mimicking.

Moreover, we intended to preserve as much as possible the regulatory regions of the gene, while modifying the encoded protein. To achieve this aim, our approach was based on exon-by-exon substitution of the *C. elegans* sequence for human coding PRPF3. (**Figure R. 30 A**).

I proceeded with the humanization of the exon 3, where s-adRP mutations occur. To substitute the desired sequence, two Cas9 cuts at each of the ends of the exon were performed, and a double-stranded DNA (dsDNA) donor containing the human homolog sequence for this region was provided. The resulting strain contains a chimeric PRP3 domain and the remaining protein intact (**Figure R. 30 A and B**). The attempt to substitute exon 3 was successful, and the resulting human-*elegans* hybrid PRP-3 protein was at least partially functional as the strain was viable.

Then, I proceeded with the humanization of the largest exon of the gene, exon 2 (**Figure R. 30 C**). Fortunately, my attempt to replace exon 2 was successful, albeit the strain was not viable in homozygosis.

Our work shows that complete humanization of an essential splicing gene in the endogenous locus might not be possible; however, I achieved partial humanization of nearly 25% of the protein. This strain might serve as a platform for variant modelling. Thus, my current work is centred on modelling two s-adRP mutations: Ala489/425Asp and Thr494/430Met (*H.s./C.e.* numbering) (**Figure R. 29**) in the WT and partially humanized backgrounds to inspect if humanization improves s-adRP modelling.

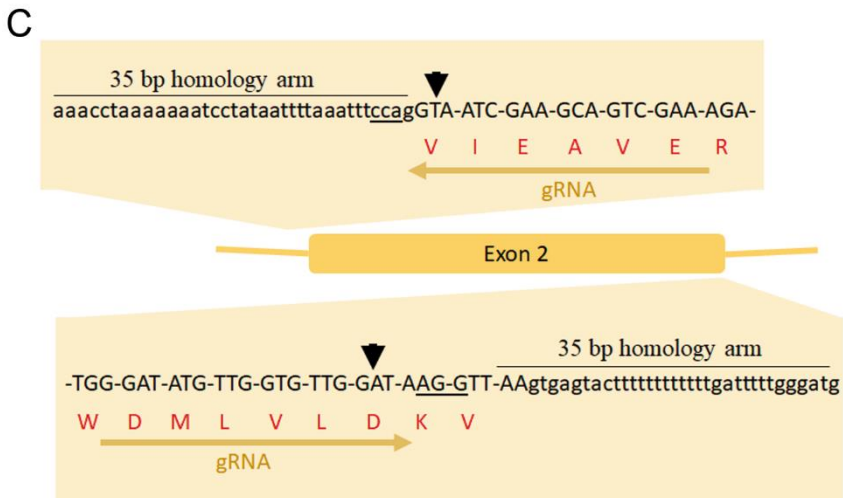
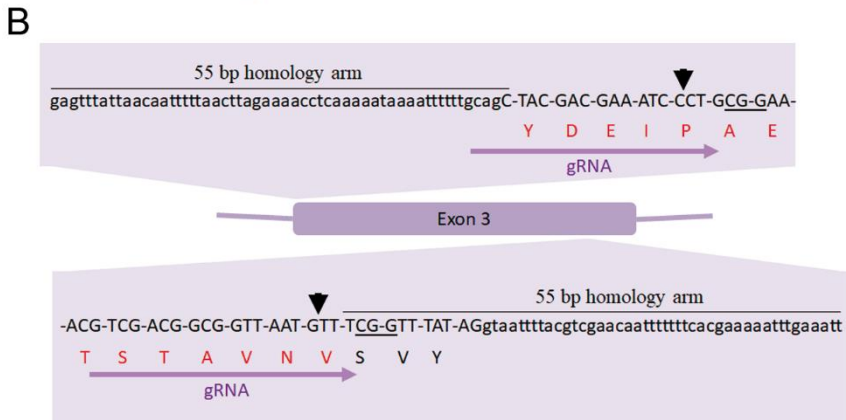
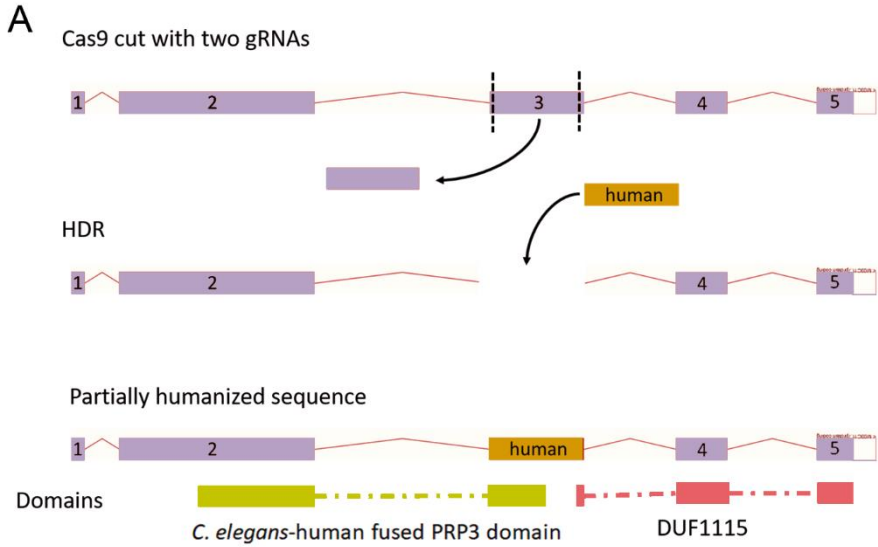


Figure R. 30: Stepwise exon replacement for humanization of *prp-3* scheme (A), and CRISPR-Cas9 designs of exon 3 (B) and 2 (C). (A) Two CRISPR-Cas9 cuts at exon boundaries followed by homology-directed repair (HDR) with a provided dsDNA donor containing the PRPF3 coding sequence leads to a partially humanized sequence. (B and C) PAM sequences are underlined with the cut site indicated by an arrow. The gRNA direction and sequences, homology arms used for HDR, and replaced residues (red) are depicted. Capital letters denote exon sequences and lowercase introns.

DISCUSSION

1. CRISPR-Cas9 for the generation of s-adRP *C. elegans* models

1. a. s-adRP proteins PRPF8/PRP-8 and SNRNP200/SNRP-200

Splicing is an ubiquitous process, meaning that s-adRP genes develop their function in different cell types. Thus, why defects in essential genes specifically affect the retina remains a mystery (Mordes *et al.*, 2006; Parmeggiani *et al.*, 2011; Růžicková & Staněk, 2017). Some studies suggest high transcriptional and splicing demands for the continuous renewal of photoreceptor discs could explain this phenomenon; however conflicting data from model organisms on splicing genes expression in the retina does not fully support this theory (Comitato *et al.*, 2007; Graziotto *et al.*, 2008; Cao *et al.*, 2011).

s-adRP genes normally present missense or small in frame mutations, being *PRPF31* the only gene which tolerates deletion and causes disease by haploinsufficiency (Rio Frio *et al.*, 2008; Růžicková & Staněk, 2017). Among s-adRP affected genes, we chose *PRPF8* and *SNRNP200* (*BRR2* in *Saccharomyces cerevisiae*) to model s-adRP alterations in *C. elegans*. Firstly, both proteins, along with PRPF6 (also affected in s-adRP), form part of the U5 snRNP, which is implicated in several genetic disorders (Schneider *et al.*, 2010; Wood *et al.*, 2021). In *C. elegans*, RNAi of these three genes produces a stronger phenotype than U4 s-adRP genes, probably because the U5 particle participates in subsequent splicing steps after recruitment while U4 is released during B^{act} complex formation (Rubio-Peña *et al.*, 2015).

PRPF8 is the largest protein of the spliceosome located in its catalytic core, interacting with U5 proteins and functioning at the 3' and 5' splice sites. The

PRPF8 C-terminal region, where all the RP-related mutations are encountered, interacts with EFTUD2 (SNU114 in *Saccharomyces cerevisiae*) and SNRNP200. Both PRPF8 and EFTUD2 regulate SNRNP200 helicase activity, essential for U4/U6 duplex unfolding required for B^{act} formation (Häcker *et al.*, 2008; Plaschka *et al.*, 2019; Wilkinson *et al.*, 2020).

In summary, these two genes were selected for s-adRP modelling due to their strong RNAi phenotype and the fact that PRPF8 and SNRNP200 proteins are physically and functionally interacting. This fact suggests mutations in both genes could be affecting splicing similarly. In our hands, combining *weak* mutations in *prp-8* and *snrp-200* points towards this direction in terms of visually observable phenotypes; however, in embryonic development the effect seems additive.

1. b. Functional impact of mimicked s-adRP mutations

In recent years, CRISPR-Cas9 genome editing technology has facilitated the development of numerous genetic disease models of inherited retinal disorders (Fuster-García *et al.*, 2020). The fast life cycle, its hermaphroditism, the ease of large population maintenance along with standard microinjection techniques for CRISPR-Cas9 delivery place multicellular *C. elegans* in a good position as a tool for genetic disease modelling (Vicencio & Cerón, 2021).

No photoreceptors, a cell type that presents high rates of transcriptional and metabolic activities due to continuous renewing of components of the outer segment, are found in *C. elegans* (Bramall *et al.*, 2010). Nonetheless, *C. elegans* presents high metabolic rate and transcriptional levels during larval development (Houthoofd *et al.*, 2002; Grün *et al.*, 2014), suggesting splicing alterations would produce postembryonic phenotypes.

Karina Rubio-Peña mimicked Arg2310Gly (R2303G in *C. elegans*) and additionally isolated a deletion allele of the equivalent human residue His2309. To date, three different missense mutations affecting Arg2310 have been identified in human patients: the mimicked change to Gly, to Lys, and to Ser. Two other mutations were reported at His2309 residue: His2309Pro and His2309Arg (Růžicková & Staněk, 2017) (**Supplementary Table I. 1**). These findings suggest Arg2310 and His2309 have a crucial functional role in splicing.

Our avatar strain *prp-8(cer22)*, which mimics Arg2310Gly variant, did not develop severe phenotypes. Still, the mortal germline phenotype and the genetic interactions support the presence of a functional alteration caused by this mutation and the value of our model. The *prp-8(cer14)*, equivalent to the deletion of His2309 residue, presents a remarkable strong temperature-dependent sterility among other phenotypes. Consistently, yeast models of R2310G, R2310K, and H2309P have previously shown temperature-sensitive phenotypes such as growing defects (Maeder, Kutach, & Guthrie, 2009; Mozaffari-Jovin *et al.*, 2013). Interestingly, patients with mutations His2309Pro and His2309Arg present worse prognosis than Arg2310Lys patients (Towns *et al.*, 2010).

At the molecular level, previous studies reported reduced formation of the U4/U6·U5 caused by PRPF8 mutations (Mozaffari-Jovin *et al.*, 2013), affecting splicing efficiency (Mayerle & Guthrie, 2016). Microarray analysis of transcripts from blood samples of His2309Arg individuals supports inefficient splicing in approximately 20% of analysed exons (Korir *et al.*, 2014). SNRNP200/BRR2 U4/U6 unwinding activity has been shown to be influenced by PRP8 C-terminus, and negatively affected by the RP-associated mutations (Maeder *et al.*, 2009). Similarly, *in vitro* studies by Malinová *et al.* (2017) reported splicing inefficiency of retina-specific genes and defects in U5 assembly. RP-associated mutations of PRPF8 seem

to misslocalize the protein to the nucleus which might be contributing to the inefficient splicing (Malinová *et al.*, 2017). Although we did not explore PRPF8 subcellular localization, it could be studied with fluorescent tags. Conveniently, a CRISPR-based approach to endogenously tag proteins was developed by our group (Vicencio *et al.*, 2019).

SNRNP200 modelled mutations are found in the active helicase domain of the protein (Santos *et al.*, 2012; Růžičková & Staněk, 2017). Val683Leu (V676L in *C. elegans*) has no previous functional data reported, while Ser1087Leu (S1080L in *C. elegans*) decreases the RNA binding activity and ATPase activity (Santos *et al.*, 2012) and is detrimental for unwinding and splicing (Zhao *et al.*, 2009). In our hands, the V683L equivalent mutation in *C. elegans* shows a range of overt phenotypes including embryonic lethality, in contrast to S1087L which has a limited phenotypic impact.

In summary, the fact that all four generated mutants present different levels of functional impact correlate with previous studies and indicates each mutation has a unique functional implication. Altogether these findings justify the use of personalized models for each of the mutations for following aims.

2. *C. elegans* is a powerful model for the identification of genetic modifiers of s-adRP mutations

Curiously, there is phenotypic variation between RP patients carrying the same mutation (Daiger *et al.*, 2007; Parmeggiani *et al.*, 2011; Verbakel *et al.*, 2018; Kiser *et al.*, 2019). This fact might be explained due to the existence of mutations in other genes that might influence disease onset and progression. *CNOT3* is a modifier in *trans* of *PRPF31*, which acts as a transcriptional regulator of the splicing factor and would modify the functional impact of any mutation on this gene (Venturini *et al.*, 2012). Other genes might be interacting with s-adRP mutations and altering disease progress too. To identify such interactors, we performed an RNAi screen in our avatar worms.

Weak alleles are an excellent choice for this aim since they have a limited functional impact, but there is room for its modulation to uncover detrimental interactions. Curiously, although the screen was done on *weak* alleles, we only identified interactors of the *prp-8(cer22)*. Three interactors were uncovered: *isy-1/ISY1*, *mog-2/SNRPA1*, and *cyn-15/PPWD-1*.

ISY1 (Ntc30 in yeast) forms part of the Nineteen Complex (NTC) and is implicated in branching, the first transesterification reaction of splicing (Wilkinson *et al.*, 2021). Interestingly, ISY1 was recently linked to base excision repair by interacting with apurinic/apyrimidinic endonuclease 1 (APE1) and enhancing its activity (Jaiswal *et al.*, 2020). This is an example of how splicing defects contribute to genome instability and is further discussed in section four of the discussion.

SNRPA1 forms part of U2 and is also localized to the catalytic spliceosome. Loss of SNRPA1 was linked to male infertility in *Drosophila* (Wu *et al.*, 2016), and its depletion is linked to DNA damage (Tanikawa *et al.*, 2016), as well as to cancer (Zeng *et al.*, 2019; Feng *et al.*, 2020).

PPWD1 is a peptidyl prolyl isomerase identified in the C complex of the spliceosome. Recent structural data suggests the tryptophan (W) aspartic acid (D) reach domain (WD40) interacts with RP-affected Jab1 Domain of PRPF8 to help in BRR2 repression. The strong interaction identified between both RNAi and the deletion allele of WD40 with an s-adRP missense mutation supports the importance of PPWD1 in splicing. PPWD1 also interacts with ISY1 and U2 and presumably plays an important role in C complex structure stabilization (Bertram *et al.*, 2020). Thus, the three identified modifiers of the *prp-8 weak* allele might be implicated in the disruption of the C complex.

We did not find an interaction with missense mutations in PPWD1 and ISY1, which might cause protein function defects in healthy individuals. Recently published structural data might point towards mutations that specifically affect ISY1-PPWD1-PRPF8 (Bertram *et al.*, 2020) interactions, supporting our findings.

The interactors described above are not only interesting for RP but can also be studied for cancer therapeutic strategies. In fact, synthetic lethality screens have been used for that means before and have an interest for the identification of novel therapeutic targets (Ceron *et al.*, 2007; Serrat *et al.*, 2019).

DISCUSSION

In summary, s-adRP *C. elegans* models allowed the identification of three modifiers of the *prp-8(cer22)*, which might point to disease progression modifiers. Our RNAi screen was restricted to splicing-related genes. A larger RNAi screen may uncover functional interactions with other pathways regulating the activity of the spliceosome.

3. *C. elegans* s-adRP models as a tool for drug screens

Currently, there is no cure for RP. Nonetheless, some management strategies in different phases of development such as cell replacement (Uyama, Mandai, & Takahashi, 2021; Holan, Palacka, & Hermankova, 2021), electronic devices (Ostad-Ahmadi, Modabberi, & Mostafaie, 2021), transcorneal electrical stimulation (Wagner *et al.*, 2017), ASO (Gemayel, Bhatwadekar, & Ciulla, 2020; Aísa-Marín *et al.*, 2021), or gene editing (Russell *et al.*, 2017), among others exist (Verbakel *et al.*, 2018). These strategies are high cost and need high specialization, hampering widespread adaptation for RP treatment. Thus, the identification and implementation of simpler treatments would be of great value.

One possibility is the identification of small molecules through drug screens to at least alleviate the disease symptoms. *C. elegans* has previously been used for drug screens and has proven to be a valuable model for identifying hit compounds (Moy *et al.*, 2006; Artal-Sanz *et al.*, 2006; Matsunami, 2018; Ikenaka *et al.*, 2019).

Conveniently, *prp-8(cer14)* strain presents a reliable temperature-sensitive sterility, allowing strain maintenance at low temperatures and screening for sterility rescue at higher temperatures. I performed a drug screen of mainly FDA-approved drugs, which would reduce the implementation time into the clinics of a potential hit. Around 16% of the tested drugs had a visually observable effect on *C. elegans*, validating our drug library. We wondered whether motility could be a helpful indicator of fitness as it has been previously used for toxicity detection (Bianchi *et al.*, 2015; Spensley *et al.*, 2018). Accordingly, we found a correlation between visually observable phenotypes induced by drugs and motility reduction. The s-adRP strain

presented reduced movement records presumably due to lack of progeny, so motility rescue might be used as an indicator for restored fertility and allows partial automation and escalation of the number of drugs screened.

Contrary to our expectations, we identified a drug that induces toxicity in *snrp-200* mutants instead of rescuing the phenotype. Dequalinium is a cytotoxic drug currently used for infection treatment (Mendling *et al.*, 2016), and its derivatives are in research for treating different cancer types (Pajuelo *et al.*, 2011; Timaner *et al.*, 2015). Different modes of action including disruption of membrane permeability, perturbation of osmotic exchange, interfering with different enzymes, or direct DNA binding were associated with dequalinium (Mendling *et al.*, 2016). Interaction between drugs and gene variants have been identified principally for cytochromes that participate in its metabolism and clearance (Westervelt *et al.*, 2014; FDA, 2020). Our study suggests that mutations in splicing factors could also interfere with the drug response. From the clinical point of view, a drug-gene interaction can result in an inefficient response or increase of adverse effects. In the case of pathogenic mutations of a degenerative disease like RP, such interactions could imply a faster disease progression. Health systems should work in this direction and fund studies to identify harmful drugs for specific conditions.

Thus, we demonstrate *C. elegans* s-adRP disease models might be used not only for a drug screen to identify compounds that rescue a phenotype and evaluate their toxicity, but also to identify specific genotype-drug interactions.

4. Genome instability might be present in s-adRP mutants

Apoptosis of photoreceptors is thought to cause visual loss in RP (Wert *et al.*, 2014; Zhang, 2016). The mechanism by which cell death occurs is still unknown; however, the degenerative nature of the disease points to a cumulative process through years. Our previously established working model stands accumulation of R-loops might expose DNA to damaging agents, and such cumulative damage may result in apoptosis (Rubio-Peña *et al.*, 2015).

The interplay between transcription and splicing, or cotranscriptional splicing, is well known (Girard *et al.*, 2012; De Conti *et al.*, 2013; Saldi *et al.*, 2016; Shenasa & Hertel, 2019). Thus, alterations in splicing might be linked to DNA damage through this process. Accordingly, depletion of splicing factors SRSF1 as well as of SLU7 has been linked to an accumulation of R-loops and increased DNA damage (Li & Manley, 2005; Paulsen *et al.*, 2009; Shkreta & Chabot, 2015; Jiménez *et al.*, 2019).

Previous data obtained from RNAi in *C. elegans* point towards the presence of genomic instability upon splicing defects (Rubio-Peña *et al.*, 2015). RNAi of splicing factors enhances the accumulation of RPA-1, a protein that coordinates DNA repair response (Haring *et al.*, 2008; Hefel *et al.*, 2021) upon UV-light-induced damage. Moreover, up-regulation of *atll-1/ATR*, which phosphorylates Ser15 in *cep-1/p53* might be critical for apoptosis activation (Tibbetts *et al.* 1999). *egl-1*, an apoptosis activator, was also upregulated upon RNAi of s-adRP genes (Rubio-Peña *et al.*, 2015). These data indicate that splicing defects have an implication in the DNA damage response and may be linked to activation of the apoptotic pathway.

Initial data on s-adRP mutants have shown sensitivity to HU-induced damage (Rubio-Peña, 2017).

In this work, I confirm DNA damaging agents HU and UV-light induce upregulation of the proapoptotic gene *egl-1*, suggesting DNA damage produces somatic cell death. s-adRP mutants did not present an evident sensitivity to these agents. However, further technical optimization seems to be needed as evidenced by reduced *egl-1* upregulation in *prp-8* mutants upon HU treatment and high interexperimental variability in UV experiments. To overcome these barriers, endogenous *egl-1* tagging might be an alternative.

Regarding DNA damage, smFISH of *atl-1* showed an increased expression in the germline. This is coherent with previous findings and its functional role during meiosis and mtDNA maintenance (Aoki *et al.*, 2000; Mori, Takanami, & Higashitani, 2008; Suetomi *et al.*, 2013; Pacheco *et al.*, 2018). Surprisingly, low expression levels were also present in somatic cells suggesting alternative functions of this gene in somatic cells. *prp-8(RNAi)* produced substantial upregulation of *atl-1*, confirming previous observations (Rubio-Peña *et al.*, 2015). This upregulation was observed in somatic cells indicating RNAi of *prp-8* produces DNA damage response in the soma. The *strong* allele of *snrp-200* did not clearly show the same effects. It is plausible to think that the mutation may have functional impact after the cumulative effect of DNA damage, meaning that *atl-1* upregulation could be visible later in life or after several generations under stressful conditions. It would be of interest to explore such effects; however, in our hands, the permeability of adults to smFISH probes was low, impeding its use in this stage.

The *weak* allele *prp-8(cer22)* showed Mrt phenotype, which consists of gradual loss of germ cell immortality. This phenotype phenocopies

observations from DNA integrity maintenance mutants (Ahmed & Hodgkin, 2000; Gartner *et al.*, 2008; Yanowitz, 2008), thus hinting that an s-adRP mutation can cause DNA damage. Moreover, the genetic interaction between this allele and an *ama-1* (Pol II) mutant demonstrates how a splicing mutation functionally interacts with transcription alteration.

Thus, we provide evidence that s-adRP mutations affect germ cell immortality in a degenerative manner, presumably through DNA damage and the interaction with altered transcription, pointing to splicing-transcription interplay as a possible disease mechanism. Linked to RP patients, the accumulation of DNA damage in photoreceptors could cause apoptosis in the retinal cells and explain the degenerative nature of the disease. If such alterations exist in s-adRP patients, exploring other DNA damage derivate conditions such as increased cancer incidence would be of interest.

5. CRISPR-Cas9 allows VUS evaluation in

C. elegans

Although more than 80 genes have been linked to RP (Daiger *et al.*, 1998; Verbakel *et al.*, 2018), different studies show only 30-50% of patients have a genetic diagnosis indicating the existence of unknown RP mutations (Salmaninejad *et al.*, 2019; Perea-Romero *et al.*, 2021). Next generation sequencing (NGS) is becoming a new standard in identifying novel variants in patients (Salmaninejad *et al.*, 2019). These techniques identify plenty of novel mutations with a causative potential, but it is not always clear which are causing the disease. Current guidelines establish criteria for a variant classification, which usually ranges from pathogenic to benign based on current evidence. In some cases, it is impossible to establish a variant as pathogenic or rule out its implication in the disease and thus these variants are generally classified as variants of unknown significance (VUS) (Richards *et al.*, 2015). Moreover, cis-mutations that affect splicing might be erroneously classified as missense, nonsense, or silent, additionally hamstringing the assessment of pathogenicity (Aísa-Marín *et al.*, 2021). Thus, functional data of the variant impact is a relevant hint on the pathogenicity of VUS.

Validation of putative pathogenic variants with functional assays in model organisms such as Zebrafish is being implemented in clinics (Zhang *et al.*, 2021). Similarly, *in vivo* and *in vitro* models along with CRISPR-Cas9 technology are being investigated for VUS functional testing (Harnish *et al.*, 2019; Nazlamova *et al.*, 2021). In this study, we propose using *C. elegans* to evaluate the functional implication of s-adRP VUS. The ease and fast generation of mutants by CRISPR-Cas, with the high conservation of splicing genes, encourages *C. elegans* use as a platform for functional study

of variants. We also demonstrate the utility of SpG Cas9 (Walton *et al.*, 2020) with a more flexible NGN PAM requirement to expand the editable genome and thus facilitate mimicking virtually any desired variant.

We established a panel of phenotypic features that were identified in *C. elegans* s-adRP mutants (**Table R. 4**). Thus, any VUS presenting similar phenotypes would be a candidate for pathogenicity.

(1) The four s-adRP strains show different degrees of developmental delay with two strains presenting overt phenotypes (Rubio-Peña, 2017; Kukhtar *et al.*, 2020). The overt phenotypes are easily detected and are an indicator of the functional impact of a mutation.

(2) Phenocopying of veiled phenotypes such as delayed growth, reduced brood size, or mortal germline could indicate altered function caused by a VUS. However, careful characterization is needed for its detection.

Interactions with (3) *cyn-15(cer173)* (splicing-related) and (4) *ama-1(cer135)* (transcription-related) uncover the functional impact of the weak allele *prp-8(cer22)*. The need for characterization and performing genetic crosses might be a difficulty in its implementation as a practical test. To facilitate uncovering of the interaction, we attempted to alter splicing pharmacologically with herboxidiene (Hasegawa *et al.*, 2011) or to inhibit transcription with α -amanitin (Montanaro *et al.*, 1971). Functional impact magnification with small compounds failed, thus not being a promising approach for VUS testing. Interestingly, we could confirm the slow Pol II mutant resistance to α -amanitin described in a previous report (Bowman *et al.*, 2011). Similarly, other spliceosome modulators could be tested, such as BRR2 inhibitors or late spliceosome assembly inhibitor N-palmitoyl-L-leucine (DeNicola & Tang, 2019).

(5) Nanopore sequencing was used to detect AS events specific to the *strong* allele of *snrp-200(cer23)*. This technology offers a small-sized and relatively inexpensive solution for long-read sequencing (Kraft & Kurth, 2020). Its use is growing in laboratories and is also being investigated for application in clinics (Miller *et al.*, 2020; Ptasinska *et al.*, 2020). We compared cDNA-PCR and direct RNA sequencing of the samples and identified a PCR enrichment of transcripts around 1000 bp in length. Since the primers used for PCR are intended to select for full transcripts, the enriched length seems to correspond to such transcripts. Direct RNA sequencing might be used for an unbiased transcriptomic study, to detect RNA modifications, and to study poly (A) tail length (Workman *et al.*, 2019; Li *et al.*, 2020; Roach *et al.*, 2020; Motorin & Marchand, 2021). Such characteristics might provide additional clues of the role of s-adRP mutations in RNA biology and additional biomarkers.

In our hands, nanopore sequencing detected novel AS transcripts and identified three reliable events on the *strong* allele *snrp-200(cer23)*: *brd-1*, *rmf-1*, and C05C10.7. These events were later confirmed in *prp-8(cer14)*. *brd-1* is a homolog of the human BARD1 involved in genome integrity maintenance in cooperation with BRCA1 (Morris & Solomon, 2004). It might be interesting to investigate if this novel isoform has any functional impact on genome instability or if it is a mere by-product of altered splicing. In the case of *rmf-1* and C05C10.7, no functional data has been published so far. Independently of its biological relevance, all three events are candidates for a panel of features for VUS evaluation.

(6) Gamma radiation induces double-strand breaks in the DNA, one of the biggest features of genome instability (Vignard, Mirey, & Salles, 2013). It seems to have a more substantial effect on *snrp-200(cer24)* *weak* allele and might be pointing to subjacent genome instability that was not uncovered

by other tests. The preliminary data shows it might be used for functional impact testing, but more investigation in this direction is needed.

We show how CRISPR-Cas9 generated *C. elegans* s-adRP mutants provide a set of phenotypic features that might be used for VUS testing. I generated a VUS in the *prp-8* gene and started with its characterization. Unfortunately, due to time constraints, I could not finish the complete evaluation.

This panel of features might be helpful in the identification of other s-adRP related genes. Systemic disruption of splicing-related genes in *C. elegans* in search of phenocopying of features in our panel might point to novel s-adRP genes. Such novel genes would be great candidates for sequencing in genetically undiagnosed patients and possibly identifying novel variants.

6. Humanization for s-adRP genes to improve *C. elegans* models

Most of the residues affected by s-adRP missense mutations are conserved in *C. elegans*, allowing their direct modelling in this model system. However, there are still not conserved residues hampering s-adRP study in *C. elegans* (**Supplementary Table I. 1**). Moreover, although the splicing process presents globally high conservation, there are still differences that might modify a conserved residue protein context, thus masking or modifying the effect of a mutation on such residues.

To better understand the impact of a mutation modelled in a model organism, we designed a strategy to replace the *C. elegans prp-3* for the human *PRPF3*. Previously, gene replacement for human orthologs or “humanization” has been made in different model organisms.

In yeast, it has been shown that roughly half of more than four hundred essential genes tested for humanization could restore viability. Thus, a functional replacement of yeast proteins was achieved with human orthologs. The number of successful humanizations was different between pathways being the success rate in transcription and translation around half of the tested genes (Kachroo *et al.*, 2015).

There are two published studies of humanization in *C. elegans*. One replaces *unc-18* with human STXBP1 encoded in plasmids that were incorporated as extrachromosomal arrays. Functional replacement was achieved, and several mutations implicated in epilepsy syndromes provoked an impact on protein function (Zhu *et al.*, 2020). The second performs a single copy replacement of *daf-18* with the open reading frame of *PTEN* in the endogenous locus. This strategy maintains the worm 3' and

5' UTRs however, it removes all worm introns. Human protein successfully functionally replaced the missing ortholog, and a cancer-related variant drastically impaired protein function (McDiarmid *et al.*, 2018). InVivoBiosystems, a company centered on the use of model organisms for disease modelling is also implementing the humanization of several non-essential genes for variant testing (Hopkins, 2021).

The studies commented above do not entirely maintain the regulatory regions of the replaced genes. Recently, a strategy based on CRISPR-Cas9 succeeded in nearly fully humanize *Drosophila* *Gao*, a gene implicated in epilepsy. This approach allowed humanizing the coding sequence but maintaining the regulatory regions almost intact (Savitsky *et al.*, 2020).

In our project, we followed a similar method replacing *prp-3* exon by exon. Its human homolog *PRPF3* presents a similar size and conserved domains. The identity is around 34% and the similarity is 52%, indicating that important differences exist between both proteins. Previous attempts of functional substitution of non-essential genes failed with protein identities lower than 53% (Hopkins, 2021).

Successful humanization of the exon three, as evidenced by at least partial functional replacement was achieved. The addition of a humanized exon two failed, as evidenced by the loss of viability in homozygosis. Thus, we partially humanized PRP-3 protein with close to a quarter of its sequence replaced. Notably, the humanized region contains the identified up to date s-adRP mutations (**Supplementary Table I. 1**)

We show how CRISPR-Cas9 can be used to humanize essential genes at the endogenous locus at least partially, thus preserving most of the regulatory regions. Our future work will be centred in modelling two s-adRP mutations of *prp-3* on the WT and humanized backgrounds to assess if humanization improves s-adRP modelling.

7. *C. elegans* role in personalized medicine and final remarks

Personalized medicine has been gaining weight in clinics. The stratification of the patients to improve treatments and to predict prognosis enhances the quality of medical care (Chan & Ginsburg, 2011). Basic and translational research are making efforts to investigate in this direction.

Patients of rare diseases can probably benefit the most from personalised medicine. One example of success in this matter is the Undiagnosed Disease Network (UDN), dedicated to investigate rare gene variants using *C. elegans*, *Dario rerio*, and *D. melanogaster*. The aim of this network is to provide useful data of novel variants for diagnosis, therapy choice, and to study disease mechanisms (Wangler *et al.*, 2017). To date, UDN took advantage of functional assays in model organisms to diagnose more than 400 patients by identifying the mutation causing their disease.

We have used CRISPR-Cas9 to generate personalized models of the rare disease s-adRP. The generation of our “avatar” relies in the aminoacidic conservation from nematodes to humans. Such conservation implies a functional relevance for the protein, although the consequence of modifications of these residues are not always evident (as in veiled phenotypes).

The implementation of *C. elegans* in the health system as a diagnostic tool is feasible. Handling and manipulation of this model organism are easy to teach in few weeks. In fact, *C. elegans* is widely used for teaching purposes even at scholar level (Deffit, Neff, & Kowalski, 2017). Moreover, *C. elegans* is a model that fits within the 3Rs principles that promote reduction of animals in experimentation. Ethical committees do not consider

invertebrates, such as *C. elegans*, as an animal. Thus, its use in the laboratory lacks ethical issues.

The ease of genetic editing in *C. elegans* allows rapid modelling of genetic variants. However, more research is needed to establish which genes are suitable for VUS studies in *C. elegans*. Once the gene list is established, the use of *C. elegans* for diagnosis could be assessed in more depth and even implemented in the health systems. Thus, it would be easy to expand the models to most of the identified s-adRP mutations thanks to CRISPR-Cas9, studying the particularity of each mutation individually.

Summarising, we made one step forward in using *C. elegans* to model a rare genetic disease with CRISPR-Cas9 and provide a valuable pre-clinical tool to support personalized medicine.

CONCLUSIONS

CONCLUSIONS

1. Strains mimicking s-adRP mutations have a functional impact but are viable in homozygosis, allowing RNAi and drug screens.
2. Genetic interactors, uncovered by RNAi, of the weak allele *prp-8(cer22)* are potential disease modifiers and might be explored for prognostic means. Expanding the RNAi screen to genes unrelated to splicing might uncover additional pathways implicated in s-adRP.
3. Drug screen on s-adRP mutant strain can identify drugs potentially harmful for s-adRP patients, as evidenced by the dequalinium sensitivity of *snrp-200* mutants.
4. s-adRP mutant strains might have genome instability that is evidenced through generations or upon DNA damage.
5. *Strong* s-adRP alleles present AS events that might serve as markers of functional alteration related to s-adRP mutations.
6. We proposed a panel of tests in *C. elegans* to assign functions to VUS in s-adRP genes. Such a panel needs to be consolidated by testing more VUS.
7. *prp-3* allows exon three substitution for the human counterpart, making a nematode-human protein chimera that is functional. However, additional replacement of exon two causes lethality. The benefit of partial gene humanization for s-adRP modelling still needs to be assessed.

MATERIALS AND METHODS

1. *C. elegans* maintenance and strains

Standard methods for culturing were applied (Brenner, 1974). Worms were grown on NGM (Nematode Growth Media) agar plates seeded with an overgrown culture of the *Escherichia coli* strain OP50 at temperatures between 15°C and 25°C. Worms were synchronized following the sodium hypochlorite treatment (Porta-de-la-Riva *et al.*, 2012). Bristol N2 was used as the WT strain.

Table M. 1: List of strains:

Strain	Genotype
CER255	<i>prp-8(cer14[2303del]) III</i>
CER240	<i>prp-8(cer22[R2303G]) III</i>
CER256	<i>snrp-200(cer23[V676L]) II</i>
CER248	<i>snrp-200(cer24[S1080L]) II</i>
CER440	<i>prp-8(cer22[R2303G]) III; snrp-200(cer24[S1080L]) II</i>
CER456	<i>isy-1(cer115[G170S]) V</i>
CER465	<i>cyn-15(cer119[D74Q]) I</i>
CER544	<i>prp-8(cer22[R2303G]) III; isy-1(cer115[G170S]) V</i>
CER545	<i>prp-8(cer22[R2303G]) III; cyn-15 (cer119[D74Q]) I</i>
CER578	<i>cyn-15(cer173[D66_D74del]) I</i>
CER580	<i>cyn-15(cer173[D66_D74del])/+ I; prp-8(cer22[R2303G]) III</i>
WS1973	<i>opIs56 [egl-1p::2xNLS::GFP]</i>
CER267	<i>prp-8(cer14[2303del]) III; opIs56 [egl-1p::2xNLS::GFP]</i>
CER268	<i>prp-8(cer22[R2303G]) III; opIs56 [egl-1p::2xNLS::GFP]</i>
CER265	<i>snrp-200(cer23[V676L]) II; opIs56 [egl-1p::2xNLS::GFP]</i>
CER266	<i>snrp-200(cer24[S1080L]) II; opIs56 [egl-1p::2xNLS::GFP]</i>
CER536	<i>ama-1(cer135[R743H]) IV</i>
CER537	<i>ama-1(cer135[R743H]) IV; prp-8(cer14[2303del]) III</i>

Strain	Genotype
CER538	<i>ama-1(cer135[R743H]) IV; prp-8(cer22[R2303G]) III</i>
CER539	<i>ama-1(cer135[R743H]) IV; snrp-200(cer23[V676L]) II</i>
CER540	<i>ama-1(cer135[R743H]) IV; snrp-200(cer24[S1080L]) II</i>
CER529	<i>sftb-1(cer144[S1090A, A1095T, I1096V, F1101Y]) III</i>
CER568	<i>sftb-1(cer144[S1090A, A1095T, I1096V, F1101Y]) III; prp-8(cer22[R2303G]) III</i>
CER569	<i>sftb-1(cer144[S1090A, A1095T, I1096V, F1101Y]) III; snrp-200(cer23[V676L]) II</i>
CER570	<i>sftb-1(cer144[S1090A, A1095T, I1096V, F1101Y]) III; snrp-200(cer23[V676L]) II</i>
CER607	<i>sftb-1(cer144[S1090A, A1095T, I1096V, F1101Y]) III; ama-1(cer135[R743H]) IV</i>
GW638	<i>met-2(n4256); set-25(n5021)</i>
CER628	<i>prp-8(cer209[T2319_E2325del]) III</i>
CER629	<i>prp-8(cer210[A2118T]) III</i>
CER611	<i>prp-3(cer194) III (exon 3 humanized)</i>
CER666	<i>prp-3(cer231/cer194) III (exon 3 humanized in homozygosis, exon 2 humanized in heterozygosis)</i>

2. Brood size, overt phenotypes, and Emb

L4 larvae were singled out in 35-mm NGM agar plates and transferred to a fresh plate every 8-12 h until egg-laying ceased. Two days after P₀ was removed, the number of F₁ larvae, overt phenotypes, and dead embryos from each plate were manually scored, and total offspring per hermaphrodite was calculated. P₀ and the previous generation were grown at experimental temperature.

For *ama-1(cer135)* and s-adRP double mutants, visually observable phenotypes were scored daily from singled L1.

3. Developmental delay assay

After worm synchronization with sodium hypochlorite treatment (Porta-de-la-Riva *et al.*, 2012), each strain was seeded on an OP50 plate for one-hour recovery. Afterward, worms were singled onto a 24-well plate containing OP50 bacteria and grown at the experimental temperature.

Stage determination based on the size and morphological structures of the worms was carried out every 24 h for three to four days. Length measurements were also made in a portion of the experiments.

4. RNAi screen

Bacteria expressing dsRNA against a library of 128 splicing-related RNAi clones (Kerins *et al.*, 2010) was obtained from the ORFeome library (Rual *et al.*, 2004) or the Ahringer library (Kamath & Ahringer, 2003). Each clone was authenticated by determining the size of the insert by PCR, and six randomly selected clones were Sanger sequenced before its usage. The result was 98 validated clones for RNAi by feeding (**Supplementary Table R. 1**). The screen was carried out in 24-well plates containing NGM agar supplemented with 12.5 µg/ml tetracycline, 50 µg/ml ampicillin, and 3 mM IPTG (RNAi plates) at 25°C. Ten to twenty of either wildtype or *weak* mutants (*prp-8(cer22)* or *snrp-200(cer24)*) worms per well from the synchronized L1 stage were tested for each clone in duplicates. *gfp(RNAi)* was used as a negative control. Worms were scored at 72 and 96 h post-seeding.

isy-1(RNAi) validation was done at 25°C, measuring worm-length as described below. Validation of *cyn-15(RNAi)* and *mog-2(RNAi)* brood sizes as previously described using RNAi plates.

6. Worm length

Synchronized L1 were seeded in 55-mm with or without treatments depending on the experiment. 72 h post-seeding, 35 to 40x magnified pictures of the plates were taken using the stereoscopic NIKON SMZ800 or Zeiss Stemi 305 microscope attached to a DS-2MV or Axiocam ERc 5s camera, respectively. To score the length of such animals, a line from the anterior to the posterior part of the body was drawn and measure using the NIS Elements 3.10 software or Fiji ImageJ 1.53c.

7. DAPI staining

Worms were recovered in M9 buffer (Stiernagle, 2006) and, after washing out bacteria were placed in a Pyrex dish. Afterward, residual M9 was removed, and Carnoy's fixative (Chloroform 30%, acetic acid 60%, and ethanol 10%) was added for 30 minutes. Next, washes of 10 minutes with PBS-Tween 20 0,1% were performed. Finally, worms were transferred to a slide, DAPI-Fluoromount-G® (Southern Biotech ref: 0100-20) was added, and a coverslip was placed on top of the slide and sealed with nail polish. Pictures were taken on a Nikon ECLIPSE TI-s inverted microscope attached to a Nikon DS-2Mv camera.

For gonad extrusion, tetramisole 0,33 mM was added to recovered worms in a Pyrex dish, and gonads extracted by cutting worms with 20 gauges

syringes. Then, 4% paraformaldehyde was added for 20-30 min and was visualized as explained.

8. CRISPR editing

Karinna Rubio-Peña generated *prp-8(cer14)*, *prp-8(cer22)*, *snrp-200(cer23)*, and *snrp-200(cer24)* mutants (Rubio-Peña, 2017; Kukhtar *et al.*, 2020) and Xenia Serrat *sftb-1(cer144)* by CRISPR-Cas9 (Serrat *et al.*, 2019). *isy-1(cer115)*, *cyn-15(cer119)*, *ama-1(cer135)*, *prp-8(cer209)*, *prp-8(cer210)*, *prp-3(cer194)*, and *prp-3(cer231)* mutant worm lines were generated via CRISPR-Cas9 following previously described methods (Paix *et al.*, 2015; Paix, Folkmann, & Seydoux, 2017; Dickinson & Goldstein, 2016).

Alt-R™ CRISPR-Cas9 tracrRNA, crRNAs, Cas9 Nuclease 3xNLS, single-stranded oligodeoxynucleotide (ssODN) repair templates (for point mutations and small deletions), gBlocks gene fragments (for exon replacement), and primers were purchased from Integrated DNA Technologies.

crRNA containing a guide sequence adjacent to a protospacer motif (PAM) was injected with purified Cas9 enzyme, repair template ssODN, and *dpy-10* crRNA with ssODN for the *dpy-10(cn64)* allele as a co-CRISPR marker. Repair templates for small mutations contained the desired modification, silent mutations to avoid re-cutting by Cas9, and homology arms of 35 bp to allow recombination (**Table M. 2, Figure R. 27, and Figure R. 30**). For exon replacement, gBlocks with the desired sequence were cloned into pDONR221 vector and transfected into DH5 α . After plasmid purification, a PCR product with primers complementary to homology arm sequences was used to amplify repair templates (**Table M. 3**).

I isolated Dpy, Rol, and pools of WT worms from the brood of injected Po. Mutants were identified by PCR using specific primers and confirmed by Sanger sequencing (Table M. 4).

Table M. 2: Summary of crRNAs and repair templates for point mutations and small deletions.

Gene	Allele	crRNA	Repair template
<i>isy-1</i>	<i>cer115</i>	<i>GGTACTTGGATGACGAAGA</i>	<i>TATTGAGAAATATCGACGCTCACTA</i> <i>TTTTGGTTACCTTGACGATGAGGAC</i> <i>TCTCGCTTAATTCCTTTGAAAAAC</i> <i>TAATTGAAGAGA</i>
<i>cyn-15</i>	<i>cer119</i>	<i>ATAATCACTGCAAGCGTCGA</i>	<i>CACGTTATCGCGACAAAAACCGAT</i> <i>TTTATAATCACAGCGTCTGTGCAAG</i> <i>GACACCTGAAATTCTGAAAAAGA</i> <i>AGCATTCCGA</i>
<i>cyn-15</i>	<i>cer173</i>	<i>ATAATCACTGCAAGCGTCGA</i>	<i>GGGACACAATTTCTCACGTTATCG</i> <i>CGACAAAAACCGACACCTGAAAT</i> <i>TCTGAAAAAGAAGCATTCCGA</i> <i>CAGACTTTTGAGAATAAAGTCAATC</i>
<i>ama-1</i>	<i>cer135</i>	<i>GAACGACGCTCGTGATCGAA</i>	<i>AGATTTTGAATGATGCACACGACC</i> <i>GTA CTGGTAGTTCTGCGCAGAAGA</i> <i>GTTTGTCTGAATTCAA</i>
<i>prp-8</i>	<i>cer209</i>	<i>TGCAAATGCATCCTCGCGAT</i>	<i>AGATAAAATAAGAAAAATGATTATG</i> <i>CAAATGCATCTCCAAGTGGATCGT</i> <i>CGAATGCCTAAAAATGAAAGAA</i> <i>ATTATCAGGTGGCGATACACCATA</i>
<i>prp-8</i>	<i>cer210</i>	<i>CATACATGAATCCAGCAATC</i>	<i>CATGAATCCAGTGATTTGTGTTCTGA</i> <i>AGATCCGAGATAGTGATGAACTTCT</i> <i>T</i>
<i>prp-3</i>	<i>cer194</i>	5' exon 3 <i>CAGCTACGACGAAATCCCTG</i> 3' exon 3 <i>GTCGACGGCGGTTAATGTTT</i>	Repair templates Table M. 3
<i>prp-3</i>	<i>cer231</i>	5' exon 3 <i>TTTCGACTGCTTCGATTACC</i> 3' exon 3 <i>GGATATGTTGGTGTGGATA</i>	Repair templates Table M. 3

Table M. 3: Repair templates *prp-3* exon 2 and 3 replacement.

prp-3 exon 3

gagttattaacaatttttaacttagaaaacctcaaaaataaaatttttgagCTACGACGAAATCC/CTGCGGAAAAC
 GACATGGAAAGATACTCACAGACAGTTTCCGAACTCGTAGAGCACCCGATTTCAATGAG
 AGCACCCACTGAGCCATTAECTCAACAATATCTGAAAGTATACTTGACAACAAAAGAAA
 AAAAGAAGATTTCGTCGTCAAAATCGTAAAGGAACTACTGAAAAGAGAAGACAGAGAAGATT
 CGTTTGGGACTGGAAAAGGCTCCGGAGCCAAAAGTCAAAATTAGTAATTTAATGAGAGT
 TCTTGGAATGAAGCAATCCAGGATCCGACGAAAATGGAAGCACAAGTTCGGAACAAA
 TGGCTGAAAGATTGAAGAAACATGAGACATTGAATGCTGAGAGAAAGCTTACCGAAGAT
 CAGAAACGCGCGAAAAAGACGAAAAAACTGTCTGAGGATACGTCGACGGCGGTTAATG
TTTCGGTTTATAGgtaattttacgtcgaacaattttttcacgaaaaatttgaatt

prp-3 exon 2

aaacctaaaaatectataattttaaatttcagAGGGTACTTGGATTTTCGGAACCGACCGTAGTTACGG
 CAGCGTTGAATTGTTGGAAAAGGCATGGATAAAAAGAAAAGCAGCGGACCATTTAAAA
 CCATTTCTTGATGACTCCACGTTACGTTTCGTAGACAACTTTTCGAGGCAGTGGAAGAA
 GGCCGTTCCAGTCGACACAGTAAATCCTCTTCGGATAGAAAGTCGTAAGCGTGAGCTGAA
 AGAAGTGTTCGGTGATGACTCAGAGATTTCCAAAGAATCCAAGTGGTGTCAAGAAAAGAC
 GTATTCCTCGTTTCGAGGAGGTCGAAGAAGAGCCTGAAGTCATTCTGGTCCGCCATCG
 GAGAGTCCAGGAATGCTTACAAAATTGCAAAATTAACAAAATGATGGAGGCAGCAACGAG
 ACAGATTGAGGAACGAAAAAGCAGCTGTCCTTTATTTCGCCTCCAACACCACAGCCTA
 AAATCCATCATCTTACAGCCGGAGCGTTTGCCGATTGGAATACGATACAACCTAGT
 CAAGCTGCAACGTTTCAATGACGCCATCGAGAAGGCGCGAAAAGGCCGAGAGTTGC
 AAGCGGAATTCAAGCACAGCTGGCCTTGAAGCCGGGCTTGATAGGCAATGCTAACATG
 GTTGGCTAGCGAACTTACATGCCATGGGAATCGCCCTCCTAAGGTAGAGTTAAAAGA
 TCAGACTAAGCCAACGCCACTTATCTTAGACGAACAGGGCAGAACTGTGGACGCCACTG
 GAAAGGAAATTGAGCTGACACACAGAATGCCTACATTGAAGGCTAATATCAGAGCCGTT
 AAGCGTGAACAGTTAAGCAGCAGCTGAAGGAAAAACCTTCGGAAGATATGGAATCAAA
 CACCTTCTTTGACCCACGAGTATCCATCGCTCCGTCAACGACAACGACGTACCTTCAA
 GTTTCATGACAAGGGTAAAGTTCGAGAAGATAGCACAAAGACTTAGAACCAAGGCACAAC
 TTGAGAAATTGCAGGCGGAAAATCTCAAGCCGCCAGAAAACTGGCATCCATACTTCT
 ACTCGACTTGCAATTAATCGACCAAAAAAAGAGCTCAAGGAAGGAGACATACCTGAAAT
 AGAATGGTGGGACTCCTATATTATCCCAAgtagactttttttttgatttttgggatg

Majuscules: exons, minuscules: introns, underlined: homology arms.

Table M. 4: Primers to genotype each allele, Sanger sequencing, and amplify repair templates for gene replacement.

Gene	Allele	Primers to genotype	Primers for Sanger
<i>isy-1</i>	<i>cer115</i>	WT specific Fwd	Sanger Fwd
		<i>TTACTTGGATGACGAAGATGG</i>	<i>TAATGCAGGGTCCTATTGC</i>
		<i>cer115</i> specific Fwd	common Rev
		<i>GTTACCTTGACGATGAGGACTC</i>	<i>CCGCTCAGTTTACTTGTATT</i>
<i>cyn-15</i>	<i>cer119</i>	WT specific Fwd	Sanger Rev
		<i>TAATCACTGCAAGCGTCGAT</i>	<i>CCTCAATTATCTTGACTGGCG</i>
		<i>cer119</i> specific Fwd	common Fwd
		<i>TAATCACAGCGTCTGTGCAA</i>	<i>CACAACTCAAGCATGAATCAG</i>
<i>cyn-15</i>	<i>cer173</i>	<i>Fwd</i>	
		<i>CACAACTCAAGCATGAATCAG</i>	
		<i>Rev</i>	Same as for <i>cer119</i>
		<i>TGACAAACTCGACTCCTTCG</i>	
WT and <i>cer173</i> discernible by size			
<i>ama-1</i>	<i>cer135</i>	WT specific Rev	Sanger Rev
		<i>AGAACTACCCGTTTCGATCAC</i>	<i>GGATCGAAGGGATCGAAGAT</i>
		<i>cer135</i> specific Rev	common Fwd
		<i>AGAACTACCAGTACGGTCTGT</i>	<i>TTCTCGCTTATCATTCTTGG</i>
<i>prp-8</i>	<i>cer209</i>	WT specific Rev	Sanger Rev
		<i>ATTATGCAAATGCATCCTCG</i>	<i>GGGGGTTTGGGAAAATACAC</i>
		<i>cer209</i> specific Rev	common Fwd
		<i>ATGATTATGCAAATGCATCTCC</i>	<i>TATGGTGTATCGCCACCTGA</i>
<i>prp-8</i>	<i>cer210</i>	WT specific Rev	Sanger Rev
		<i>CCATACATGAATCCAGCAATC</i>	<i>GCAGTCAGAGAAACAGATCC</i>
		<i>cer210</i> specific Rev	common Fwd
		<i>ACCATACATGAATCCTGTGATT</i>	<i>AAGACTACTATCACCGAGCC</i>
<i>prp-3</i>	<i>cer194</i>	repair amplification Fwd	repair amplification Rev
		<i>GAGTTTATTAACAATTTTAAAC</i>	<i>AATTTCAAATTTTTCGTG</i>
		WT specific Fwd	WT specific Rev
		<i>ATACTCACAGACAGTTTCCG</i>	<i>ATACTCACAGACAGTTTCCG</i>
		<i>cer194</i> specific Fwd	<i>cer194</i> specific Rev
		<i>CGGCTTTGATCTTACAGAGG</i>	<i>ACCGATATGTGTACCCCTG</i>
Sanger Fwd	Sanger Rev		
<i>CTTTTCGTTAAAAGTGGCG</i>	<i>GACTTTTTCATTTTCATCAC</i>		

Gene	Allele	Primers to genotype	Primers for Sanger
		repair amplification Fwd <i>AAACCTAAAAAATCCTATA</i>	repair amplification Rev <i>CATCCCAAAAATCAAAA</i>
	<i>cer231</i>	Fwd A <i>TGCGACCAGTATTTGAGCAG</i>	Rev B <i>ATTTCCTTCCAGTGGCGTC</i>
		Fwd C <i>CCAACACCACAGCCTAAAAC</i>	Rev E <i>GGCAAATTGCGAGTTACCG</i>
<i>prp-3</i>	<i>cer231</i>		

Exon 2 humanized

Fwd A Rev B Fwd C Rev D

Combinations of A+B, C+D to genotype *cer231* specifically and Sanger.
A+D to distinguish WT and *cer231* by size.

Fwd: forward primer, Rev: reverse primer.

9. Genetic crosses

Males were induced by placing six plates with six L4 larvae each at 31°C for 4 h. Male worms were recovered from the F₁ and used for crosses (directly between strains or self-cross to generate more males). I placed five males with two hermaphrodites in 35-mm plates in triplicates. P₀ males and hermaphrodites were passed to a fresh plate daily and maintained at 20°C. Hermaphrodites were singled from plates containing F₁ males, indicative of successful cross, and genotyped once laid eggs. Homozygous double mutants were isolated by singling out from individual hermaphrodites and PCR genotyping.

10. Drug screen and drug treatment

10.a. Drug screen and validation

I tested a library of 929 drugs (853 FDA approved and 76 epigenetic drugs) from Selleck Chemicals DMSO-diluted at 10 mM (www.selleckchem.com). The screen was performed in 96-well plates containing 50 μ M of each drug in S-basal (Stiernagle, 2006) supplemented with 5 μ g/ml cholesterol, 50 μ g/ml ampicillin, 12.5 μ g/ml tetracycline, and OP50 as a food source. Approximately 10 of either WT or *prp-8(cer14)* synchronized L1 worms were seeded to each well and maintained in a humidified chamber at 25°C. The scoring was done on day three and day four by visual observation and a 15 min WmicrotrackerTM (PhylumTech, Santa Fe, Argentina) measurement. DMSO 0.5% was used as a negative control. Potential candidates were retested under the same condition in triplicates, and the four selected candidates proceeded to validation in agar plates.

Further validation was done in duplicate in 35-mm plates containing NGM agar with OP50 that was freeze-thawed three times at -80°C as a food source. Drugs obtained from Sigma-Aldrich were used: dequalinium chloride (ref: PHR1300), flutamide (ref: F9397), dronedarone hydrochloride (ref: D9696), and doxycycline hyclate (ref: D9891). Drugs were added on top of the agar and kept at 4°C overnight to allow its diffusion. Around 50 synchronized L1 worms of each strain were added to each plate and kept at 25°C. At 48 h post-seeding, pictures of the worms were taken, and length measured as described in part six.

10. b. Herboxidiene and α -amanitin treatment

Herboxidiene and α -amanitin were dissolved in DMSO. *C. elegans* were treated in liquid as described above, adjusting final concentrations of the drug. For herboxidiene, after 48 h, worms were recovered and seeded onto NGM plates to take pictures for worm length measurement. For α -amanitin, worms were scored on day two, three, and four to check the progress. For representative pictures, worms were recovered in NGM plates as described for herboxidiene.

11. UV-C and HU treatment

11. a. UV-C treatment

Synchronized worms 24 h post-seeding were recovered and washed in M9. Then, transferred to a bacteria-free 55-mm NGM plate and irradiated with 100 J/m² UV in a UV crosslinker (model 2400, Stratagene). After, worms were returned to OP50-containing plates for additional 24 h and mounted on slides with levamisole 0,3 M for GFP signal scoring through an inverted fluorescence microscope Nikon ECLIPSE TI-s.

11. b. HU treatment

500 μ l of H₂O diluted HU (Sigma, H8627) was added to 55-mm NGM OP50-containing plates and let dry and diffuse for three hours minimum. Afterward, synchronized L1s were seeded on and left for 24 h. Finally, worms were mounted on slides with levamisole 0,3 M for GFP signal scoring through an inverted fluorescence microscope Nikon ECLIPSE TI-s.

12. smFISH

Quasar 570 labeled Stellaris FISH Probes against *atl-1* transcript were ordered from Bioresearch Technologies.

Worms were recovered in M9 and washed three times. Next, fixed with 3.7% vol/vol formaldehyde in PBS (Sigma, P4417) for 45 min in agitation. After a couple of washes permeabilized overnight in 70% ethanol. Then, washed for two to five minutes in Stellaris RNA FISH Wash Buffer A (Bioresearch Technologies Cat# SMF-WA1-60) and hybridized with probes in the formamide containing Stellaris RNA FISH Hybridization Buffer (Bioresearch Technologies Cat# SMF-HB1-10) overnight at 37°C. Finally, after a 30 min wash in Stellaris RNA FISH WASH Buffer A, counterstaining with DAPI along with a short five minutes wash with Stellaris RNA FISH WASH Buffer B (Bioresearch Technologies Cat# SMF-WB1-20), worms were mounted and visualized on an inverted fluorescence microscope (Zeiss Axio Observer Z1).

13. Mortal germline

Before the experiment beginning, all the strains were outcrossed. Six L1 larvae were transferred to a fresh 55-mm OP50 containing plates every two generations and maintained at 25°C until complete sterility of *prp-8(cer22)*. In the first replicate, during the experiment brood size of the worms was tracked weekly following the methodology of part two.

14. Nanopore sequencing and semiquantitative PCR

14.a. RNA extraction

Total RNA for cDNA-PCR sequencing was extracted using Invitrogen Purelink RNA Mini Kit (Thermo Fischer, 12183020). Before direct RNA sequencing mRNA was isolated from the total RNA with Poly (A) mRNA Magnetic Beads (New England BioLabs, E7490G). For semiquantitative PCR of synchronized populations and re-extracted RNA an in-house RNA extraction protocol was used. Shortly, worms were recovered in M9 and after several washes resuspended in TRI Reagent (Molecular Research Center, TR118). Then, five freeze-thaw cycles were applied, and chloroform was added. Samples were allowed to separate phases, and after a centrifuge, the aqueous phase was recovered. Nucleic acids were precipitated with isopropanol, and the pellet after two washes with 75% ethanol was resuspended in nuclease-free water.

14.b. Nanopore sequencing

For cDNA-PCR sequencing, the SQK-PCS108 kit was employed following the manufacturer's instructions. Briefly, retrotranscription and strand switching steps were performed. The sample was then amplified with primers intended to select for full transcripts, and sequencing adapters were added to the library prior to loading into the flow cell (**Figure R. 18**).

For direct RNA sequencing, the SQK-RNA001 kit was used, and the manufacturer's instructions were followed. The initial amount of mRNA was >500 ng. The optional retrotranscription step to improve sequencing

quality was performed. Note that despite retrotranscription of the first strand, the sequenced molecule is still RNA (**Figure R. 18**).

14.c. Bioinformatic pipeline

I used a pipeline intended to identify novel transcripts (<https://community.nanoporetech.com/knowledge/bioinformatics/using-pinfish-for-gene-tra/tutorial> consulted 25/04/2021) and developed by the Nanopore community. This pipeline uses *pychopper* tool to select for full-length cDNA, then it maps these reads to an annotated genome and creates a genome index with *minimap2* (Li, 2018). Afterward, the selected reads are mapped to the genome (*minimap2*), sorted, and indexed with *samtools* (Li *et al.*, 2009). A GFF annotation file from mapped reads is then generated with *Pinfish*, and a consensus sequence correction with *Racon* (Vaser *et al.*, 2017) of *Pinfish* clustered reads is done. Next, clustered and polished reads are remapped to the genome with *minimap2*, to generate a new GFF file from such clean reads (*Pinfish*). Finally, partial and redundant transcript annotations are collapsed (*Pinfish*), and *GFFcompare* is used to compare reference genome annotation with our generated GFF in order to identify novel isoforms. In parallel, a FASTA file from collapsed annotations is generated (*gffread*) (**Figure R. 20 and Table R. 3**).

After the candidates were retrieved from the pipeline, a manual revision in Integrative Genomic Viewer was done to select candidates for validation.

14.d. Semiquantitative PCR

For the initial validation of AS events, the same RNA as for sequencing was used. RNA was purified by an in-house extraction method described above for synchronized populations and re-extraction of mixed populations. Prior to retrotranscription, DNase (ThermoFischer, EN0521) treatment of extracted nucleic acids was performed. cDNA was prepared with ReverseAid H Minus First Strand cDNA sequencing Kit (Fermentas,

K1632) from 1 µg of initial total RNA. Then, cDNA was amplified by PCR with selected primers (**Table M. 5 and Figure R. 22**) and products resolved by electrophoresis.

Table M. 5: Primers used for semiquantitative PCR.

Gene	Forward primer	Reverse primer
<i>brd-1</i>	AGTGTGAAATCAGAGCAACG	AACTCTCTGTTTCAGTCTTGA
<i>rnf-1</i>	CTGCTATCAGCCTTTTAATG	AGTCTCAGAATCGCTGTCTC
C05C10.7	TTGCCCTGAAAAACAACCTAG	CAACAAATAGGAATGACGGC
F11A10.6	TACGGAATAATGCGTTACCG	CAATGGTGTTCAGGAAGAAAC
<i>pcm-1</i>	TGCCAGTCAAAGAGCCTACG	AATCCTTGACGACCGTCTCCCT
<i>ugt-50</i>	GGATAGATATGTGTGCAGAT	TAGGTTCCACGCAACCTTGT
<i>act-1</i>	GAGGCCAATCCAAGAGAGGTATC	TCAGCGGTGGTGGTAAAGAGTAA

15. Gamma radiation

Synchronized L1 populations seeded on 55-mm NGM agar plates with OP50 were exposed to different doses of gamma radiation at Scientific and Technologic Centres of University of Barcelona (CCiTUB). Afterward, worms were left at 20°C for 72 h and length measured as explained above.

16. Statistical analyses and figures

"N" stands for the number of experimental replicates, and "n" the total number of individual worms for each group. The parametricity of the data was assessed using the Kolmogorov-Smirnov test. Figure legends indicate the statistical analysis used for each of the experiments. Results in Figures R 1, R. 2, R. 3B-C, R. 7, R. 8, and R. 26 are analyzed using GraphPad Prism v6 and v8.3.0 software. Figures R. 10, R. 11, R. 12, R. 17, R. 24, and Suppl. Figures R. 1 and R. 4C were analyzed in R 4.0.3. Data from the effect of the drugs on worm length was processed using the aligned rank transformation approach with *ARTool* v0.10.6. Later, the interaction

between drug concentrations and strains was compared by regular two-way ANOVA. To determine which groups presented differences in worm length, F-test with Bonferroni correction was applied using *TestInteraction* function from the package *phia* v0.2-1. Figures A. 1, R. 9, R. 13 A, and R. 18 are created with BioRender.com.

SUPPLEMENTARY
DATA

Supplementary Table I. 1: Missense mutations of the s-adRP genes with a clear *C. elegans* ortholog reported in scientific articles.

Gene	Nucleotide mutation	Amino acid consequence	<i>C. elegans</i> equivalent residue	References
<i>PRPF3</i> <i>prp-3</i>	c.1345C>G	p.Arg449Gly	p.Arg385	(Zhong <i>et al.</i> , 2016)
	c.1466C>A	p.Ala489Asp	p.Ala425	(Gamundi <i>et al.</i> , 2008)
	c.1478C>T	p.Pro493Ser	p.Pro429	(Chakarova <i>et al.</i> , 2002; Sullivan <i>et al.</i> , 2006)
	c.1482C>T	p.Thr494Met	p.Thr430	(Chakarova <i>et al.</i> , 2002; Martinez-Gimeno <i>et al.</i> , 2003; Wada <i>et al.</i> , 2004; Sullivan <i>et al.</i> , 2006; Vaclavik <i>et al.</i> , 2010; Audo <i>et al.</i> , 2012; Kim <i>et al.</i> , 2012; Xu <i>et al.</i> , 2014; Martin-Merida <i>et al.</i> , 2018; Gao <i>et al.</i> , 2019; Zampaglione <i>et al.</i> , 2020)
<i>PRPF4</i> <i>prp-4</i>	c.1532A>C	p.His511Pro	p.His447	(Zhong <i>et al.</i> , 2016)
	c.556C>G	p.Pro187Ala	*p.Arg160	(Benaglio <i>et al.</i> , 2014)
	c.575G>A	p.Arg192His	p.Arg165	(Linder <i>et al.</i> , 2014)
	c.944C>T	p.Pro315Leu	p.Pro288	(Chen <i>et al.</i> , 2014)
<i>PRPF6</i> <i>prp-6</i>	c.515G>A	p.Arg172Gln	p.Arg185	(Gao <i>et al.</i> , 2019)
	c.514C>T	p.Arg172Trp		(Huang <i>et al.</i> , 2015; Koyanagi <i>et al.</i> , 2019; Gao <i>et al.</i> , 2019)
	c.542C>T	p.Pro181Leu	p.Pro194	(Huang <i>et al.</i> , 2017)
	c.551A>G	p.Asp184Gly		(Huang <i>et al.</i> , 2015)
	c.550G>C	p.Asp184His	p.Asp197	(Oishi <i>et al.</i> , 2014)
	c.550G>A	p.Asp184Asn		(Zampaglione <i>et al.</i> , 2020)
	c.2185C>T	p.Arg729Trp	p.Arg756	(Tanackovic <i>et al.</i> , 2011)

Gene	Nucleotide mutation	Amino acid consequence	<i>C. elegans</i> equivalent residue	References
<i>PRPF8</i> <i>prp-8</i>	c.5041C>T	p.Arg1681Trp	p.Arg1674	(Zhang <i>et al.</i> , 2016)
	c.5792C>T	p.Thr1931Met	p.Thr1924	(Jones <i>et al.</i> , 2017)
	c.5804G>A	p.Arg1935His	p.Arg1928	(Xu <i>et al.</i> , 2014; Lunghi <i>et al.</i> , 2019)
	c.6353C>T	p.Ser2118Phe	p.Ser2111	(Towns <i>et al.</i> , 2010; Maubaret <i>et al.</i> , 2011)
	c.6470T>A	p.Val2157Glu	p.Val2150	(Ellingford <i>et al.</i> , 2016; Avela <i>et al.</i> , 2018)
	c.6840C>A	p.Asn2280Lys	p.Asn2273	(Van Cauwenbergh <i>et al.</i> , 2017)
	c.6901C>A	p.Pro2301Thr	p.Pro2294	(McKie <i>et al.</i> , 2001)
	c.6901C>T	p.Pro2301Ser		(Ziviello <i>et al.</i> , 2005; Testa <i>et al.</i> , 2006; Sullivan <i>et al.</i> , 2013)
	c.6912C>G	p.Phe2304Leu	*p.Tyr2297	(McKie <i>et al.</i> , 2001; Sullivan <i>et al.</i> , 2006, 2013; Xu <i>et al.</i> , 2014; Van Cauwenbergh <i>et al.</i> , 2017; Koyanagi <i>et al.</i> , 2019; Zampaglione <i>et al.</i> , 2020)
	c.6910T>C			
	c.6926A>C	p.His2309Pro	p.His2302	(McKie <i>et al.</i> , 2001; Towns <i>et al.</i> , 2010)
	c.6926A>G	p.His2309Arg		(McKie <i>et al.</i> , 2001; Walia <i>et al.</i> , 2008; Towns <i>et al.</i> , 2010; Bravo-Gil <i>et al.</i> , 2017; Riera <i>et al.</i> , 2017; Zampaglione <i>et al.</i> , 2020)
	c.6926G>A	p.Arg2310Lys	p.Arg2303	(McKie <i>et al.</i> , 2001; Towns <i>et al.</i> , 2010)
	c.6928A>G	p.Arg2310Gly		(McKie <i>et al.</i> , 2001; Martínez-Gimeno <i>et al.</i> , 2003; Sullivan <i>et al.</i> , 2006; Towns <i>et al.</i> , 2010; Martín-Merida <i>et al.</i> , 2018; Koyanagi <i>et al.</i> , 2019; Zenteno <i>et al.</i> , 2020)
	c.6930G>C	p.Arg2310Ser	p.Phe2307	(Towns <i>et al.</i> , 2010; Maubaret <i>et al.</i> , 2011; Carrigan <i>et al.</i> , 2016; Wu <i>et al.</i> , 2018)
c.6942C>A	p.Phe2314Leu	(McKie <i>et al.</i> , 2001; Avela <i>et al.</i> , 2019)		

Gene	Nucleotide mutation	Amino acid consequence	<i>C. elegans</i> equivalent residue	References
<i>PRPF8</i> <i>prp-8</i>	c.6985G>A	p.Asp2329Asn	p.Asp2323	(Xu <i>et al.</i> , 2014)
	c.6992A>G	p.Glu2331Gly	p.Glu2325	(Audo <i>et al.</i> , 2012)
	c.7000T>A	p.Tyr2334Asn	*p.Phe2328	(De Erkenez, Berson, & Dryja, 2002; Towns <i>et al.</i> , 2010)
	c.7006T>C	p.Ter2336Arg	Ter2330	(Martínez-Gimeno <i>et al.</i> , 2003; Van Cauwenbergh <i>et al.</i> , 2017)
	c.7008A>G	p.Ter2336Trp	Ter2330	(Gao <i>et al.</i> , 2019)
	c.7007G>C	p.Ter2336Serext Ter41	Ter2330	(Zampaglione <i>et al.</i> , 2020)
	c.319C>G	p.Leu107Val	*p.Ile116	(Rivolta <i>et al.</i> , 2006; Rio Frio <i>et al.</i> , 2008)
c.341T>A	p.Ile114Asn	*p.Val123	(Ellingford <i>et al.</i> , 2016; Wheway <i>et al.</i> , 2019)	
c.413C>A	p.Thr138Lys	p.Thr147	(Waseem <i>et al.</i> , 2007)	
c.581C>A	p.Ala194Glu	p.Ala203	(Vithana <i>et al.</i> , 2001)	
c.590T>C	p.Leu197Pro	p.Leu206	(Wu <i>et al.</i> , 2018; Bryant <i>et al.</i> , 2018, 2019)	
c.646G>C	p.Ala216Pro	p.Ala225	(Vithana <i>et al.</i> , 2001)	
c.736G>A	p.Ala246Thr	*p.Ser255	(Xu <i>et al.</i> , 2014; Martín-Merida <i>et al.</i> , 2018)	
c.764A>T	p.Gln255Leu	*p.Thr264	(Oishi <i>et al.</i> , 2014)	
c.815G>T	p.Gly272Val	p.Gly281	(Sullivan <i>et al.</i> , 2006; Daiger <i>et al.</i> , 2014)	
c.839T>G	p.Val280Gly	p.Val289	(Birtel <i>et al.</i> , 2018)	
c.896G>A	p.Cys299Tyr	*p.Val308	(Bhatia <i>et al.</i> , 2018)	
c.895T>C	p.Cys299Arg	*p.Val308	(Sullivan <i>et al.</i> , 2006; Blanco-Kelly <i>et al.</i> , 2012; Xu <i>et al.</i> , 2012; Martín-Merida <i>et al.</i> , 2017, 2018; Myers, Iannaccone, & Bidelman, 2017)	
<i>PRPF31</i> <i>prp-31</i>				

Gene	Nucleotide mutation	Amino acid consequence	<i>C. elegans</i> equivalent residue	References
<i>PRPF31</i> <i>prp-31</i>	c.910C>T	p.Arg304Cys	p.Arg313	(Huang <i>et al.</i> , 2015; Zampaglione <i>et al.</i> , 2020)
	c.1222C>T	p.Arg408Trp	p.Arg419	(Huang <i>et al.</i> , 2017; Xiao <i>et al.</i> , 2017; Jespersgaard <i>et al.</i> , 2019)
	c.1547G>T	p.Cys516Phe	*p.Thr510	(Yusuf <i>et al.</i> , 2019)
	c.1614T>G	p.Ile538Met	p.Ile532	(Huang <i>et al.</i> , 2015)
	c.1625C>T	p.Ala542Val	p.Ala536	(Bowne <i>et al.</i> , 2013; Daiger <i>et al.</i> , 2014)
	c.1631T>C	p.Met544Thr	p.Met538	(Huang <i>et al.</i> , 2015)
	c.1634G>A	**p.Arg545His	*p.Lys539	(Gerth-Kahlert <i>et al.</i> , 2019)
	c.1871G>A	p.Arg624Lys	p.Arg618	(Oishi <i>et al.</i> , 2014; Ellingford <i>et al.</i> , 2016)
	c.1981G>T	p.Val661Leu	p.Val655	Van Cauwenbergh <i>et al.</i> 2017
	c.2041C>T	p.Arg681Cys		(Benaglio <i>et al.</i> , 2011; Bowne <i>et al.</i> , 2013; Wang <i>et al.</i> , 2014a; Xu <i>et al.</i> , 2014; Coussa <i>et al.</i> , 2015; Ellingford <i>et al.</i> , 2016; Van Cauwenbergh <i>et al.</i> , 2017; Martin-Merida <i>et al.</i> , 2018; Yusuf <i>et al.</i> , 2019; Gao <i>et al.</i> , 2019; Jespersgaard <i>et al.</i> , 2019)
<i>SNRNP200</i> <i>snrp-200</i>	c.2042G>A	p.Arg681His	p.Arg674	(Benaglio <i>et al.</i> , 2011; Bowne <i>et al.</i> , 2013; Pan <i>et al.</i> , 2014; Oishi <i>et al.</i> , 2014; Van Cauwenbergh <i>et al.</i> , 2017; Martin-Merida <i>et al.</i> , 2018; Wu <i>et al.</i> , 2018; Koyanagi <i>et al.</i> , 2019; Gao <i>et al.</i> , 2019; Zampaglione <i>et al.</i> , 2020)
	Not stated	p.Arg681Lys		(Daiger <i>et al.</i> , 2014)
	c.2044C>T	p.Pro682Ser	p.Pro675	(Bowne <i>et al.</i> , 2013; Koyanagi <i>et al.</i> , 2019)
	c.25047G>T	p.Val683Leu	p.Val676	(Benaglio <i>et al.</i> , 2011; Oishi <i>et al.</i> , 2014; Koyanagi <i>et al.</i> , 2019)

Gene	Nucleotide mutation	Amino acid consequence	<i>C. elegans</i> equivalent residue	References
<i>SNRNP200</i> <i>snrp-200</i>	c.2066A>G	p.Tyr689Cys	p.Tyr682	(Benaglio <i>et al.</i> , 2011)
	c.2359G>A	p.Ala787Thr	p.Ala780	(Wang <i>et al.</i> , 2014b; Xu <i>et al.</i> , 2014; Costa <i>et al.</i> , 2017; Martin-Merida <i>et al.</i> , 2018; Yusuf <i>et al.</i> , 2019)
	c.2593G>A	p.Gly865Ser	p.Gly858	(Koyanagi <i>et al.</i> , 2019)
	c.2653C>G	p.Gln885Glu	p.Gln878	(Liu <i>et al.</i> , 2012)
	c.2879C>T	p.Ala960Val	p.Ala958	(Ellingford <i>et al.</i> , 2016; van Doormaal <i>et al.</i> , 2017)
	c.3260C>T	p.Ser1087Leu	p.Ser1080	(Zhao <i>et al.</i> , 2009; Benaglio <i>et al.</i> , 2011; Bowne <i>et al.</i> , 2013; Fernandez-San Jose <i>et al.</i> , 2015; Coussa <i>et al.</i> , 2015; Ellingford <i>et al.</i> , 2016; Martin-Merida <i>et al.</i> , 2018; Gerth-Kahlert <i>et al.</i> , 2019; Koyanagi <i>et al.</i> , 2019; Gao <i>et al.</i> , 2019; Zenteno <i>et al.</i> , 2020; Zampaglione <i>et al.</i> , 2020)
	c.3269G>T	p.Arg1090Leu	p.Arg1083	(Li <i>et al.</i> , 2010; Cvačková, Matějů, & Staněk, 2014)
	c.3454C>T	p.Arg1152Cys	p.Arg1145	(Huang <i>et al.</i> , 2017)
	c.5356G>A	p.Arg1779His	p.Arg1778	(Zhang <i>et al.</i> , 2013; Gao <i>et al.</i> , 2019)
	c.6025C>T	p.Arg2009Cys	p.Arg2008	(Huang <i>et al.</i> , 2017)
<i>DHX38</i>	c.971G>A	**p.Arg324Gln	p.Arg231	(Latif <i>et al.</i> , 2018)
<i>mog-1</i>	c.995G>A	**p.Gly332Asp	*p.Ala239	(Ajmal <i>et al.</i> , 2014)

*Not conserved in *C. elegans*. ** Autosomal recessive mutations. *CWC27* and *PAPI* excluded as non of the *CWC27* mutations is missense and *PAPI* lacks of a *C. elegans* ortholog.

Supplementary Table R. 1. List of genes tested in the RNAi screen with the phenotypes obtained.

RNAi library	RNAi clone	<i>C. elegans</i> locus	WT (N2)	<i>prp-8(cer22[R22303G])</i>	WT (N2)	<i>snrp-200(cer24[S1080L])</i>	<i>snrp-200(cer24)</i>
A	T08A11.2	<i>sftb-1</i>	Lva	Lva	Lva	Lva	Lva
V	K02F2.3	<i>teg-4</i>	Rbs, Emb	Rbs, Emb	pSte, Emb	pSte, Emb	pSte, Emb
V	H20J04.8	<i>mog-2</i>	No phenotype	Rbs, pEmb, pLet	No phenotype	No phenotype	No phenotype
V	Y71D11A.2	<i>smr-1</i>	No phenotype	No phenotype	No phenotype	No phenotype	No phenotype
A	F11A10.2	<i>repo-1</i>	No phenotype	No phenotype	Rbs	Rbs	Rbs
A	C08B11.5	<i>sap-49</i>	Ste, Lva, pPvl	Ste, Lva, pPvl	Ste, Lva	Ste, Lva	Ste, Lva
V	F56D2.6	<i>ddx-15</i>	Ste, pLva, pPvl	Ste, pLva, pPvl	Ste, pLvl, pPvl	Ste, pLvl, pPvl	Ste, pLvl, pPvl
V	C33H5.12	<i>rsp-6</i>	No phenotype	No phenotype	No phenotype	No phenotype	No phenotype
V	D1081.8	<i>cdc-5L</i>	Lva, movement	Lva, movement	Lva, pLvl, movement	Lva, movement	Lva, movement
V	T10F2.4	<i>prp-19</i>	abnormal	abnormal	abnormal	abnormal	abnormal
V	D1054.15	<i>plr-1</i>	Ste, pLet	Ste, pLet	Ste, pLet, pPvl	Ste, pLet, pPvl	Ste, pLet, pPvl
V	T11G6.8	<i>rhm-22</i>	pPvl, pLva, pSte	pPvl, pLva, pSte	Lva, pPvl	Lva, pPvl	Lva, pPvl
A	Y116A8C.32	<i>sfa-1</i>	Ste, pPvl, pLva, pLet	Ste, pPvl, pLva, pLet	pPvl, Lva, pLet	pPvl, Lva, pLet	pPvl, Lva, pLet
V	F43G9.10	<i>mfpap-1</i>	pEmb, pSte, Rbs	pEmb, pSte, Rbs	pEmb, Rbs	pEmb, Rbs	pEmb, Rbs
V	F33A8.1	<i>let-858</i>	pPvl, Ste	pPvl, Ste	Rbs	Rbs	Rbs
A	C04H5.6	<i>mog-4</i>	Lva	Lva	Lva	Lva	Lva
A	M03C11.7	<i>prp-3</i>	pSte, pLva	pSte, pLva	pSte	pSte	pSte
V	C36B1.5	<i>prp-4</i>	No phenotype	No phenotype	No phenotype	No phenotype	No phenotype
A	ZK328.2	<i>eft-1</i>	pPvl, pLva, Ste	pPvl, pLva, Ste	pPvl, pLva, Ste	pPvl, pLva, Ste	pPvl, pLva, Ste
V	F44G4.4	<i>tdp-1</i>	Lva, Sck, pLvl	Lva, Sck, pLvl	Lva	Lva	Lva
A	F08B4.1	<i>dic-1</i>	No phenotype	No phenotype	No phenotype	No phenotype	No phenotype
			Ste, pEmb	Ste, pPvl	Ste, pEmb	Ste, pEmb	Ste, pEmb

RNAi library	RNAi clone	<i>C. elegans</i> locus	WT (N2)	<i>prp-8(cer22[R2303G])</i>	WT (N2)	<i>snrp-200(cer24[S1080L])</i>	<i>snrp-200(cer24)</i>
V	F43G9.12		pPvl, Ste, pLva	pPvl, Ste, pLva	pPvl, Ste, pLva, Sck, pLet	pPvl, Ste, pLva, Sck, pLet	pPvl, Ste, pLva, Sck, pLet
V	Y75B12B.2	<i>cyn-7</i>	No phenotype	No phenotype	No phenotype	No phenotype	No phenotype
V	R08D7.1		Ste, pPvl	Ste, pPvl	Ste, Emb	Ste, Emb	Ste, Emb
V	K07C5.6		Lva (also pPvl, pLet)	Lva	pLvl, Ste	pLvl, Ste, pLet	pLvl, Ste, pLet
V	W08E3.1	<i>snr-2</i>	pPvl, pLva, pLvl	pPvl, pLva, pLvl	Lva, pLvl	Lva, pLvl	Lva, pLvl
A	F58B3.7		No phenotype	No phenotype	No phenotype	No phenotype	No phenotype
A	ZK686.4	<i>snu-23</i>	No phenotype	No phenotype	No phenotype	No phenotype	No phenotype
A	F43G9.5	<i>cfim-1</i>	No phenotype	No phenotype	No phenotype	No phenotype	No phenotype
A	Y54E10A.9	<i>vbh-1</i>	No phenotype	No phenotype	No phenotype	No phenotype	No phenotype
V	B0336.9	<i>swp-1</i>	No phenotype	No phenotype	No phenotype	No phenotype	No phenotype
A	B0495.8		No phenotype	No phenotype	No phenotype	No phenotype	No phenotype
V	B0511.7		No phenotype	No phenotype	No phenotype	No phenotype	No phenotype
A	C07A4.1	<i>tiar-3</i>	No phenotype	No phenotype	No phenotype	No phenotype	No phenotype
V	C07E3.1	<i>stip-1</i>	No phenotype	No phenotype	No phenotype	No phenotype	No phenotype
A	C07H6.4		No phenotype	No phenotype	No phenotype	No phenotype	No phenotype
A	C14A4.4	<i>crn-3</i>	Ste	Ste	Ste	Ste	Ste
A	C16A3.8	<i>thoc-2</i>	No phenotype	No phenotype	No phenotype	No phenotype	No phenotype
V	C26D10.2	<i>hel-1</i>	Lva, Sck, pLvl, movement abnormal	Lva, Sck, pLvl, movement abnormal	Lva, pLvl, movement abnormal	Lva, pLvl	Lva, pLvl
V	C30B5.4		pPvl, pLva, pLet	pPvl, pLva, pLet	pPvl, pLva, pLet, pEmb	pPvl, pLva, pLet, pEmb	pPvl, pLva, pLet, pEmb
V	C34D4.12	<i>cyp-12</i>	No phenotype	No phenotype	No phenotype	No phenotype	No phenotype
V	C50D2.5		No phenotype	No phenotype	Lva, pLvl	Lva, pLvl	Lva, pLvl
V	C50F2.3	<i>syf-1</i>	Lva, Sck	Lva, pLvl	Gro	Gro	Gro

RNAi library	RNAi clone	<i>C. elegans</i> locus	WT (N2)	<i>prp-8(cer22[R22303G])</i>	WT (N2)	<i>snrp-200(cer24[S1080L])</i>
				<i>prp-8(cer22)</i>		<i>snrp-200(cer24)</i>
V	CC4.3	<i>smu-1</i>	No phenotype	No phenotype	Rbs	Rbs
V	D2089.1	<i>rsp-7</i>	Lva, Sck	Lva, Sck	Lva	Lva
V	E01A2.2		No phenotype	No phenotype	No phenotype	No phenotype
A	EEED8.5	<i>mog-5</i>	Lva, pPvl, Sck	Lva, pPvl, Sck	Lva, pPvl	Lva, pPvl
A	EEED8.7	<i>rsp-4</i>	No phenotype	No phenotype	No phenotype	No phenotype
A	F01F1.7	<i>ddx-23</i>	Ste	Ste	Ste	Ste
V	F09D1.1	<i>usp-39</i>	pPvl,pSte, pLet	pPvl,pSte, pLet	pPvl,pSte, pLet, pLva	pPvl,pSte, pLet, pLva
A	F19F10.9		Ste, pPvl, pLva	Ste, pPvl, pLva	Ste, pPvl, pLva, movement abnormal,	Ste, pPvl, pLva, movement abnormal, pLet
V	F22D6.5	<i>prpf-4</i>	No phenotype	No phenotype	No phenotype	No phenotype
A	F25B4.5		No phenotype	No phenotype	No phenotype	No phenotype
V	F26A3.2	<i>ncbp-2</i>	Ste, pPvl, movement abnormal	Ste, pPvl, movement abnormal	Ste, pPvl, movement abnormal	Ste, pPvl, movement abnormal
V	F32B6.3		pEmb	pEmb	No phenotype	No phenotype
V	F37E3.1	<i>ncbp-1</i>	Ste, pPvl	Ste, pPvl	Ste, pPvl	Ste, pPvl
V	F42H10.7	<i>ess-2</i>	No phenotype	No phenotype	No phenotype	No phenotype
A	F45C12.3	<i>ceh-81</i>	No phenotype	No phenotype	No phenotype	No phenotype
A	F49D11.1	<i>prp-17</i>	Ste, pPvl	Ste, pPvl	Ste, pGro	Ste, pPvl
V	F53B7.3	<i>isy-1</i>	pPvl, Lva	pPvl,Lva (much earlier than N2)	pPvl, Lva,pLet	pPvl, Lva,pLet
A	F53H1.1		No phenotype	No phenotype	No phenotype	No phenotype
V	F59E10.2	<i>mog-6</i>	No phenotype	No phenotype	No phenotype	No phenotype
V	K01G5.1	<i>rnf-113</i>	No phenotype	No phenotype	No phenotype	No phenotype
V	K02F3.11	<i>rnp-5</i>	No phenotype	No phenotype	No phenotype	No phenotype

RNAi library	RNAi clone	<i>C. elegans</i> locus	<i>prp-8(cer22)[R2303G]</i>		<i>snrp-200(cer24)[S1080L]</i>	
			WT (N2)	<i>prp-8(cer22)</i>	WT (N2)	<i>snrp-200(cer24)</i>
A	K03H1.2	<i>mog-1</i>	pLet, pEmb	pLet, pEmb	Rbs, Sck	Rbs, Sck
V	K04G7.10	<i>rnp-7</i>	No phenotype	No phenotype	No phenotype	No phenotype
V	K08D10.4	<i>rnp-2</i>	No phenotype	No phenotype	No phenotype	No phenotype
A	M03F8.3	<i>phi-12</i>	pPvl, Lva, pLet, Ste	pPvl, Lva, pLet, Ste	Lva	Lva
V	M28.5		No phenotype	No phenotype	No phenotype	No phenotype
V	R07E5.1		No phenotype	No phenotype	No phenotype	No phenotype
A	R07E5.14	<i>rnp-4</i>	Ste	Ste pLva, pLvl	Lva, pPvl, pLvl	Lva, pLvl
V	R09B3.5	<i>mag-1</i>	pSte	pSte	pSte	pSte
A	R107.8	<i>lin-12</i>	No phenotype	No phenotype	Rbs	Rbs
A	T03F6.2	<i>daj-17</i>	No phenotype	No phenotype	No phenotype	No phenotype
A	T07D4.3	<i>rha-1</i>	No phenotype	No phenotype	No phenotype	No phenotype
A	T13H5.4	<i>phi-8</i>	Ste, pPvl, Lva, pLvl	Ste, pPvl, Lva, pLvl	Lva, Sck	Lva, Sck, pLet
V	T27F2.1	<i>skp-1</i>	Lva, pLet, movement abnormal	Lva, pLet, movement abnormal	Lva, Sck	Lva, Sck, pLet
V	T28D9.2	<i>rsp-5</i>	No phenotype	No phenotype	Rbs, pEmb	Rbs, pEmb
V	W02B12.2	<i>rsp-2</i>	No phenotype	No phenotype	No phenotype	No phenotype
V	W02B12.3	<i>rsp-1</i>	No phenotype	No phenotype	No phenotype	No phenotype
V	W03H9.4	<i>cacn-1</i>	pLva, pPvl	pLva, pPvl	pLva, pPvl, pLet, pSte	pLva, pPvl, pLet, pSte
V	W07E6.4	<i>prp-21</i>	pPvl, Lva	pPvl, Lva	Lva	Lva
A	W08D2.7	<i>mtr-4</i>	pPvl, pLva	pPvl, pLva	Ste, pLet	Ste, pLet
V	Y116A8C.42	<i>snr-1</i>	Lva, movement variant	Lva, movement variant	Lva	Lva
V	Y32H12A.2	<i>thoc-5</i>	No phenotype	No phenotype	No phenotype	No phenotype
A	Y41E3.11	<i>hrpu-1</i>	No phenotype	No phenotype	Rbs	Rbs

RNAi library	RNAi clone	<i>C. elegans</i> locus	WT (N2)	<i>prp-8(cer22)[R2303G]</i>	WT (N2)	<i>snrp-200(cer24[S1080L])</i>	<i>snrp-200(cer24)</i>
V	Y47G6A.20	<i>rnp-6</i>	Rup, pLva, pLet, pPvl	Rup, pLva, pLet, pPvl	Ste, pEmb, pPvl	Ste, pEmb, pPvl	
V	Y49E10.15	<i>snr-6</i>	Lva, pLvl	Lva, pLvl	Lva	Lva	
V	Y49F6B.4	<i>smu-2</i>	No phenotype	No phenotype	No phenotype	No phenotype	
A	Y52B11A.9	<i>dxbp-1</i>	No phenotype	No phenotype	No phenotype	No phenotype	
V	Y55F3AM.3	<i>rbm-39</i>	No phenotype	No phenotype	No phenotype	No phenotype	
V	Y59A8B.6	<i>prp-6</i>	Lva	Lva, pLvl	Lva	Lva	
V	Y65B4A.6		Lva, pLvl, movement abnormal	Lva, pLvl, movement abnormal	Lva, pLvl	Lva, pLvl	
V	Y71F9B.4	<i>snr-7</i>	pLva, Ste, Sck	pLva, Ste, Sck	Lva	Lva	
V	Y87G2A.6	<i>cyn-15</i>	No phenotype	Emb, Ste, Gro	No phenotype	No phenotype	
V	ZK1067.6	<i>sym-2</i>	No phenotype	No phenotype	No phenotype	No phenotype	
V	ZK1127.9	<i>tcer-1</i>	No phenotype	pGro	No phenotype	No phenotype	
V	ZK652.1	<i>snr-5</i>	No phenotype	No phenotype	No phenotype	No phenotype	

The source for the RNAi clone (Ahringer library (A) or ORFeome library (V)), the name for the corresponding *C. elegans* genes, the yeast and human orthologs, the spliceosome complex in which it participates, from which class or family of genes it belongs and the observed phenotype in *cer22* and *cer24* screens, are indicated. The selected interactors are highlighted in yellow. Phenotype abbreviations: Ste: sterility, Rbs: reduced brood size, Gro: developmental delay, Lva: larval arrest, Pvl: protruding vulva, Let: lethality, Lvl: larval lethality, Emb: embryonic lethal, Sck: sick, Rup: ruptured. “p” before a phenotype indicates “partial”.

Supplementary Figure R. 2: List of drugs used in the drug screen, phenotypes obtained in the primary screen

DRUG	Resume of phenotypes (Subtracting existing Gro, Lva and Ste in <i>cer14</i>)		Microtracker read (day 4)	
	N2	<i>prp-8(cer14)</i>	N2	<i>prp-8(cer14)</i>
<i>trans</i> -Resveratrol	DMSO like	DMSO like	44	40
2,4-DPD	DMSO like	DMSO like	49	14
DMOG	DMSO like	DMSO like	35	20
Trichostatin A	DMSO like	DMSO like	31	12
CAY10398	DMSO like	DMSO like	28	29
2,4-Pyridinedicarboxylic Acid	DMSO like	DMSO like	50	6
CAY10433	DMSO like	DMSO like	44	12
Piceatannol	DMSO like	DMSO like	40	12
CAY10591	Gro	DMSO like	16	0
EX-527	Gro	DMSO like	50	0
SAHA	DMSO like	DMSO like	30	0
2-PCPA (hydrochloride)	DMSO like	DMSO like	42	0
1-Naphthoic Acid	DMSO like	DMSO like	19	0
Sinefungin	DMSO like	DMSO like	36	3
Suramin (sodium salt)	DMSO like	DMSO like	46	7
3-amino Benzamide	DMSO like	DMSO like	50	13
SB 939	DMSO like	DMSO like	9	17
PCI34051	DMSO like	DMSO like	38	20
4-iodo-SAHA	DMSO like	DMSO like	36	24
Sirtinol	DMSO like	DMSO like	46	8
C646	DMSO like	DMSO like	36	0
Tubastatin A (trifluoroacetat salt)	DMSO like	DMSO like	58	16
Garcinol	Gro	DMSO like	5	27
Suberohydroxamic Acid	DMSO like	DMSO like	50	4
Apicidin	Ste, Emb, Egl	DMSO like	46	22
UNC0321 (trifluoroacetate salt)	DMSO like	DMSO like	52	0
(-)-Neplanocin A	DMSO like	DMSO like	70	24
Cl-Amidine	DMSO like	DMSO like	48	21
F-Amidine (trifluoroacetate salt)	DMSO like	DMSO like	44	4
JGB1741	DMSO like	DMSO like	68	4
UNC0638	Gro	DMSO like	36	5
Isoliquiritigenin	Gro, Rbs	Lva	2	2
CCG-100602	DMSO like	DMSO like	42	30
CAY10669	Lva, Lvl	Lva, Lvl	0	0
Zebularine	DMSO like	DMSO like	70	48
Delphinidin chloride	DMSO like	DMSO like	72	42
PFI-1	DMSO like	DMSO like	70	12
5-Azacytidine	DMSO like	DMSO like	63	0
(+)-JQ1	Gro, Ste	Lva	6	10
(-)-JQ1	Ste, Emb, Egl	Lva	8	1
BSI-201	DMSO like	DMSO like	42	32
AG-014699	DMSO like	DMSO like	44	18
IOX1	DMSO like	DMSO like	73	7
MI-2 (hydrochloride)	DMSO like	DMSO like	67	13

DRUG	Resume of phenotypes (Subtracting existing Gro, Lva and Ste in <i>cer14</i>)		Microtracker read (day 4)	
	N2	<i>prp-8(cer14)</i>	N2	<i>prp-8(cer14)</i>
MI-nc (hydrochloride)	DMSO like	DMSO like	50	7
Lomeguatrib	DMSO like	DMSO like	52	41
Daminozide	DMSO like	DMSO like	44	1
GSK-J1 (sodium salt)	DMSO like	DMSO like	23	2
GSK-J2 (sodium salt)	DMSO like	DMSO like	48	22
GSK-J4 (hydrochloride)	Lva, Lvl	Lva, Lvl	3	0
GSK-J5 (hydrochloride)	Ste, Emb, Egl	Gro	14	1
Valproic acid (sodium salt)	DMSO like	DMSO like	57	14
Tenovin-1	DMSO like	DMSO like	53	48
Tenovin-6	DMSO like	DMSO like	35	2
Anacardic Acid	Gro	DMSO like	36	9
AGK2	DMSO like	DMSO like	42	2
CAY10603	DMSO like	DMSO like	28	10
Chaetocin	Lva	Lva	0	1
Splitomicin	DMSO like	DMSO like	52	0
CBHA	DMSO like	DMSO like	19	2
M 344	DMSO like	DMSO like	84	14
Oxamflatin	DMSO like	DMSO like	40	0
Salermide	DMSO like	DMSO like	47	3
Mirin	DMSO like	DMSO like	40	0
Pimelic	DMSO like	DMSO like	52	32
Diphenylamide 106				
(S)-HDAC-42	DMSO like	DMSO like	46	0
MS-275	DMSO like	DMSO like	32	1
RG-108	DMSO like	DMSO like	30	22
2',3',5'-triacetyl-5-Azacytidine	DMSO like	DMSO like	47	25
S-Adenosylhomocysteine	DMSO like	DMSO like	52	8
UNC0224	DMSO like	DMSO like	48	0
Chidamide	DMSO like	DMSO like	48	33
3-Deazaneplanocin A	DMSO like	DMSO like	39	34
N-Oxalyglycine	DMSO like	DMSO like	36	0
AMI-1 (sodium salt)	DMSO like	DMSO like	50	0
UNC1215	DMSO like	DMSO like	30	6
Rapamycin (Sirolimus)	DMSO like	DMSO like	64	14
Abiraterone (CB-7598)	DMSO like	DMSO like	68	6
Anastrozole	DMSO like	DMSO like	50	37
Melatonin	DMSO like	DMSO like	78	24
Clofarabine	DMSO like	DMSO like	48	10
Leucovorin Calcium	DMSO like	DMSO like	57	10
Posaconazole	DMSO like	DMSO like	63	5
Artemisinin	DMSO like	DMSO like	48	2
Sorafenib (Nexavar)	Lva, Lvl	Lva, Lvl	0	1
Pemetrexed	Gro	DMSO like	26	12
Aprepitant (MK-0869)	Lva, Lvl	Lva, Lvl	0	1
Bisoprolol	DMSO like	DMSO like	76	12
Dacarbazine (DTIC-Dome)	DMSO like	DMSO like	32	15

SUPPLEMENTARY DATA

DRUG	Resume of phenotypes (Subtracting existing Gro, Lva and Ste in <i>cer14</i>)		Microtracker read (day 4)	
	N2	<i>prp-8(cer14)</i>	N2	<i>prp-8(cer14)</i>
Methazolastone	DMSO like	DMSO like	67	14
Prasugrel (Effient)	DMSO like	DMSO like	72	4
Asenapine	Lvl	Lvl	5	4
Axitinib	Ste, pPvl	pPvl	6	9
Sunitinib Malate (Sutent)	DMSO like	DMSO like	46	2
Malotilate	DMSO like	DMSO like	78	24
Bicalutamide (Casodex)	DMSO like	DMSO like	64	34
Doxorubicin (Adriamycin)	Gro	DMSO like	70	9
Dexrazoxane Hydrochloride	DMSO like	DMSO like	78	14
Vincristine	DMSO like	DMSO like	45	2
Ramelteon (TAK-375)	DMSO like	DMSO like	70	10
Bortezomib (Velcade)	Lvl	Lvl	0	0
Temsirolimus (Torisel)	DMSO like	DMSO like	91	2
Ivacaftor (VX-770)	Gro	DMSO like	30	5
Fulvestrant (Faslodex)	DMSO like	DMSO like	78	12
Adrucil (Fluorouracil)	DMSO like	DMSO like	74	2
Epirubicin Hydrochloride	DMSO like	DMSO like	84	9
Agomelatine	DMSO like	DMSO like	68	20
AMG-073 HCl (Cinacalcet hydrochloride)	Lva, Lvl	Lva, Lvl	0	2
Bosutinib (SKI-606)	Ste, pPvl, Gro	Gro	16	6
Vandetanib (Zactima)	DMSO like	DMSO like	86	4
Docetaxel (Taxotere)	Gro	DMSO like	44	3
Thalidomide	DMSO like	DMSO like	68	10
Abitrexate (Methotrexate)	Emb, Rbs	DMSO like	40	2
Oxaliplatin (Eloxatin)	DMSO like	DMSO like	73	11
Leflunomide	DMSO like	DMSO like	74	32
Celecoxib	Gro	DMSO like	68	40
Dasatinib (BMS-354825)	Rbs	DMSO like	55	4
Vorinostat (SAHA)	DMSO like	DMSO like	87	12
Paclitaxel (Taxol)	Let, Rbs, Movement abnormal	Lva, Lvl	10	0
Exemestane	DMSO like	DMSO like	76	24
Imiquimod	DMSO like	DMSO like	18	22
Etoposide (VP-16)	DMSO like	DMSO like	80	1
Vinblastine	Let	DMSO like	59	40
Vemurafenib (PLX4032)	DMSO like	DMSO like	45	1
Erlotinib HCl	DMSO like	DMSO like	82	8
Masitinib (AB1010)	DMSO like	DMSO like	96	14
Capecitabine (Xeloda)	DMSO like	DMSO like	78	26

DRUG	Resume of phenotypes (Subtracting existing Gro, Lva and Ste in <i>cer14</i>)		Microtracker read (day 4)	
	N2	<i>prp-8(cer14)</i>	N2	<i>prp-8(cer14)</i>
Finasteride	DMSO like	DMSO like	86	6
Bendamustine HCL	DMSO like	DMSO like	64	8
Evista (Raloxifene Hydrochloride)	DMSO like	DMSO like	53	24
MDV3100 (Enzalutamide)	Lva, Lvl	Lva, Lvl	0	0
Acarbose	DMSO like	DMSO like	60	10
Gefitinib (Iressa)	Lva	DMSO like	0	4
Crizotinib (PF-02341066)	DMSO like	DMSO like	46	30
Cisplatin	DMSO like	DMSO like	59	2
Irinotecan	DMSO like	DMSO like	57	30
Nelarabine (Arranon)	DMSO like	DMSO like	42	12
Idarubicin HCl	Lva	Lva	1	0
Dienogest	DMSO like	DMSO like	78	22
Adapalene	DMSO like	DMSO like	69	3
Imatinib Mesylate	DMSO like	DMSO like	96	8
Vismodegib (GDC-0449)	DMSO like	DMSO like	90	22
Valproic acid sodium salt (Sodium valproate)	DMSO like	DMSO like	82	2
Cladribine	DMSO like	DMSO like	78	4
Bleomycin sulfate	Lva, Lvl	Lva, Lvl	2	1
Topotecan HCl	DMSO like	DMSO like	76	37
Entecavir hydrate	DMSO like	DMSO like	69	26
Altretamine (Hexalen)	DMSO like	DMSO like	76	1
Lenalidomide XL-184 (Cabozantinib)	DMSO like Lva	DMSO like Lva	72 0	4 1
Regorafenib (BAY 73-4506)	Lva, Lvl	Lva, Lvl	0	0
Decitabine	DMSO like	DMSO like	73	6
Carboplatin	DMSO like	DMSO like	72	8
2-Methoxyestradiol	DMSO like	DMSO like	86	36
Nepafenac	DMSO like	DMSO like	82	16
Amisulpride	DMSO like	DMSO like	64	11
Nilotinib (AMN-107)	DMSO like	DMSO like	75	14
Everolimus (RAD001)	DMSO like	DMSO like	86	10
Ritonavir	DMSO like	DMSO like	69	24
Dutasteride	DMSO like	DMSO like	89	22
Clafen (Cyclophosphamide)	DMSO like	DMSO like	46	22
Letrozole	DMSO like	DMSO like	90	4
Rufinamide (Banzel)	DMSO like	DMSO like	58	3
Aniracetam	DMSO like	DMSO like	73	0
Allylthiourea	DMSO like	DMSO like	18	0
Diphemanil methylsulfate	DMSO like	DMSO like	54	22
Carbimazole	DMSO like	DMSO like	28	2
Ronidazole	DMSO like	DMSO like	26	13
Sodium nitrite	DMSO like	DMSO like	25	6
Avanafil	DMSO like	DMSO like	70	19
Vitamin D2	DMSO like	DMSO like	57	36

SUPPLEMENTARY DATA

DRUG	Resume of phenotypes (Subtracting existing Gro, Lva and Ste in <i>cer14</i>)		Microtracker read (day 4)	
	N2	<i>prp-8(cer14)</i>	N2	<i>prp-8(cer14)</i>
Bextra (valdecoxib)	DMSO like	DMSO like	24	14
Vitamin D3 (Cholecalciferol)	DMSO like	DMSO like	42	10
Pyrithione zinc	Ste, Egl, Gro	Lva	16	0
Pemirolast (BMY 26517) potassium	DMSO like	DMSO like	52	2
Sodium Picosulfate	DMSO like	DMSO like	54	1
Doxapram HCl	DMSO like	DMSO like	20	2
valganciclovir hydrochloride	DMSO like	DMSO like	34	0
Escitalopram oxalate	DMSO like	DMSO like	31	0
Propranolol HCl	DMSO like	DMSO like	32	2
Mirabegron (YM178)	DMSO like	DMSO like	42	31
Tolcapone	DMSO like	DMSO like	25	4
Dibucaine HCL	DMSO like	DMSO like	26	22
Nabumetone	DMSO like	DMSO like	57	30
Guanabenz acetate	DMSO like	DMSO like	47	27
Mequinol	DMSO like	DMSO like	41	8
Acebutolol HCl	DMSO like	DMSO like	60	4
Probenecid (Benemid)	DMSO like	DMSO like	50	18
Methazolamide	DMSO like	DMSO like	35	22
Netilmicin Sulfate	DMSO like	DMSO like	44	0
Dequalinium chloride	Lva, Lvl	Lva, Lvl (much earlier than N2)	6	2
Mefenamic acid	DMSO like	DMSO like	42	6
Ampiroxicam	DMSO like	DMSO like	46	2
Procaine (Novocaine) HCl	DMSO like	DMSO like	50	2
norethindrone	DMSO like	DMSO like	50	10
Sertraline HCl	Lva, Lvl	Lva, Lvl	0	2
Deferiprone	DMSO like	DMSO like	57	4
Ticagrelor	Ste, Sck	Sck	5	2
Desloratadine	DMSO like	DMSO like	50	22
Homatropine Bromide	DMSO like	DMSO like	60	11
olsalazine sodium	DMSO like	DMSO like	34	1
Spironolactone	DMSO like	DMSO like	43	0
tinidazole	DMSO like	DMSO like	44	17
triamterene	DMSO like	DMSO like	68	2
Sodium Monofluorophosphate	DMSO like	DMSO like	58	19
Hydroxyzine 2HCl	DMSO like	DMSO like	52	2
nafcillin sodium monohydrate	DMSO like	DMSO like	26	0
Retapamulin	DMSO like	DMSO like	56	0
Hexamethonium bromide	DMSO like	DMSO like	41	0
sulfacetamide sodium	DMSO like	DMSO like	33	28
Hyoscyamine (Daturine)	DMSO like	DMSO like	44	1
Flavoxate HCl	DMSO like	DMSO like	21	8
tetrahydrozoline hydrochloride	DMSO like	DMSO like	34	1
Methyclothiazide	DMSO like	DMSO like	41	12
Guanidine HCl	DMSO like	DMSO like	20	2

DRUG	Resume of phenotypes (Subtracting existing Gro, Lva and Ste in <i>cer14</i>)		Microtracker read (day 4)	
	N2	<i>prp-8(cer14)</i>	N2	<i>prp-8(cer14)</i>
FK-506 (Tacrolimus)	Gro, Emb, Egl, Reduced brod size	DMSO like	6	6
Cyclamic acid	DMSO like	DMSO like	51	34
Aclidinium Bromide	DMSO like	DMSO like	48	1
toltrazuril	Gro, Ste	Lva	10	1
Ropivacaine HCl	DMSO like	DMSO like	50	1
Decamethonium bromide	DMSO like	DMSO like	54	26
Pimecrolimus	DMSO like	DMSO like	28	6
Ouabain	DMSO like	DMSO like	34	1
Bismuth	DMSO like	DMSO like	42	28
Subsalicylate				
Bisacodyl	DMSO like	DMSO like	44	0
Sodium	DMSO like	DMSO like	44	13
Nitroprusside				
Aminosalicylate sodium	DMSO like	DMSO like	40	16
Plerixafor (AMD3100)	DMSO like	DMSO like	54	0
Floxuridine	Ste, Emb, Egl	DMSO like	10	25
Ellagic acid	DMSO like	DMSO like	64	54
Granisetron HCl	DMSO like	DMSO like	66	16
Cefoselis sulfate	DMSO like	DMSO like	73	14
Minoxidil	DMSO like	DMSO like	56	26
Tigecycline	DMSO like	DMSO like	84	8
Sildenafil citrate	DMSO like	DMSO like	82	0
Zonisamide	DMSO like	DMSO like	68	10
Ftorafur	DMSO like	DMSO like	90	2
Etodolac (Lodine)	DMSO like	DMSO like	80	16
Daptomycin	DMSO like	DMSO like	66	31
Mosapride citrate	DMSO like	DMSO like	95	30
Trilostane	DMSO like	DMSO like	56	6
Sumatriptan succinate	DMSO like	DMSO like	91	35
Atazanavir sulfate	DMSO like	Let	7	2
Benazepril hydrochloride	DMSO like	DMSO like	68	18
Ifosfamide	DMSO like	DMSO like	88	18
Etomidate	DMSO like	DMSO like	48	7
Ivermectin	Lva, Lvl	Lva, Lvl	0	1
Doripenem Hydrate	DMSO like	DMSO like	94	22
Nafamostat mesylate	DMSO like	DMSO like	70	16
Vecuronium Bromide	DMSO like	DMSO like	81	7
Tianeptine sodium	DMSO like	DMSO like	77	0
Biperiden HCl	DMSO like	DMSO like	60	12
Megestrol Acetate	DMSO like	DMSO like	90	5
Felbamate	DMSO like	DMSO like	70	12
Ketoconazole	DMSO like	DMSO like	80	3
Dorzolamide HCL	DMSO like	DMSO like	74	8
Omeprazole (Prilosec)	DMSO like	DMSO like	48	4
Bimatoprost	DMSO like	DMSO like	80	24
Tizanidine HCl	DMSO like	DMSO like	57	6
Budesonide	DMSO like	DMSO like	86	15
Mercaptopurine	DMSO like	DMSO like	78	3
Fluconazole	DMSO like	DMSO like	62	3

SUPPLEMENTARY DATA

DRUG	Resume of phenotypes (Subtracting existing Gro, Lva and Ste in <i>cer14</i>)		Microtracker read (day 4)	
	N2	<i>prp-8(cer14)</i>	N2	<i>prp-8(cer14)</i>
Lansoprazole	DMSO like	DMSO like	70	17
Gestodene	DMSO like	DMSO like	58	14
Oxcarbazepine	DMSO like	DMSO like	90	24
Linezolid (Zyvox)	DMSO like	DMSO like	79	0
Topiramate	Rbs	DMSO like	32	2
Bumetanide	DMSO like	DMSO like	10	30
			0	
Pamidronate Disodium	DMSO like	DMSO like	81	3
Flumazenil	DMSO like	DMSO like	41	8
Levetiracetam	DMSO like	DMSO like	58	2
Drospirenone	DMSO like	DMSO like	80	14
Pizotifen malate	DMSO like	DMSO like	70	11
Alfuzosin hydrochloride (Uroxatral)	DMSO like	DMSO like	60	38
Tranilast (SB 252218)	DMSO like	DMSO like	61	2
Camptothecin	Lva, Lvl	Lva, Lvl	0	4
Streptozotocin (Zanosar)	Rbs	DMSO like	62	10
Fluoxetine HCl	Gro	DMSO like	54	14
Lidocaine (Alphacaine)	DMSO like	DMSO like	83	24
Ruxolitinib (INCB018424)	DMSO like	DMSO like	72	22
Resveratrol	DMSO like	DMSO like	68	24
Clopidogrel (Plavix)	DMSO like	DMSO like	62	0
Varenicline tartrate	DMSO like	DMSO like	80	8
Carmofur	Rbs, Emb, Egl	DMSO like	42	4
Zoledronic Acid (Zoledronate)	DMSO like	DMSO like	80	33
Fluvoxamine maleate	DMSO like	DMSO like	56	8
Loratadine	DMSO like	DMSO like	76	3
Isotretinoin	DMSO like	DMSO like	74	4
Rocuronium bromide	DMSO like	DMSO like	67	8
Prazosin HCl	DMSO like	DMSO like	72	8
Venlafaxine	DMSO like	DMSO like	76	16
Cetirizine Dihydrochloride	DMSO like	DMSO like	83	11
Dexamethasone	DMSO like	DMSO like	64	11
Gatifloxacin	DMSO like	DMSO like	47	1
Lopinavir (ABT-378)	DMSO like	DMSO like	78	2
Stavudine	DMSO like	DMSO like	72	13
Repaglinide	DMSO like	DMSO like	70	27
Voriconazole	DMSO like	DMSO like	80	1
Cilnidipine	DMSO like	DMSO like	70	6
Doxazosin mesylate	DMSO like	DMSO like	58	0
Genistein	DMSO like	DMSO like	70	20
Acitretin	DMSO like	DMSO like	61	14
Meropenem	DMSO like	DMSO like	68	6
Teicoplanin	DMSO like	DMSO like	79	18
Risedronate sodium	Lva, Lvl	Lva, Lvl	0	0
Zileuton	DMSO like	DMSO like	56	1
Cilostazol	DMSO like	DMSO like	66	4
Edaravone (MCI- 186)	DMSO like	DMSO like	69	28

DRUG	Resume of phenotypes (Subtracting existing Gro, Lva and Ste in <i>cer14</i>)		Microtracker read (day 4)	
	N2	<i>prp-8(cer14)</i>	N2	<i>prp-8(cer14)</i>
Glimepiride	DMSO like	DMSO like	50	4
Biapenem	DMSO like	DMSO like	52	2
Mianserin hydrochloride	DMSO like	DMSO like	56	2
Tenofovir (Viread)	DMSO like	DMSO like	58	2
Rolipram	DMSO like	DMSO like	80	30
Ziprasidone hydrochloride	DMSO like	DMSO like	70	8
Ponatinib (AP24534)	Lva, Lvl	Lva, Lvl	0	1
Alprostadil (Caverject)	DMSO like	DMSO like	80	8
Pimobendan (Vetmedin)	Lva	Lva	2	30
Clotrimazole (Canesten)	Lva, Lvl	Lva, Lvl	1	0
Prilocaine	DMSO like	DMSO like	81	4
Erythromycin (E- Mycin)	DMSO like	DMSO like	96	18
Ketorolac (Toradol)	DMSO like	DMSO like	69	46
Isradipine (Dynacirc)	Gro, Rbs	Gro	14	4
Fludarabine (Fludara)	DMSO like	DMSO like	70	14
Norfloracin (Norxacin)	DMSO like	DMSO like	61	11
Pomalidomide	DMSO like	DMSO like	62	4
Rizatriptan Benzoate (Maxalt)	DMSO like	DMSO like	10	16
			0	
Darunavir Ethanolate (Prezista)	DMSO like	DMSO like	91	24
Amphotericin B (Abelcet)	DMSO like	DMSO like	84	16
Adenosine (Adenocard)	DMSO like	DMSO like	89	12
Estrone	DMSO like	DMSO like	81	0
Ofloxacin (Floxin)	DMSO like	DMSO like	61	2
Pralatrexate (Foloty)	DMSO like	DMSO like	82	22
Tadalafil (Cialis)	DMSO like	DMSO like	78	0
Tazarotene (Avage)	DMSO like	DMSO like	79	20
Pyridostigmine Bromide (Mestinon)	DMSO like	DMSO like	92	0
Prednisone (Adasone)	DMSO like	DMSO like	66	8
Docosanol (Abreva)	DMSO like	DMSO like	71	8
Cytarabine	DMSO like	DMSO like	77	30
Marbofloxacin	DMSO like	DMSO like	10	6
			2	
Cefaclor (Ceclor)	DMSO like	DMSO like	64	0
Cyclosporine (Neoral)	DMSO like	DMSO like	64	33
Sulfasalazine (Azulfidine)	DMSO like	DMSO like	79	2
Methimazole (Tapazole, Northyx)	DMSO like	DMSO like	80	2
Acetylcysteine	DMSO like	DMSO like	80	15
Ibuprofen (Advil)	DMSO like	DMSO like	60	19
Zolmitriptan (Zomig)	DMSO like	DMSO like	71	1

SUPPLEMENTARY DATA

DRUG	Resume of phenotypes (Subtracting existing Gro, Lva and Ste in <i>cer14</i>)		Microtracker read (day 4)	
	N2	<i>prp-8(cer14)</i>	N2	<i>prp-8(cer14)</i>
Moxifloxacin hydrochloride	DMSO like	DMSO like	67	9
Betamethasone (Celestone)	DMSO like	DMSO like	64	8
Cidofovir (Vistide)	DMSO like	DMSO like	52	2
Candesartan (Atacand)	DMSO like	DMSO like	72	0
Metolazone (Zaroxolyn)	DMSO like	DMSO like	84	30
Alendronate (Fosamax)	DMSO like	DMSO like	72	14
Amprenavir (Agenerase)	DMSO like	DMSO like	97	11
Telbivudine (Sebivo, Tyzeka)	DMSO like	DMSO like	70	29
Calcitriol (Rocaltrol)	DMSO like	DMSO like	85	8
Mycophenolate mofetil (CellCept)	DMSO like	DMSO like	66	18
Natamycin (Pimaricin)	DMSO like	DMSO like	90	20
Ubenimex (Bestatin)	DMSO like	DMSO like	89	7
Cefoperazone (Cefobid)	DMSO like	DMSO like	56	22
Ethinyl Estradiol	DMSO like	DMSO like	95	30
Albendazole (Albenza)	Prz	Prz	1	3
Monobenzone (Benoquin)	DMSO like	DMSO like	75	20
Doxercalciferol (Hectorol)	DMSO like	DMSO like	11	52
Cephalexin (Cefalexin)	DMSO like	DMSO like	94	8
Vinorelbine (Navelbine)	DMSO like	DMSO like	86	16
Apixaban	DMSO like	DMSO like	84	32
Sildenafil (Rapaflo)	DMSO like	DMSO like	11	5
Naproxen (Aleve)	DMSO like	DMSO like	90	3
Chlorothiazide	DMSO like	DMSO like	93	36
Tretinoin (Aberela)	Gro, Rbs	Gro	54	4
Alfacalcidol	DMSO like	DMSO like	82	14
Dyphylline (Dilor)	DMSO like	DMSO like	84	4
Telaprevir (VX-950)	DMSO like	DMSO like	86	6
Reserpine	DMSO like	DMSO like	93	8
Riluzole (Rilutek)	DMSO like	DMSO like	92	4
Nitazoxanide (Alinia, Annita)	DMSO like	DMSO like	86	36
Methyldopa (Aldomet)	DMSO like	DMSO like	82	5
Phenylbutazone (Butazolidin, Butatron)	DMSO like	DMSO like	71	9
Calcifediol	DMSO like	DMSO like	84	2
Aztreonam (Azactam, Cayston)	DMSO like	DMSO like	86	18
Saxagliptin (BMS-477118, Onglyza)	DMSO like	DMSO like	80	1

DRUG	Resume of phenotypes (Subtracting existing Gro, Lva and Ste in <i>cer14</i>)		Microtracker read (day 4)	
	N2	<i>prp-8(cer14)</i>	N2	<i>prp-8(cer14)</i>
Furosemide (Lasix)	DMSO like	DMSO like	82	36
Risperidone (Risperdal)	DMSO like	DMSO like	79	0
Orlistat (Alli, Xenical)	DMSO like	DMSO like	82	2
Ursodiol (Actigal Urso)	DMSO like	DMSO like	84	4
Ezetimibe (Zetia)	Rbs	DMSO like	66	7
Iloperidone (Fanapt)	DMSO like	DMSO like	86	12
Perindopril	DMSO like	DMSO like	78	0
Erbumine (Aceon)				
Febuxostat (Uloric)	DMSO like	DMSO like	68	23
Olmесartan medoxomil (Benicar)	DMSO like	DMSO like	62	15
Sulfapyridine (Dagenan)	DMSO like	DMSO like	68	26
Allopurinol (Zyloprim)	DMSO like	DMSO like	69	34
Nitrofurazone (Nitrofurazone)	DMSO like	DMSO like	76	2
Enalaprilat dihydrate	DMSO like	DMSO like	82	5
Naratriptan HCl	DMSO like	DMSO like	70	19
Irbesartan (Avapro)	DMSO like	DMSO like	36	20
Nebivolol (Bystolic)	DMSO like	Lva, Gro	64	0
Cefdinir (Omnicef)	DMSO like	DMSO like	72	10
Sulfameter (Bayrena)	DMSO like	DMSO like	60	5
Zafirlukast (Accolate)	DMSO like	DMSO like	81	33
Ketoprofen (Actron)	Gro	DMSO like	60	2
Dofetilide (Tikosyn)	DMSO like	DMSO like	76	10
Disulfiram (Antabuse)	DMSO like	DMSO like	46	16
Didanosine (Videx)	DMSO like	DMSO like	48	22
Glipizide (Glucotrol)	DMSO like	DMSO like	49	6
Indapamide (Lozol)	DMSO like	DMSO like	74	16
Nevirapine (Viramune)	DMSO like	DMSO like	66	38
Pyrazinamide (Pyrazinoic acid amide)	DMSO like	DMSO like	46	32
Trifluridine (Viroptic)	DMSO like	DMSO like	57	22
Ranitidine (Zantac)	DMSO like	DMSO like	64	16
Mesalamine (Lialda)	DMSO like	DMSO like	68	24
Divalproex sodium	DMSO like	DMSO like	64	18
Glyburide (Diabeta)	DMSO like	DMSO like	38	6
Mitotane (Lysodren)	Lva, Lvl	Lva, Lvl	0	0
Niacin (Nicotinic acid)	DMSO like	DMSO like	46	26
Quetiapine fumarate (Seroquel)	DMSO like	DMSO like	68	28
Azacitidine (Vidaza)	DMSO like	DMSO like	38	34
Acadesine	DMSO like	DMSO like	68	6
Flucytosine (Ancobon)	DMSO like	DMSO like	76	10
Ipratropium bromide	DMSO like	DMSO like	50	16

SUPPLEMENTARY DATA

DRUG	Resume of phenotypes (Subtracting existing Gro, Lva and Ste in <i>cer14</i>)		Microtracker read (day 4)	
	N2	<i>prp-8(cer14)</i>	N2	<i>prp-8(cer14)</i>
Emtricitabine (Emtriva)	DMSO like	DMSO like	79	6
Adefovir Dipivoxil (Preveon, Hepsera)	DMSO like	DMSO like	75	10
Methylprednisolone	DMSO like	DMSO like	53	0
Nimodipine (Nimotop)	DMSO like	DMSO like	94	17
Rifampin (Rifadin, Rimactane)	DMSO like	DMSO like	53	58
Vidarabine (Vira-A)	DMSO like	DMSO like	8	2
Trichlormethiazide (Achletin)	DMSO like	DMSO like	76	33
Sulfanilamide	DMSO like	DMSO like	96	14
Progesterone (Prometrium)	DMSO like	DMSO like	59	2
Zalcitabine	DMSO like	DMSO like	76	8
Meloxicam (Mobic)	DMSO like	DMSO like	79	2
Nisoldipine (Sular)	DMSO like	DMSO like	68	0
Beta Carotene	DMSO like	DMSO like	86	4
Verteporfin (Visudyne)	DMSO like	DMSO like	18	4
Loteprednol etabonate	DMSO like	DMSO like	36	22
Betapar (Meprednisone)	DMSO like	DMSO like	50	10
Lamivudine (Epivir)	DMSO like	DMSO like	65	12
Azathioprine (Azasan, Imuran)	DMSO like	DMSO like	58	29
Mesna (Uromitexan, Mesnex)	DMSO like	DMSO like	24	19
L-Glutamine	DMSO like	DMSO like	73	35
Cefditoren pivoxil	Gro	DMSO like	43	24
Teniposide (Vumon)	DMSO like	DMSO like	46	8
Aminocaproic acid (Amicar)	DMSO like	DMSO like	70	18
Praziquantel (Biltricide)	DMSO like	DMSO like	46	15
Eplerenone	DMSO like	DMSO like	38	15
Indomethacin (Indocid, Indocin)	DMSO like	DMSO like	69	20
Methocarbamol (Robaxin)	DMSO like	DMSO like	78	32
Gadodiamide (Omniscan)	DMSO like	DMSO like	76	16
Sulfadiazine	DMSO like	DMSO like	36	8
Rifaximin (Xifaxan)	DMSO like	DMSO like	52	11
Aminoglutethimide (Cytadren)	DMSO like	DMSO like	31	26
Busulfan (Myleran, Busulfex)	DMSO like	DMSO like	57	24
Hydrochlorothiazide	DMSO like	DMSO like	56	4
Paliperidone (Invega)	Gro, Rbs	DMSO like	36	16
Prednisolone (Hydroretrocortine)	DMSO like	DMSO like	70	20
Oxybutynin (Ditropan)	DMSO like	DMSO like	69	29
Chlorprothixene	Gro, Rbs	Gro	81	50

DRUG	Resume of phenotypes (Subtracting existing Gro, Lva and Ste in <i>cer14</i>)		Microtracker read (day 4)	
	N2	<i>prp-8(cer14)</i>	N2	<i>prp-8(cer14)</i>
Bacitracin zinc	DMSO like	DMSO like	42	12
Aminophylline (Truphylline)	DMSO like	DMSO like	80	36
Carbamazepine (Carbatrol)	DMSO like	DMSO like	40	16
Estradiol	Gro	Gro	65	5
Terbinafine (Lamisil, Terbinex)	DMSO like	DMSO like	36	40
Telmisartan (Micardis)	DMSO like	DMSO like	37	19
Enoxacin (Penetrex)	Gro, Rbs	DMSO like	32	34
Oxytetracycline (Terramycin)	DMSO like	DMSO like	53	27
Simvastatin (Zocor)	Gro, Rbs	Gro	21	25
Amorolfine Hydrochloride	Gro	Gro	56	3
Hydrocortisone (Cortisol)	DMSO like	DMSO like	68	25
Deferasirox (Exjade)	DMSO like	DMSO like	45	25
Levodopa (Sinemet)	DMSO like	DMSO like	44	7
Thiabendazole	Movement abnormal	Movement abnormal	15	0
Pitavastatin calcium (Livalo)	Gro	DMSO like	30	48
Thioguanine	DMSO like	DMSO like	60	16
Ramipril (Altace)	DMSO like	DMSO like	68	12
Chloramphenicol (Chloromycetin)	DMSO like	DMSO like	52	14
Torseamide (Demadex)	DMSO like	DMSO like	44	36
Piroxicam (Feldene)	DMSO like	DMSO like	52	22
Levonorgestrel (Levonelle)	DMSO like	DMSO like	56	15
Guaifenesin (Guaiphenesin)	DMSO like	DMSO like	33	22
Rifapentine (Priftin)	DMSO like	DMSO like	50	10
Toremifene Citrate (Fareston, Acapodene)	Lva, Lvl	Lva, Lvl	0	0
Fenofibrate (Tricor, Trilipix)	DMSO like	DMSO like	64	15
Flurbiprofen (Ansaid)	DMSO like	DMSO like	71	26
Desonide	DMSO like	DMSO like	83	20
Gemcitabine (Gemzar)	DMSO like	DMSO like	64	17
Gemfibrozil (Lopid)	DMSO like	DMSO like	55	12
Rifabutin (Mycobutin)	DMSO like	DMSO like	74	27
Suprofen (Profenal)	DMSO like	DMSO like	50	41
Ethionamide	DMSO like	DMSO like	66	22
Ranolazine (Ranexa)	DMSO like	DMSO like	58	12
Proparacaine HCl	DMSO like	DMSO like	65	22
Cimetidine (Tagamet)	DMSO like	DMSO like	53	38
Diltiazem HCl (Tiazac)	DMSO like	DMSO like	40	42

SUPPLEMENTARY DATA

DRUG	Resume of phenotypes (Subtracting existing Gro, Lva and Ste in <i>cer14</i>)		Microtracker read (day 4)	
	N2	<i>prp-8(cer14)</i>	N2	<i>prp-8(cer14)</i>
Felodipine (Plendil)	Gro, Rbs	Gro	52	3
Vitamin B12	DMSO like	DMSO like	61	8
Sulfamethoxazole	DMSO like	DMSO like	60	22
Levofloxacin (Levaquin)	DMSO like	DMSO like	40	24
Primidone (Mysoline)	DMSO like	DMSO like	56	10
Pranlukast	DMSO like	DMSO like	61	5
Clemastine Fumarate	Ste, Gro	Gro	13	4
Diphenhydramine HCl (Benadryl)	DMSO like	DMSO like	29	20
Deflazacort (Calcort)	DMSO like	DMSO like	50	9
Diclofenac	DMSO like	DMSO like	54	3
Sulfisoxazole	DMSO like	DMSO like	66	17
Enalapril maleate (Vasotec)	DMSO like	DMSO like	44	13
Nefiracetam (Translon)	DMSO like	DMSO like	61	4
Acetylcholine chloride	DMSO like	DMSO like	62	30
Oxfendazole	Ste, Egl, Dpy, Movement abnormal	Dpy, Movement abnormal	0	0
Curcumin	Gro, Ste, Egl	Gro	2	8
Dapoxetine hydrochloride (Priligy)	DMSO like	DMSO like	40	14
Nizatidine	DMSO like	DMSO like	46	37
Avobenzone (Parsol 1789)	DMSO like	DMSO like	40	24
Crystal violet	Lva, Lvl	Lva, Lvl	0	0
Menadione	Gro	DMSO like	48	12
Acipimox	DMSO like	DMSO like	71	14
Carvedilol	DMSO like	DMSO like	48	31
Daidzein	DMSO like	DMSO like	70	38
Risedronic acid (Actonel)	DMSO like	DMSO like	68	33
Carbidopa	DMSO like	DMSO like	35	36
Amlodipine (Norvasc)	DMSO like	DMSO like	74	48
Haloperidol (Haldol)	DMSO like	DMSO like	50	30
Metformin hydrochloride (Glucophage)	DMSO like	DMSO like	58	26
Acyclovir (Aciclovir)	DMSO like	DMSO like	77	20
Atracurium besylate	Gro	DMSO like	80	30
Oxibendazole	Prz	Prz	24	0
Tranexamic acid (Transamin)	DMSO like	DMSO like	73	12
Valsartan (Diovan)	DMSO like	DMSO like	78	42
Metronidazole (Flagyl)	DMSO like	DMSO like	73	42
Phenindione (Rectadione)	DMSO like	DMSO like	74	10
Methoxsalen (Oxsoralen)	DMSO like	DMSO like	74	20
Nifedipine (Adalat)	DMSO like	DMSO like	53	14
Butoconazole nitrate	Lva, Lvl	Lva, Lvl	0	0

DRUG	Resume of phenotypes (Subtracting existing Gro, Lva and Ste in <i>cer14</i>)		Microtracker read (day 4)	
	N2	<i>prp-8(cer14)</i>	N2	<i>prp-8(cer14)</i>
Penicillamine (Cuprimine)	DMSO like	DMSO like	62	21
Valaciclovir HCl	DMSO like	DMSO like	42	8
Dipyridamole (Persantine)	DMSO like	DMSO like	68	19
Flutamide (Eulexin)	Ste, Egl, Emb	Gro (more than usual)	31	12
Alibendol	DMSO like	DMSO like	80	24
Sulfamethizole (Proklar)	DMSO like	DMSO like	54	42
Amiloride hydrochloride (Midamor)	DMSO like	DMSO like	62	52
Azithromycin (Zithromax)	DMSO like	DMSO like	57	3
Bifonazole	Lva, Lvl	Lva, Lvl	4	0
Ganciclovir	DMSO like	DMSO like	64	6
Hydroxyurea (Cytodrox)	DMSO like	DMSO like	50	34
Fluvastatin sodium (Lescol)	Gro	DMSO like	45	24
Irsogladine	DMSO like	DMSO like	59	32
Sulbactam	DMSO like	DMSO like	58	24
Chlorpheniramine Maleate	DMSO like	DMSO like	77	16
Flubendazole (Flutelmium)	DMSO like	DMSO like	10	19
Pefloxacin mesylate	DMSO like	DMSO like	54	30
Roxatidine acetate HCl	DMSO like	DMSO like	57	21
Potassium iodide	DMSO like	DMSO like	48	22
Tioconazole	Lva	Lva	2	10
Triamcinolone (Aristocort)	DMSO like	DMSO like	66	34
Tolfenamic acid	DMSO like	DMSO like	59	21
Clofibrate (Atromid- S)	DMSO like	DMSO like	50	6
Chloroxine	DMSO like	DMSO like	44	30
Metoprolol tartrate	DMSO like	DMSO like	58	12
Prothionamide (Prothionamide)	DMSO like	DMSO like	47	18
Tropisetron	DMSO like	DMSO like	44	1
Disodium Cromoglycate	DMSO like	DMSO like	40	26
Nystatin (Mycostatin)	DMSO like	DMSO like	48	2
Pranoprofen	DMSO like	DMSO like	49	10
Fenoprofen calcium	DMSO like	DMSO like	66	25
Lomustine (CeeNU)	Ste, Egl, Emb	DMSO like	46	18
Etidronate (Didronel)	DMSO like	DMSO like	49	8
Idoxuridine	DMSO like	DMSO like	62	0
Nicotinamide (Niacinamide)	DMSO like	DMSO like	62	0
Tropicamide	DMSO like	DMSO like	56	10
Isoniazid (Tubizid)	DMSO like	DMSO like	41	24
Sulphadimethoxine	DMSO like	DMSO like	63	8
Erdosteine	DMSO like	DMSO like	57	9
Chenodeoxycholic acid	DMSO like	DMSO like	71	20

SUPPLEMENTARY DATA

DRUG	Resume of phenotypes (Subtracting existing Gro, Lva and Ste in <i>cer14</i>)		Microtracker read (day 4)	
	N2	<i>prp-8(cer14)</i>	N2	<i>prp-8(cer14)</i>
Diethylstilbestrol (Stilbestrol)	Gro	DMSO like	41	42
Sparfloxacin	DMSO like	DMSO like	44	26
Talc	DMSO like	DMSO like	49	17
Pregnenolone	DMSO like	DMSO like	59	14
Levamisole Hydrochloride (Ergamisol)	pDpy, pRup	Dpy	41	0
Rimantadine (Flumadine)	DMSO like	DMSO like	33	16
ATP (Adenosine- Triphosphate)	DMSO like	DMSO like	67	24
Sodium orthovanadate	Ste	DMSO like	4	12
Chlormezanone (Trancopal)	DMSO like	DMSO like	24	2
Aspartame	DMSO like	DMSO like	46	26
Orphenadrine citrate (Norflex)	DMSO like	DMSO like	44	11
Mitiglinide calcium	DMSO like	DMSO like	58	22
Ivabradine HCl (Procoralan)	DMSO like	DMSO like	58	0
Rasagiline mesylate	DMSO like	DMSO like	70	1
Meclizine 2HCl	Lva	Lva	7	1
Elvitegravir (GS- 9137)	Lva	Lva	6	0
Ketotifen fumarate (Zaditor)	DMSO like	DMSO like	52	24
Phentolamine mesilate	DMSO like	DMSO like	61	2
Gimeracil	DMSO like	DMSO like	51	0
Mecarbinatate	DMSO like	DMSO like	48	13
Rivastigmine tartrate (Exelon)	DMSO like	DMSO like	34	0
Naltrexone HCl	DMSO like	DMSO like	56	0
Nicorandil (Ikorel)	DMSO like	DMSO like	22	24
Mometasone furoate	DMSO like	DMSO like	41	17
Maraviroc	DMSO like	DMSO like	48	12
Urapidil HCl	DMSO like	DMSO like	56	18
Nimesulide	DMSO like	DMSO like	21	8
Tolnaftate	DMSO like	DMSO like	42	0
Lisinopril (Zestril)	DMSO like	DMSO like	38	14
Dexmedetomidine HCl (Precedex)	Gro	DMSO like	34	38
Tamoxifen Citrate (Nolvadex)	Lva	Lva	2	0
Propylthiouracil	DMSO like	DMSO like	48	0
Vicriviroc Malate	DMSO like	DMSO like	27	19
Ginkgolide A	DMSO like	DMSO like	51	0
Dyclonine HCl	DMSO like	DMSO like	72	34
Terazosin HCl (Hytrin)	DMSO like	DMSO like	76	1
Atorvastatin calcium (Lipitor)	Gro	DMSO like	34	0
Betaxolol (Betoptic)	DMSO like	DMSO like	32	0
Meglumine	DMSO like	DMSO like	40	4

DRUG	Resume of phenotypes (Subtracting existing Gro, Lva and Ste in <i>cer14</i>)		Microtracker read (day 4)	
	N2	<i>prp-8(cer14)</i>	N2	<i>prp-8(cer14)</i>
Fluticasone propionate (Flonase, Veramyst)	DMSO like	DMSO like	50	8
Raltegravir (MK-0518)	DMSO like	DMSO like	56	11
Ciprofloxacin (Cipro)	DMSO like	DMSO like	64	14
Memantine HCl (Namenda)	DMSO like	DMSO like	49	18
Bromhexine HCl	DMSO like	DMSO like	56	2
Famotidine (Pepcid)	DMSO like	DMSO like	66	0
Detomidine HCl	DMSO like	DMSO like	76	22
Aripiprazole (Abilify)	DMSO like	DMSO like	42	14
Lacidipine (Lacipil, Motens)	Egl, Rbs, Movement abnormal	DMSO like	12	2
Pyrimethamine	DMSO like	DMSO like	58	18
Diclazuril	Lva	Lva	0	0
Cyproheptadine HCl (Periactin)	DMSO like	DMSO like	32	4
Lovastatin (Mevacor)	DMSO like	DMSO like	52	16
Moexipril HCl	DMSO like	DMSO like	44	0
Fosinopril sodium (Monopril)	Gro, Rbs	Gro	40	8
Sarafloxacin HCl	DMSO like	DMSO like	64	16
Procarbazine HCl (Matulane)	DMSO like	DMSO like	80	8
Sulindac (Clinoril)	DMSO like	DMSO like	41	0
Uridine	DMSO like	DMSO like	69	12
Doxifluridine	Emb, Egl, Ste	DMSO like	8	12
Tiopronin (Thiola)	DMSO like	DMSO like	40	16
Cleviprex (Clevipine)	DMSO like	DMSO like	66	41
Almotriptan malate (Axert)	DMSO like	DMSO like	60	8
Methscopolamine (Pamine)	DMSO like	DMSO like	70	4
Ondansetron (Zofran)	DMSO like	DMSO like	30	15
Taurine	DMSO like	DMSO like	38	10
Flunarizine 2HCl	Lva, Lvl	Lva, Lvl	0	3
Lornoxicam (Xefo)	DMSO like	DMSO like	29	3
Balofloxacin	DMSO like	DMSO like	47	28
Cilazapril monohydrate (Inhibace)	DMSO like	DMSO like	46	14
Ambrisentan	DMSO like	DMSO like	48	7
Amiodarone HCl	Lva, Lvl	Lva, Lvl	0	0
Liranaftate	DMSO like	DMSO like	54	10
Suplatast tosylate	DMSO like	DMSO like	49	18
Fenticonazole nitrate	Lva, Lvl	Lva, Lvl	0	0
Strontium ranelate (Protelos)	DMSO like	DMSO like	64	4
Lafutidine	DMSO like	DMSO like	43	16
Adiphenine HCl	DMSO like	DMSO like	48	22
Bexarotene	DMSO like	DMSO like	62	10
Adenine	DMSO like	DMSO like	59	8
D-Cycloserine	DMSO like	DMSO like	49	4

SUPPLEMENTARY DATA

DRUG	Resume of phenotypes (Subtracting existing Gro, Lva and Ste in <i>cer14</i>)		Microtracker read (day 4)	
	N2	<i>prp-8(cer14)</i>	N2	<i>prp-8(cer14)</i>
Mirtazapine (Remeron, Avanza)	DMSO like	DMSO like	70	36
Rebamipide	DMSO like	DMSO like	69	4
Captopril (Capoten)	DMSO like	DMSO like	62	0
Moxonidine	DMSO like	DMSO like	40	2
Duloxetine HCl (Cymbalta)	pGro, pLet, Ste, Egl	Gro	0	2
Temocapril HCl	DMSO like	DMSO like	54	6
Ticlopidine HCl	DMSO like	DMSO like	58	4
Sodium butyrate	DMSO like	DMSO like	52	4
Formoterol hemifumarate	DMSO like	DMSO like	32	6
Epalrestat	DMSO like	DMSO like	38	18
Cytidine	DMSO like	DMSO like	48	10
Argatroban	DMSO like	DMSO like	64	0
Trimebutine	DMSO like	DMSO like	42	25
Gabexate mesylate	DMSO like	DMSO like	65	20
Ibutilide fumarate	DMSO like	DMSO like	45	7
Gabapentin (Neurontin)	DMSO like	DMSO like	38	10
TAME	DMSO like	DMSO like	62	43
10-DAB (10- Deacetylbaecatin)	DMSO like	DMSO like	46	0
Bethanechol chloride	DMSO like	DMSO like	27	16
Fleroxacin (Quinodis)	DMSO like	DMSO like	48	2
Nateglinide (Starlix)	DMSO like	DMSO like	41	14
Propafenone (Rytmonorm)	DMSO like	DMSO like	39	0
Probuco	DMSO like	DMSO like	54	12
Sitafloxacin hydrate	DMSO like	DMSO like	52	6
Eltrombopag (SB- 497115-GR)	Gro	DMSO like	34	6
Paeoniflorin	DMSO like	DMSO like	43	7
Chlorpromazine (Sonazine)	Lva	Lva	0	20
Fluocinolone acetone (Flucort-N)	DMSO like	DMSO like	55	19
Neostigmine bromide (Prostigmin)	DMSO like	DMSO like	58	1
Quinine hydrochloride dihydrate	DMSO like	DMSO like	52	16
Azasetron HCl (Y- 25130)	DMSO like	DMSO like	76	19
Arbidol HCl	Egl, Ste, Gro	Lva	21	0
BIBR-1048 (Dabigatran)	Ste, pLet	Lva	0	2
Esomeprazole sodium (Nexium)	Gro	DMSO like	16	4
Geniposide	DMSO like	DMSO like	61	38
Clindamycin hydrochloride (Dalacin)	DMSO like	DMSO like	62	0
Gallamine triethiodide (Flaxedil)	DMSO like	DMSO like	65	31

DRUG	Resume of phenotypes (Subtracting existing Gro, Lva and Ste in <i>cer14</i>)		Microtracker read (day 4)	
	N2	<i>prp-8(cer14)</i>	N2	<i>prp-8(cer14)</i>
Nitrendipine	DMSO like	DMSO like	46	5
Mizolastine (Mizollen)	DMSO like	DMSO like	52	12
Dextrose (D-glucose)	DMSO like	DMSO like	58	5
Tebipenem pivoxil (L-084)	DMSO like	DMSO like	44	4
Fesoterodine fumarate (Toviaz)	DMSO like	DMSO like	54	20
Genipin	DMSO like	DMSO like	74	0
Clonidine hydrochloride (Catapres)	DMSO like	DMSO like	46	6
Itraconazole (Sporanox)	DMSO like	DMSO like	69	0
Novobiocin sodium (Albamylin)	DMSO like	DMSO like	54	4
Flunixin meglumin	DMSO like	DMSO like	62	10
Xylose	DMSO like	DMSO like	54	20
Rosuvastatin calcium (Crestor)	DMSO like	DMSO like	39	2
Artemether (SM-224)	DMSO like	DMSO like	30	0
Geniposidic acid	DMSO like	DMSO like	45	7
Clozapine (Clozaril)	DMSO like	DMSO like	68	13
Lincomycin hydrochloride (Lincocin)	DMSO like	DMSO like	49	23
Olanzapine (Zyprexa)	DMSO like	DMSO like	53	12
Vinpocetine (Cavinton)	DMSO like	DMSO like	50	3
Mestranol	DMSO like	DMSO like	62	16
Dichlorphenamide (Diclofenamide)	DMSO like	DMSO like	36	17
Nalidixic acid (NegGram)	DMSO like	DMSO like	50	6
Tolbutamide	DMSO like	DMSO like	34	4
Pramipexole (Mirapex)	DMSO like	DMSO like	32	18
Loperamide hydrochloride	Rbs	DMSO like	10	8
Olopatadine hydrochloride (Opatanol)	DMSO like	DMSO like	38	17
Lapatinib	Rbs	DMSO like	24	1
Naftopidil (Flivas)	Gro, Rbs	DMSO like	26	7
BIBR 953 (Dabigatran etexilate, Pradaxa)	DMSO like	DMSO like	54	6
Ammonium Glycyrrhizinate (AMGZ)	DMSO like	DMSO like	43	20
Levosimendan	Gro, Ste, Egl, Movement abnormalo	Gro, Movement abnormal	5	7
Domperidone (Motilium)	DMSO like	DMSO like	60	2

SUPPLEMENTARY DATA

DRUG	Resume of phenotypes (Subtracting existing Gro, Lva and Ste in <i>cer14</i>)		Microtracker read (day 4)	
	N2	<i>prp-8(cer14)</i>	N2	<i>prp-8(cer14)</i>
Manidipine (Manyper)	Lva	Lva	1	0
Oxymetazoline hydrochloride	DMSO like	DMSO like	62	10
Blonanserin (Lonasen)	DMSO like	DMSO like	69	18
S-(+)-Rolipram	DMSO like	DMSO like	72	14
Aliskiren hemifumarate	DMSO like	DMSO like	44	13
D-Mannitol (Osmitrol)	DMSO like	DMSO like	52	24
Amantadine hydrochloride (Symmetrel)	DMSO like	DMSO like	73	8
Donepezil HCl (Aricept)	DMSO like	DMSO like	56	1
Milrinone (Primacor)	DMSO like	DMSO like	56	42
Ozagrel	DMSO like	DMSO like	43	17
Cisatracurium besylate (Nimbex)	DMSO like	DMSO like	33	4
Fudosteine	DMSO like	DMSO like	58	14
OSI-420 (Desmethyl Erlotinib)	DMSO like	DMSO like	37	13
L-carnitine (Levocarnitine)	DMSO like	DMSO like	56	20
Amfebutamone (Bupropion)	DMSO like	DMSO like	65	6
Estriol	DMSO like	DMSO like	60	2
Mitoxantrone Hydrochloride	Lva	Lva	18	0
Pancuronium (Pavulon)	DMSO like	DMSO like	65	10
Dronedarone HCl (Multaq)	Lva	Lvl?	0	0
Atropine	DMSO like	DMSO like	76	20
DAPT (GSI-IX)	DMSO like	DMSO like	44	0
Sorbitol (Glucitol)	DMSO like	DMSO like	52	11
Benserazide	DMSO like	DMSO like	43	22
Famciclovir (Famvir)	DMSO like	DMSO like	63	13
Moroxydine	DMSO like	DMSO like	72	4
Pantothenic acid (pantothenate)	DMSO like	DMSO like	53	18
Conivaptan HCl (Vaprisol)	DMSO like	DMSO like	44	34
Roflumilast (Daxas)	DMSO like	DMSO like	70	12
Apatinib (YN968D1)	Lva	Lva	0	0
Cephalomannine	Lva	Lva	2	0
Bupivacaine hydrochloride (Marcaïn)	DMSO like	DMSO like	42	12
Fenbendazole (Panacur)	Lva	Lva	0	0
Mycophenolic (Mycophenolate)	DMSO like	DMSO like	60	25
Phenoxybenzamine HCl	Gro, Emb, Egl	DMSO like	6	4
Tobramycin	DMSO like	DMSO like	72	6

DRUG	Resume of phenotypes (Subtracting existing Gro, Lva and Ste in <i>cer14</i>)		Microtracker read (day 4)	
	N2	<i>prp-8(cer14)</i>	N2	<i>prp-8(cer14)</i>
Ciclopirox (Penlac)	DMSO like	DMSO like	30	23
Trospium chloride (Sanctura)	DMSO like	DMSO like	61	18
Amoxicillin sodium (Amox)	DMSO like	DMSO like	74	12
Zidovudine (Retrovir)	DMSO like	DMSO like	44	12
Pramiracetam	DMSO like	DMSO like	42	12
Ethisterone	DMSO like	DMSO like	57	1
Aspirin (Acetylsalicylic acid)	DMSO like	DMSO like	60	6
Vardenafil (Vivanza)	DMSO like	DMSO like	46	20
Dopamine hydrochloride (Inotropin)	DMSO like	DMSO like	65	34
Tolterodine tartrate (Detrol LA)	DMSO like	DMSO like	44	16
Isoprenaline hydrochloride	DMSO like	DMSO like	52	29
Quinapril HCl (Accupril)	DMSO like	DMSO like	62	6
Oseltamivir phosphate (Tamiflu)	DMSO like	DMSO like	54	2
Clorsulon	DMSO like	DMSO like	50	10
Niflumic acid	DMSO like	DMSO like	44	23
Racecadotril (Acetorphan)	DMSO like	DMSO like	60	46
Xylazine HCl	DMSO like	DMSO like	16	4
Ritodrine hydrochloride (Yutopar)	DMSO like	DMSO like	52	15
Azelastine hydrochloride (Astelin)	Gro	DMSO like	41	2
Medroxyprogesteron e acetate	DMSO like	DMSO like	60	4
Trazodone hydrochloride (Desyrel)	DMSO like	DMSO like	41	2
L-Thyroxine	DMSO like	DMSO like	62	0
Arecoline	DMSO like	DMSO like	34	2
Ribavirin (Copegus)	DMSO like	DMSO like	71	48
Maprotiline hydrochloride	DMSO like	DMSO like	56	4
Econazole nitrate (Spectazole)	Lva, Lvl	Lva, Lvl	0	0
5-Aminolevulinic acid hydrochloride	DMSO like	DMSO like	64	17
Neomycin sulfate	DMSO like	DMSO like	48	0
Thiamphenicol (Thiophenicol)	DMSO like	DMSO like	60	6
Acemetacin (Emflex)	Emb, Egl, Rbs	DMSO like	18	2
Noradrenaline bitartrate monohydrate (Levophed)	DMSO like	DMSO like	56	20

SUPPLEMENTARY DATA

DRUG	Resume of phenotypes (Subtracting existing Gro, Lva and Ste in <i>cer14</i>)		Microtracker read (day 4)	
	N2	<i>prp-8(cer14)</i>	N2	<i>prp-8(cer14)</i>
Roxithromycin (Roxl-150)	DMSO like	DMSO like	36	18
NAD+	DMSO like	DMSO like	70	9
Miconazole (Monistat)	Lva, Lvl	Lva, Lvl	0	0
Clarithromycin (Biaxin, Klacid)	DMSO like	DMSO like	55	4
Phenylephrine HCl	DMSO like	DMSO like	37	0
Clobetasol propionate	Lva, Lvl	Lva, Lvl	0	0
Tioxolone	DMSO like	DMSO like	50	24
Peramivir Trihydrate	DMSO like	DMSO like	44	4
Salbutamol sulfate (Albuterol)	DMSO like	DMSO like	56	10
Naphazoline hydrochloride (Naphcon)	DMSO like	DMSO like	31	9
Lomefloxacin hydrochloride (Maxaquin)	DMSO like	DMSO like	52	6
Rosiglitazone (Avandia)	DMSO like	DMSO like	26	2
Streptomycin sulfate	DMSO like	DMSO like	22	15
Brompheniramine	DMSO like	DMSO like	41	16
Idebenone	Ste	DMSO like	25	2
Nilvadipine (ARC029)	Gro	Gro	13	13
Scopolamine hydrobromide	DMSO like	DMSO like	60	8
Epinephrine bitartrate (Adrenalinium)	DMSO like	DMSO like	54	16
Riboflavin (Vitamin B2)	DMSO like	DMSO like	28	4
Cortisone acetate (Cortone)	DMSO like	DMSO like	47	0
Tetracaine hydrochloride (Pontocaine)	DMSO like	DMSO like	54	6
Dimethyl Fumarate	DMSO like	DMSO like	48	16
Mifepristone (Mifeprex)	DMSO like	DMSO like	17	1
Hygromycin B	Lva	Lva	0	0
Sotalol (Betapace)	DMSO like	DMSO like	67	9
L-Adrenaline (Epinephrine)	DMSO like	DMSO like	43	2
Clomipramine hydrochloride (Anafranil)	Emb, Egl, Ste	Gro	0	14
Clomifene citrate (Serophene)	Lva	Lva	0	0
Tetracycline HCl	DMSO like	DMSO like	58	14
Calcium levofolinate (Calcium Folate)	DMSO like	DMSO like	47	12
Buflomedil HCl	DMSO like	DMSO like	54	1
Carbazochrome sodium sulfonate	DMSO like	DMSO like	48	54

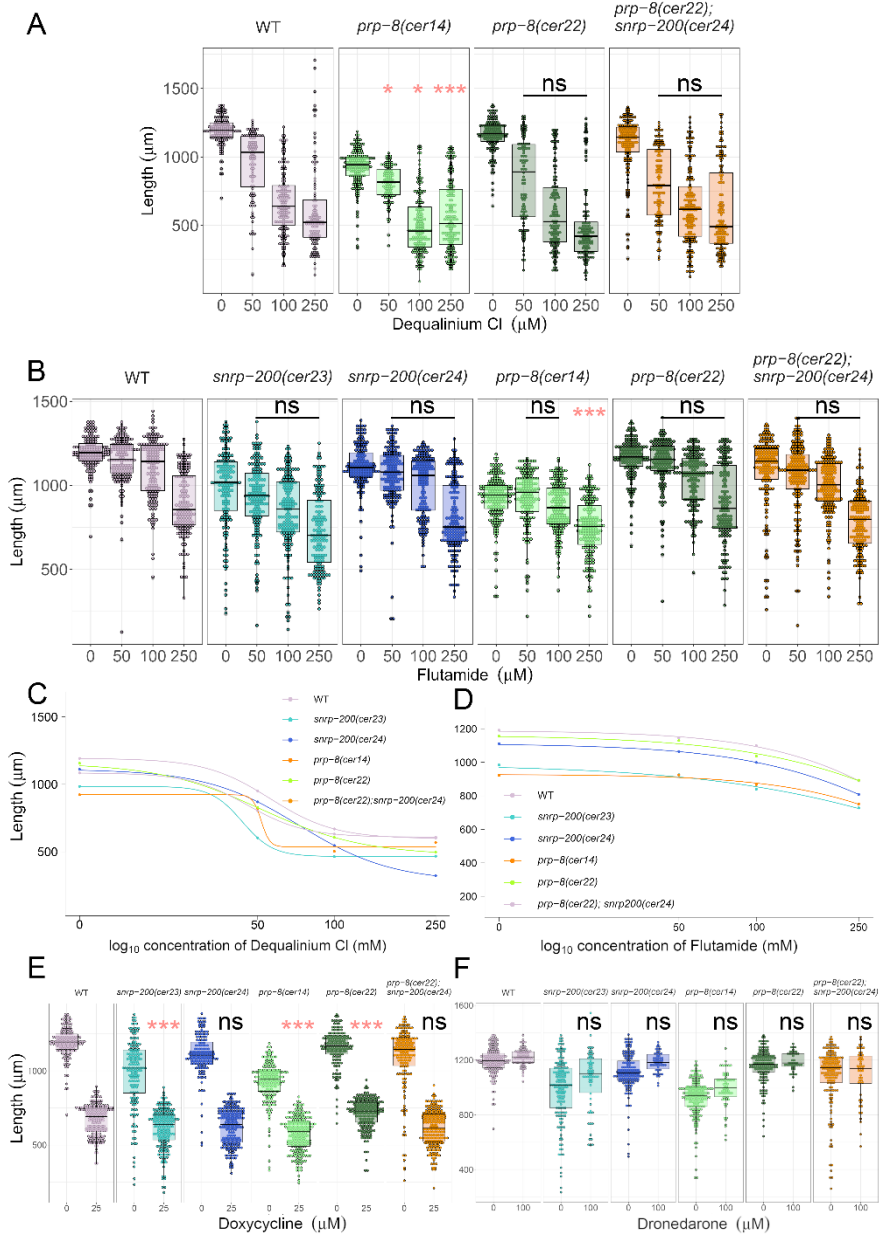
DRUG	Resume of phenotypes (Subtracting existing Gro, Lva and Ste in <i>cer14</i>)		Microtracker read (day 4)	
	N2	<i>prp-8(cer14)</i>	N2	<i>prp-8(cer14)</i>
Spectinomycin hydrochloride	DMSO like	DMSO like	46	20
DL-Adrenaline	DMSO like	DMSO like	60	0
Cefprozil hydrate (Cefzil)	DMSO like	DMSO like	38	0
Hydralazine hydrochloride	DMSO like	DMSO like	32	0
Vancomycin HCl (Vancocin)	DMSO like	DMSO like	43	16
Miglitol (Glyset)	DMSO like	DMSO like	42	0
Fluocinonide (Vanos)	DMSO like	DMSO like	38	6
Paroxetine HCl	Lva	Lva	12	6
Sulfadoxine (Sulphadoxine)	DMSO like	DMSO like	54	2
Phenytoin (Lepitoin)	DMSO like	DMSO like	62	17
Scopine	DMSO like	DMSO like	31	11
Oxacillin sodium monohydrate	DMSO like	DMSO like	33	0
Xylometazoline HCl	DMSO like	DMSO like	38	10
Pioglitazone (Actos)	DMSO like	DMSO like	43	22
Pazopanib	DMSO like	DMSO like	48	9
Tenoxicam (Mobiflex)	Lva	DMSO like	6	0
Methacycline hydrochloride (Physiomycine)	Gro	DMSO like	6	4
Tiotropium Bromide hydrate	DMSO like	DMSO like	53	0
Cloxacillin sodium (Cloxacap)	DMSO like	DMSO like	32	26
Phenacetin	DMSO like	DMSO like	29	3
Tolvaptan (OPC-41061)	Gro, Rbs	DMSO like	8	4
Lonidamine	Gro, Rbs	DMSO like	12	1
Amoxicillin (Amoxycillin)	DMSO like	DMSO like	46	10
Daunorubicin HCl (Daunomycin HCl)	Eg1, Emb, Rbs	DMSO like	5	26
Palonosetron HCl	DMSO like	DMSO like	53	4
Etravirine (TMC125)	DMSO like	DMSO like	48	6
Trimethoprim	DMSO like	DMSO like	51	8
Ibandronate sodium	DMSO like	DMSO like	43	2
Anagrelide HCl	DMSO like	DMSO like	43	0
Triflusal	DMSO like	DMSO like	68	4
Clinafloxacin (PD127391)	DMSO like	DMSO like	30	6
Pravastatin sodium	DMSO like	DMSO like	58	0
Azelmidipine	Ste, Eg1, Let	Lva	15	6
Ulipristal	DMSO like	DMSO like	12	14
Biotin (Vitamin B7)	DMSO like	DMSO like	48	33
Articaine HCl	DMSO like	DMSO like	34	0
Antipyrine	DMSO like	DMSO like	50	36
Trifluoperazine 2HCl	Lva	Lva	1	0
Pentamidine	DMSO like	DMSO like	38	0
Rimonabant (SR141716)	Lva, Lvl	Lva, Lvl	0	0
Bepotastine Besilate	DMSO like	DMSO like	51	10

SUPPLEMENTARY DATA

DRUG	Resume of phenotypes (Subtracting existing Gro, Lva and Ste in <i>cer14</i>)		Microtracker read (day 4)	
	N2	<i>prp-8(cer14)</i>	N2	<i>prp-8(cer14)</i>
Alverine Citrate	DMSO like	DMSO like	30	1
Indacaterol Maleate	pGro, Rbs	DMSO like	34	25
Sulfamerazine	DMSO like	DMSO like	58	28
Gliquidone	Gro, Rbs	DMSO like	32	0
L-Arginine HCl	DMSO like	DMSO like	48	4
Catharanthine	DMSO like	DMSO like	54	12
Cabazitaxel (Jevtana)	Lva	Lva	2	0
Fosoprepitant dimeglumine	Lva	Lva	0	0
Besifloxacin HCl (Besivance)	DMSO like	DMSO like	30	20
2-Thiouracil	DMSO like	DMSO like	46	16
Sulfamethazine	DMSO like	DMSO like	54	16
Butenafine HCl	Ste, Egl, Emb	Gro	10	4
Betahistine 2HCl	DMSO like	DMSO like	50	12
Meptazinol HCl	DMSO like	DMSO like	39	2
Bufexamac	DMSO like	DMSO like	38	6
Droxidopa (L-DOPS)	DMSO like	DMSO like	40	9
Danofloxacin Mesylate	DMSO like	DMSO like	46	2
Creatinine	DMSO like	DMSO like	60	10
Sodium salicylate	DMSO like	DMSO like	37	2
Mepivacaine HCl	DMSO like	DMSO like	52	22
Carbenicillin disodium	DMSO like	DMSO like	43	42
Fexofenadine HCl	DMSO like	DMSO like	51	32
Lamotrigine	DMSO like	DMSO like	64	6
Rofecoxib (Vioxx)	DMSO like	DMSO like	34	1
Enrofloxacin	DMSO like	DMSO like	57	3
Moguisteine	DMSO like	DMSO like	50	2
Methylthiouracil	DMSO like	DMSO like	60	1
Naftifine HCl	Gro, Rbs	DMSO like	26	2
Flumequine	DMSO like	DMSO like	38	29
Amidopyrine	DMSO like	DMSO like	58	26
PMSF (Phenylmethylsulfon yl Fluoride)	DMSO like	DMSO like	30	6
Lurasidone HCl	Ste, Egl, Emb	DMSO like	8	11
Medetomidine HCl	Gro	DMSO like	31	0
Nadifloxacin	DMSO like	DMSO like	68	36
Methenamine (Mandelamine)	DMSO like	DMSO like	60	34
Tylosin tartrate	DMSO like	DMSO like	45	26
Amitriptyline HCl	DMSO like	DMSO like	67	8
Moclobemide	DMSO like	DMSO like	48	48
Niclosamide (Niclocide)	DMSO like	DMSO like	42	2
Cinepazide maleate	DMSO like	DMSO like	49	4
Diclofenac Diethylamine	DMSO like	DMSO like	35	29
Vitamin C (Ascorbic acid)	DMSO like	DMSO like	47	2
Milnacipran HCl	DMSO like	DMSO like	26	32
Benzotropine mesylate	DMSO like	DMSO like	44	22
Azatadine dimaleate	DMSO like	DMSO like	75	36
Pergolide mesylate	DMSO like	DMSO like	32	35
Linagliptin (BI-1356)	DMSO like	DMSO like	48	12

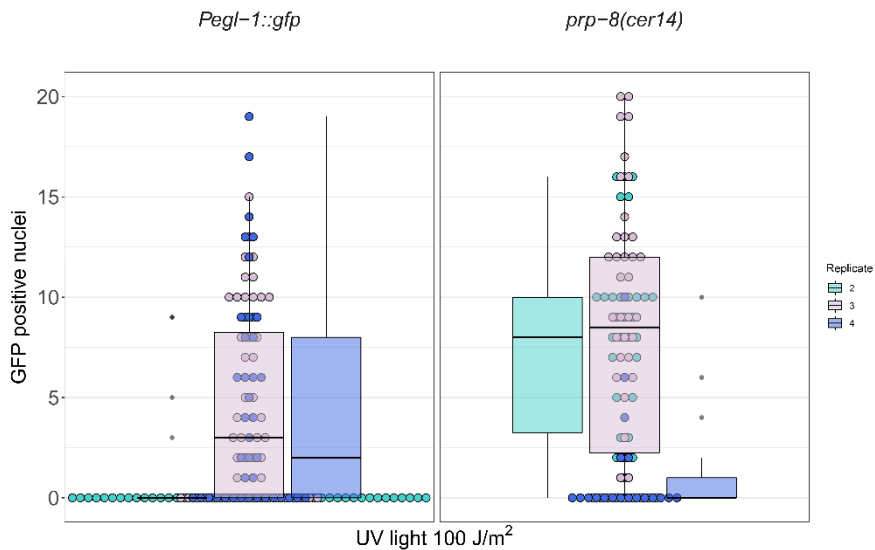
DRUG	Resume of phenotypes (Subtracting existing Gro, Lva and Ste in <i>cer14</i>)		Microtracker read (day 4)	
	N2	<i>prp-8(cer14)</i>	N2	<i>prp-8(cer14)</i>
Azilsartan (TAK-536)	DMSO like	DMSO like	40	18
Naloxone HCl	DMSO like	DMSO like	32	4
Sulfathiazole	DMSO like	DMSO like	65	18
Darifenacin HBr	DMSO like	DMSO like	28	18
Abacavir sulfate	DMSO like	DMSO like	43	28
(+,-)-Octopamine HCl	DMSO like	DMSO like	51	8
Lithocholic acid	Gro, Rbs	Gro	17	1
Bindarit	Lva, Lvl	Lva, Lvl	0	0
Otilonium Bromide (R)-baclofen	Lva, Lvl	Lva, Lvl	0	0
Ornidazole	DMSO like	DMSO like	36	9
Ornidazole	DMSO like	DMSO like	38	1
Tripeleennamine HCl	DMSO like	DMSO like	36	18
Altrenogest	Rbs	DMSO like	44	0
Azlocillin sodium salt	DMSO like	DMSO like	38	19
Ethambutol HCl	DMSO like	DMSO like	29	10
Vildagliptin (LAF-237)	DMSO like	DMSO like	68	10
Solifenacin succinate	DMSO like	DMSO like	50	19
Atovaquone (Atovaquone)	DMSO like	DMSO like	46	2
Amikacin hydrate	DMSO like	DMSO like	43	0
Entacapone	DMSO like	DMSO like	62	9
Ampicillin sodium	DMSO like	DMSO like	47	0
Azacyclonol	DMSO like	DMSO like	44	0
Doxycycline HCl	Gro, Ste	Lva	2	0

Phenotype abbreviations: Ste: sterility, Rbs: reduced brood size, Gro: slow growth, Lva: larval arrest, Pvl: protruding vulva, Let: lethality, Lvl: larval lethality, Emb: embryonic lethal, Sck: sick, Rup: ruptured, Egl: egg laying defective, Dpy: dumpy. Shaded area denotes drugs that were selected for re-testing

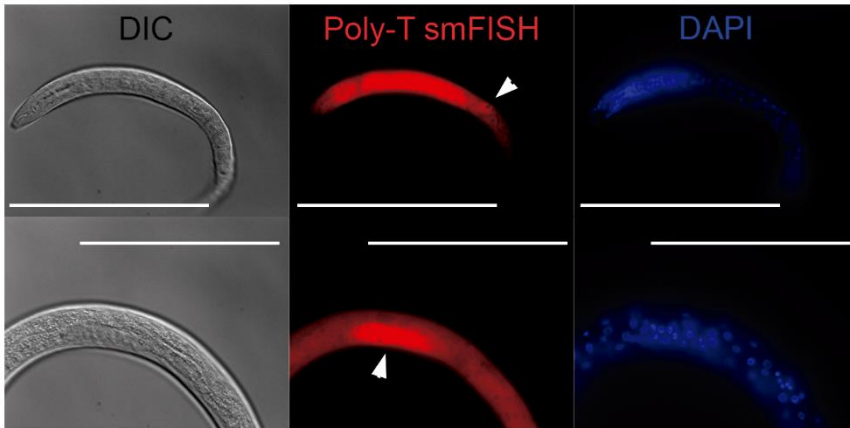


Supplementary Figure R. 1: Validation of candidates for sensitivity obtained from drug screen.

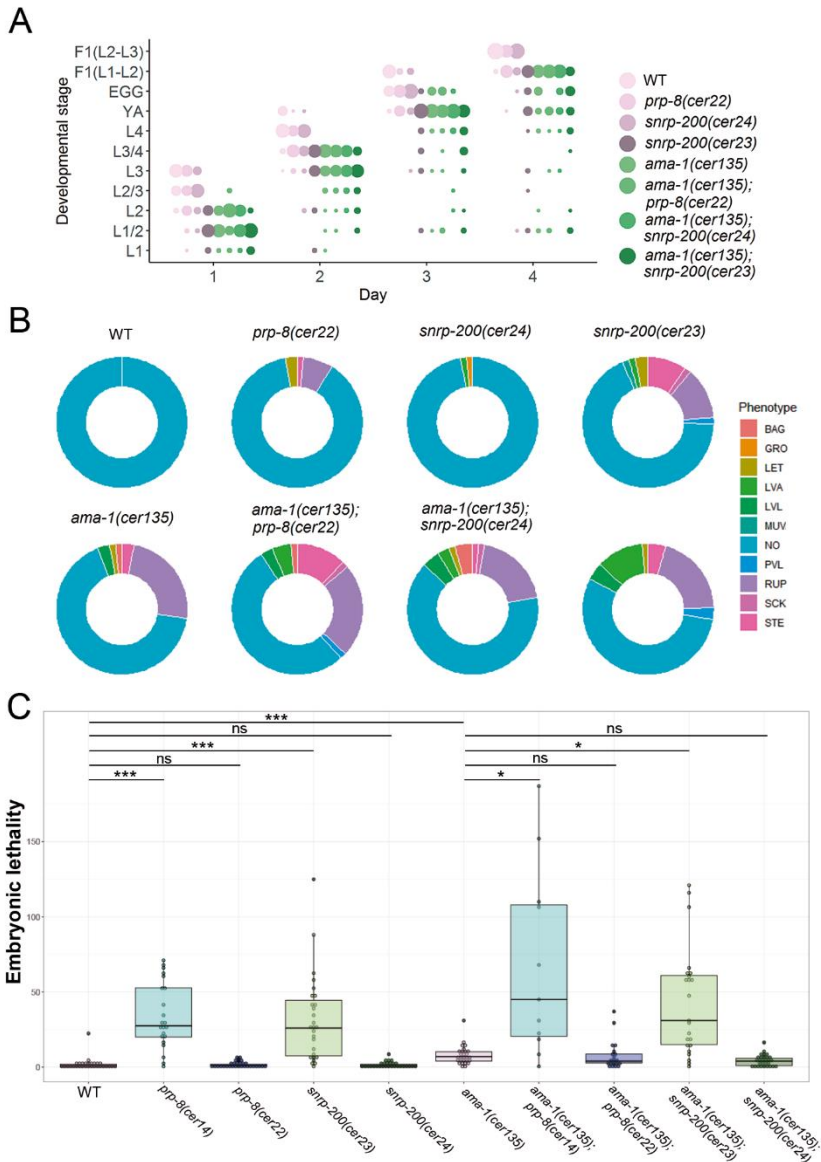
Worm length of WT and s-adRP strains upon treatment with dequalinium Cl (A, N=3, except N=2 at 50 μ M; $n \geq 69$), flutamide (B, N=3, $n \geq 147$), doxycycline hyclate (E, N=3, $n \geq 174$) and dronedarone (E, N=1, $n \geq 44$). Panels C and D show dose-response curve for dequalinium Cl (N=3, except N=2 at 50 μ M; $n \geq 69$) and flutamide (N=3, $n \geq 147$), respectively. (A, B, E and F) Each dot represents the length of an individual worm, box plot indicates the median with the IQR and whiskers the ± 1.5 product of IQR. The difference between control concentration 0 and the tested drug concentrations of the WT was compared to the difference of the mutants'. Aligned rank transformation followed by two-way ANOVA and F test to test interaction was applied. *ns* indicates not significant, * $p < 0.05$ and *** $p < 0.001$. Red color of the asterisks indicates that the observed differences stand against our initial hypothesis of sensitivity. Note that *prp-8(cer14)* and *snrp-200(cer23)* have a highly reduced length even at control conditions, producing an artefactual low reduction in size upon any effective drug treatment, and thus hamstringing the correct interpretation of such reduction. (C and D) Each dot represents the median length at each condition and the line represents log-logistic distribution.



Supplementary Figure R. 2: High inter-replicate variability of *Pegl-1::gfp* reporter hinders the conclusion of sensitivity in the *strong prp-8(cer14)* mutant background. Results of *prp-8(cer14)* strains crossed with *Pegl-1::gfp* (simplified with the name of s-adRP strain) upon exposure to UV light with boxplots for each replicate. The GFP signal varies greatly in different replicates being two that show sensitivity of *cer14* than WT and one resistance. Each dot represents the number of GFP expressing cells, bars represent the median with the ± 1.5 product of IQR. N=3, $n \geq 19$. Kruskal-Wallis with Dunn's post-hoc analysis: *ns* indicates not significant, *** $p < 0.01$ and **** $p < 0.0001$.



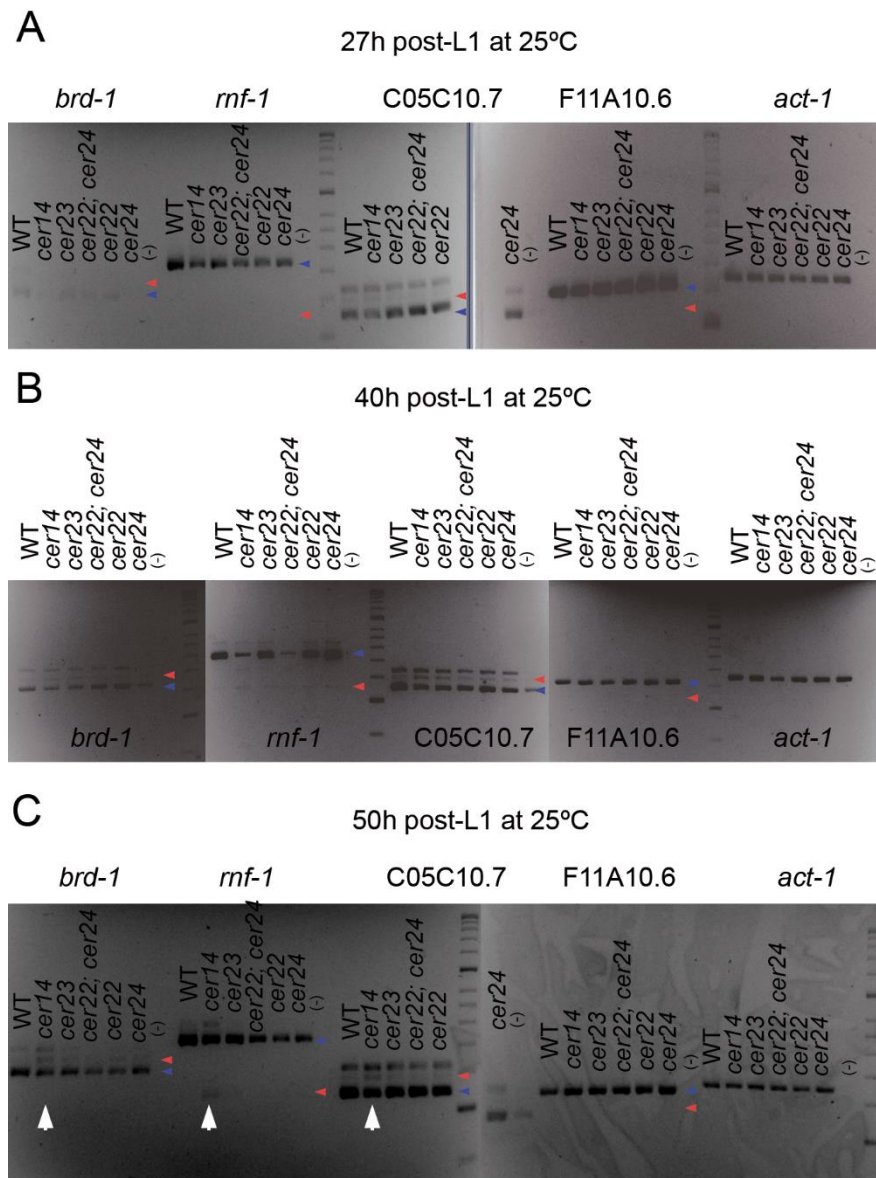
Supplementary Figure R. 3: Poly (T) smFISH of L1 and L2 animals. Most of the body cells present a diffuse signal with the exception of perinuclear foci resembling P-granules encountered in the germ cells (white arrow).



Supplementary Figure R. 4: Characterization of developmental delay (A), overt phenotypes (B), and embryonic lethality (C) of *ama-1(cer135)* and s-adRP double mutants.

(A) Developmental timing. The size of each dot is proportional to the percentage of the population at a given developmental stage, starting with a synchronized population and grown at 20°C (N=1, n≥71). (B) Donnut plots representing visually observable phenotypes detected in mutant strains. (N=1, n≥72). Abbreviations: Bag: bag of worms, Dpy: dumpy, Gro: slow growth, Let: lethality, Lvl: larval lethality, Muv: multivulva, Pvl: protruding vulva, Rup: ruptured, Sck: sick, Ste:

sterile. NO: No observable phenotype. (C) Each dot represents the number of death embryos of a single worm, and bars represent the median with the IQR and whiskers ± 1.5 product of IQR (N=2, $n \geq 21$). Kruskal-Wallis with Dunn's post-hoc analysis: *ns* indicates not significant, * $p < 0.05$, and *** $p < 0.001$.



Supplementary Figure R. 5: Semi-quantitative PCR results of synchronized populations show the strong allele *prp-8(cer14)* present AS events in *brd-1*, *rmf-1*, and C05C10.7 at 50h (white arrows).

Gels showing electrophoresis results with the AS events (red arrows) and canonically spliced transcript sizes (blue arrows) depicted. Only allele names of *prp-8(cer14)*, *prp-8(cer22)*, *snrp-200(cer23)*, and *snrp-200(cer24)* are shown for simplicity. (A) Gels from RNA extracted 25h post-L1, (B) 40h post-L1, and (C) 50h post-L1.

BIBLIOGRAPHY

- ABRAMOWICZ, A. & GOS, M. (2018) Splicing mutations in human genetic disorders: examples, detection, and confirmation. *Journal of Applied Genetics* **59**, 253–268.
- ADLER, A.S., MCCLELAND, M.L., YEE, S., YAYLAOGLU, M., HUSSAIN, S., COSINO, E., QUINONES, G., MODRUSAN, Z., SESHAGIRI, S., TORRES, E., CHOPRA, V.S., HALEY, B., ZHANG, Z., BLACKWOOD, E.M., SINGH, M., ET AL. (2014) An integrative analysis of colon cancer identifies an essential function for PRPF6 in tumor growth. *Genes and Development* **28**, 1068–1084.
- ADLI, M. (2018) The CRISPR tool kit for genome editing and beyond. *Nature Communications* **9**, 1911.
- AHMED, S. & HODGKIN, J. (2000) MRT-2 checkpoint protein is required for germline immortality and telomere replication in *C. elegans*. *Nature* **403**, 159–164.
- AÍSA-MARÍN, I., GARCÍA-ARROYO, R., MIRRA, S. & MARFANY, G. (2021) The alter retina: Alternative splicing of retinal genes in health and disease. *International Journal of Molecular Sciences* **22**, 1–28.
- AJMAL, M., KHAN, M.I., NEVELING, K., KHAN, Y.M., AZAM, M., WAHEED, N.K., HAMEL, C.P., BEN-YOSEF, T., DE BAERE, E., KOENEKOOP, R.K., COLLIN, R.W.J., QAMAR, R. & CREMERS, F.P.M. (2014) A missense mutation in the splicing factor gene *DHX38* is associated with early-onset retinitis pigmentosa with macular coloboma. *Journal of Medical Genetics* **51**, 444–448.
- ALLEN, M.A., HILLIER, L.D.W., WATERSTON, R.H. & BLUMENTHAL, T. (2011) A global analysis of *C. elegans* trans-splicing. *Genome Research* **21**, 255–264.
- ALLISON, D.F. & WANG, G.G. (2019) R-loops: formation, function, and relevance to cell stress. *Cell Stress* **3**, 38–46.
- AOKI, H., SATO, S., TAKANAMI, T., ISHIHARA, T., KATSURA, I., TAKAHASHI, H. & HIGASHITANI, A. (2000) Characterization of *Ce-atl-1*, an ATM-like gene from *Caenorhabditis elegans*. *Molecular and General Genetics* **264**, 119–126.
- ARNOLD, E.S., LING, S.C.S.-C., HUELGA, S.C., LAGIER-TOURENNE, C., POLYMERIDOU, M., DITSWORTH, D., KORDASIEWICZ, H.B., MCALONIS-DOWNES, M., PLATOSHYN, O., PARONE, P.A., DA CRUZ, S., CLUTARIO, K.M., SWING, D., TESSAROLLO, L., MARSALA, M., ET AL. (2013) ALS-linked *TDP-43* mutations produce aberrant RNA splicing and adult-onset motor neuron disease without aggregation or loss of nuclear TDP-43. *Proceedings of the National Academy of Sciences* **110**, E736–E745.
- ARRIBERE, J.A., BELL, R.T., FU, B.X.H., ARTILES, K.L., HARTMAN, P.S. & FIRE, A.Z. (2014) Efficient marker-free recovery of custom genetic modifications with CRISPR/Cas9 in *Caenorhabditis elegans*. *Genetics* **198**, 837–846.
- ARTAL-SANZ, M., DE JONG, L. & TAVERNARAKIS, N. (2006) *Caenorhabditis elegans*: A versatile platform for drug discovery. *Biotechnology Journal* **1**, 1405–1418.
- ASIKAINEN, S., VARTIAINEN, S., LAKSO, M., NASS, R. & WONG, G. (2005) Selective sensitivity of *Caenorhabditis elegans* neurons to RNA interference. *NeuroReport* **16**, 1995–1999.
- AUDO, I., BUJAKOWSKA, K.M., LÉVEILLARD, T., MOHAND-SAD, S., LANCELOT, M.E., GERMAIN, A., ANTONIO, A., MICHIELS, C., SARAIVA, J.P., LETEXIER, M., SAHEL, J.A., BHATTACHARYA, S.S. & ZEITZ, C. (2012) Development and application of a next-generation-sequencing (NGS) approach to detect known and novel gene defects underlying retinal diseases. *Orphanet Journal of Rare Diseases* **7**, 8.
- AVELA, K., SALONEN-KAJANDER, R., LAITINEN, A., RAMSDEN, S., BARTON, S. & RUDANKO, S. (2019) The genetic aetiology of retinal degeneration in children in Finland – new founder mutations identified. *Acta Ophthalmologica* **97**, 805–814.
- AVELA, K., SANKILA, E.-M., SEITSONEN, S., KUULUVAINEN, L., BARTON, S., GILLIES, S. & AITTO-MÄKI, K. (2018) A founder mutation in *CERKL* is a major cause of retinal dystrophy in Finland. *Acta Ophthalmologica* **96**, 183–191.

- BACCHI, N., CASAROSA, S. & DENTI, M.A. (2014) Splicing-correcting therapeutic approaches for retinal dystrophies: Where endogenous gene regulation and specificity matter. *Investigative Ophthalmology and Visual Science* **55**, 3285–3294.
- BARALLE, M. & BARALLE, F.E. (2018) The splicing code. *BioSystems* **164**, 39–48.
- BARBERAN-SOLER, S. & ZAHLER, A.M. (2008) Alternative splicing and the steady-state ratios of mRNA isoforms generated by it are under strong stabilizing selection in *Caenorhabditis elegans*. *Molecular biology and evolution* **25**, 2431–2437.
- BARRANGOU, R., FREMAUX, C., DEVEAU, H., RICHARDS, M., BOYAVAL, P., MOINEAU, S., ROMERO, D.A. & HORVATH, P. (2007) CRISPR provides acquired resistance against viruses in prokaryotes. *Science* **315**, 1709–1712.
- BENAGLIO, P., MCGEE, T.L., CAPELLI, L.P., HARPER, S., BERSON, E.L. & RIVOLTA, C. (2011) Next generation sequencing of pooled samples reveals new *SNRN200* mutations associated with retinitis pigmentosa. *Human Mutation* **32**, E2246–E2258.
- BENAGLIO, P., SAN JOSE, P.F., AVILA-FERNANDEZ, A., ASCARI, G., HARPER, S., MANES, G., AYUSO, C., HAMEL, C., BERSON, E.L. & RIVOLTA, C. (2014) Mutational screening of splicing factor genes in cases with autosomal dominant retinitis pigmentosa. *Molecular vision* **20**, 843–851.
- BERGET, S.M., MOORE, C. & SHARP, P.A. (1977) Spliced segments at the 5' terminus of adenovirus 2 late mRNA. *Proceedings of the National Academy of Sciences of the United States of America* **74**, 3171–3175.
- BERK, A.J. (2016) Discovery of RNA splicing and genes in pieces. *Proceedings of the National Academy of Sciences of the United States of America* **113**, 801–805.
- BERTRAM, K., EL AYOUBI, L., DYBKOV, O., AGAFONOV, D.E., WILL, C.L., HARTMUTH, K., URLAUB, H., KASTNER, B., STARK, H. & LÜHRMANN, R. (2020) Structural Insights into the Roles of Metazoan-Specific Splicing Factors in the Human Step 1 Spliceosome. *Molecular Cell* **80**, 127-139.e6.
- BHATIA, S., GOYAL, S., SINGH, I.R., SINGH, D. & VANITA, V. (2018) A novel mutation in the *PRPF31* in a North Indian adRP family with incomplete penetrance. *Documenta Ophthalmologica* **137**, 103–119.
- BIANCHI, J.I., STOCKERT, J.C., BUZZI, L.I., BUZZ, L.I., BLÁZQUEZ-CASTRO, A. & SIMONETTA, S.H. (2015) Reliable Screening of Dye Phototoxicity by Using a *Caenorhabditis elegans* Fast Bioassay. *PLoS one* **10**, e0128898.
- BIEBERSTEIN, N.I., OESTERREICH, F.C., STRAUBE, K. & NEUGEBAUER, K.M. (2012) First exon length controls active chromatin signatures and transcription. *Cell Reports* **2**, 62–68.
- BILLI, A.C., FISCHER, S.E.J. & KIM, J.K. (2014) Endogenous RNAi pathways in *C. elegans*. In *WormBook: the online review of C. elegans biology* pp. 1–49.
- BIRTEL, J., GLIEM, M., MANGOLD, E., MÜLLER, P.L., HOLZ, F.G., NEUHAUS, C., LENZNER, S., ZAHNLEITER, D., BETZ, C., EISENBERGER, T., BOLZ, H.J. & ISSA, P.C. (2018) Next-generation sequencing identifies unexpected genotype-phenotype correlations in patients with retinitis pigmentosa. *PLoS ONE* **13**.
- BIRTEL, J., GLIEM, M., OISHI, A., MÜLLER, P.L., HERRMANN, P., HOLZ, F.G., MANGOLD, E., KNAPP, M., BOLZ, H.J. & CHARBEL ISSA, P. (2019) Genetic testing in patients with retinitis pigmentosa: Features of unsolved cases. *Clinical & Experimental Ophthalmology* **47**, ceo.13516.
- BLANCO-KELLY, F., GARCÍA-HOYOS, M., CORTÓN, M., AVILA-FERNÁNDEZ, A., RIVEIRO-ÁLVAREZ, R., GIMÉNEZ, A., HERNAN, I., CARBALLO, M. & AYUSO, C. (2012) Genotyping microarray: mutation screening in Spanish families with autosomal dominant retinitis pigmentosa. *Molecular vision* **18**, 1478–1483.

- BLUMENTHAL, T. (2012) Trans-splicing and operons in *C. elegans*. In *WormBook : the online review of C. elegans biology* pp. 1–11.
- BONNAL, S.C., LÓPEZ-OREJA, I. & VALCÁRCEL, J. (2020) Roles and mechanisms of alternative splicing in cancer — implications for care. *Nature Reviews Clinical Oncology* **17**, 457–474.
- BONNET, A., GROSSO, A.R., ELKAOUTARI, A., COLENO, E., PRESLE, A., SRIDHARA, S.C., JANBON, G., GÉLI, V., DE ALMEIDA, S.F. & PALANCADE, B. (2017) Introns Protect Eukaryotic Genomes from Transcription-Associated Genetic Instability. *Molecular Cell* **67**, 608–621.e6.
- BOQUE-SASTRE, R., SOLER, M., OLIVEIRA-MATEOS, C., PORTELA, A., MOUTINHO, C., SAYOLS, S., VILLANUEVA, A., ESTELLER, M. & GUIL, S. (2015) Head-to-head antisense transcription and R-loop formation promotes transcriptional activation. *Proceedings of the National Academy of Sciences of the United States of America* **112**, 5785–5790.
- BOWMAN, E.A., RIDDLE, D.L. & KELLY, W. (2011) Amino Acid Substitutions in the *Caenorhabditis elegans* RNA Polymerase II Large Subunit AMA-1/RPB-1 that Result in α -Amanitin Resistance and/or Reduced Function. *G3 Genes/Genomes/Genetics* **1**, 411–416.
- BOWNE, S.J., SULLIVAN, L.S., AVERY, C.E., SASSER, E.M., ROORDA, A., DUNCAN, J.L., WHEATON, D.H., BIRCH, D.G., BRANHAM, K.E., HECKENLIVELY, J.R., SIEVING, P.A. & DAIGER, S.P. (2013) Mutations in the small nuclear riboprotein 200 kDa gene (*SNRNP200*) cause 1.6% of autosomal dominant retinitis pigmentosa. *Molecular vision* **19**, 2407–2417.
- BRABERG, H., JIN, H., MOEHLE, E.A., CHAN, Y.A., WANG, S., SHALES, M., BENSCHOP, J.J., MORRIS, J.H., QIU, C., HU, F., TANG, L.K., FRASER, J.S., HOLSTEGE, F.C.P., HIETER, P., GUTHRIE, C., ET AL. (2013) From structure to systems: High-resolution, quantitative genetic analysis of RNA polymerase II. *Cell* **154**, 775–788.
- BRAMALL, A.N., WRIGHT, A.F., JACOBSON, S.G. & MCINNES, R.R. (2010) The genomic, biochemical, and cellular responses of the retina in inherited photoreceptor degenerations and prospects for the treatment of these disorders. *Annual Review of Neuroscience* **33**, 441–472.
- BRAVO-GIL, N., GONZÁLEZ-DEL POZO, M., MARTÍN-SÁNCHEZ, M., MÉNDEZ-VIDAL, C., RODRÍGUEZ-DE LA RÚA, E., BORREGO, S. & ANTIÑOLO, G. (2017) Unravelling the genetic basis of simplex Retinitis Pigmentosa cases. *Scientific Reports* **7**, 41937.
- BRENA, D., BERTRAN, J., PORTA-DE-LA-RIVA, M., GUILLÉN, Y., CORNES, E., KUKHTAR, D., CAMPOS-VICENS, L., FERNÁNDEZ, L., PECHARROMAN, I., GARCÍA-LÓPEZ, A., ISLAM, A.B.M.M.K., MARRUECOS, L., BIGAS, A., CERÓN, J. & ESPINOSA, L. (2020) Ancestral function of Inhibitors-of-kappaB regulates *Caenorhabditis elegans* development. *Scientific reports* **10**, 16153.
- BRENNER, S. (1973) The genetics of behaviour. *British Medical Bulletin* **29**, 269–271.
- BRENNER, S. (1988) Foreword. In *The Nematode Caenorhabditis elegans*, Edited by William B. Wood
- BRENNER, S. (1974) The genetics of *Caenorhabditis elegans*. *Genetics* **77**, 71–94.
- BRYANT, L., LOZYSKA, O., MAGUIRE, A.M., ALEMAN, T.S. & BENNETT, J. (2018) Prescreening whole exome sequencing results from patients with retinal degeneration for variants in genes associated with retinal degeneration. *Clinical Ophthalmology* **12**, 49–63.
- BRYANT, L., LOZYSKA, O., MARSH, A., PAPP, T.E., VAN GORDER, L., SERRANO, L.W., GAI, X., MAGUIRE, A.M., ALEMAN, T.S. & BENNETT, J. (2019) Identification of a novel pathogenic missense mutation in *PRPF31* using whole exome sequencing: A case report. *British Journal of Ophthalmology* **103**, 761–767.
- BYRDON, E.M., BRONSTEIN, R., BUSKIN, A., LAKO, M., PIERCE, E.A. & FERNANDEZ-GODINO, R. (2019) AAV-Mediated Gene Augmentation Therapy Restores Critical Functions in Mutant *PRPF31*^{+/-} iPSC-Derived RPE Cells. *Molecular Therapy - Methods and Clinical Development* **15**, 392–402.

- BURGE, C.B., PADGETT, R.A. & SHARP, P.A. (1998) Evolutionary fates and origins of U12-type introns. *Molecular Cell* **2**, 773–785.
- CAO, H., WU, J., LAM, S., DUAN, R., NEWNHAM, C., MOLDAI, R.S., GRAZIOTTO, J.J., PIERCE, E.A. & HU, J. (2011) Temporal and tissue specific regulation of RP-Associated splicing factor genes *PRPF3*, *PRPF31* and *PRPC8*-implications in the pathogenesis of RP. *PLoS ONE* **6**, 1–10.
- CARRIGAN, M., DUIGNAN, E., MALONE, C.P.G., STEPHENSON, K., SAAD, T., MCDERMOTT, C., GREEN, A., KEEGAN, D., HUMPHRIES, P., KENNA, P.F. & FARRAR, G.J. (2016) Panel-Based Population Next-Generation Sequencing for Inherited Retinal Degenerations. *Scientific Reports* **6**, 33248.
- VAN CAUWENBERGH, C., COPPIETERS, F., ROELS, D., DE JAEGERE, S., FLIPTS, H., DE ZAEYTIJD, J., WALRAEDT, S., CLAES, C., FRANSEN, E., VAN CAMP, G., DEPASSE, F., CASTEELS, I., DE RAVEL, T., LEROY, B.P. & DE BAERE, E. (2017) Mutations in splicing factor genes are a major cause of autosomal dominant retinitis pigmentosa in Belgian families. *PLoS one* **12**, e0170038.
- CERON, J., RUAL, J.-F., CHANDRA, A., DUPUY, D., VIDAL, M. & VAN DEN HEUVEL, S. (2007) Large-scale RNAi screens identify novel genes that interact with the *C. elegans* retinoblastoma pathway as well as splicing-related components with synMuv B activity. *BMC developmental biology* **7**, 30.
- CHAKAROVA, C.F., HIMS, M.M., BOLZ, H., ABU-SAFIEH, L., PATEL, R.J., PAPAIOANNOU, M.G., INGLEHEARN, C.F., KEEN, T.J., WILLIS, C., MOORE, A.T., ROSENBERG, T., WEBSTER, A.R., BIRD, A.C., GAL, A., HUNT, D., ET AL. (2002) Mutations in HPRP3, a third member of pre-mRNA splicing factor genes, implicated in autosomal dominant retinitis pigmentosa. *Human Molecular Genetics* **11**, 87–92.
- CHALFIE, M., TU, Y., EUSKIRCHEN, G., WARD, W.W. & PRASHER, D.C. (1994) Green fluorescent protein as a marker for gene expression. *Science* **263**, 802–805.
- CHAN, I.S. & GINSBURG, G.S. (2011) Personalized medicine: Progress and promise. *Annual Review of Genomics and Human Genetics* **12**, 217–244.
- CHEN, F.C., WANG, S.S., CHEN, C.J., LI, W.H. & CHUANG, T.J. (2006) Alternatively and constitutively spliced exons are subject to different evolutionary forces. *Molecular Biology and Evolution* **23**, 675–682.
- CHEN, X., LIU, Y., SHENG, X., TAM, P.O.S., ZHAO, K., CHEN, X., RONG, W., LIU, Y., LIU, X., PAN, X., CHEN, L.J., ZHAO, Q., VOLLRATH, D., PANG, C.P. & ZHAO, C. (2014) *PRPF4* mutations cause autosomal dominant retinitis pigmentosa. *Human Molecular Genetics* **23**, 2926–2939.
- CHEN, Y., CHAFIN, D., PRICE, D.H. & GREENLEAF, A.L. (1996) Drosophila RNA polymerase II mutants that affect transcription elongation. *Journal of Biological Chemistry* **271**, 5993–5999.
- CHEN, Y., WEEKS, J., MORTIN, M.A. & GREENLEAF, A.L. (1993) Mapping mutations in genes encoding the two large subunits of Drosophila RNA polymerase II defines domains essential for basic transcription functions and for proper expression of developmental genes. *Molecular and Cellular Biology* **13**, 4214–4222.
- CHIU, H., SCHWARTZ, H.T., ANTOSHECHKIN, I. & STERNBERG, P.W. (2013) Transgene-free genome editing in *Caenorhabditis elegans* using CRISPR-Cas. *Genetics* **195**, 1167–1171.
- CHO, S.W., LEE, J., CARROLL, D., KIM, J.S. & LEE, J. (2013) Heritable gene knockout in *Caenorhabditis elegans* by direct injection of Cas9-sgRNA ribonucleoproteins. *Genetics* **195**, 1177–1180.
- CHOI, D. & WOO, M. (2010) Executioners of apoptosis in pancreatic-cells: not just for cell death. *Am J Physiol Endocrinol Metab* **298**, 735–741.
- CHOW, L.T., GELINAS, R.E., BROKER, T.R. & ROBERTS, R.J. (1977) An amazing sequence arrangement at the 5' ends of adenovirus 2 messenger RNA. *Cell* **12**, 1–8.

- CHU, C.S., TRAPNELL, B.C., CURRISTIN, S., CUTTING, G.R. & CRYSTAL, R.G. (1993) Genetic basis of variable exon 9 skipping in cystic fibrosis transmembrane conductance regulator mRNA. *Nature Genetics* **3**, 151–156.
- COMITATO, A., SPAMPANATO, C., CHAKAROVA, C., SANGES, D., BHATTACHARYA, S.S. & MARIGO, V. (2007) Mutations in splicing factor *PRPF3*, causing retinal degeneration, form detrimental aggregates in photoreceptor cells. *Human Molecular Genetics* **16**, 1699–1707.
- CONG, L., RAN, F.A., COX, D., LIN, S., BARRETTO, R., HABIB, N., HSU, P.D., WU, X., JIANG, W., MARRAFFINI, L.A. & ZHANG, F. (2013) Multiplex genome engineering using CRISPR/Cas systems. *Science* **339**, 819–823.
- CONRAD, R., THOMAS, J., SPIETH, J. & BLUMENTHAL, T. (1991) Insertion of part of an intron into the 5' untranslated region of a *Caenorhabditis elegans* gene converts it into a trans-spliced gene. *Molecular and Cellular Biology* **11**, 1921–1926.
- CONTE, D., MACNEIL, L.T., WALHOUT, A.J.M. & MELLO, C.C. (2015) RNA Interference in *Caenorhabditis elegans*. *Current Protocols in Molecular Biology* **109**, 26.3.1–26.3.30.
- DE CONTI, L., BARALLE, M. & BURATTI, E. (2013) Exon and intron definition in pre-mRNA splicing. *Wiley Interdisciplinary Reviews: RNA* **4**, 49–60.
- CORSI, A.K., WIGHTMAN, B. & CHALFIE, M. (2015) A Transparent window into biology: A primer on *Caenorhabditis elegans*. In *WormBook : the online review of C. elegans biology* pp. 1–31.
- COSTA, K.A., SALLES, M.V., WHITEBIRCH, C., CHIANG, J. & SALLUM, J.M.F. (2017) Gene panel sequencing in Brazilian patients with retinitis pigmentosa. *International Journal of Retina and Vitreous* **3**, 33.
- COUSSA, R.G., CHAKAROVA, C., AJLAN, R., TAHA, M., KAVALEC, C., GOMOLIN, J., KHAN, A., LOPEZ, I., REN, H., WASEEM, N., KAMENAROVA, K., BHATTACHARYA, S.S. & KOENEKOOP, R.K. (2015) Genotype and Phenotype Studies in Autosomal Dominant Retinitis Pigmentosa (adRP) of the French Canadian Founder Population. *Investigative Ophthalmology & Visual Science* **56**, 8297.
- CRAIG VENTER, J., ADAMS, M.D., MYERS, E.W., LI, P.W., MURAL, R.J., SUTTON, G.G., SMITH, H.O., YANDELL, M., EVANS, C.A., HOLT, R.A., GOCAYNE, J.D., AMANATIDES, P., BALLEW, R.M., HUSON, D.H., WORTMAN, J.R., ET AL. (2001) The sequence of the human genome. *Science* **291**, 1304–1351.
- CULETTO, E. & SATTELLE, D.B. (2000) A role for *Caenorhabditis elegans* in understanding the function and interactions of human disease genes. In *Human Molecular Genetics* p.
- CVAČKOVÁ, Z., MATĚJŮ, D. & STANĚK, D. (2014) Retinitis Pigmentosa Mutations of *SNRNP200* Enhance Cryptic Splice-Site Recognition. *Human Mutation* **35**, 308–317.
- DAIGER, S., ROSSITER, B., GREENBERG, J., CHRISTOFFELS, A. & HIDE, W. (1998) RetNet. Data services and software for identifying genes and mutations causing retinal degeneration. *Invest. Ophthalmol. Vis. Sci.* <https://sph.uth.edu/RetNet/>.
- DAIGER, S.P., BOWNE, S.J. & SULLIVAN, L.S. (2007) Perspective on genes and mutations causing retinitis pigmentosa. *Archives of Ophthalmology* **125**, 151–158.
- DAIGER, S.P., BOWNE, S.J. & SULLIVAN, L.S. (2015) Genes and mutations causing autosomal dominant retinitis pigmentosa. *Cold Spring Harbor Perspectives in Medicine* **5**, a017129.
- DAIGER, S.P., BOWNE, S.J., SULLIVAN, L.S., BLANTON, S.H., WEINSTOCK, G.M., KOBOLDT, D.C., FULTON, R.S., LARSEN, D., HUMPHRIES, P., HUMPHRIES, M.M., PIERCE, E.A., CHEN, R. & LI, Y. (2014) Application of next-generation sequencing to identify genes and mutations causing autosomal dominant retinitis pigmentosa (adRP). *Advances in Experimental Medicine and Biology* **801**, 123–129.

- DEFFIT, S.N., NEFF, C. & KOWALSKI, J.R. (2017) Exploring *Caenorhabditis elegans* Behavior: An Inquiry-Based Laboratory Module for Middle or High School Students. *The American Biology Teacher* **79**, 661–667.
- DENICOLA, A.B. & TANG, Y. (2019) Therapeutic approaches to treat human spliceosomal diseases. *Current Opinion in Biotechnology* **60**, 72–81.
- DESHAIES, J.-E., SHKRETA, L., MOSZCZYNSKI, A.J., SIDIBÉ, H., SEMMLER, S., FOUILLEN, A., BENNETT, E.R., BEKENSTEIN, U., DESTROISMAISONS, L., TOUTANT, J., DELMOTTE, Q., VOLKENING, K., STABILE, S., AULAS, A., KHALFALLAH, Y., ET AL. (2018) TDP-43 regulates the alternative splicing of hnRNP A1 to yield an aggregation-prone variant in amyotrophic lateral sclerosis. *Brain : a journal of neurology* **141**, 1320–1333.
- DICKINSON, D.J. & GOLDSTEIN, B. (2016) CRISPR-Based Methods for *Caenorhabditis elegans* Genome Engineering. *Genetics* **202**, 885–901.
- DING, F. & ELOWITZ, M.B. (2019) Constitutive splicing and economies of scale in gene expression. *Nature Structural and Molecular Biology* **26**, 424–432.
- DOCKERY, A., STEPHENSON, K., KEEGAN, D., WYNNE, N., SILVESTRI, G., HUMPHRIES, P., KENNA, P.F., CARRIGAN, M. & FARRAR, G.J. (2017) Target 5000: Target Capture Sequencing for Inherited Retinal Degenerations. *Genes* **8**, 304.
- DOKSHIN, G.A., GHANTA, K.S., PISCOPO, K.M. & MELLO, C.C. (2018) Robust Genome Editing with Short Single-Stranded and Long, Partially Single-Stranded DNA Donors in *Caenorhabditis elegans*. *Genetics* **210**, 781–787.
- DOMÍNGUEZ-SÁNCHEZ, M.S., BARROSO, S., GÓMEZ-GONZÁLEZ, B., LUNA, R. & AGUILERA, A. (2011) Genome Instability and Transcription Elongation Impairment in Human Cells Depleted of THO/TREX. *PLoS Genetics* **7**, e1002386.
- VAN DOORMAAL, P.T.C., TICOZZI, N., WEISHAUP, J.H., KENNA, K., DIEKSTRA, F.P., VERDE, F., ANDERSEN, P.M., DEKKER, A.M., TILOCA, C., MARROQUIN, N., OVERSTE, D.J., PENSATO, V., NÜRNBERG, P., PULIT, S.L., SCHELLEVIS, R.D., ET AL. (2017) The role of de novo mutations in the development of amyotrophic lateral sclerosis. *Human Mutation* **38**, 1534–1541.
- DRYJA, T.P., MCGEE, T.L., REICHEL, E., HAHN, L.B., COWLEY, G.S., YANDELL, D.W., SANDBERG, M.A. & BERSON, E.L. (1990) A point mutation of the rhodopsin gene in one form of retinitis pigmentosa. *Nature* **343**, 364–366.
- ELLINGFORD, J.M., BARTON, S., BHASKAR, S., O’SULLIVAN, J., WILLIAMS, S.G., LAMB, J.A., PANDA, B., SERGOUNIOTIS, P.I., GILLESPIE, R.L., DAIGER, S.P., HALL, G., GALE, T., CHRISTOPHER LLOYD, I., BISHOP, P.N., RAMSDEN, S.C., ET AL. (2016) Molecular findings from 537 individuals with inherited retinal disease. *Journal of Medical Genetics* **53**, 761–767.
- ELLIS, H.M. & HORVITZ, H.R. (1986) Genetic control of programmed cell death in the nematode *C. elegans*. *Cell* **44**, 817–829.
- DE ERKENEZ, A., BERSON, E. & DRYJA, T. (2002) Novel Mutations in the *PRPC8* Gene, Encoding a Pre-mRNA Splicing Factor in Patients with Autosomal Dominant Retinitis Pigmentosa | IOVS | ARVO Journals.
- FAHIM, A.T., DAIGER, S.P. & WELEBER, R.G. (1993) Nonsyndromic Retinitis Pigmentosa Overview. In *GeneReviews*® (eds R.A. PAGON, M.P. ADAM, H.H. ARDINGER, S.E. WALLACE, A. AMEMIYA, L.J.H. BEAN, T.D. BIRD, N. LEDBETTER, H.C. MEFFORD, R.J.H. SMITH & K. STEPHENS), p.
- FDA (2020) Table of Pharmacogenetic Associations | FDA. <https://www.fda.gov/medical-devices/precision-medicine/table-pharmacogenetic-associations> [accessed 15 April 2021].
- FENG, J., GUO, J., ZHAO, P., SHEN, J., CHAI, B. & WANG, J. (2020) mTOR up-regulation of SNRPA1 contributes to hepatocellular carcinoma development. *Bioscience reports* **40**.

- FERNANDEZ-SAN JOSE, P., CORTON, M., BLANCO-KELLY, F., AVILA-FERNANDEZ, A., LOPEZ-MARTINEZ, M.A., SANCHEZ-NAVARRO, I., SANCHEZ-ALCUDIA, R., PEREZ-CARRO, R., ZURITA, O., SANCHEZ-BOLIVAR, N., LOPEZ-MOLINA, M.I., GARCIA-SANDOVAL, B., RIVEIRO-ALVAREZ, R. & AYUSO, C. (2015) Targeted next-generation sequencing improves the diagnosis of autosomal dominant retinitis pigmentosa in Spanish patients. *Investigative Ophthalmology and Visual Science* **56**, 2173–2182.
- FIRE, A., XU, S., MONTGOMERY, M.K., KOSTAS, S.A., DRIVER, S.E. & MELLO, C.C. (1998) Potent and specific genetic interference by double-stranded RNA in *Caenorhabditis elegans*. *Nature* **391**, 806–811.
- FONG, N., KIM, H., ZHOU, Y., JI, X., QIU, J., SALDI, T., DIENER, K., JONES, K., FU, X.D. & BENTLEY, D.L. (2014) Pre-mRNA splicing is facilitated by an optimal RNA polymerase II elongation rate. *Genes and Development* **28**, 2663–2676.
- FONTRDONA, L., PORTA-DE-LA-RIVA, M., MORÁN, T., NIU, W., DÍAZ, M., ARISTIZÁBAL-CORRALES, D., VILLANUEVA, A., SCHWARTZ, S., REINKE, V. & CERÓN, J. (2013) RSR-2, the *Caenorhabditis elegans* Ortholog of Human Spliceosomal Component SRm300/SRRM2, Regulates Development by Influencing the Transcriptional Machinery. *PLoS Genetics* **9**, e1003543.
- FRASER, A.G., KAMATH, R.S., ZIPPERLEN, P., MARTINEZ-CAMPOS, M., SOHRMANN, M. & AHRINGER, J. (2000) Functional genomic analysis of *C. elegans* chromosome I by systematic RNA interference. *Nature* **408**, 325–330.
- FRIEDLAND, A.E., TZUR, Y.B., ESVELT, K.M., COLAIÁCOVO, M.P., CHURCH, G.M. & CALARCO, J.A. (2013) Heritable genome editing in *C. elegans* via a CRISPR-Cas9 system. *Nature Methods* **10**, 741–743.
- FUSTER-GARCÍA, C., GARCÍA-BOHÓRQUEZ, B., RODRÍGUEZ-MUÑOZ, A., MILLÁN, J.M. & GARCÍA-GARCÍA, G. (2020) Application of CRISPR Tools for Variant Interpretation and Disease Modeling in Inherited Retinal Dystrophies. *Genes* **11**, 473.
- GAMMON, D.B. (2017) *Caenorhabditis elegans* as an Emerging Model for Virus-Host Interactions. *Journal of Virology* **91**, e00509-17.
- GAMUNDI, M.J., HERNAN, I., MUNTANYOLA, M., MASERAS, M., LÓPEZ-ROMERO, P., ÁLVAREZ, R., DOPAZO, A., BORREGO, S. & CARBALLO, M. (2008) Transcriptional expression of *cis*-acting and *trans*-acting splicing mutations cause autosomal dominant retinitis pigmentosa. *Human Mutation* **29**, 869–878.
- GAO, F.J., LI, J.K., CHEN, H., HU, F.Y., ZHANG, S.H., QI, Y.H., XU, P., WANG, D.D., WANG, L.S., CHANG, Q., ZHANG, Y.J., LIU, W., LI, W., WANG, M., CHEN, F., ET AL. (2019) Genetic and Clinical Findings in a Large Cohort of Chinese Patients with Suspected Retinitis Pigmentosa. *Ophthalmology* **126**, 1549–1556.
- GARCÍA-RODRÍGUEZ, F.J., MARTÍNEZ-FERNÁNDEZ, C., BRENA, D., KUKHTAR, D., SERRAT, X., NADAL, E., BOXEM, M., HONNEN, S., MIRANDA-VIZUETE, A., VILLANUEVA, A. & CERÓN, J. (2018) Genetic and cellular sensitivity of *Caenorhabditis elegans* to the chemotherapeutic agent cisplatin. *Disease models & mechanisms* **11**, dmm033506.
- GARTNER, A., BOAG, P.R. & BLACKWELL, T.K. (2008) Germline survival and apoptosis. *WormBook: the online review of C. elegans biology*. .
- GASIUNAS, G., BARRANGOU, R., HORVATH, P. & SIKSNYS, V. (2012) Cas9-crRNA ribonucleoprotein complex mediates specific DNA cleavage for adaptive immunity in bacteria. *Proceedings of the National Academy of Sciences of the United States of America* **109**, E2579–E2586.
- GEMAYEL, M.C., BHATWADEKAR, A.D. & CIULLA, T. (2020) RNA therapeutics for retinal diseases. *Expert Opinion on Biological Therapy*, 1–11.

- GERTH-KAHLERT, C., KOLLER, S., HANSON, J.V.M., BAEHR, L., TIWARI, A., KIVRAK-PFIFNER, F., BAHR, A. & BERGER, W. (2019) Genotype–Phenotype Analysis of a Novel Recessive and a Recurrent Dominant *SNRNP200* Variant Causing Retinitis Pigmentosa. *Investigative Ophthalmology & Visual Science* **60**, 2822.
- GIRARD, C., WILL, C.L., PENG, J., MAKAROV, E.M., KASTNER, B., LEMM, I., URLAUB, H., HARTMUTH, K. & LUHRMANN, R. (2012) Post-transcriptional spliceosomes are retained in nuclear speckles until splicing completion. *Nature Communications* **3**, 1–12.
- GÓMEZ-GONZÁLEZ, B. & AGUILERA, A. (2007) Activation-induced cytidine deaminase action is strongly stimulated by mutations of the THO complex. *Proceedings of the National Academy of Sciences of the United States of America* **104**, 8409–8414.
- GRAZIOTTO, J.J., FARKAS, M.H., BUJAKOWSKA, K., DERAMAUDT, B.M., ZHANG, Q., NANDROT, E.F., INGLEHEARN, C.F., BHATTACHARYA, S.S. & PIERCE, E.A. (2011) Three gene-targeted mouse models of RNA splicing factor RP show late-onset RPE and retinal degeneration. *Investigative Ophthalmology and Visual Science* **52**, 190–198.
- GRAZIOTTO, J.J., INGLEHEARN, C.F., PACK, M.A. & PIERCE, E.A. (2008) Decreased levels of the RNA splicing factor Prpf3 in mice and zebrafish do not cause photoreceptor degeneration. *Investigative Ophthalmology and Visual Science* **49**, 3830–3838.
- GRISHOK, A. (2005) RNAi mechanisms in *Caenorhabditis elegans*. *FEBS letters* **579**, 5932–5939.
- GRÜN, D., KIRCHNER, M., THIERFELDER, N., STOECKIUS, M., SELBACH, M. & RAJEWSKY, N. (2014) Conservation of mRNA and protein expression during development of *C. elegans*. *Cell Reports* **6**, 565–577.
- HÄCKER, I., SANDER, B., GOLAS, M.M., WOLF, E., KARAGÖZ, E., KASTNER, B., STARK, H., FABRIZIO, P. & LÜHRMANN, R. (2008) Localization of Prp8, Brp2, Snu14 and U4/U6 proteins in the yeast tri-snRNP by electron microscopy. *Nature Structural and Molecular Biology* **15**, 1206–1212.
- HANNON, G.J., MARONEY, P.A. & NILSEN, T.W. (1991) U Small Nuclear Ribonucleoprotein Requirements for Nematode cis- and trans-Splicing in Vitro*. *J Biol Chem* **266**, 22792–22695.
- HARING, S.J., MASON, A.C., BINZ, S.K. & WOLD, M.S. (2008) Cellular functions of human RPA1: Multiple roles of domains in replication, repair, and checkpoints. *Journal of Biological Chemistry* **283**, 19095–19111.
- HARNISH, J.M., DEAL, S.L., CHAO, H.-T., WANGLER, M.F. & YAMAMOTO, S. (2019) In Vivo Functional Study of Disease-associated Rare Human Variants Using *Drosophila*. *Journal of Visualized Experiments* **2019**.
- HARRIS, T.W., ARNABOLDI, V., CAIN, S., CHAN, J., CHEN, W.J., CHO, J., DAVIS, P., GAO, S., GROVE, C.A., KISHORE, R., LEE, R.Y.N., MULLER, H.-M., NAKAMURA, C., NUIN, P., PAULINI, M., ET AL. (2019) WormBase: a modern Model Organism Information Resource. *Nucleic Acids Research* **48**, D762–D767.
- HARTONG, D.T., BERSON, E.L. & DRYJA, T.P. (2006) Retinitis pigmentosa. *Lancet (London, England)* **368**, 1795–1809.
- HASEGAWA, M., MIURA, T., KUZUYA, K., INOUE, A., KI, S.W., HORINOUCHE, S., YOSHIDA, T., KUNOH, T., KOSEKI, K., MINO, K., SASAKI, R., YOSHIDA, M. & MIZUKAMI, T. (2011) Identification of SAP155 as the target of GEX1A (Herboxidiene), an antitumor natural product. *ACS Chemical Biology* **6**, 229–233.
- HEFEL, A., HONDA, M., CRONIN, N., HARRELL, K., PATEL, P., SPIES, M. & SMOLIKOVE, S. (2021) RPA complexes in *Caenorhabditis elegans* meiosis; unique roles in replication, meiotic recombination and apoptosis. *Nucleic acids research* **49**, 2005–2026.
- HOHMAN, T.C. (2017) Hereditary retinal dystrophy. In *Handbook of Experimental Pharmacology* pp. 337–367.

- HOLAN, V., PALACKA, K. & HERMANKOVA, B. (2021) Mesenchymal Stem Cell-Based Therapy for Retinal Degenerative Diseases: Experimental Models and Clinical Trials. *Cells* **10**, 588.
- HOLLINS, C., ZORIO, D.A.R., MACMORRIS, M. & BLUMENTHAL, T. (2005) U2AF binding selects for the high conservation of the *C. elegans* 3' splice site. *RNA* **11**, 248–253.
- HOPKINS, C. (2021) Whole Gene Humanization for Personalized Medicine Applications - InVivo Biosystems.
- HOUTHOOFD, K., BRAECKMAN, B.P., LENAERTS, I., BRYNS, K., DE VREESE, A., VAN EYGEN, S. & VANFLETEREN, J.R. (2002) Ageing is reversed, and metabolism is reset to young levels in recovering dauer larvae of *C. elegans*. *Experimental Gerontology* **37**, 1015–1021.
- HSU, P.D., SCOTT, D.A., WEINSTEIN, J.A., RAN, F.A., KONERMANN, S., AGARWALA, V., LI, Y., FINE, E.J., WU, X., SHALEM, O., CRADICK, T.J., MARRAFFINI, L.A., BAO, G. & ZHANG, F. (2013) DNA targeting specificity of RNA-guided Cas9 nucleases. *Nature Biotechnology* **31**, 827–832.
- HUANG, L., ZHANG, Q., HUANG, X., QU, C., MA, S., MAO, Y., YANG, J., LI, Y., LI, Y., TAN, C., ZHAO, P. & YANG, Z. (2017) Mutation screening in genes known to be responsible for Retinitis Pigmentosa in 98 Small Han Chinese Families. *Scientific Reports* **7**, 1–10.
- HUANG, X.F., HUANG, F., WU, K.C., WU, J., CHEN, J., PANG, C.P., LU, F., QU, J. & JIN, Z.B. (2015) Genotype-phenotype correlation and mutation spectrum in a large cohort of patients with inherited retinal dystrophy revealed by next-generation sequencing. *Genetics in Medicine* **17**, 271–278.
- HUNT, S.E., MCLAREN, W., GIL, L., THORMANN, A., SCHULENBURG, H., SHEPPARD, D., PARTON, A., ARMEAN, I.M., TREVANION, S.J., FLICEK, P. & CUNNINGHAM, F. (2018) Ensembl variation resources. *Database* **2018**.
- IKENAKA, K., TSUKADA, Y., GILES, A.C., ARAI, T., NAKADERA, Y., NAKANO, S., KAWAI, K., MOCHIZUKI, H., KATSUNO, M., SOBUE, G. & MORI, I. (2019) A behavior-based drug screening system using a *Caenorhabditis elegans* model of motor neuron disease. *Scientific Reports* **9**, 10104.
- IRIMIA, M. & ROY, S.W. (2014) Origin of Spliceosomal Introns and Alternative Splicing. *Cold Spring Harbor Perspectives in Biology* **6**, a016071–a016071.
- JAIN, B.P. & PANDEY, S. (2018) WD40 Repeat Proteins: Signalling Scaffold with Diverse Functions. *The Protein Journal* **37**, 391–406.
- JAISWAL, A.S., WILLIAMSON, E.A., SRINIVASAN, G., KONG, K., LOMELINO, C.L., MCKENNA, R., WALTER, C., SUNG, P., NARAYAN, S. & HROMAS, R. (2020) The splicing component ISY1 regulates APE1 in base excision repair. *DNA Repair* **86**, 102769.
- JANGI, M., FLEET, C., CULLEN, P., GUPTA, S. V., MEKHOUBAD, S., CHIAO, E., ALLAIRE, N., BENNETT, C.F., RIGO, F., KRAINER, A.R., HURT, J.A., CARULLI, J.P. & STAROPOLI, J.F. (2017) SMN deficiency in severe models of spinal muscular atrophy causes widespread intron retention and DNA damage. *Proceedings of the National Academy of Sciences of the United States of America* **114**, E2347–E2356.
- JESPERGAARD, C., FANG, M., BERTELSEN, M., DANG, X., JENSEN, H., CHEN, Y., BECH, N., DAI, L., ROSENBERG, T., ZHANG, J., MØLLER, L.B., TÜMER, Z., BRØNDUM-NIELSEN, K. & GRØNSKOV, K. (2019) Molecular genetic analysis using targeted NGS analysis of 677 individuals with retinal dystrophy. *Scientific Reports* **9**, 1–7.
- JIMÉNEZ, M., JIMÉNEZ, J., URTASUN, R., ELIZALDE, M., AZKONA, M., UJUE LATASA, M., URIARTE, I., ARECHEDERRA, M., ALIGNANI, D., BÁRCENA-VARELA, M., ALVAREZ-SOLA, G., COLYN, L., SANTAMARÍA, E., SANGRO, B., RODRIGUEZ-ORTIGOSA, C., ET AL. (2019) Splicing events in the control of genome integrity: role of SLU7 and truncated SRSF3 proteins. *Nucleic Acids Research* **47**, 3450–3466.

- JINEK, M., CHYLINSKI, K., FONFARA, I., HAUER, M., DOUDNA, J.A. & CHARPENTIER, E. (2012) A programmable dual-RNA-guided DNA endonuclease in adaptive bacterial immunity. *Science* **337**, 816–821.
- JONES, K.D., WHEATON, D.K., BOWNE, S.J., SULLIVAN, L.S., BIRCH, D.G., CHEN, R. & DAIGER, S.P. (2017) Next-generation sequencing to solve complex inherited retinal dystrophy: A case series of multiple genes contributing to disease in extended families. *Molecular Vision* **23**, 470–481.
- KACHROO, A.H., LAURENT, J.M., YELLMAN, C.M., MEYER, A.G., WILKE, C.O. & MARCOTTE, E.M. (2015) Systematic humanization of yeast genes reveals conserved functions and genetic modularity. *Science* **348**, 921–925.
- KALETTA, T. & HENGARTNER, M.O. (2006) Finding function in novel targets: *C. elegans* as a model organism. *Nature Reviews Drug Discovery* **5**, 387–399.
- KAMATH, R.S. & AHRINGER, J. (2003) Genome-wide RNAi screening in *Caenorhabditis elegans*. *Methods (San Diego, Calif.)* **30**, 313–321.
- KAMATH, R.S., FRASER, A.G., DONG, Y., POULIN, G., DURBIN, R., GOTTA, M., KANAPIN, A., LE BOT, N., MORENO, S., SOHRMANN, M., WELCHMAN, D.P., ZIPPERLEN, P., AHRINGER, J., ZIPPERIEN, P. & AHRINGER, J. (2003) Systematic functional analysis of the *Caenorhabditis elegans* genome using RNAi. *Nature* **421**, 231–237.
- KAMATH, R.S., MARTINEZ-CAMPOS, M., ZIPPERLEN, P., FRASER, A.G. & AHRINGER, J. (2001) Effectiveness of specific RNA-mediated interference through ingested double-stranded RNA in *Caenorhabditis elegans*. *Genome biology* **2**, RESEARCH0002.1.
- KARCZEWSKI, K.J., FRANCIOLI, L.C., TIAO, G., CUMMINGS, B.B., ALFÖLDI, J., WANG, Q., COLLINS, R.L., LARICCHIA, K.M., GANNA, A., BIRNBAUM, D.P., GAUTHIER, L.D., BRAND, H., SOLOMONSON, M., WATTS, N.A., RHODES, D., ET AL. (2020) The mutational constraint spectrum quantified from variation in 141,456 humans. *Nature* **581**, 434–443.
- KASTNER, B., WILL, C.L., STARK, H. & LÜHRMANN, R. (2019) Structural Insights into Nuclear pre-mRNA Splicing in Higher Eukaryotes. *Cold Spring Harbor Perspectives in Biology* **11**, a032417.
- KENT, W.J. & ZAHLER, A.M. (2000) Conservation, regulation, synteny, and introns in a large-scale *C. briggsae-C. elegans* genomic alignment. *Genome Research* **10**, 1115–1125.
- KERINS, J.A., HANAZAWA, M., DORSETT, M. & SCHEDL, T. (2010) PRP-17 and the pre-mRNA splicing pathway are preferentially required for the proliferation versus meiotic development decision and germline sex determination in *Caenorhabditis elegans*. *Developmental dynamics: an official publication of the American Association of Anatomists* **239**, 1555–1572.
- KIM, C., JOONG KIM, K., BOK, J., LEE, E.-J.J., KIM, D.-J.J., HEE OH, J., PYO PARK, S., YOUNG SHIN, J., LEE, J.-Y.Y., GON YU, H., KIM, K.J., BOK, J., LEE, E.-J.J., KIM, D.-J.J., OH, J.H., ET AL. (2012) Microarray-based mutation detection and phenotypic characterization in Korean patients with retinitis pigmentosa. In *Molecular Vision* pp. 2398–2410.
- KIM, H., ISHIDATE, T., GHANTA, K.S., SETH, M., CONTE, D., SHIRAYAMA, M. & MELLO, C.C. (2014) A Co-CRISPR Strategy for Efficient Genome Editing in *Caenorhabditis elegans*. *Genetics* **197**, 1069–1080.
- KIMBLE, J. & HIRSH, D. (1979) The postembryonic cell lineages of the hermaphrodite and male gonads in *Caenorhabditis elegans*. *Developmental Biology* **70**, 396–417.
- KISER, K., WEBB-JONES, K.D., BOWNE, S.J., SULLIVAN, L.S., DAIGER, S.P. & BIRCH, D.G. (2019) Time Course of Disease Progression of *PRPF31*-mediated Retinitis Pigmentosa. *American Journal of Ophthalmology* **200**, 76–84.
- KOGA, M., HAYASHI, M. & KAIDA, D. (2015) Splicing inhibition decreases phosphorylation level of Ser2 in Pol II CTD. *Nucleic Acids Research* **43**, 8258–8267.

- KORIR, P.K., ROBERTS, L., RAMESAR, R. & SEOIGHE, C. (2014) A mutation in a splicing factor that causes retinitis pigmentosa has a transcriptome-wide effect on mRNA splicing. *BMC Research Notes* **7**, 401.
- KOYANAGI, Y., AKIYAMA, M., NISHIGUCHI, K.M., MOMOZAWA, Y., KAMATANI, Y., TAKATA, S., INAI, C., IWASAKI, Y., KUMANO, M., MURAKAMI, Y., OMODAKA, K., ABE, T., KOMORI, S., GAO, D., HIRAKATA, T., ET AL. (2019) Genetic characteristics of retinitis pigmentosa in 1204 Japanese patients. *Journal of Medical Genetics* **56**, 662–670.
- KRAFT, F. & KURTH, I. (2020) Long-read sequencing to understand genome biology and cell function. *International Journal of Biochemistry and Cell Biology* **126**, 105799.
- KUKHTAR, D., RUBIO-PEÑA, K., SERRAT, X. & CERÓN, J. (2020) Mimicking of splicing-related retinitis pigmentosa mutations in *C. elegans* allow drug screens and identification of disease modifiers. *Human Molecular Genetics* **29**, 756–765.
- KURTOVIC-KOZARIC, A., PRZYCHODZEN, B., SINGH, J., KONARSKA, M.M., CLEMENTE, M.J., OTROCK, Z.K., NAKASHIMA, M., HSI, E.D., YOSHIDA, K., SHIRAISHI, Y., CHIBA, K., TANAKA, H., MIYANO, S., OGAWA, S., BOULTWOOD, J., ET AL. (2015) PRPF8 defects cause missplicing in myeloid malignancies. *Leukemia* **29**, 126–136.
- KWOK, T.C.Y., RICKER, N., FRASER, R., CHAN, A.W., BURNS, A., STANLEY, E.F., MCCOURT, P., CUTLER, S.R. & ROY, P.J. (2006) A small-molecule screen in *C. elegans* yields a new calcium channel antagonist. *Nature* **441**, 91–95.
- DE LA MATA, M., ALONSO, C.R., KADENER, S., FEDEDA, J.P., BLAUSTEIN, M., PELISCH, F., CRAMER, P., BENTLEY, D. & KORNBLIHT, A.R. (2003) A slow RNA polymerase II affects alternative splicing in vivo. *Molecular Cell* **12**, 525–532.
- DE LA MATA, M. & KORNBLIHT, A.R. (2006) RNA polymerase II C-terminal domain mediates regulation of alternative splicing by SRp20. *Nature Structural and Molecular Biology* **13**, 973–980.
- LANDER, E.S. (2016) The Heroes of CRISPR. *Cell* **164**, 18–28.
- LANDER, E.S., LINTON, L.M., BIRREN, B., NUSBAUM, C., ZODY, M.C., BALDWIN, J., DEVON, K., DEWAR, K., DOYLE, M., FITZHUGH, W., FUNKE, R., GAGE, D., HARRIS, K., HEAFORD, A., HOWLAND, J., ET AL. (2001) Initial sequencing and analysis of the human genome. *Nature* **409**, 860–921.
- LATIF, Z., CHAKCHOUK, I., SCHRAUWEN, I., LEE, K., SANTOS-CORTEZ, R.L.P., ABBE, I., ACHARYA, A., JARRAL, A., ALI, I., ULLAH, E., KHAN, M.N., ALI, G., TAHIR, T.H., BAMSHAD, M.J., NICKERSON, D.A., ET AL. (2018) Confirmation of the Role of DHX38 in the Etiology of Early-Onset Retinitis Pigmentosa. *Investigative Ophthalmology & Visual Science* **59**, 4552.
- LEE, Y. & RIO, D.C. (2015) Mechanisms and Regulation of Alternative Pre-mRNA Splicing. *Annual Review of Biochemistry* **84**, 291–323.
- LEV-MAOR, G., GOREN, A., SELA, N., KIM, E., KEREN, H., DORON-FAIGENBOIM, A., LEIBMAN-BARAK, S., PUPKO, T. & AST, G. (2007) The ‘alternative’ choice of constitutive exons throughout evolution. *PLoS Genetics* **3**, 2221–2234.
- LI, D.K., TISDALE, S., LOTTI, F. & PELLIZZONI, L. (2014) SMN control of RNP assembly: From post-transcriptional gene regulation to motor neuron disease. *Seminars in Cell & Developmental Biology* **32**, 22–29.
- LI, H. (2018) Minimap2: pairwise alignment for nucleotide sequences. *Bioinformatics* **34**, 3094–3100.
- LI, H., HANDSAKER, B., WYSOKER, A., FENNEL, T., RUAN, J., HOMER, N., MARTH, G., ABECASIS, G. & DURBIN, R. (2009) The Sequence Alignment/Map format and SAMtools. *Bioinformatics* **25**, 2078–2079.

- LI, N., MEI, H., MACDONALD, I.M., JIAO, X.D. & FIELDING HEJTMANCIK, J. (2010) Mutations in *ASCC3L1* on 2q11.2 are associated with autosomal dominant retinitis pigmentosa in a chinese family. *Investigative Ophthalmology and Visual Science* **51**, 1036–1043.
- LI, R., REN, X., DING, Q., BI, Y., XIE, D. & ZHAO, Z. (2020) Direct full-length RNA sequencing reveals unexpected transcriptome complexity during *Caenorhabditis elegans* development. *Genome Research* **30**, 287–298.
- LI, X. & MANLEY, J.L. (2005) Inactivation of the SR protein splicing factor ASF/SF2 results in genomic instability. *Cell* **122**, 365–378.
- LI, Y.I., SANCHEZ-PULIDO, L., HAERTY, W. & PONTING, C.P. (2015) RBFOX and PTBPI proteins regulate the alternative splicing of micro-exons in human brain transcripts. *Genome Research* **25**, 1–13.
- LIN, S.-L., MILLER, J.D. & YING, S.-Y. (2006) Intronic microRNA (miRNA). *Journal of biomedicine & biotechnology* **2006**, 26818.
- LINDER, B., HIRMER, A., GAL, A., RÜTHER, K., BOLZ, H.J., WINKLER, C., LAGGERBAUER, B. & FISCHER, U. (2014) Identification of a *PRPF4* loss-of-function variant that abrogates U4/U6.U5 Tri-snRNP integration and is associated with retinitis pigmentosa. *PLoS ONE* **9**, e111754.
- LIU, S., MOZAFFARI-JOVIN, S., WOLLENHAUPT, J., SANTOS, K.F., THEUSER, M., DUNIN-HORKAWICZ, S., FABRIZIO, P., BUJNICKI, J.M., LÜHRMANN, R. & WAHL, M.C. (2015) A composite double-/single-stranded RNA-binding region in protein Prp3 supports tri-snRNP stability and splicing. *eLife* **4**, e07320.
- LIU, T., JIN, X., ZHANG, X., YUAN, H., CHENG, J., LEE, J., ZHANG, B., ZHANG, M., WU, J., WANG, L., TIAN, G. & WANG, W. (2012) A Novel Missense *SNRNP200* Mutation Associated with Autosomal Dominant Retinitis Pigmentosa in a Chinese Family. *PLoS ONE* **7**, e45464.
- LUNGI, C., GALLI-RESTA, L., BINDA, P., CICCINI, G.M., PLACIDI, G., FALSINI, B. & MORRONE, M.C. (2019) Visual Cortical Plasticity in Retinitis Pigmentosa. *Investigative Ophthalmology & Visual Science* **60**, 2753.
- LUYTEN, W., ANTAL, P., BRAECKMAN, B.P., BUNDY, J., CIRULLI, F., FANG-YEN, C., FUELLEN, G., LEROI, A., LIU, Q., MARTORELL, P., METSPALU, A., PEROLA, M., RISTOW, M., SAUL, N., SCHOofs, L., ET AL. (2016) Ageing with elegans: a research proposal to map healthspan pathways. *Biogerontology* **17**, 771–782.
- MAEDER, C., KUTACH, A.K. & GUTHRIE, C. (2009) ATP-dependent unwinding of U4/U6 snRNAs by the Brr2 helicase requires the C terminus of Prp8. *Nature Structural and Molecular Biology* **16**, 42–48.
- MALINOVÁ, A., CVAČKOVÁ, Z., MATĚJŮ, D., HOŘEJŠÍ, Z., ABÉZA, C., VANDERMOERE, F., BERTRAND, E., STANĚK, D. & VERHEGGEN, C. (2017) Assembly of the U5 snRNP component PRPF8 is controlled by the HSP90/R2TP chaperones. *The Journal of Cell Biology* **216**, 1579–1596.
- MARTIN-MERIDA, I., AGUILERA-GARCIA, D., JOSE, P.F.-S., BLANCO-KELLY, F., ZURITA, O., ALMOGUERA, B., GARCIA-SANDOVAL, B., AVILA-FERNANDEZ, A., ARTECHE, A., MINGUEZ, P., CARBALLO, M., CORTON, M., AYUSO, C., FERNANDEZ-SAN JOSE, P., BLANCO-KELLY, F., ET AL. (2018) Toward the mutational landscape of autosomal dominant retinitis pigmentosa: A comprehensive analysis of 258 Spanish families. *Investigative Ophthalmology & Visual Science* **59**, 2345–2354.
- MARTIN-MERIDA, I., SANCHEZ-ALCUDIA, R., JOSE, P.F.S., BLANCO-KELLY, F., PEREZ-CARRO, R., DA SILVA, L.R.J., ALMOGUERA, B., GARCIA-SANDOVAL, B., LOPEZ-MOLINA, M.I., AVILA-FERNANDEZ, A., CARBALLO, M., CORTON, M. & AYUSO, C. (2017) Analysis of the *PRPF31* gene in spanish autosomal dominant retinitis pigmentosa patients: A novel genomic rearrangement. *Investigative Ophthalmology and Visual Science* **58**, 1045–1053.

- MARTÍNEZ-GIMENO, M., GAMUNDI, M.J., HERNAN, I., MASERAS, M., MILLÁ, E., AYUSO, C., GARCÍA-SANDOVAL, B., BENEYTO, M., VILELA, C., BAIGET, M., ANTIÑOLO, G. & CARBALLO, M. (2003) Mutations in the pre-mRNA splicing-factor genes *PRPF3*, *PRPF8*, and *PRPF31* in Spanish families with autosomal dominant retinitis pigmentosa. *Investigative ophthalmology & visual science* **44**, 2171–2177.
- MATSOUKAS, I.G. (2018) Commentary: RNA editing with CRISPR-Cas13. *Frontiers in Genetics* **9**, 1019–1027.
- MATSUNAMI, K. (2018) Frailty and *Caenorhabditis elegans* as a Benchtop Animal Model for Screening Drugs Including Natural Herbs. *Frontiers in Nutrition* **5**, 111.
- MAUBARET, C.G., VACLAVIK, V., MUKHOPADHYAY, R., WASEEM, N.H., CHURCHILL, A., HOLDER, G.E., MOORE, A.T., BHATTACHARYA, S.S. & WEBSTER, A.R. (2011) Autosomal dominant retinitis pigmentosa with intrafamilial variability and incomplete penetrance in two families carrying mutations in *prpf8*. *Investigative Ophthalmology and Visual Science* **52**, 9304–9309.
- MAYERLE, M. & GUTHRIE, C. (2016) Prp8 retinitis pigmentosa mutants cause defects in the transition between the catalytic steps of splicing. *RNA (New York, N.Y.)* **22**, 793–809.
- MCDIARMID, T.A., AU, V., LOEWEN, A.D., LIANG, J., MIZUMOTO, K., MOERMAN, D.G. & RANKIN, C.H. (2018) CRISPR-Cas9 human gene replacement and phenomic characterization in *Caenorhabditis elegans* to understand the functional conservation of human genes and decipher variants of uncertain significance. *Disease Models & Mechanisms* **11**.
- MCKIE, A.B., MCHALE, J.C., KEEN, T.J., TARTTELIN, E.E., GOLIATH, R., VAN LITH-VERHOEVEN, J.J.C., GREENBERG, J., RAMESAR, R.S., HOYNG, C.B., CREMERS, F.P.M., MACKAY, D.A., BHATTACHARYA, S.S., BIRD, A.C., MARKHAM, A.F. & INGLEHEARN, C.F. (2001) Mutations in the pre-mRNA splicing factor gene *PRPC8* in autosomal dominant retinitis pigmentosa (RP13). *Human Molecular Genetics* **10**, 1555–1562.
- MENDLING, W., WEISSENBACHER, E.R., GERBER, S., PRASAUSKAS, V. & GROB, P. (2016) Use of locally delivered dequalinium chloride in the treatment of vaginal infections: a review. *Archives of Gynecology and Obstetrics* **293**, 469–484.
- MEYLEMANS, A. & DE BLEECKER, J. (2019) Current evidence for treatment with nusinersen for spinal muscular atrophy: a systematic review. *Acta Neurologica Belgica* **119**, 523–533.
- MILLER, D.E., SULOVARI, A., WANG, T., LOUCKS, H., HOEKZEMA, K., MUNSON, K.M., LEWIS, A.P., ALMANZA FUERTE, E.P., PASCHAL, C.R., THIES, J., BENNETT, J.T., GLASS, I., DIPPLE, K.M., PATTERSON, K., BONKOWSKI, E.S., ET AL. (2020) Targeted long-read sequencing resolves complex structural variants and identifies missing disease-causing variants. *bioRxiv*.
- MIN, K. & LEE, J. (2007) RNA interference in *C. elegans*: History, application, and perspectives. *Integrative Biosciences* **11**, 99–104.
- MOJICA, F.J.M., DÍEZ-VILLASEÑOR, C., GARCÍA-MARTÍNEZ, J. & SORIA, E. (2005) Intervening sequences of regularly spaced prokaryotic repeats derive from foreign genetic elements. *Journal of Molecular Evolution* **60**, 174–182.
- MONTANARO, N., NOVELLO, F. & STIRPE, F. (1971) Effect of alpha-amanitin on ribonucleic acid polymerase II of rat brain nuclei and on retention of avoidance conditioning. *The Biochemical journal* **125**, 1087–1090.
- MONTES, M., SANFORD, B.L., COMISKEY, D.F. & CHANDLER, D.S. (2019) RNA Splicing and Disease: Animal Models to Therapies. *Trends in Genetics* **35**, 68–87.
- MORDES, D., LUO, X., KAR, A., KUO, D., XU, L., FUSHIMI, K., YU, G., STERNBERG, P. & WU, J.Y. (2006) Pre-mRNA splicing and retinitis pigmentosa. *Molecular vision* **12**, 1259–1271.
- MORI, C., TAKANAMI, T. & HIGASHITANI, A. (2008) Maintenance of Mitochondrial DNA by the *Caenorhabditis elegans* ATR Checkpoint Protein ATL-1. *Genetics* **180**, 681–686.

- MORRIS, J.R. & SOLOMON, E. (2004) BRCA1: BARD1 induces the formation of conjugated ubiquitin structures, dependent on K6 of ubiquitin, in cells during DNA replication and repair. *Human Molecular Genetics* **13**, 807–817.
- MOTORIN, Y. & MARCHAND, V. (2021) Analysis of RNA Modifications by Second- and Third-Generation Deep Sequencing: 2020 Update. *Genes* **12**, 278.
- MOY, T.I., BALL, A.R., ANKLESARIA, Z., CASADEI, G., LEWIS, K. & AUSUBEL, F.M. (2006) Identification of novel antimicrobials using a live-animal infection model. *Proceedings of the National Academy of Sciences of the United States of America* **103**, 10414–10419.
- MOZAFFARI-JOVIN, S., WANDERSLEBEN, T., SANTOS, K.F., WILL, C.L., LUHRMANN, R. & WAHL, M.C. (2013) Inhibition of RNA helicase Brr2 by the C-terminal tail of the spliceosomal protein Prp8. *Science* **341**, 80–84.
- MYERS, M.H., IANNACONE, A. & BIDELMAN, G.M. (2017) A pilot investigation of audiovisual processing and multisensory integration in patients with inherited retinal dystrophies. *BMC ophthalmology* **17**, 240.
- NAZLAMOVA, L., THOMAS, N.S., CHEUNG, M.-K., LEGBEKE, J., LORD, J., PENGELLY, R.J., TAPPER, W.J. & WHEWAY, G. (2021) A CRISPR and high-content imaging assay compliant with ACMG/AMP guidelines for clinical variant interpretation in ciliopathies. *Human Genetics* **140**, 593–607.
- O'REILLY, L.P., LUKE, C.J., PERLMUTTER, D.H., SILVERMAN, G.A. & PAK, S.C. (2014) *C. elegans* in high-throughput drug discovery. *Advanced Drug Delivery Reviews* **69–70**, 247–253.
- OISHI, M., OISHI, A., GOTOH, N., OGINO, K., HIGASA, K., IIDA, K., MAKIYAMA, Y., MOROOKA, S., MATSUDA, F. & YOSHIMURA, N. (2014) Comprehensive molecular diagnosis of a large cohort of Japanese retinitis pigmentosa and usher syndrome patients by next-generation sequencing. *Investigative Ophthalmology and Visual Science* **55**, 7369–7375.
- OSTAD-AHMADI, Z., MODABBERI, M.-R. & MOSTAFAIE, A. (2021) Safety, effectiveness, and cost-effectiveness of Argus II in patients with retinitis pigmentosa: a systematic review. *International Journal of Ophthalmology* **14**, 310–316.
- PACHECO, S., MALDONADO-LINARES, A., MARCET-ORTEGA, M., ROJAS, C., MARTÍNEZ-MARCHAL, A., FUENTES-LAZARO, J., LANGE, J., JASIN, M., KEENEY, S., FERNÁNDEZ-CAPETILLO, O., GARCIA-CALDÉS, M. & ROIG, I. (2018) ATR is required to complete meiotic recombination in mice. *Nature Communications* **9**, 1–14.
- PAIX, A., FOLKMANN, A., RASOLOSON, D. & SEYDOUX, G. (2015) High Efficiency, Homology-Directed Genome Editing in *Caenorhabditis elegans* Using CRISPR-Cas9 Ribonucleoprotein Complexes. *Genetics* **201**, 47–54.
- PAIX, A., FOLKMANN, A. & SEYDOUX, G. (2017) Precision genome editing using CRISPR-Cas9 and linear repair templates in *C. elegans*. *Methods* **121–122**, 86–93.
- PAJUELO, L., CALVIÑO, E., DIEZ, J.C., BOYANO-ADÁNEZ, M. DEL C., GIL, J. & SANCHO, P. (2011) Dequalinium induces apoptosis in peripheral blood mononuclear cells isolated from human chronic lymphocytic leukemia. *Investigational New Drugs* **29**, 1156–1163.
- PAN, Q., SHAI, O., LEE, L.J., FREY, B.J. & BLENCOWE, B.J. (2008) Deep surveying of alternative splicing complexity in the human transcriptome by high-throughput sequencing. *Nature Genetics* **40**, 1413–1415.
- PAN, X., CHEN, X., LIU, X., GAO, X., KANG, X., XU, Q., CHEN, X., ZHAO, K., ZHANG, X., CHU, Q., WANG, X. & ZHAO, C. (2014) Mutation analysis of pre-mRNA splicing genes in Chinese families with retinitis pigmentosa. *Molecular vision* **20**, 770–779.
- PARMEGGIANI, F., S. SORRENTINO, F., PONZIN, D., BARBARO, V., FERRARI, S., DI IORIO, E., BARBARO, V., PONZIN, D., SORRENTINO, F.S. & PARMEGGIANI, F. (2011) Retinitis pigmentosa: genes and disease mechanisms. *Current Genomics* **12**, 238–249.

- PARTRIDGE, F.A., BROWN, A.E., BUCKINGHAM, S.D., WILLIS, N.J., WYNNE, G.M., FORMAN, R., ELSE, K.J., MORRISON, A.A., MATTHEWS, J.B., RUSSELL, A.J., LOMAS, D.A. & SATTELLE, D.B. (2018) An automated high-throughput system for phenotypic screening of chemical libraries on *C. elegans* and parasitic nematodes. *International Journal for Parasitology: Drugs and Drug Resistance* **8**, 8–21.
- PAULSEN, R.D., SONI, D. V., WOLLMAN, R., HAHN, A.T., YEE, M.C., GUAN, A., HESLEY, J.A., MILLER, S.C., CROMWELL, E.F., SOLOW-CORDERO, D.E., MEYER, T. & CIMPRICH, K.A. (2009) A Genome-wide siRNA Screen Reveals Diverse Cellular Processes and Pathways that Mediate Genome Stability. *Molecular Cell* **35**, 228–239.
- PEREA-ROMERO, I., GORDO, G., IANCU, I.F., DEL POZO-VALERO, M., ALMOGUERA, B., BLANCO-KELLY, F., CARREÑO, E., JIMENEZ-ROLANDO, B., LOPEZ-RODRIGUEZ, R., LORDA-SANCHEZ, I., MARTIN-MERIDA, I., PÉREZ DE AYALA, L., RIVEIRO-ALVAREZ, R., RODRIGUEZ-PINILLA, E., TAHSIN-SWAFIRI, S., ET AL. (2021) Genetic landscape of 6089 inherited retinal dystrophies affected cases in Spain and their therapeutic and extended epidemiological implications. *Scientific Reports* **11**, 1526.
- PEREZ-GOMEZ, A., CARRETERO, M., WEBER, N., PETERKA, V., TO, A., TITOVA, V., SOLIS, G., OSBORN, O. & PETRASCHECK, M. (2018) A phenotypic *Caenorhabditis elegans* screen identifies a selective suppressor of antipsychotic-induced hyperphagia. *Nature Communications* **9**, 5272.
- PÉREZ-JIMÉNEZ, M.M., MONJE-MORENO, J.M., BROKATE-LLANOS, A.M., VENEGAS-CALERÓN, M., SÁNCHEZ-GARCÍA, A., SANSIGRE, P., VALLADARES, A., ESTEBAN-GARCÍA, S., SUÁREZ-PEREIRA, I., VITORICA, J., RÍOS, J.J., ARTAL-SANZ, M., CARRIÓN, Á.M. & MUÑOZ, M.J. (2021) Steroid hormones sulfatase inactivation extends lifespan and ameliorates age-related diseases. *Nature Communications* **12**, 1–12.
- PLASCHKA, C., NEWMAN, A.J. & NAGAI, K. (2019) Structural Basis of Nuclear pre-mRNA Splicing: Lessons from Yeast. *Cold Spring Harbor Perspectives in Biology* **11**, a032391.
- POLAK, P. & ARNDT, P.F. (2008) Transcription induces strand-specific mutations at the 5' end of human genes. *Genome Research* **18**, 1216–1223.
- PORTA-DE-LA-RIVA, M., FONTRODONA, L., VILLANUEVA, A. & CERÓN, J. (2012) Basic *Caenorhabditis elegans* methods: synchronization and observation. *Journal of visualized experiments : JoVE* **64**, e4019.
- PTASINSKA, A., WHALLEY, C., BOSWORTH, A., POXON, C., BRYER, C., MACHIN, N., GRIPPON, S., WISE, E.L., ARMSON, B., HOWSON, E.L.A., GORING, A., SNELL, G., FORSTER, J., MATTOCKS, C., FRAMPTON, S., ET AL. (2020) Diagnostic accuracy of loop mediated isothermal amplification coupled to nanopore sequencing (LamPORE) for the detection of SARS-CoV-2 infection at scale in symptomatic and asymptomatic populations. *medRxiv*.
- RAMANI, A.K., CALARCO, J.A., PAN, Q., MAVANDADI, S., WANG, Y., NELSON, A.C., LEE, L.J., MORRIS, Q., BLENOWE, B.J., ZHEN, M. & FRASER, A.G. (2011) Genome-wide analysis of alternative splicing in *Caenorhabditis elegans*. *Genome Research* **21**, 342–348.
- REARICK, D., PRAKASH, A., MCSWEENEY, A., SHEPARD, S.S., FEDOROVA, L. & FEDOROV, A. (2011) Critical association of ncRNA with introns. *Nucleic acids research* **39**, 2357–2366.
- RICHARDS, S., AZIZ, N., BALE, S., BICK, D., DAS, S., GASTIER-FOSTER, J., GRODY, W.W., HEGDE, M., LYON, E., SPECTOR, E., VOELKERDING, K. & REHM, H.L. (2015) Standards and guidelines for the interpretation of sequence variants: A joint consensus recommendation of the American College of Medical Genetics and Genomics and the Association for Molecular Pathology. *Genetics in Medicine* **17**, 405–424.
- RIDDLE, D.L., BLUMENTHAL, T., MEYER, B.J. & PRIESS, J.R. (1997a) Cis -Splicing in Worms. In *C. elegans II. 2nd edition*.
- RIDDLE, D.L., BLUMENTHAL, T., MEYER, B.J. & PRIESS, J.R. (1997b) The Biological Model. In *C. elegans II. 2nd edition*.

- RIERA, M., NAVARRO, R., RUIZ-NOGALES, S., MÉNDEZ, P., BURÉS-JELSTRUP, A., CORCÓSTEGUI, B. & POMARES, E. (2017) Whole exome sequencing using Ion Proton system enables reliable genetic diagnosis of inherited retinal dystrophies. *Scientific reports* **7**, 42078.
- RIO FRIO, T., WADE, N.M., RANSIJN, A., BERSON, E.L., BECKMANN, J.S. & RIVOLTA, C. (2008) Premature termination codons in *PRPF31* cause retinitis pigmentosa via haploinsufficiency due to nonsense-mediated mRNA decay. *Journal of Clinical Investigation* **118**, 1519–1531.
- RIVOLTA, C., MCGEE, T.L., FRIO, T.R., JENSEN, R. V., BERSON, E.L. & DRYJA, T.P. (2006) Variation in retinitis pigmentosa-11 (*PRPF31* or RP11) gene expression between symptomatic and asymptomatic patients with dominant RP11 mutations. *Human Mutation* **27**, 644–653.
- ROACH, N.P., SADOWSKI, N., ALESSI, A.F., TIMP, W., TAYLOR, J. & KIM, J.K. (2020) The full-length transcriptome of *C. elegans* using direct RNA sequencing. *Genome Research* **30**, 299–312.
- ROGALSKI, T.M., BULLERJAHN, A.M. & RIDDLE, D.L. (1988) Lethal and amanitin-resistance mutations in the *Caenorhabditis elegans ama-1* and *ama-2* genes. *Genetics* **120**, 409–422.
- RUAL, J.-F., CERON, J., KORETH, J., HAO, T., NICOT, A.-S., HIROZANE-KISHIKAWA, T., VANDENHAUTE, J., ORKIN, S.H., HILL, D.E., VAN DEN HEUVEL, S. & VIDAL, M. (2004) Toward improving *Caenorhabditis elegans* phenome mapping with an ORFeome-based RNAi library. *Genome research* **14**, 2162–2168.
- RUBIO-PEÑA, K. (2017) Modeling splicing-related autosomal dominant retinitis pigmentosa in *Caenorhabditis elegans*. In *Doctoral thesis* p.
- RUBIO-PEÑA, K., FONTRDONA, L., ARISTIZÁBAL-CORRALES, D., TORRES, S., CORNES, E., GARCÍA-RODRÍGUEZ, F.J., SERRAT, X., GONZÁLEZ-KNOWLES, D., FOISSAC, S., PORTA-DE-LA-RIVA, M. & CERÓN, J. (2015) Modeling of autosomal-dominant retinitis pigmentosa in *Caenorhabditis elegans* uncovers a nexus between global impaired functioning of certain splicing factors and cell type-specific apoptosis. *RNA (New York, N.Y.)* **21**, 2119–2131.
- RUSSELL, S., BENNETT, J., WELLMAN, J.A., CHUNG, D.C., YU, Z.F., TILLMAN, A., WITTES, J., PAPPAS, J., ELCI, O., MCCAGUE, S., CROSS, D., MARSHALL, K.A., WALSHIRE, J., KEHOE, T.L., REICHERT, H., ET AL. (2017) Efficacy and safety of voretigene neparvovec (AAV2-hRPE65v2) in patients with RPE65-mediated inherited retinal dystrophy: a randomised, controlled, open-label, phase 3 trial. *The Lancet* **390**, 849–860.
- RŮŽIČKOVÁ, Š. & STANĚK, D. (2017) Mutations in spliceosomal proteins and retina degeneration. *RNA biology* **14**, 544–552.
- SALDI, T., CORTAZAR, M.A., SHERIDAN, R.M. & BENTLEY, D.L. (2016) Coupling of RNA Polymerase II Transcription Elongation with Pre-mRNA Splicing. *Journal of Molecular Biology* **428**, 2623–2635.
- SALMANNEJAD, A., MOTAEE, J., FARJAMI, M., ALIMARDANI, M., ESMAELIE, A. & PASDAR, A. (2019) Next-generation sequencing and its application in diagnosis of retinitis pigmentosa. *Ophthalmic Genetics* **40**, 393–402.
- SANTOS, K.F., JOVIN, S.M., WEBER, G., PENA, V., LUHRMANN, R. & WAHLA, M.C. (2012) Structural basis for functional cooperation between tandem helicase cassettes in Brr2-mediated remodeling of the spliceosome. *Proceedings of the National Academy of Sciences of the United States of America* **109**, 17418–17423.
- SAVAGE, K.I., GORSKI, J.J., BARROS, E.M., IRWIN, G.W., MANTI, L., POWELL, A.J., PELLAGATTI, A., LUKASHCHUK, N., MCCANCE, D.J., MCCLUGGAGE, W.G., SCHETTINO, G., SALTO-TELLEZ, M., BOULTWOOD, J., RICHARD, D.J., MCDADE, S.S., ET AL. (2014) Identification of a *BRCA1*-mRNA Splicing Complex Required for Efficient DNA Repair and Maintenance of Genomic Stability. *Molecular Cell* **54**, 445–459.
- SAVITSKY, M., SOLIS, G.P., KRYUCHKOV, M. & KATANAIEV, V.L. (2020) Humanization of *Drosophila* Gao to Model GNAO1 Paediatric Encephalopathies. *Biomedicines* **8**, 395.

- SCHNEIDER, M., HSIAO, H.H., WILL, C.L., GIET, R., URLAUB, H. & LÜHRMANN, R. (2010) Human PRP4 kinase is required for stable tri-snRNP association during spliceosomal B complex formation. *Nature Structural and Molecular Biology* **17**, 216–221.
- SCHWARTZ, S.H., SILVA, J., BURSTEIN, D., PUPKO, T., EYRAS, E. & AST, G. (2008) Large-scale comparative analysis of splicing signals and their corresponding splicing factors in eukaryotes. *Genome Research* **18**, 88–103.
- SCOTTI, M.M. & SWANSON, M.S. (2016) RNA mis-splicing in disease. *Nature Reviews Genetics* **17**, 19–32.
- SERRAT, X., KUKHTAR, D., CORNES, E., ESTEVE-CODINA, A., BENLLOCH, H., CECERE, G. & CERÓN, J. (2019) CRISPR editing of *sfib-1/SF3B1* in *Caenorhabditis elegans* allows the identification of synthetic interactions with cancer-related mutations and the chemical inhibition of splicing. *PLoS Genetics* **15**, e1008464.
- SHAN, G. & WALTHALL, W.W. (2008) Copulation in *C. elegans* males requires a nuclear hormone receptor. *Developmental Biology* **322**, 11–20.
- SHAYE, D.D. & GREENWALD, I. (2011) OrthoList: A Compendium of *C. elegans* Genes with Human Orthologs. *PLoS ONE* **6**, e20085.
- SHENASA, H. & HERTEL, K.J. (2019) Combinatorial regulation of alternative splicing. *Biochimica et Biophysica Acta - Gene Regulatory Mechanisms* **1862**, 194392.
- SHKRETA, L. & CHABOT, B. (2015) The RNA Splicing Response to DNA Damage. *Biomolecules* **5**, 2935–2977.
- SIBLEY, M.H., JOHNSON, J.J., MELLO, C.C. & KRAMER, J.M. (1993) Genetic identification, sequence, and alternative splicing of the *Caenorhabditis elegans* alpha 2(IV) collagen gene. *Journal of Cell Biology* **123**, 255–264.
- SKOURTI-STATHAKI, K., KAMIENIARZ-GDULA, K. & PROUDFOOT, N.J. (2014) R-loops induce repressive chromatin marks over mammalian gene terminators. *Nature* **516**, 436–439.
- SKOURTI-STATHAKI, K. & PROUDFOOT, N.J. (2014) A double-edged sword: R loops as threats to genome integrity and powerful regulators of gene expression. *Genes & Development* **28**, 1384–1396.
- SPENSLEY, M., DEL BORRELLO, S., PAJKIC, D. & FRASER, A.G. (2018) Acute Effects of Drugs on *Caenorhabditis elegans* Movement Reveal Complex Responses and Plasticity. *G3 Genes/Genomes/Genetics* **8**, 2941–2952.
- SPIETH, J., BROOKE, G., KUERSTEN, S., LEA, K. & BLUMENTHAL, T. (1993) Operons in *C. elegans*: Polycistronic mRNA precursors are processed by trans-splicing of SL2 to downstream coding regions. *Cell* **73**, 521–532.
- STERNE-WEILER, T. & SANFORD, J.R. (2014) Exon identity crisis: Disease-causing mutations that disrupt the splicing code. *Genome Biology* **15**, 201.
- STIERNAGLE, T. (2006) Maintenance of *C. elegans*. In *WormBook* p.
- SUETOMI, K., MEREITER, S., MORI, C., TAKANAMI, T. & HIGASHITANI, A. (2013) *Caenorhabditis elegans* ATR checkpoint kinase ATL-1 influences life span through mitochondrial maintenance. *Mitochondrion* **13**, 729–735.
- SULLIVAN, L.S., BOWNE, S.J., BIRCH, D.G., HUGHBANKS-WHEATON, D., HECKENLIVELY, J.R., LEWIS, R.A., GARCIA, C.A., RUIZ, R.S., BLANTON, S.H., NORTHRUP, H., GIRE, A.I., SEAMAN, R., DUZKALE, H., SPELLICY, C.J., ZHU, J., ET AL. (2006) Prevalence of disease-causing mutations in families with autosomal dominant retinitis pigmentosa: A screen of known genes in 200 families. *Investigative Ophthalmology and Visual Science* **47**, 3052–3064.

- SULLIVAN, L.S., BOWNE, S.J., REEVES, M.J., BLAIN, D., GOETZ, K., DIFOR, V.N., VITEZ, S., WANG, X., TUMMINIA, S.J. & DAIGER, S.P. (2013) Prevalence of mutations in eyeGENE probands with a diagnosis of autosomal dominant retinitis pigmentosa. *Investigative Ophthalmology and Visual Science* **54**, 6255–6261.
- SULSTON, J., DEW, M. & BRENNER, S. (1975) Dopaminergic neurons in the nematode *Caenorhabditis elegans*. *The Journal of Comparative Neurology* **163**, 215–226.
- SULSTON, J. & HODGKIN, J. (1988) Methods. In *The Nematode Caenorhabditis elegans*, Edited by William B. Wood pp. 587–606.
- SULSTON, J.E., SCHIERENBERG, E., WHITE, J.G. & THOMSON, J.N. (1983) The embryonic cell lineage of the nematode *Caenorhabditis elegans*. *Developmental Biology* **100**, 64–119.
- SUÑÉ-POU, M., PRIETO-SÁNCHEZ, S., BOYERO-CORRAL, S., MORENO-CASTRO, C., EL YOUSFI, Y., SUÑÉ-NEGRE, J., HERNÁNDEZ-MUNAIN, C. & SUÑÉ, C. (2017) Targeting Splicing in the Treatment of Human Disease. *Genes* **8**, 87.
- SYED, Y.Y. (2016) Eteplirsén: First Global Approval. *Drugs* **76**, 1699–1704.
- TABARA, H. (1998) REVERSE GENETICS:RNAi in *C. elegans*: Soaking in the Genome Sequence. *Science* **282**, 430–431.
- TAM, A.S., SIHOTA, T.S., MILBURY, K.L., ZHANG, A., MATHEW, V. & STIRLING, P.C. (2019) Selective defects in gene expression control genome instability in yeast splicing mutants. *Molecular Biology of the Cell* **30**, 191–200.
- TAM, A.S. & STIRLING, P.C. (2019) Splicing, genome stability and disease: splice like your genome depends on it! *Current Genetics* **65**, 905–912.
- TAN, J.H. & FRASER, A.G. (2017) The combinatorial control of alternative splicing in *C. elegans*. *PLOS Genetics* **13**, e1007033.
- TANACKOVIC, G., RANSIJN, A., AYUSO, C., HARPER, S., BERSON, E.L. & RIVOLTA, C. (2011) A missense mutation in *PRPF6* causes impairment of pre-mRNA splicing and autosomal-dominant retinitis pigmentosa. *American Journal of Human Genetics* **88**, 643–649.
- TANIKAWA, M., SANJIV, K., HELLEDAY, T., HERR, P. & MORTUSEWICZ, O. (2016) The spliceosome U2 snRNP factors promote genome stability through distinct mechanisms; transcription of repair factors and R-loop processing. *Oncogenesis* **5**, e280–e280.
- TESTA, F., ZIVIELLO, C., RINALDI, M., ROSSI, S., DI IORIO, V., INTERLANDI, E., CICCOCICOLA, A., BANFI, S. & SIMONELLI, F. (2006) Clinical Phenotype of an Italian Family with a New Mutation in the *PRPF8* Gene. *European Journal of Ophthalmology* **16**, 779–781.
- THE C.ELEGANS SEQUENCING CONSORTIUM (1998) Genome Sequence of the Nematode *C.elegans*: A Platform for Investigating Biology. *Science* **282**, 2012–2018.
- TIEMANN, K. & ROSSI, J.J. (2009) RNAi-based therapeutics—current status, challenges and prospects. *EMBO Molecular Medicine* **1**, 142–151.
- TIMANER, M., BRIL, R., KAIDAR-PERSON, O., RACHMAN-TZEMAH, C., ALISHEKEVITZ, D., KOTSOFRUK, R., MILLER, V., NEVELSKY, A., DANIEL, S., RAVIV, Z., ROTENBERG, S.A. & SHAKED, Y. (2015) Dequalinium blocks macrophage-induced metastasis following local radiation. *Oncotarget* **6**, 27537–27554.
- TIMMONS, L. & FIRE, A. (1998) Specific interference by ingested dsRNA. *Nature* **395**, 854–854.
- TOURASSE, N.J., MILLET, J.R.M. & DUPUY, D. (2017) Quantitative RNA-seq meta-analysis of alternative exon usage in *C. elegans*. *Genome Research* **27**, 2120–2128.

- TOWNS, K. V., KIPLOTI, A., LONG, V., MCKIBBIN, M., MAUBARET, C., VACLAVIK, V., EHSANI, P., SPRINGELL, K., KAMAL, M., RAMESAR, R.S., MACKEY, D.A., MOORE, A.T., MUKHOPADHYAY, R., WEBSTER, A.R., BLACK, G.C.M., ET AL. (2010) Prognosis for splicing factor *PRPF8* retinitis pigmentosa, novel mutations and correlation between human and yeast phenotypes. *Human Mutation* **31**, E1361–E1376.
- TUDURI, S., CRABBÉ, L., CONTI, C., TOURRIÈRE, H., HOLTGREVE-GREZ, H., JAUCH, A., PANTESCO, V., DE VOS, J., THOMAS, A., THEILLET, C., POMMIER, Y., TAZI, J., COQUELLE, A. & PASERO, P. (2009) Topoisomerase I suppresses genomic instability by preventing interference between replication and transcription. *Nature Cell Biology* **11**, 1315–1324.
- USTIANENKO, D., WEYN-VANHENTENRYCK, S.M. & ZHANG, C. (2017) Microexons: discovery, regulation, and function. *Wiley Interdisciplinary Reviews: RNA* **8**, e1418.
- UYAMA, H., MANDAI, M. & TAKAHASHI, M. (2021) Stem-cell-based therapies for retinal degenerative diseases: Current challenges in the establishment of new treatment strategies. *Development Growth and Differentiation* **63**, 59–71.
- VACLAVIK, V., GAILLARD, M.-C., TIAB, L., SCHORDERET, D.F. & MUNIER, F.L. (2010) Variable phenotypic expressivity in a Swiss family with autosomal dominant retinitis pigmentosa due to a T494M mutation in the *PRPF3* gene. *Molecular vision* **16**, 467–475.
- VASER, R., SOVIĆ, I., NAGARAJAN, N. & ŠIKIĆ, M. (2017) Fast and accurate de novo genome assembly from long uncorrected reads. *Genome Research* **27**, 737–746.
- VENTURINI, G., ROSE, A.M., SHAH, A.Z., BHATTACHARYA, S.S. & RIVOLTA, C. (2012) *CNOT3* is a modifier of *PRPF31* mutations in retinitis pigmentosa with incomplete penetrance. *PLoS Genetics* **8**, e1003040.
- VERBAKEL, S.K., VAN HUET, R.A.C., BOON, C.J.F., DEN HOLLANDER, A.I., COLLIN, R.W.J., KLAVER, C.C.W., HOYNG, C.B., ROEPMAN, R. & KLEVERING, B.J. (2018) Non-syndromic retinitis pigmentosa. *Progress in Retinal and Eye Research* **66**, 157–186.
- VICENCIO, J. & CERÓN, J. (2021) A Living Organism in your CRISPR Toolbox: *Caenorhabditis elegans* Is a Rapid and Efficient Model for Developing CRISPR-Cas Technologies. *The CRISPR Journal* **4**, 32–42.
- VICENCIO, J., MARTÍNEZ-FERNÁNDEZ, C., SERRAT, X. & CERÓN, J. (2019) Efficient Generation of Endogenous Fluorescent Reporters by Nested CRISPR in *Caenorhabditis elegans*. *Genetics* **211**, 1143–1154.
- VIGNARD, J., MIREY, G. & SALLES, B. (2013) Ionizing-radiation induced DNA double-strand breaks: A direct and indirect lighting up. *Radiotherapy and Oncology* **108**, 362–369.
- VITHANA, E.N., ABU-SAFIEH, L., ALLEN, M.J., CAREY, A., PAPAIOANNOU, M., CHAKAROVA, C., AL-MAGHTHEH, M., EBENEZER, N.D., WILLIS, C., MOORE, A.T., BIRD, A.C., HUNT, D.M. & BHATTACHARYA, S.S. (2001) A Human Homolog of Yeast Pre-mRNA Splicing Gene, *PRP31*, Underlies Autosomal Dominant Retinitis Pigmentosa on Chromosome 19q13.4 (RP11). *Molecular Cell* **8**, 375–381.
- VOLPATTI, J.R., ENDO, Y., KNOX, J., GROOM, L., BRENNAN, S., NOCHE, R., ZUERCHER, W.J., ROY, P., DIRKSEN, R.T. & DOWLING, J.J. (2020) Identification of drug modifiers for RYR1-related myopathy using a multi-species discovery pipeline. *eLife* **9**, e52946.
- WADA, Y., ITABASHI, T., SATO, H. & TAMAI, M. (2004) Clinical features of a Japanese family with autosomal dominant retinitis pigmentosa associated with a Thr494Met mutation in the *HPRP3* gene. *Graefes' Archive for Clinical and Experimental Ophthalmology* **242**, 956–961.
- WAGNER, S.K., JOLLY, J.K., PEFKIANAKI, M., GEKELER, F., WEBSTER, A.R., DOWNES, S.M. & MACLAREN, R.E. (2017) Transcorneal electrical stimulation for the treatment of retinitis pigmentosa: Results from the TESOLAUK trial. *BMJ Open Ophthalmology* **2**, e000096.

- WAHL, M.C., WILL, C.L. & LÜHRMANN, R. (2009) The spliceosome: design principles of a dynamic RNP machine. *Cell* **136**, 701–718.
- WALIA, S., FISHMAN, G.A., ZERNANT-RAJANG, J., RAIME, K. & ALLIKMETS, R. (2008) Phenotypic expression of a *PRPF8* gene mutation in a large African American family. *Archives of Ophthalmology* **126**, 1127–1132.
- WALTON, R.T., CHRISTIE, K.A., WHITTAKER, M.N. & KLEINSTIVER, B.P. (2020) Unconstrained genome targeting with near-PAMless engineered CRISPR-Cas9 variants. *Science* **368**, 290–296.
- WAN, Y., ZHENG, X., CHEN, H., GUO, Y., JIANG, H., HE, X., ZHU, X. & ZHENG, Y. (2015) Splicing function of mitotic regulators links R-loop-mediated DNA damage to tumor cell killing. *Journal of Cell Biology* **209**, 235–246.
- WANG, E.T., SANDBERG, R., LUO, S., KHREBTUKOVA, I., ZHANG, L., MAYR, C., KINGSMORE, S.F., SCHROTH, G.P. & BURGE, C.B. (2008) Alternative isoform regulation in human tissue transcriptomes. *Nature* **456**, 470–476.
- WANG, F., WANG, H., TUAN, H.F., NGUYEN, D.H., SUN, V., KESER, V., BOWNE, S.J., SULLIVAN, L.S., LUO, H., ZHAO, L., WANG, X., ZANEVELD, J.E., SALVO, J.S., SIDDIQUI, S., MAO, L., ET AL. (2014a) Next generation sequencing-based molecular diagnosis of retinitis pigmentosa: Identification of a novel genotype-phenotype correlation and clinical refinements. *Human Genetics* **133**, 331–345.
- WANG, J., ZHANG, V.W., FENG, Y., TIAN, X., LI, F.Y., TRUONG, C., WANG, G., CHIANG, P.W., LEWIS, R.A. & WONG, L.J.C. (2014b) Dependable and efficient clinical utility of target capture-based deep sequencing in molecular diagnosis of retinitis pigmentosa. *Investigative Ophthalmology and Visual Science* **55**, 6213–6223.
- WANGLER, M.F., YAMAMOTO, S., CHAO, H.-T., POSEY, J.E., WESTERFIELD, M., POSTLETHWAIT, J., HIETER, P., BOYCOTT, K.M., CAMPEAU, P.M. & BELLEN, H.J. (2017) Model Organisms Facilitate Rare Disease Diagnosis and Therapeutic Research. *Genetics* **207**, 9–27.
- WANI, S. & KUROYANAGI, H. (2017) An emerging model organism *Caenorhabditis elegans* for alternative pre-mRNA processing in vivo. *Wiley Interdisciplinary Reviews: RNA* **8**, e1428.
- WARD, J.D. (2015) Rapid and Precise Engineering of the *Caenorhabditis elegans* Genome with Lethal Mutation Co-Conversion and Inactivation of NHEJ Repair. *Genetics* **199**, 363–377.
- WARD, S., THOMSON, N., WHITE, J.G. & BRENNER, S. (1975) Electron microscopical reconstruction of the anterior sensory anatomy of the nematode *Caenorhabditis elegans*. *The Journal of Comparative Neurology* **160**, 313–337.
- WASEEM, N.H., VACLAVIK, V., WEBSTER, A., JENKINS, S.A., BIRD, A.C. & BHATTACHARYA, S.S. (2007) Mutations in the Gene Coding for the Pre-mRNA Splicing Factor, *PRPF31*, in Patients with Autosomal Dominant Retinitis Pigmentosa. *Investigative Ophthalmology & Visual Science* **48**, 1330.
- WERT, K.J., LIN, J.H. & TSANG, S.H. (2014) General Pathophysiology in Retinal Degeneration. In *Cell-Based Therapy for Retinal Degenerative Disease* pp. 33–43.
- WESTERVELT, P., CHO, K., BRIGHT, D.R. & KISOR, D.F. (2014) Drug-gene interactions: inherent variability in drug maintenance dose requirements. *P & T: a peer-reviewed journal for formulary management* **39**, 630–637.
- WESTHOLM, J.O. & LAI, E.C. (2011) Mirtrons: microRNA biogenesis via splicing. *Biochimie* **93**, 1897–1904.
- WHEWAY, G., NAZLAMOVA, L., MESHAD, N., HUNT, S., JACKSON, N. & CHURCHILL, A. (2019) A Combined *in silico*, *in vitro* and Clinical Approach to Characterize Novel Pathogenic Missense Variants in *PRPF31* in Retinitis Pigmentosa. *Frontiers in Genetics* **10**, 248.

- WHITE, J., SOUTHGATE, E., THOMSON, J. & BRENNER, S. (1986) The structure of the nervous system of the nematode *Caenorhabditis elegans*. *Philosophical Transactions of the Royal Society of London. B, Biological Sciences* **314**, 1–340.
- WHITE, J.G., SOUTHGATE, E., THOMSON, J.N. & BRENNER, S. (1976) The structure of the ventral nerve cord of *Caenorhabditis elegans*. *Philosophical Transactions of the Royal Society of London. B, Biological Sciences* **275**, 327–348.
- WILKINSON, M.E., CHARENTON, C. & NAGAI, K. (2020) RNA Splicing by the Spliceosome. *Annual Review of Biochemistry* **89**, 359–388.
- WILKINSON, M.E., FICA, S.M., GALEJ, W.P. & NAGAI, K. (2021) Structural basis for conformational equilibrium of the catalytic spliceosome. *Molecular Cell* **81**, 1439-1452.e9.
- WILL, C.L. & LÜHRMANN, R. (2011) Spliceosome structure and function. *Cold Spring Harbor perspectives in biology* **3**, 1–2.
- WOOD, K.A., EADSFORTH, M.A., NEWMAN, W.G. & O'KEEFE, R.T. (2021) The Role of the U5 snRNP in Genetic Disorders and Cancer. *Frontiers in Genetics* **12**, 20.
- WORKMAN, R.E., TANG, A.D., TANG, P.S., JAIN, M., TYSON, J.R., RAZAGHI, R., ZUZARTE, P.C., GILPATRICK, T., PAYNE, A., QUICK, J., SADOWSKI, N., HOLMES, N., DE JESUS, J.G., JONES, K.L., SOULETTE, C.M., ET AL. (2019) Nanopore native RNA sequencing of a human poly(A) transcriptome. *Nature Methods* **16**, 1297–1305.
- WU, H., SUN, L., WEN, Y., LIU, Y., YU, J., MAO, F., WANG, Y., TONG, C., GUO, X., HU, Z., SHA, J., LIU, M. & XIA, L. (2016) Major spliceosome defects cause male infertility and are associated with nonobstructive azoospermia in humans. *Proceedings of the National Academy of Sciences of the United States of America* **113**, 4134–4139.
- WU, Z., ZHONG, M., LI, M., HUANG, H., LIAO, J., LU, A., GUO, K., MA, N., LIN, J., DUAN, J., LIU, L., XU, F., ZHONG, Z. & CHEN, J. (2018) Mutation Analysis of Pre-mRNA Splicing Genes *PRPF31*, *PRPF8*, and *SNRNP200* in Chinese Families with Autosomal Dominant Retinitis Pigmentosa. *Current Molecular Medicine* **18**, 287–294.
- XIAO, X., CAO, Y., ZHANG, Z., XU, Y., ZHENG, Y., CHEN, L.J., PANG, C.P. & CHEN, H. (2017) Novel Mutations in *PRPF31* Causing Retinitis Pigmentosa Identified Using Whole-Exome Sequencing. *Investigative Ophthalmology & Visual Science* **58**, 6342.
- XU, F., SUI, R., LIANG, X., LI, H., JIANG, R. & DONG, F. (2012) Novel *PRPF31* mutations associated with Chinese autosomal dominant retinitis pigmentosa patients. *Molecular vision* **18**, 3021.
- XU, Y., GUAN, L., SHEN, T., ZHANG, J., XIAO, X., JIANG, H., LI, S., YANG, J., JIA, X., YIN, Y., GUO, X., WANG, J. & ZHANG, Q. (2014) Mutations of 60 known causative genes in 157 families with retinitis pigmentosa based on exome sequencing. *Human Genetics* **133**, 1255–1271.
- YAN, C., WAN, R. & SHI, Y. (2019) Molecular mechanisms of pre-mRNA splicing through structural biology of the spliceosome. *Cold Spring Harbor Perspectives in Biology* **11**, a032409.
- YANOWITZ, J.L. (2008) Genome Integrity Is Regulated by the *Caenorhabditis elegans* Rad51D Homolog *rfs-1*. *Genetics* **179**, 249–262.
- YIN, J., BROCHER, J., FISCHER, U. & WINKLER, C. (2011) Mutant Prpf31 causes pre-mRNA splicing defects and rod photoreceptor cell degeneration in a zebrafish model for Retinitis pigmentosa. *Molecular Neurodegeneration* **6**, 56.
- YU, K., CHEDIN, F., HSIEH, C.L., WILSON, T.E. & LIEBER, M.R. (2003) R-loops at immunoglobulin class switch regions in the chromosomes of stimulated B cells. *Nature Immunology* **4**, 442–451.
- YUSUF, I.H., BIRTEL, J., SHANKS, M.E., CLOUSTON, P., DOWNES, S.M., CHARBEL ISSA, P. & MACLAREN, R.E. (2019) Clinical Characterization of Retinitis Pigmentosa Associated with Variants in *SNRNP200*. *JAMA Ophthalmology* **137**, 1295–1300.

- ZÄHLER, A. (2018) Pre-mRNA splicing and its regulation in *Caenorhabditis elegans*. In *In: WormBook: The Online Review of C. elegans Biology [Internet]* p.
- ZAMPAGLIONE, E., KINDE, B., PLACE, E.M., NAVARRO-GOMEZ, D., MAHER, M., JAMSHIDI, F., NASSIRI, S., MAZZONE, J.A., FINN, C., SCHLEGEL, D., COMANDER, J., PIERCE, E.A. & BUJAKOWSKA, K.M. (2020) Copy-number variation contributes 9% of pathogenicity in the inherited retinal degenerations. *Genetics in Medicine* **22**, 1079–1087.
- ZELLER, P., PADEKEN, J., VAN SCHENDEL, R., KALCK, V., TIJSTERMAN, M. & GASSER, S.M. (2016) Histone H3K9 methylation is dispensable for *Caenorhabditis elegans* development but suppresses RNA:DNA hybrid-associated repeat instability. *Nature Genetics* **48**, 1385–1395.
- ZENG, L., LIU, W., FENG, W., WANG, X., DANG, H., GAO, L., YAO, J. & ZHANG, X. (2013) A novel donor splice-site mutation of major intrinsic protein gene associated with congenital cataract in a Chinese family. *Molecular Vision* **19**, 2244–2249.
- ZENG, Q., LEI, F., CHANG, Y., GAO, Z., WANG, Y., GAO, Q., NIU, P. & LI, Q. (2019) An oncogenic gene, *SNRPA1*, regulates *PIK3R1*, *VEGFC*, *MKI67*, *CDK1* and other genes in colorectal cancer. *Biomedicine & pharmacotherapy = Biomedecine & pharmacotherapie* **117**, 109076.
- ZENTENO, J.C., GARCÍA-MONTAÑO, L.A., CRUZ-AGUILAR, M., RONQUILLO, J., RODAS-SERRANO, A., AGUILAR-CASTUL, L., MATSUI, R., VENCEDOR-MERAZ, C.I., ARCE-GONZÁLEZ, R., GRAUE-WIECHERS, F., GUTIÉRREZ-PAZ, M., URREA-VICTORIA, T., DIOS CUADRAS, U. & CHACÓN-CAMACHO, O.F. (2020) Extensive genic and allelic heterogeneity underlying inherited retinal dystrophies in Mexican patients molecularly analyzed by next-generation sequencing. *Molecular Genetics & Genomic Medicine* **8**, mgg3.1044.
- ZERBINO, D.R., ACHUTHAN, P., AKANNI, W., AMODE, M.R., BARRELL, D., BHAI, J., BILLIS, K., CUMMINS, C., GALL, A., GIRÓN, C.G., GIL, L., GORDON, L., HAGGERTY, L., HASKELL, E., HOURLIER, T., ET AL. (2018) Ensembl 2018. *Nucleic Acids Research* **46**, D754–D761.
- ZHANG, Q. (2016) Retinitis Pigmentosa: Progress and Perspective. *Asia-Pacific journal of ophthalmology (Philadelphia, Pa.)* **5**, 265–271.
- ZHANG, Q., XU, M., VERRIOTTO, J.D., LI, Y., WANG, H., GAN, L., LAM, B.L. & CHEN, R. (2016) Next-generation sequencing-based molecular diagnosis of 35 Hispanic retinitis pigmentosa probands. *Scientific reports* **6**, 32792.
- ZHANG, T., BAI, J., ZHANG, X., ZHENG, X., LU, N., LIANG, Z., LIN, L. & CHEN, Y. (2021) *SNRNP200* Mutations Cause Autosomal Dominant Retinitis Pigmentosa. *Frontiers in Medicine* **7**, 1108.
- ZHANG, X., LAI, T.Y.Y., CHIANG, S.W.Y., TAM, P.O.S., LIU, D.T.L., CHAN, C.K.M., PANG, C.P., ZHAO, C. & CHEN, L.J. (2013) Contribution of *SNRNP200* sequence variations to retinitis pigmentosa. *Eye (Basingstoke)* **27**, 1204–1213.
- ZHAO, C., BELLUR, D.L., LU, S., ZHAO, F., GRASSI, M.A., BOWNE, S.J., SULLIVAN, L.S., DAIGER, S.P., CHEN, L.J., PANG, C.P., ZHAO, K., STALEY, J.P. & LARSSON, C. (2009) Autosomal-dominant retinitis pigmentosa caused by a mutation in *SNRNP200*, a gene required for unwinding of U4/U6 snRNAs. *American journal of human genetics* **85**, 617–627.
- ZHONG, Z., YAN, M., SUN, W., WU, Z., HAN, L., ZHOU, Z., ZHENG, F. & CHEN, J. (2016) Two novel mutations in *PRPF3* causing autosomal dominant retinitis pigmentosa. *Scientific Reports* **6**, 37840.
- ZHU, B., MAK, J.C.H., MORRIS, A.P., MARSON, A.G., BARCLAY, J.W., SILLS, G.J. & MORGAN, A. (2020) Functional analysis of epilepsy-associated variants in *STXBP1/Munc18-1* using humanized *Caenorhabditis elegans*. *Epilepsia* **61**, 810–821.
- ZIVIELLO, C., SIMONELLI, F., TESTA, F., ANASTASI, M., MARZOLI, S.B., FALSINI, B., GHIGLIONE, D., MACALUSO, C., MANITTO, M.P., GARRÈ, C., CICCODICOLA, A., RINALDI, E. & BANFI, S. (2005) Molecular genetics of autosomal dominant retinitis pigmentosa (ADRP): a comprehensive study of 43 Italian families. *Journal of Medical Genetics* **42**, e47–e47.

BIBLIOGRAPHY

- ZORIO, D.A.R. & BLUMENTHAL, T. (1999) Both subunits of U2AF recognize the 3' splice site in *Caenorhabditis elegans*. *Nature* **402**, 835–838.
- ZORIO, D.A.R., CHENG, N.N., BLUMENTHAL, T. & SPIETH, J. (1994) Operons as a common form of chromosomal organization in *C. elegans*. *Nature* **372**, 270–272.

LIST OF PUBLICATIONS

Brena D, Bertran J, Porta-de-la-Riva M, Guillén Y, Cornes E, **Kukhtar D**, Campos-Vicens L, Fernández L, Pecharroman I, García-López A, Islam ABMMK, Marruecos L, Bigas A, Cerón J, Espinosa L. Ancestral function of Inhibitors-of-kappaB regulates *Caenorhabditis elegans* development. *Sci Rep*. 2020 Sep 30;10(1):16153.

Kukhtar D, Rubio-Peña K, Serrat X, Cerón J. Mimicking of splicing-related retinitis pigmentosa mutations in *C. elegans* allow drug screens and identification of disease modifiers. *Hum Mol Genet*. 2020 Mar 27;29(5):756-765.

Serrat X, **Kukhtar D**, Cornes E, Esteve-Codina A, Benlloch H, Cecere G, Cerón J. CRISPR editing of *sftb-1/SF3B1* in *Caenorhabditis elegans* allows the identification of synthetic interactions with cancer-related mutations and the chemical inhibition of splicing. *PLoS Genet*. 2019 Oct 21;15(10):e1008464.

García-Rodríguez FJ, Martínez-Fernández C, Brena D, **Kukhtar D**, Serrat X, Nadal E, Boxem M, Honnen S, Miranda-Vizueté A, Villanueva A, Cerón J. Genetic and cellular sensitivity of *Caenorhabditis elegans* to the chemotherapeutic agent cisplatin. *Dis Model Mech*. 2018 Jun 21;11(6):dmm033506

Saura-Esteller J, Sánchez-Vera I, Núñez-Vázquez S, Jabalquinto-Carrasco J, Cosiáls AM, Mendive-Tapia L, **Kukhtar D**, Martínez-Bueno MD, Lavilla R, Cerón J, Artal-Sanz M, Pons G, Iglesias-Serret D, Gil J. Fluorizoline-induced apoptosis requires prohibitins in nematodes and human cells. *Apoptosis*. 2021 Feb;26(1-2):83-95.

